

1992

# A study of the structures and properties of some binuclear copper complexes

Gregory William Diven  
*University of Wollongong*

## **NOTE**

This online version of the thesis may have different page formatting and pagination from the paper copy held in the University of Wollongong Library.

## **UNIVERSITY OF WOLLONGONG**

### **COPYRIGHT WARNING**

You may print or download ONE copy of this document for the purpose of your own research or study. The University does not authorise you to copy, communicate or otherwise make available electronically to any other person any copyright material contained on this site. You are reminded of the following:

Copyright owners are entitled to take legal action against persons who infringe their copyright. A reproduction of material that is protected by copyright may be a copyright infringement. A court may impose penalties and award damages in relation to offences and infringements relating to copyright material. Higher penalties may apply, and higher damages may be awarded, for offences and infringements involving the conversion of material into digital or electronic form.

**A STUDY OF THE STRUCTURES AND PROPERTIES OF SOME  
BINUCLEAR COPPER COMPLEXES**

A Thesis Submitted in Fulfillment of the Requirements for the Award of the Degree

of

**DOCTOR OF PHILOSOPHY**

from

**THE UNIVERSITY OF WOLLONGONG**

by

**GREGORY WILLIAM DIVEN** B.Sc(HONS)



DEPARTMENT OF CHEMISTRY

1992





This is to certify that the work described in  
this thesis has not been submitted for a  
degree at any other university or institution.

I dedicate this thesis to

the

memory of my mother

and

to my father.

No one could wish for better parents.

## Acknowledgements

I wish to acknowledge those people who supported and assisted me during this project.

I wish to thank Dr G.M.Mockler my supervisor for his encouragement, tolerance and perseverance. I wish also to thank Peter Riley for his considerable assistance and advice in conducting the electrochemical studies, Dr E.Sinn and Dr R.Butcher for the crystal structures presented in this thesis.

For allowing me to undertake this project I thank the chairman of the chemistry department Prof L.Kane-Maguire.

I thank the technical staff for assistance in keeping the instruments functioning.

I wish to thank my postgraduate colleagues; David Cheesman, Gary Erickson, Ulrich Senff, Branko Dikic, Maribel Nonato, Michael Manthey and Mark Stewart.

Special thanks to the Wilson family for providing a peaceful haven over the years to which I could retreat occasionally to recharge the batteries.

Finally my greatest thanks and love goes to my family for all their support and encouragement even though they do not really understand anything to do with this project.

## Table of Contents

<u>Acknowledgements</u>	iv
<u>Abstract</u>	x
<u>Aim of Project</u>	xi
 <u>1: Introduction</u>	
1.1 General Introduction	1
1.2 Copper Proteins	4
1.2.1 Hemocyanin	8
1.2.2 Tyrosinase	10
1.2.3 Blue Oxidases	12
1.2.4 Studies of the Type III Active Site	16
1.3 Model Compounds	24
1.4 Requirements for a Type III Active Site Model	26
1.5 Model Compounds for a Type III Copper Proteins	27
1.5.1 Compounds with no Endogenous Bridge	28
1.5.2 Compounds with an Endogenous Phenol Oxygen Bridge	36
1.5.3 Compounds with an Endogenous Alcohol Oxygen Bridge	46
1.5.4 Multi-Copper Oxidase Models	56
1.5.5 Reactions of Model Compounds with Phenols and Catechols	62
1.5.6 The Electrochemistry of Model Compounds of Type III Copper Proteins	69
 <u>2: Empirical Formulae</u>	 74
 <u>3: Infra-red Spectra</u>	 79

4: <u>UV-Vis Spectra</u>	88
4a) Pyrazole-Type Bridged Complexes	92
4b) Oxygen-Type Bridged Complexes	93
4c) Pyridine-N-Oxide-Type Bridged Complexes	94
5: <u>Magnetism</u>	99
5.1 Strongly Interacting Complexes	107
5.1.1 Pyrazole Bridged Complexes	107
5.1.2 Cu <sub>2</sub> (SAL-DPE)XCATH	109
5.2 Weakly Interacting Complexes	110
5.2.1 Cu <sub>2</sub> (SAL-DPL)(XCATH) <sub>0.5</sub>	110
5.2.2 Mono-Oxygen Type Bridged Complexes	112
5.2.3 Di-Oxygen Type Bridged Complexes	113
5.2.4 Pyridine-N-Oxide Type Bridged Complexes	116
6: <u>Crystal Structure</u>	
6.1 Hydroxylamine Complex	122
6.2 Cu <sub>2</sub> (SAL-DPL)6Al	126
6.3 Cu <sub>2</sub> (M <sup>2</sup> BP-DPL)3,5-Me <sup>2</sup> Pz	131
7: <u>Mass Spectra</u>	135

8: <u>Electrochemistry</u>	141
8.1 Cyclic Voltammetry	142
8.2 Differential Pulse Voltammetry	143
8.3 Coulometry	145
8.4 Polarography	146
8.5 Summary	147
8.6 Coulometry of the Copper Complexes	149
8.7 Cu(SAL-DPLH)	155
8.8 Cu <sub>2</sub> (SAL-DPL)OH.3H <sub>2</sub> O	162
8.9 Cu <sub>2</sub> (SAL-DPE)OH	168
8.10 Cu <sub>2</sub> (SAL-DPL)(CAT) <sub>0.5</sub> .(H <sub>2</sub> O) <sub>0.5</sub>	172
8.11 Cu <sub>2</sub> (SAL-DPE)CATH.(H <sub>2</sub> O) <sub>0.5</sub>	176
8.12 Cu <sub>2</sub> (SAL-DPL)Pz	180
8.13 Cu <sub>2</sub> (SAL-DPE)Pz	187
8.14 Cu <sub>2</sub> (SAL-DPL)PyO.(H <sub>2</sub> O) <sub>0.5</sub>	192
8.15 Cu <sub>2</sub> (SAL-DPL)4-OHBzCOO	197
8.16 Cu <sub>5</sub> (SAL-DPL.PAB.SAL) <sub>2</sub> .3H <sub>2</sub> O	201
8.17 Cu <sub>5</sub> (SAL-DPL.4ABA.SAL) <sub>2</sub> .2H <sub>2</sub> O	206
8.18 Cu <sub>5</sub> (ESAL-DPL.6AIESAL) <sub>2</sub> .2H <sub>2</sub> O	211

9: <u>Discussion</u>	
9.1 Models of Tyrosinase	215
9.1.1 $\text{Cu}_2(\text{SAL-DPE})\text{XCATH}(\text{H}_2\text{O})_{0.5}$	216
9.1.2 $\text{Cu}_2(\text{SAL-DPL})(\text{XCAT})_{0.5}(\text{H}_2\text{O})_{0.5}$	220
9.2 Electrochemistry of Models of Tyrosinase and Multi-Copper Oxidases	224
9.2.1 $\text{Cu}(\text{SAL-DPLH})$	224
9.2.2 $\text{Cu}_2(\text{SAL-DPE})\text{CATH}(\text{H}_2\text{O})_{0.5}$	225
9.2.3 $\text{Cu}_2(\text{SAL-DPL})(\text{CATH})_{0.5}(\text{H}_2\text{O})_{0.5}$	227
9.2.4 Binuclear Complexes	228
9.2.5 Multi-Copper Oxidase Model Compounds	231
10: <u>Other Work</u>	236
11: <u>Conclusion</u>	243
12: <u>Experimental</u>	
12.1 Synthesis of 1,5-diamino-3-pentanol (DPE)	244
12.1.1 1,5-dichloro-3-pentanone	244
12.1.2 1,5-diamino-3-pentanone.dihychloride	245
12.1.3 1,5-diamino-3-pentanol.dihydrochloride	246
12.2 4,5'-dimethyl-2-hydroxybenzophenone ( $\text{M}^2\text{BP}$ )	247
12.3 Synthesis of the Schiff Bases	248
12.4 Synthesis of $\text{Cu}(\text{XSAL})_2$	250
12.5.1 Synthesis of the Binuclear Copper Complexes of the Propanol (DPL)	250
Schiff Base	

12.5.2 Synthesis of the Binuclear Copper Complexes of the Pentanol (DPE)	250
Schiff Base	
12.6 Synthesis of the Pentanuclear Complexes	
12.6.1 Pentanuclear Complexes not Bridged by 6-Aminoindazole	252
12.6.2 Pentanuclear Complexes Bridged by 6-Aminoindazole	253
12.7 Microanalyse	254
12.8 Infra-red Spectra	255
12.9 UV-Vis Spectra	256
12.10 Magnetism	256
12.11 Mass Spectra	256
12.12 Thermogravimetry	257
12.13 Crystal Structure	257
12.14 Electrochemistry	257
 13: <u>Appendix</u>	
13.1 Crystal Structure Data for $\text{Cu}_2(\text{SAL-DPL})\text{NH}_2\text{O}$	259
13.2 Crystal Structure Data for $\text{Cu}_2(\text{SAL-DPL})6\text{AI}$	266
13.3 Crystal Structure Data for $\text{Cu}_2(\text{M}^2\text{BP-DPL})3,5\text{-Me}_2\text{Pz}$	275
13.4 Variable Temperature Magnetic Data for the Binuclear Complexes	285
 14: <u>References</u>	294



## Abstract

Thirty two binuclear copper (II) complexes based on 1,3-bis(salicylaldimino)propan-2-ol (SAL-DPLH<sub>3</sub>), 1,5-bis(salicylaldimino)pentan-3-ol (SAL-DPEH<sub>3</sub>) and 1,3-bis(4,5'-dimethyl-2-hydroxybenzophenimino)propan-2-ol (M<sup>2</sup>BP-DPLH<sub>3</sub>) have been prepared as models of the structure of the Type III copper centre of Tyrosinase. A further four complexes (one mononuclear and three pentanuclear complexes) based on the above ligands were prepared and added to the thirty two compounds in a study of models of the electrochemical activity of the Type II and Type III copper centres of multicopper oxidases. A new synthetic method was developed using Cu(XSAL)<sub>2</sub> as the copper source.

A series of binuclear copper (II) complexes with a catechol exogenous bridge were synthesised. The infra-red spectra, visible spectra, mass spectra, magnetism and electrochemistry of these complexes were measured. The crystal structures of "Cu<sub>2</sub>(SAL-DPL)NH<sub>2</sub>O", Cu<sub>2</sub>(SAL-DPL)6-AI and Cu<sub>2</sub>(M<sup>2</sup>BP-DPL)M<sup>2</sup>Pz were obtained.

The complexes were found to undergo reduction from copper (II) to copper metal in DMF solutions against a variety of electrodes with the electrode material being a mercury pool, dropping mercury, hanging mercury drop, platinum and glassy carbon. Coulometry, polarography, differential pulse voltammetry and cyclic voltammetry were used to elucidate the electrochemistry of these complexes. The complexes all were reduced in the range 0 to -2000mV. Some of these complexes were found to have quasi-reversible redox properties and the rest were found to have irreversible redox properties.

### Aim of Project

The project had two aims:

1) the synthesis and study of the physio-chemical properties of catechol bridged binuclear copper complexes as model compounds of the suggested copper-catechol-copper bridge in tyrosinase.

11) the study in detail of the electrochemistry of

a)  $\text{Cu}(\text{SAL-DPLH})$

b)  $\text{Cu}_2(\text{SAL-DPL})\text{X}$ , where  $\text{X} = \text{Hydroxide}$

Catecholate

Pyrazolate

substituted Benzoate

c) the pentanuclear model compounds of multicopper oxidases

**1:**

## **Introduction**

### 1.1. General Introduction

In nature, twenty nine, of the ninety naturally occurring elements are known to be essential for life and of these, nine are transition metals (Table 1.1.). These metals are referred to as 'trace elements' as they constitute only 0.1% of the composition of organisms. Approximately one third of all known enzymes require metal ions to function.<sup>1</sup>

There are a wide range of functions involved with these metal ions (Table 1.2.).<sup>2</sup> They can be basically summarised into four broad categories:-<sup>3</sup>

1. in trigger and control mechanisms,
2. in a structural context, including template reactions,
3. as Lewis acids, and
4. as redox catalysts.

Some metalloproteins still have no known function.

The study of the functions of metalloproteins and metalloenzymes is made easier by the presence of metal ions which have distinctive physical properties. In particular, proteins and enzymes which contain transition metals lend themselves to analysis through the standard techniques of inorganic chemistry e.g. magnetochemistry, electronic spectra, optical rotation measurements and electrochemistry. These techniques indicate that the metal has a significant effect on the electronic and structural characteristics of the protein and that the protein can force unusual stereochemistries upon the metal ion.

The study of these metal compounds has been given the general name of Bioinorganic Chemistry. It is concerned with the study of both the metal and non-metal components and their interaction in biologically occurring compounds.<sup>4</sup>

[illegible]

**TABLE 1.1: Essential Trace Elements**

**Element****Roles***nontransition metals***K, Na**

electric carrier; activator for Na/K-ATPase

**Mg**activator for ATPase, kinases, and other  
enzymes**Ca**component of bones and shells; messenger for  
hormonal action; trigger for muscle contraction;  
structural role (in proteins)*transition and post-transition metals***Fe**

active sites of metalloenzymes for redox

**Cu**reactions, oxygenation, and O<sub>2</sub>-carrying  
proteins**Mo**redox enzymes and N<sub>2</sub> fixation**Mn, Co, Zn**

Lewis acids + structural role for Zn

**Co**

component of B12

*heavy metals***Hg, Pb, As, Cd**

inhibitors for enzymes

TABLE 1.2:2 Functions of Various Metals

## 1.2. Copper Proteins

Copper is found to occur in all living organisms and is the third most abundant transition metal after iron and zinc. Copper proteins are involved in electron transfer reactions, the binding and activation of molecular oxygen<sup>1</sup> and the transport and storage of oxygen.<sup>5-8</sup>

Examples of copper proteins are shown in Table 1.3.<sup>9</sup>

The copper in these proteins is classified into three "Types". The "Type" of copper present, in a protein, is based on certain specific properties exhibited by the active site.<sup>10</sup> These properties are as follows;

### Type 1:

These are known as the "blue" copper proteins due to their unique spectral feature of a very intense absorbance ( $\epsilon = 3\text{-}5000 \text{ M}^{-1}\text{cm}^{-1}$ ) in the 580-620 nm region.<sup>11</sup> This charge transfer band is attributed to a copper to cysteine sulphur bond.

Plastocyanin, the most thoroughly studied blue copper protein, has tetrahedral coordination around the copper atom, with two histidine nitrogens, one cysteine sulphur and a weakly co-ordinating methionine thioether sulphur atom, bound to the copper atom (Fig1.1).<sup>12</sup>

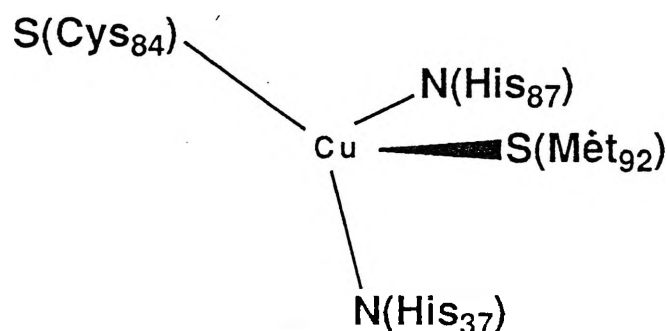


FIG 1.1:<sup>12</sup> Plastocyanin Active Site Structure

<u>Protein</u>	<u>Type</u>	<u>where found</u>	<u>Biological function</u>
<i>Blue electron carriers</i>			
Azurin	I	Green algae	Electron Transfer
Plastocyanin	I	leaves and other plants	(photosynthesis)
Stellacyanin	I	leaves and other plants	(photosynthesis)
<i>Blue oxidases</i>			
Laccase	I,II,III	Tree, Fungal	Oxidation of Phenols and Diamines
Ceruloplasmin	I,II,III	Human, Animal Serum	Weak oxidase activity Fe and Cu transport
Ascorbate oxidase	I,II,III	Plants	Oxidation of L-Ascorbic acid
<i>Non Blue oxidases</i>			
Amine oxidase	II	Most animals	Elastin, Collagen Formation
Galactose oxidase	II	Moulds	Galactose Oxidation
<i>Oxygen Carrier</i>			
Hemocyanins	III	Molluscs, Arthropods	Oxygen transport
<i>Copper Mono-oxygenases</i>			
Phenol o-mono-oxygenase (Tyrosinase)	III	Animal skin, Melanoma, insects, plants, fungi	Tyrosinase oxidation Pigment (melanin) formation
Dopamine $\beta$ -hydroxylase	III	Adrenals	Converts dopamine to norepinephrine

Table 1.3: Types of Copper Proteins, Function and Distribution<sup>9</sup>



Plastocyanin, Azurin and the multicopper oxidases, Laccase and Ceruloplasmin are involved in electron transfer reactions.

#### Type II:

This type of copper is known as normal copper. This is a result of the similarity of its spectral and magnetic properties compared to simple square planar or square pyramidal copper II complexes. It is found in, and is essential for the functioning of, the multicopper oxidases.

The copper is believed to exist in either a square planar or square pyramidal environment. In Galactose Oxidase the copper is co-ordinated to two histidine nitrogens, two tyrosine oxygens and one acetate oxygen (Fig1.2).<sup>12b</sup>

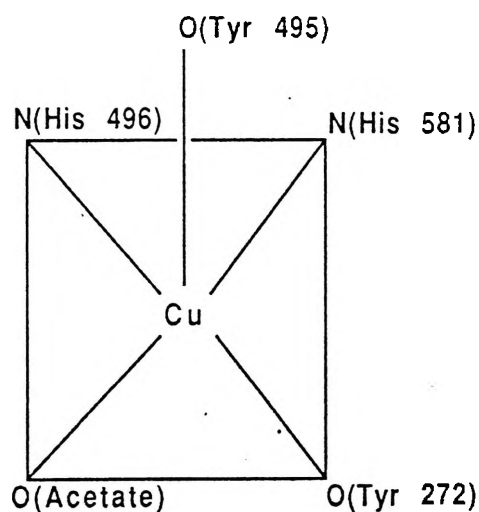


FIG 1.2:<sup>12b</sup> Galactose Oxidase Structure

The main function of proteins containing a Type II centre is the oxidation of a particular substance, which gives the protein its name, e.g. Galactose Oxidase oxidises many primary alcohols to the corresponding aldehydes (Fig1.3),<sup>12</sup> and at the same time reduces dioxygen to water.

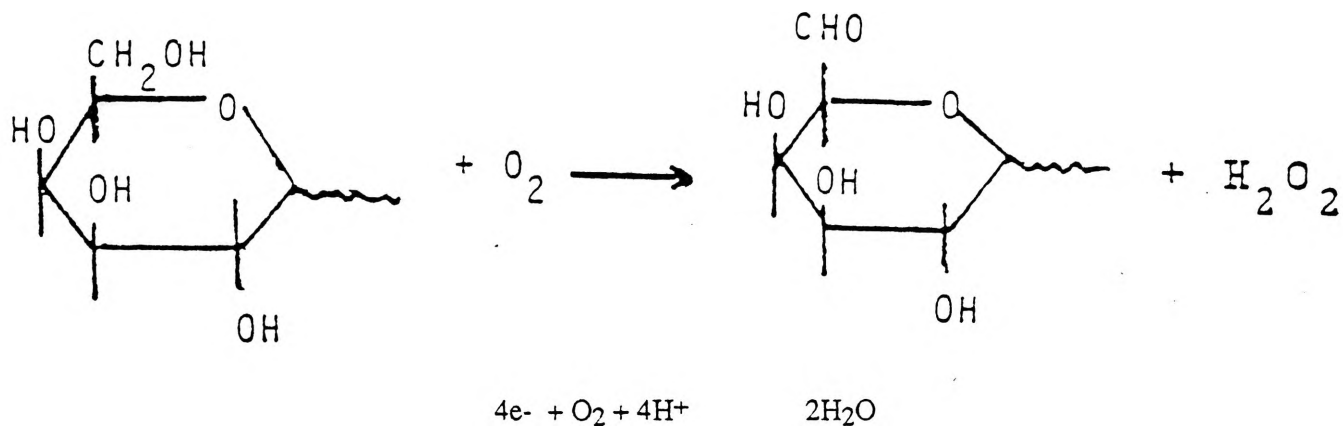


FIG 1.3:<sup>12</sup> Proposed Galactose Oxidase Reaction

#### Type III:

The Type III site is the most functionally variable of all the copper active sites. It functions as an oxygen carrier in Hemocyanin and as a catalyst for the hydroxylation of phenols to catechols and the oxidation of catechols to quinones in Tyrosinases.

The active site consists of a pair of copper atoms that are diamagnetic (Electron Spin Resonance silent) at room temperature in the oxidised and reduced protein (Fig1.4).<sup>12</sup>

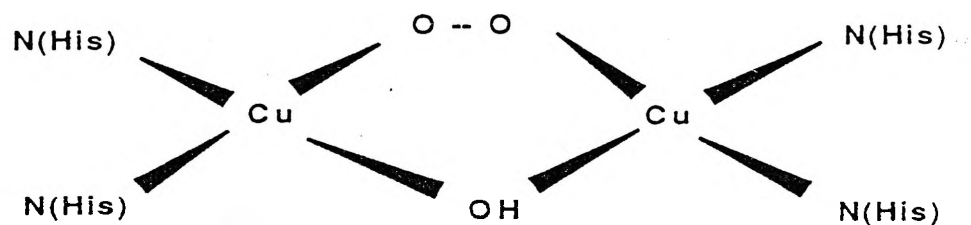


FIG 1.4:<sup>12</sup> Proposed Oxyhemocyanin Active Site

The copper atoms undergo a two electron oxidation/reduction cycle between two copper I atoms and two copper II atoms.

### 1.2.1. Hemocyanin

In nature, Hemocyanin is the most widely distributed oxygen carrying pigment after Hemoglobin.<sup>13</sup> It occurs mainly in the marine organisms of two phyla, although terrestrial forms are known.

The two phyla are Arthropoda e.g. funnel web spiders and Mollusca e.g. abalone and squid.

The oxygenated form was first isolated in 1847 by Harless<sup>14</sup> from *Helix pomatia* while the deoxy form was isolated in 1878 by Fredericq<sup>15</sup> from *Octopus vulgaris*.

The molecular weight of Hemocyanins varies widely depending on their source (Table 1.4)<sup>12,16,17</sup> and they are among the largest proteins known.<sup>18</sup> Despite this large variation, the size of the subunits in the two phyla vary little per copper ion with Arthropod subunits being approximately 36,700 and Mollusca 25,100.

The main function of hemocyanin is the uptake and transportation of dioxygen in both the Mollusca and Arthropoda. It has also been reported that Molluscan Hemocyanin catalyses the decomposition of hydrogen peroxide to water and dioxygen.<sup>19</sup>

Species	%Cu	M/Cu	M.W. (*10 <sup>6</sup> )
<u>Arthropoda:</u>			
Merostomata			3.3
<i>Limulus Polyphemus</i>	0.170	37,400	
Arachnida			---
<i>Androctonus australis</i>	0.180	35,300	
Crustacea			0.40-0.95
<i>Jasus lalandii</i>	0.176	36,100	
<i>Palinurus vulgaris</i>	0.170	37,400	
<i>Homarus americanus</i>	0.175	36,300	
<i>H. vulgaris</i>	0.169	37,600	
<i>Eriphia spinifrons</i>	0.167	38,000	
<i>Cancer magister</i>	0.166	38,300	
<i>Carcinus maenas</i>	0.173	36,700	
<i>Maja sguinado</i>	0.182	<u>34,900</u>	
	Mean	<u>36,700</u>	
<u>Mollusca:</u>			
Gastropoda			6.8-8.7
<i>Busycon canaliculatum</i>	0.245	25,900	
<i>Helix promatia</i>	0.250	25,400	
<i>Murex trunculus</i>	0.257	24,700	
Cephalopoda			2.8-3.2
<i>Sepia officinalis</i>	0.256	24,800	
<i>Loligo pealei</i>	0.260	24,400	
<i>Octopus vulgaris</i>	0.250	25,400	
<i>Eledone moschata</i>	0.252	<u>25,200</u>	
	Mean	<u>25,100</u>	

TABLE 1.4:12,16,17 Molecular Weights of Hemocyanins

### 1.2.2. Tyrosinase

Tyrosinase, which was discovered over eighty years ago,<sup>20</sup> is a mixed function oxidase<sup>7</sup> which is found in plants, animals, fungal tissue and some bacteria.<sup>21</sup> Its role in plants is uncertain, while in insects it is involved in the sclerotization of the cuticle<sup>22</sup> and in higher animals it is involved in the synthesis of dihydroxyphenylalanine (DOPA) and its subsequent reaction to form melanin (Fig 1.5).<sup>23</sup>

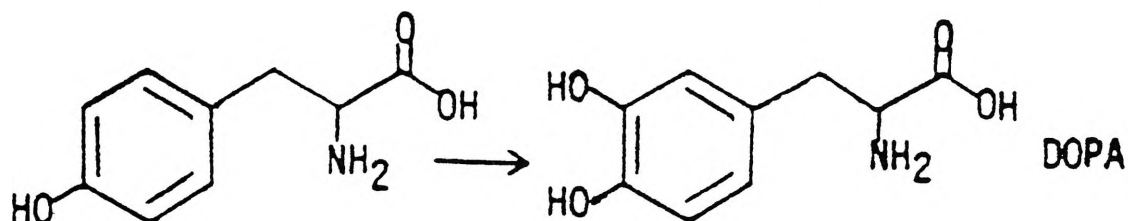


FIG 1.5:<sup>23</sup> Dopa Synthesis Catalysed by Tyrosinase

Tyrosinase is also involved in the oxidation of catechols to quinones (Fig1.6).<sup>12</sup>

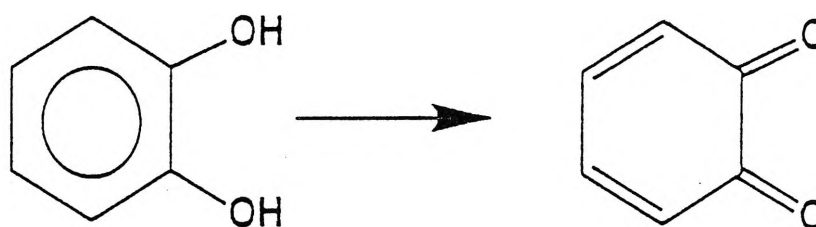


FIG 1.6:<sup>12</sup> Catechol Oxidation Catalysed by Tyrosinase

Tyrosinase varies in both the size of its subunits (30-70,000 MW) and the number of subunits, with mammalian, prokaryotic and fungal forms being monomeric, while the others are dimeric, tetrameric or pentameric (Table 1.5).<sup>12,16,17</sup>

*Neurospora* and other mushroom Tyrosinases have been well studied, with four histidine residues being implicated<sup>24</sup> per copper atom, as copper ligands in the oxidised protein. Spectroscopic and magnetic studies indicate the presence of an endogenous bridge<sup>25</sup> and Resonance Raman spectroscopy of the oxygenated Tyrosinase indicates the presence of a cis-μ-1,2-peroxo bridge ( $\nu_{O_2} = \sim 750\text{cm}^{-1}$ ).<sup>8</sup>

Tyrosinase has been found to undergo a single two electron oxidation at +0.36V.<sup>21</sup> Hemocyanin probably has a similar value, bearing in mind the closeness of other properties between these two proteins.

The close similarities between the chemical, EPR, and spectral properties of Hemocyanin and Tyrosinase imply that they have a similar active site consisting of a Type III copper centre.<sup>8</sup>

NAME	MW	SUBUNIT MW	NUMBER OF SUBUNITS	% Cu	Cu/ mol SUBUNIT
Prokaryotes					
<i>Vibrio tyrosinaticus</i>	29,000	41,000	1	0.21	2
Fungi					
<i>Neurospora crassa</i>	35-120,000		1-4	0.195	2
	46-170,000	46,000	1-4		
<i>Agaricus bisporus</i>	128,000			0.20	
	32-118,000	26,000		0.15-0.22	
	61,000			0.20	
Higher Plants					
Potato	36-300,000	36,000		0.17	
Tea Catechol Oxidase	144,000			0.32	
Spinach Catechol Oxidase		42,000	1-4		
Insects					
Housefly	340,000	61,000	5		
Silkworm Proenz	36-72,000	40,000		0.15	
Amphibia					
Frog Proenz (1)	70-90,000	33,000			
(2)	30-40,000	33,000			
Mammals					
Mouse (1)	66,000		1		
(2)	56,000				
Hamster (1)		70,000	1		
(2)		53,000			
Man		67,000	1		2

TABLE 1.5:<sup>12,16,17</sup> Molecular Weights of Tyrosinase

1.2.3. Blue Oxidases

The most widely studied oxidases are Laccases from *Rhus vernicifera* and *Polyporus verisicolor*. Ceruloplasmin and Ascorbate Oxidase.<sup>26</sup> Their molecular weights and optical properties are listed in Table 1.6.<sup>12,16,17</sup>

NAME	SOURCE	MW	OPTICAL PROPS M <sup>-1</sup> cm <sup>-1</sup> / nm	OXID/RED POT mV/ pH
ABSCORBATE OXIDASE				
	Cucumber, Squash	140,000	3,300/ 610 per blue Cu	---
CERULOPLASMIN				
	Human Serum	150,000	4,400/ 610 per blue Cu	490,580/ 5.5
LACCASE				
	<i>Polyporus verisicolor</i>	64,400	4,900/ 610	785/ 5.5
	<i>Rhus vernicifera</i>	110,000	5,700/ 615	395/ 7.5

TABLE 1.6:<sup>12,16,17</sup> Molecular Weights, Redox and Optical Properties of Blue Oxidases

Laccase from *Polyporus*<sup>2</sup> contains four copper atoms; one Type I, one Type II and a Type III binuclear pair. Their proposed structures are shown in Fig 1.7.<sup>27</sup> The same structure is proposed for *Rhus vernicifera* with the Type I centre giving the Laccase its characteristic blue colour ( $\lambda_{\max} = 615 \text{ nm}$ ). Little is known about the Type II site although it is believed to be tetragonal with a bound water molecule and three or four nitrogen ligands. The Type III site is thought to be where the oxygen interacts with the protein.<sup>27</sup>

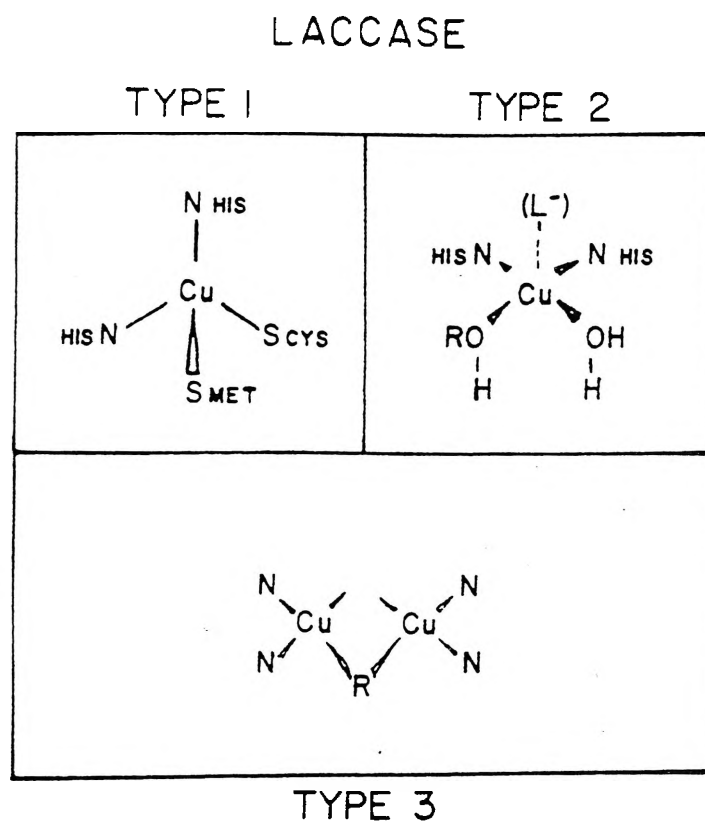


**FIG 1.7:**<sup>27</sup> Copper Centres of Laccase

The Type II/III copper site may be similar to the trinuclear copper site in Ascorbate Oxidase,<sup>55</sup> rather than that suggested in the above diagram.

The function of Laccases is the oxidative catalysis, by dioxygen, of diphenols and aromatic diamines, in which the dioxygen undergoes a four electron reduction to water (Fig 1.8).<sup>2</sup> The proposed reaction pathway is shown in Fig 1.9.<sup>2</sup> The pathway involves two one electron transfers from the substrate to the protein followed by a two electron transfer. Dioxygen then reoxidises the protein.



The Type I centre has been found to reduce at +0.42V, the Type II copper centre at +0.39V with each centre undergoing a single one electron reduction. The Type III binuclear copper centre undergoes a single two electron reduction at +0.46V.<sup>162</sup>

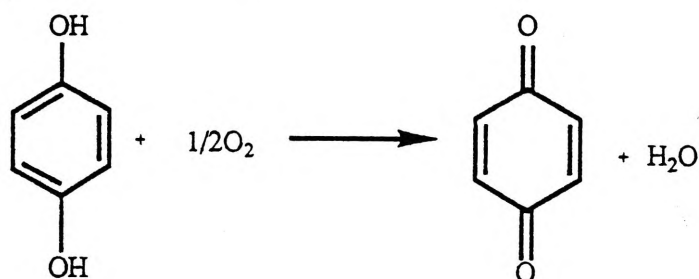


FIG 1.8:<sup>2</sup> Reduction of Oxygen by Laccase

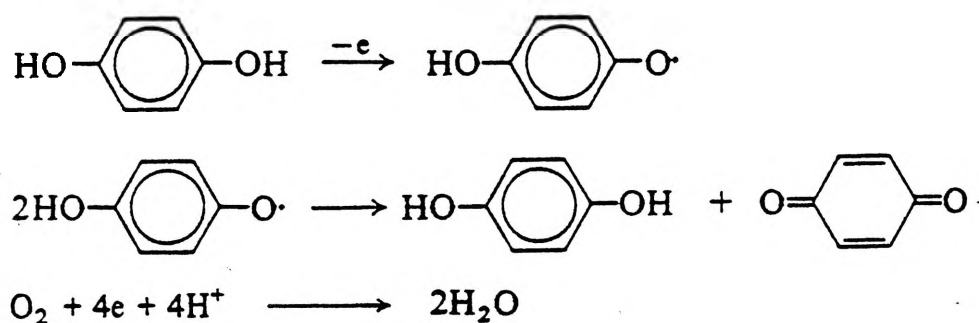


FIG 1.9:<sup>2</sup> Laccase: Proposed Reaction Pathway

Ascorbate Oxidase catalyses the oxidation of ascorbic acid (Fig 1.10).<sup>2</sup> It is found in a wide range of plants and some bacteria. In the case of *Curcubita pepo* (squash), the protein has a molecular weight of 140,000 which is made up of two subunits containing four copper atoms each. The protein has been found to contain two Type I, two Type II and two Type III binuclear copper centres. Each subunit has two chains of molecular weights 38,000 and 28,000. The reaction mechanism is believed to be similar to that of Laccases.<sup>2</sup>

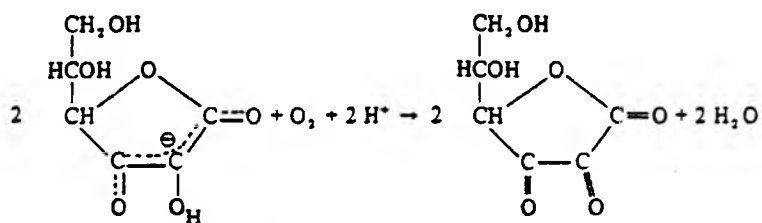


FIG 1.10:2 Oxidation of Ascorbic Acid

Ceruloplasmin<sup>3</sup> is the major copper containing protein of mammalian blood, accounting for ninety-eight per cent of all the copper in mammals. It catalyses the reoxidation of iron II to iron III for binding to Transferrin and also a four electron reduction of dioxygen to water.<sup>3</sup> It also functions as a copper storage protein.<sup>1</sup> The protein contains eight copper atoms, two Type I, two Type II and two binuclear Type III centres (Fig 1.11).<sup>2</sup> Its molecular weight is 150,000 and it probably consists of two subunits.

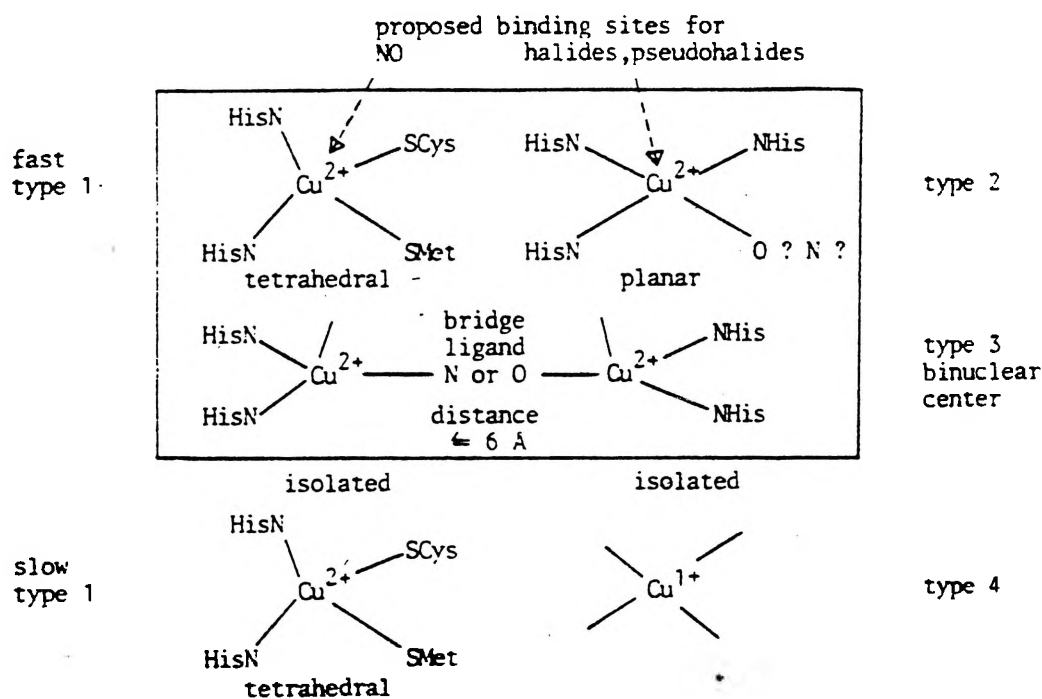


FIG 1.11:2 Ceruloplasmin: Types of Copper Centres

In both Laccases and Ceruloplasmin histidine is believed to be a ligand at both the Type I and Type II sites.<sup>3</sup>

#### 1.2.4. Studies of the Type III Active Site

The structure and properties of the Type III active site have been elucidated by a number of techniques which can be classified into two groups:-

##### 1. Chemical Techniques<sup>19,25,28-33</sup>

This involves the modification of the active site by;

- a) removal of one or more of the copper atoms.<sup>28a,b,30</sup>
- b) replacement of copper by other metal ions e.g. cobalt.<sup>29a-c</sup>
- c) changing the oxidation state of the metal ion.<sup>19,25,28</sup>
- d) substitution of different bridging groups e.g.  $\text{N}_3^-$  or CO for  $\text{O}_2^{2-}$ .<sup>29d,31-33</sup>

##### 11. Instrumental Techniques

They are used on both the unmodified and modified protein;

- a) UV-Vis Spectroscopy.<sup>34-37</sup>
- b) Electron Paramagnetic Resonance (EPR).<sup>34,35,38,39</sup>
- c) Resonance Raman Spectroscopy.<sup>40-42</sup>
- d) Magnetism.<sup>43</sup>
- e) X-Ray Crystallography.<sup>44-45</sup>
- f) Extended X-Ray Absorption Fine Structure (EXAFS).<sup>46-47</sup>
- g) Amino Acid Sequencing.<sup>48-49</sup>
- h) Electron Microscopy.<sup>50-53</sup>

The crystal structure of *Panulirus interruptus* Deoxyhemocyanin was recently resolved down to 3.2Å (Figs 1.12 and 1.13).<sup>44</sup> This structure showed that most of the ideas based on EXAFS data were correct. The two copper I atoms are separated by a distance of 3.8Å, with each copper atom coordinated to three histidine residues. From the crystal structure and amino acid sequences<sup>49</sup> it is clear that two of these histidines are separated by three amino acid residues, while the third is separated by another thirty seven amino acid residues. This arrangement allows the flexibility in the structure for the Cu I/Cu II oxidation/reduction cycle to occur. The question of the presence or absence of a bridging endogenous group could not be answered as its presence, based on spectral data, has only been predicted in the oxygenated form.

A number of groups have carried out studies on Hemocyanin and Tyrosinase using Extended X-Ray Absorption Fine Structure (EXAFS).<sup>46-47</sup> The results indicate that each copper atom is bound to two or three histidine nitrogen atoms and that the copper atoms are separated by 3.55Å in the oxygenated form. These copper atoms are in an approximately square planar or square pyramidal environment.<sup>47</sup> Two oxygen bridges are also indicated in Oxyhemocyanin. EXAFS for Deoxyhemocyanin<sup>47c</sup> indicates the presence of at least two histidine nitrogens with each copper separated by either 4.0Å or 6.0Å, with the lower value believed to be more accurate. No Cu-oxygen bonds are indicated in Deoxyhemocyanin.<sup>47c</sup>

Dioxygen has been proposed to bind exogenously as peroxide ( $O_2^{2-}$ ) in oxyhemocyanin. This is based on Resonance Raman studies conducted by Kirchner and Loew.<sup>41</sup>

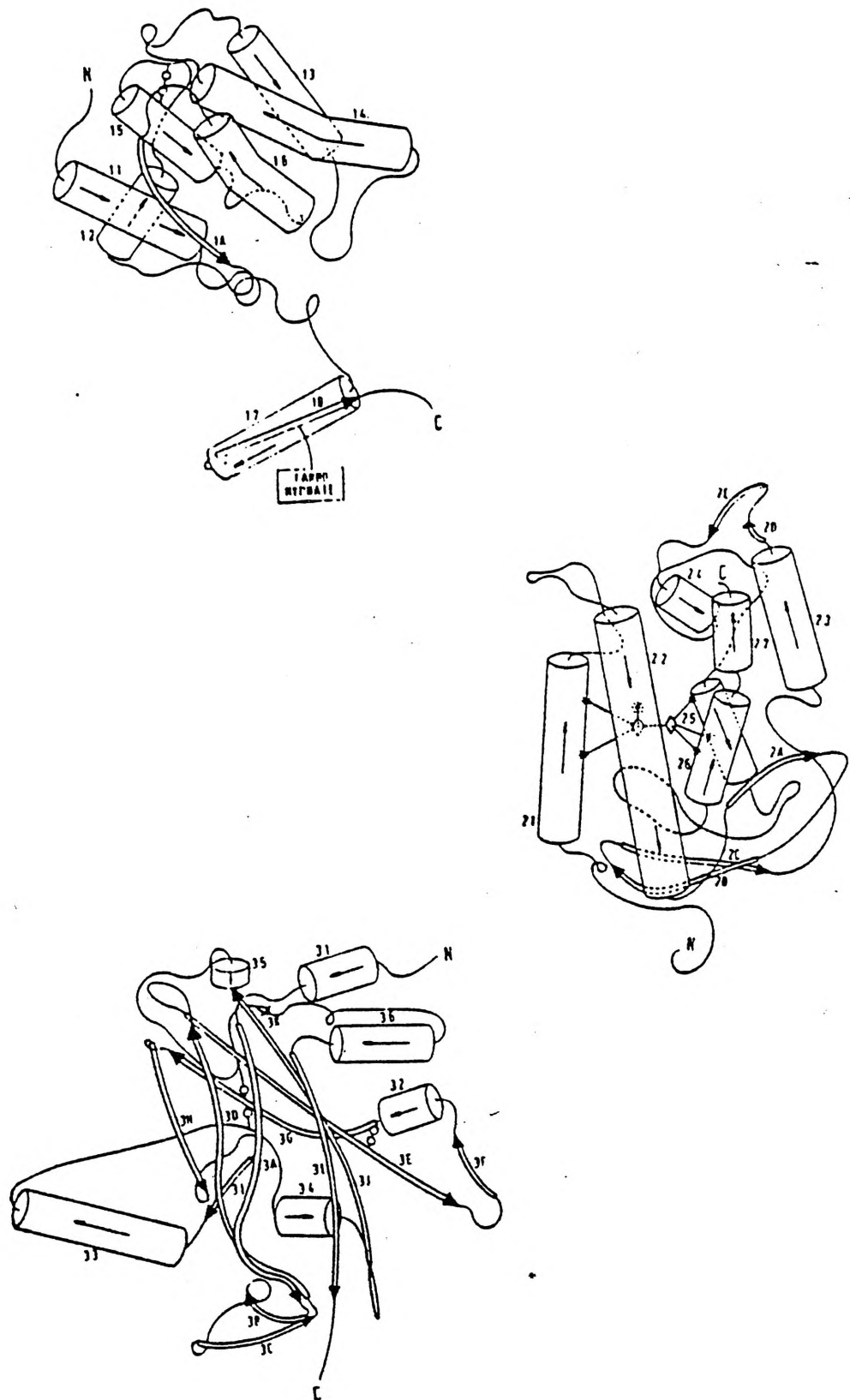


FIG 1.12:44 Deoxyhemocyanin Structure

Solomon<sup>28</sup> has proposed the presence of an endogenous oxygen bridge based on spectral and magnetic properties of Oxyhemocyanin. The nature of this bridge is still uncertain but, if present, is almost certainly a hydroxide ion.

This endogenous bridge is proposed to act as the superexchange pathway between the copper(II) atoms which gives rise to the antiferromagnetism observed for Oxyhemocyanin and Oxytyrosinase. Two possible methods of oxygen binding in Oxyhemocyanin are shown in Fig 1.13.<sup>54</sup>

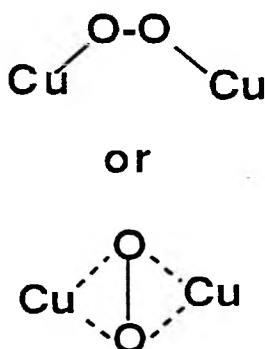
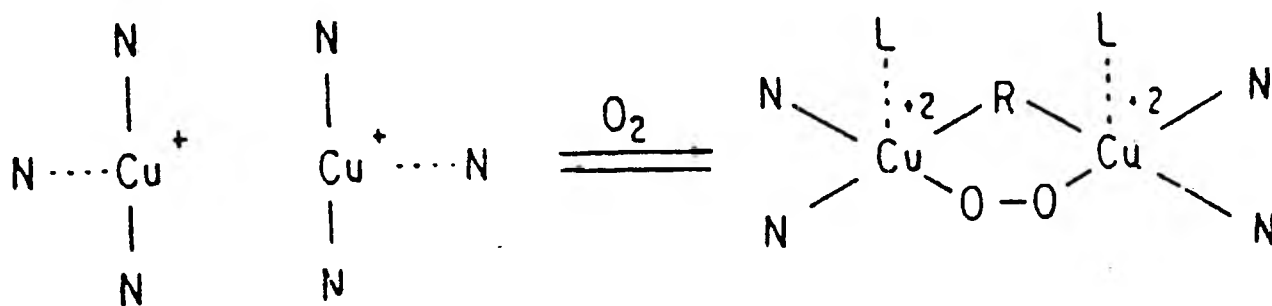


FIG 1.13:<sup>54</sup> Proposed Method of Oxygen Binding in Oxyhemocyanin Structure

Oxytyrosinase is believed to have a water molecule attached to each copper which assists in the oxidation of catechols and phenols.<sup>19</sup>

The proposed method of Hemocyanin action is shown in Fig 1.14, while that of Tyrosinase is shown in Figs 1.15-1.16.



N = Histidine

L = Histidine (?)

R = Tyrosine ("O") or Hydroxide

Diamagnetic

FIG 1.14:12 Hemocyanin

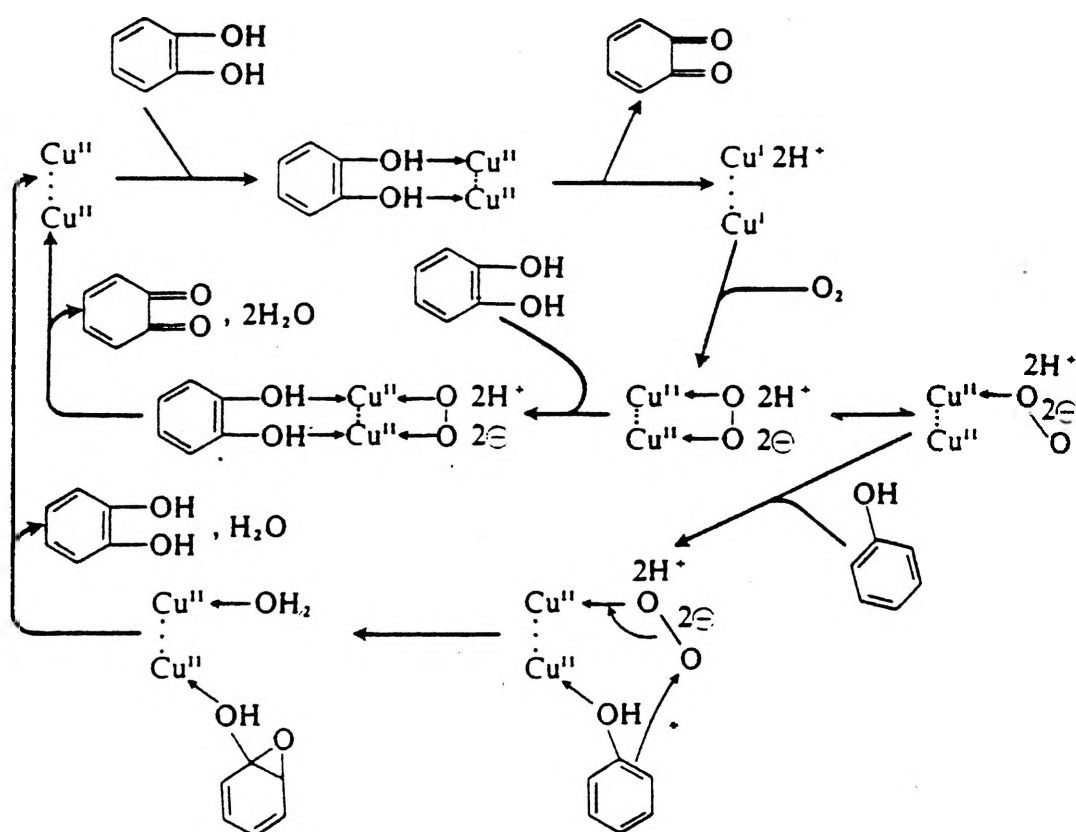
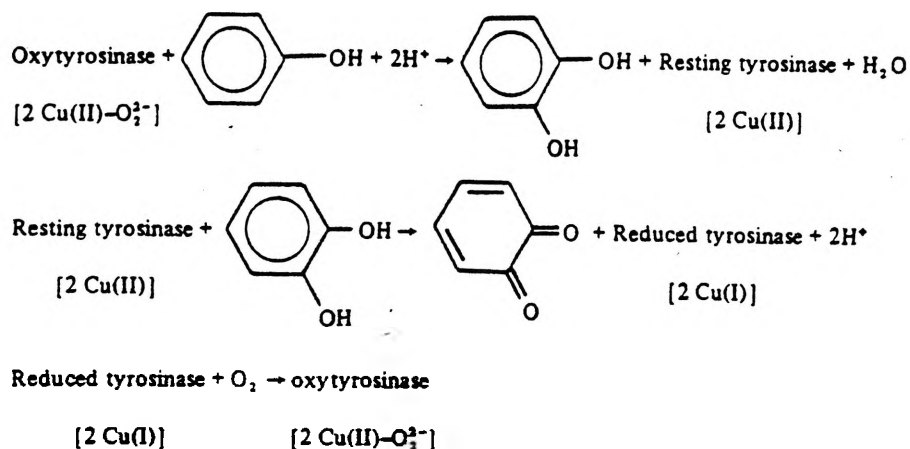


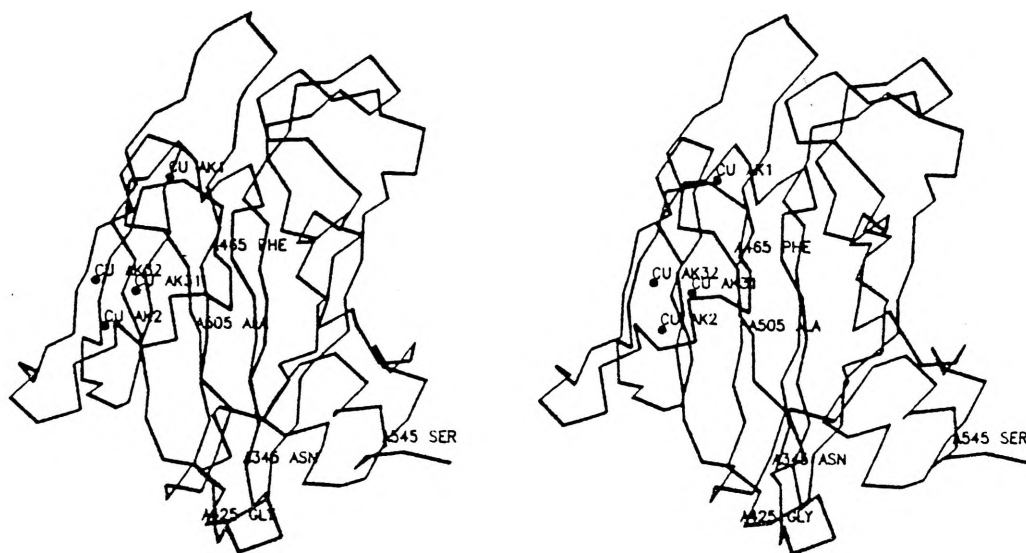
FIG 1.15:2 Tyrosinase: Proposed Reaction Pathway

FIG 1.16:<sup>24</sup> Tyrosinase

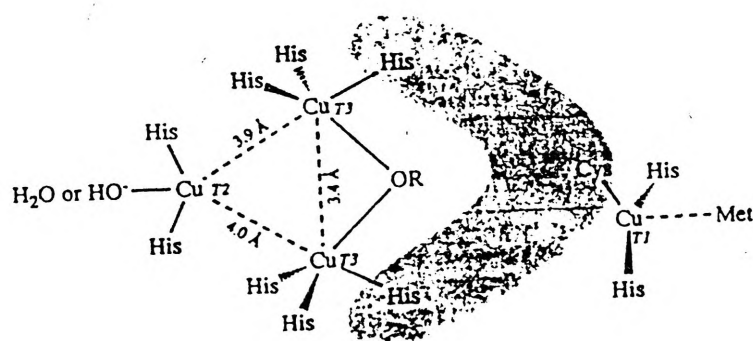
The crystal structure of Ascorbate Oxidase isolated from zucchini has recently been solved down to 2.5Å.<sup>55</sup> Two crystals were studied with one being a dimer of molecular weight 140,000 and the other a tetramer of molecular weight 280,000 with the dimer consisting of two subunits and a total of eight copper atoms. Each subunit contains four copper atoms bound as a mononuclear and a trinuclear species (Fig 1.17(a)). The mononuclear species represents the Type I copper(II) with the copper bound to two histidines, a cysteine and a methionine ligand in a tetrahedral configuration. The trinuclear species has eight histidine ligands and consists of a pair of copper atoms bound to six histidines in a trigonal prism and represent the Type III copper. The other copper is bound to two histidine ligands. Its third coordination site (Fig 1.17(b)) is formed by the Type III copper pair and its fourth ligand maybe either hydroxide or water. This copper is probably the Type II copper. It is proposed that the trinuclear cluster is the dioxygen binding and electron storage site. The Type III copper pair are ~3.4Å apart and ~3.9 to 4.0Å from the Type II copper and all three copper atoms are more than 12Å from the Type I copper.



Solomon et al.<sup>56</sup> have proposed that Laccase binds oxygen as  $\mu$ -1,1-hydroperoxide during the reduction of the Type II and Type III copper sites (Fig 1.18). This binding is proposed based on spectrochemical examination of the oxygenated and deoxygenated forms of Laccase and the ascorbate oxidase structure.



(a)



(b)

**Fig 1.17:<sup>55</sup> Stereo Drawing of Ascorbate Oxidase Subunit Structure**

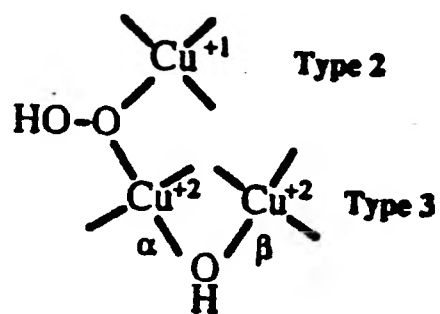


FIG 1.18;<sup>56</sup> Proposed Oxygen Binding in Reduced Laccase

### 1.3. Model Compounds

Due to the large size of metalloproteins (M.W. 10,000 to 200,000) compared to the number of metal ions in metalloproteins, (the metal accounts for only 0.2 to 0.3% of the total mass), model compounds are often used to study the active site of the metalloproteins.

These compounds are designed to mimic some or all of the structural and chemical properties of the active sites of metallo-proteins.

The use of model compounds can be organized into two parts;<sup>57</sup>

#### 1. Concepts:

a) attempt to mimic the following features:

1) spectral features.

11) structural features.

111) reactivity.

b) elucidate the basic structural features contributing to the characteristics of the protein.

c) determine the effect upon the active site, as represented by the model, of changes in substituents.

#### 2. Approach:

a) design of the ligand system:

1) appropriate ligand donors.

11) set coordination number.

111) mono or polynucleating ligands.

1V) bridging groups.

b) systematically vary pertinent features, e.g.

1) ligand donor types.

11) coordination geometry, e.g.

a) metal-metal distance.

b) chelate ring size in polydentate ligands.

111) bridging groups.

One of the major problems in studying the Type III copper active site is the fact that the protein backbone does not retain its form upon removal of the copper atoms, unlike Hemoglobin. This means that the specific details of the protein chain around the active site is difficult to study.<sup>21,40</sup>

To overcome this a versatile model system is required. This system should:-

1) be easy to synthesise .

11) systematic modification should be possible.

111) analysis of how the modification relates to the observed protein characteristics, should be possible.

#### 1.4. Requirements for a Type III Active Site Model

- I) A good model of the oxygenated Type III site should contain two copper atoms bridged by an endogenous oxygen bridge at a metal-metal distance of approximately 3.6Å.
- II) There should be room for an exogenous bridge (preferably the peroxo group, O<sub>2</sub><sup>2-</sup>).
- III) The ligand should contain two or three nitrogen atoms (preferably histidine or imidazole) per copper atom, which can coordinate to the copper atoms in a square planar or square pyramidal geometry.
- IV) The reduced or deoxygenated Type III site should retain two or three nitrogen donors per copper. The copper atoms should be three coordinate and stable in the copper I state. These copper atoms should be separated by approximately 3.8Å.
- V) This compound should be able to reversibly bind dioxygen in a ratio of one dioxygen molecule per two copper atoms.
- VI) The copper atoms should be able to undergo fully reversible oxidation/reduction with no breakdown in structure.

Model compounds are rarely able to meet all these requirements. The best models are those which satisfy the largest number of these requirements.

### 1.5 Model Compounds of Type III Copper Proteins

The research work published on model compounds of Type III copper proteins has concentrated on the following:-

- I) the synthesis of binuclear copper(II) complexes with the copper atoms bridged by an endogenous oxygen atom.
- II) the synthesis of stable binuclear copper(I) complexes and their reaction with dioxygen.
- III) the nature of the exogenous bridge in binuclear copper(II) complexes.
- IV) investigation of reactions between binuclear copper(II) complexes and phenols and catechols.
- V) the electrochemistry of binuclear copper(II)/copper(I) complexes.

The types of model compounds of Type III copper proteins investigated so far can be broadly classified into compounds containing:-

- I) no endogenous bridge.
- II) an endogenous phenolic oxygen bridge.
- III) an endogenous alcohol oxygen bridge.

### 1.5.1. Compounds with No Endogenous Bridge

Three research groups who have reported binuclear copper(II) model complexes containing no endogenous bridge are Karlin et al.,<sup>58-60,62-65</sup> Thompson<sup>66</sup> and Kitajima et al.<sup>67</sup>

The first ligands synthesised by Karlin et al. are shown in Fig 1.19.<sup>56-60</sup> The binuclear copper(I) complexes of these ligands (Fig 1.20) reversibly bind dioxygen (Fig 1.21) (at  $-80^{\circ}\text{C}$ ) and carbon monoxide, and irreversibly bind the methoxide ion.<sup>58</sup>

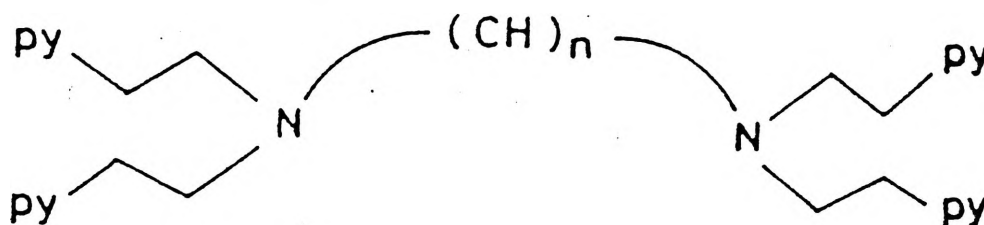


Fig 1.19:<sup>58b</sup> Karlin et al.'s Complex Ligand NnPy<sub>2</sub>

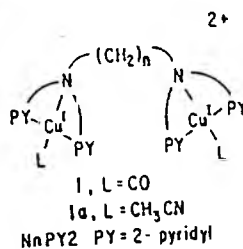


Fig 1.20:<sup>59a</sup> Binuclear Copper (I) Complex of NnPy<sub>2</sub>

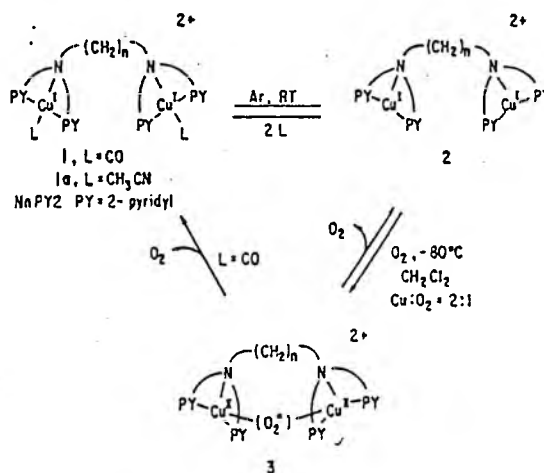


Fig 1.21:<sup>59a</sup> Reaction of Copper (I) Complex with Oxygen and Carbon Monoxide

The reversible binding of dioxygen involves the cycling of the copper atoms between the copper(I) and copper(II) oxidation states. Each cycle results in a ten percent decomposition of the complex. Manometry results indicate a 2:1 ratio of copper to dioxygen.

The dioxygen bridged complexes have similar visible spectra to that of oxyhemocyanin (Table 1.7).

TABLE 1.7\*: Cu(II)LO<sub>2</sub> complexes<sup>58b</sup>

L = OXYHc6, 61	N <sub>3</sub> Py <sub>2</sub>	N <sub>4</sub> Py <sub>2</sub>	N <sub>5</sub> Py <sub>2</sub>
345(20,000)	365(15,000)	360(16,700)	360(21,400)
425(sh, 400)	490(5,300)	458(5,300)	423(3,600)
570(1,000)	600sh(1,200)	550sh(1,200)	520(1,200)

\* = values are in nm(M<sup>-1</sup>cm<sup>-1</sup>).

These complexes are EPR silent.

The available data indicates that the exogenous dioxygen bridge occurs in the form of the peroxo (O<sub>2</sub><sup>2-</sup>) group, the same as proposed for oxyhemocyanin. A possible method of binding has been proposed (Fig 1.22).<sup>59b</sup>

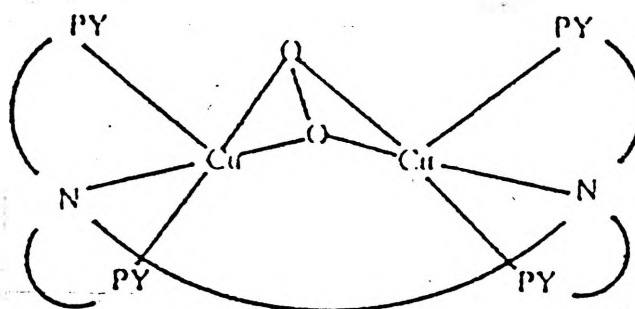
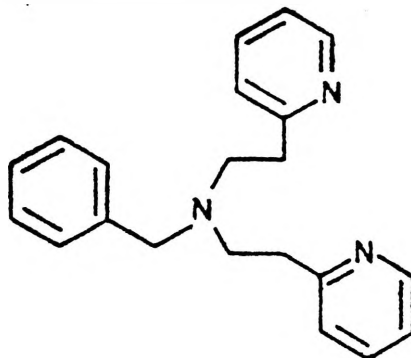


Fig 1.22:<sup>59b</sup> Model of Dioxygen Binding

Based on the above data Karlin et al. proposed that hemocyanin may also have no endogenous bridge in the oxygenated form.



Karlin's group have also used a mononucleating ligand (Fig1.23).<sup>62-65</sup>



**Bpy2**

Fig 1.23:<sup>64</sup> Karlin et al.'s Mononucleating Ligand

The copper(I) complex is able to reversibly bind dioxygen as the peroxo ( $O_2^{2-}$ ) group, carbon monoxide and triphenylphosphine at low temperature. A low temperature crystal structure shows that the dioxygen bridged complex has the following structure (Fig1.24).<sup>65</sup>

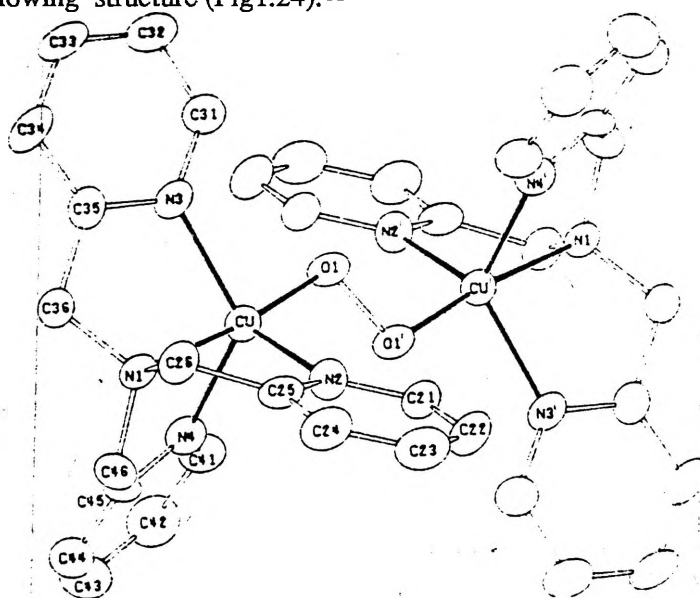


Fig1.24:<sup>65</sup> Binuclear Copper (II)  $L_2O_2$  complex

As in Oxyhemocyanin this complex is EPR silent. The copper copper distance is much larger ( $4.36\text{\AA}$  as against  $3.6\text{\AA}$ )

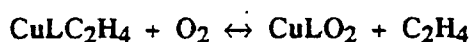
This binuclear copper(II) complex has quite different spectral properties compared to that of oxyhemocyanin (Table 1.8)

Table 1.8: Comparison of the Binucleating Complex and Oxyhemocyanin

OxyHc <sup>6,61</sup>	Cu <sub>2</sub> L <sub>2</sub> O <sub>2</sub> <sup>65</sup>
345(20,000M <sup>-1</sup> cm <sup>-1</sup> )nm	525(11,500M <sup>-1</sup> cm <sup>-1</sup> )nm
425(sh,400M <sup>-1</sup> cm <sup>-1</sup> )nm	590(sh,7600M <sup>-1</sup> cm <sup>-1</sup> )nm
570(1000M <sup>-1</sup> cm <sup>-1</sup> )nm	1035(160M <sup>-1</sup> cm <sup>-1</sup> )nm.

Due to the trigonal bipyramidal geometry around each copper atom the UV-Vis spectra of this complex differs from that of oxyhemocyanin. Also the  $\mu$ -1,2- O<sub>2</sub><sup>2-</sup> bridging is of trans configuration in the complex while the oxyhemocyanin is believed to be cis configuration or  $\mu$ -1,2- O<sub>2</sub><sup>2-</sup>.

Thompson<sup>66</sup> has synthesised copper(II)-dioxygen complexes using the ligands shown in Fig1.25. In the case of the ligand HB(3,5-Me(Pz))<sub>3</sub>,<sup>66a</sup> the ethylene adduct of the copper(I) complex reacts with dioxygen reversibly at -40°C in solution (Scheme 1).



Scheme 1: Reversible Dioxygen Uptake

The oxygen adduct is diamagnetic. The coordinated dioxygen stretch in the O<sup>16</sup> bridged complex cannot be identified because of its  $\nu_{\text{O-O}}$  being obscured by the spectra of the trispyrazoyl borate ligand. However use of O<sup>18</sup> results in an IR peak at 1015 cm<sup>-1</sup> for the complex. The presence and position of this peak leads to the proposal that the dioxygen occurs as the superoxide (O<sub>2</sub><sup>-</sup>) ion in this complex.

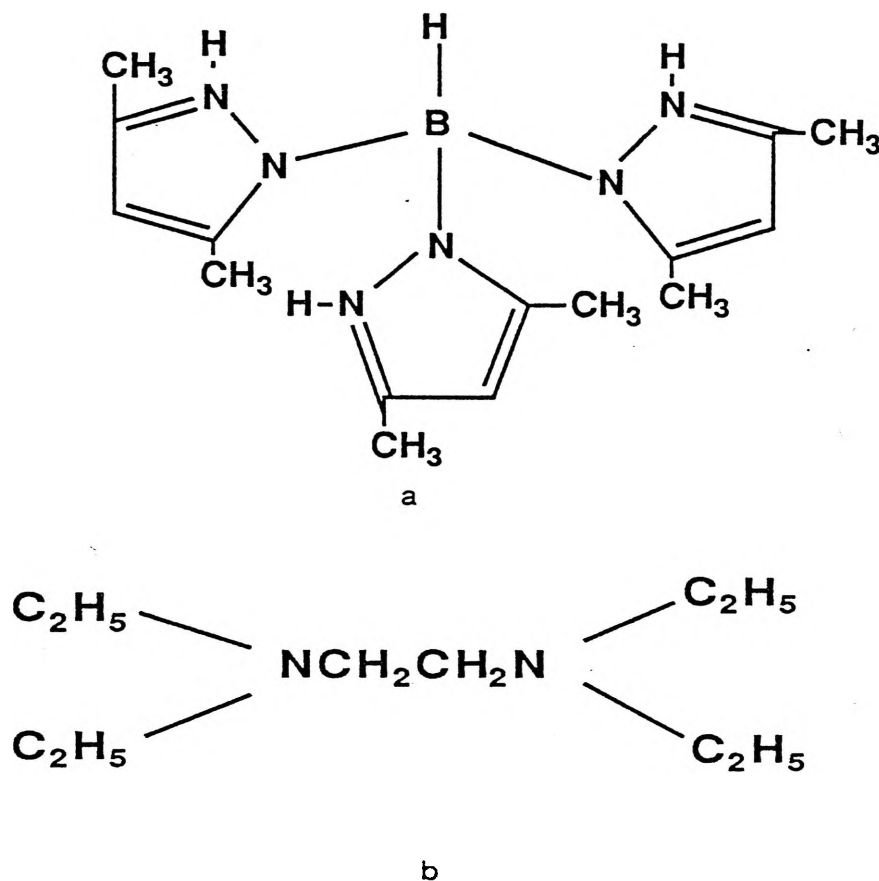


Fig 1.25:<sup>66</sup> Thompson's Ligands a) HB(3,5-Me<sub>2</sub>Pz)<sub>3</sub>, b) TEEN

The copper(I) complex of TEEN<sup>66b</sup> reacts with dioxygen reversibly, at -40°C, in solution to form a dioxygen bridged copper(II) complex Cu<sub>2</sub>L<sub>2</sub>O<sub>2</sub>·H<sub>2</sub>O. The proposed structure of this complex, based on the spectral data, is shown in Fig1.26.

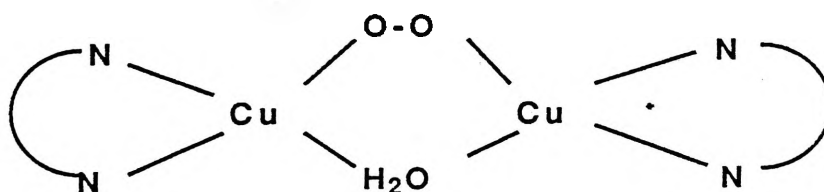


Fig 1.26:<sup>66b</sup> Proposed Cu<sub>2</sub>L<sub>2</sub>O<sub>2</sub> Complex

This complex is EPR silent at  $-160^{\circ}\text{C}$  as is oxyhemocyanin. The infra-red spectrum contains a band at  $825\text{ cm}^{-1}$  indicating that the dioxygen is bound as the peroxide ( $\text{O}_2^{2-}$ ) ion.

Kitajima et al.<sup>67</sup> have recently reported the synthesis of two peroxo bridged binuclear copper (II) complexes. The ligand used is an i-propyl derivative of Thompson et al's trispyrazoyl borate ligand (Fig 1.27).

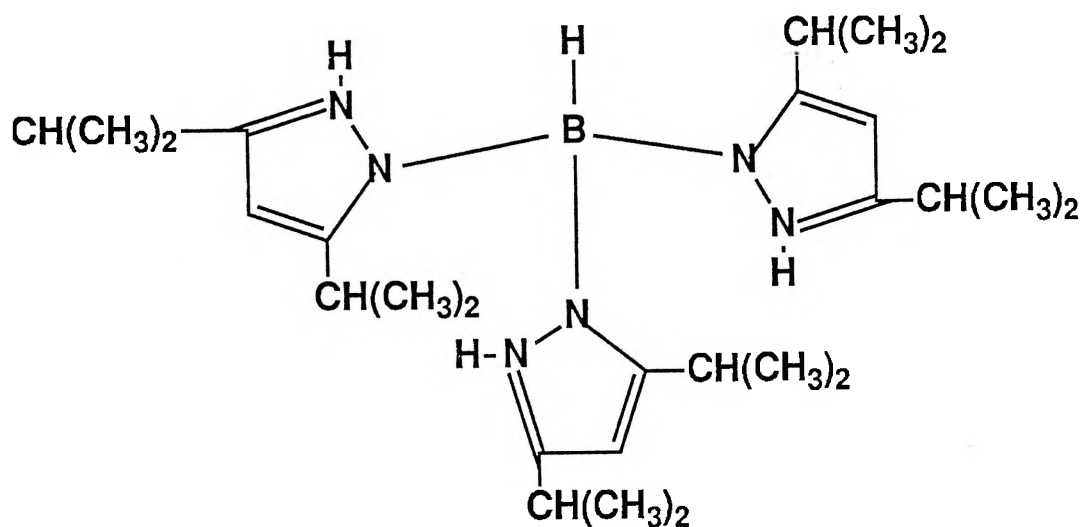


Fig 1.27:<sup>67</sup> Kitajima et al.'s Ligand

The crystal structure of the complex has been solved (Fig 1.28)<sup>67b</sup> and shows the oxygen to be bound as  $\mu$ -1,2-peroxo with the copper atoms being  $3.56\text{ \AA}$  apart, close to oxyhemocyanin ( $3.58$ - $3.66\text{ \AA}$ ) (Table 1.9) and oxytyrosinase ( $3.63\text{ \AA}$ ) with each copper atom having a square pyramidal  $\text{N}_3\text{O}_2$  coordination site.

Significantly the binuclear complex has no other bridge between the copper atoms other than the peroxo group.<sup>67a</sup> The  $\nu_{\text{O-O}}$  stretch is close to oxyhemocyanin (Table 1.9).<sup>67a</sup> The complexes are EPR silent and their UV-Vis spectra are similar to oxyhemocyanin (Table 1.9).<sup>67a</sup>

an  
abl  
n a  
cop

	(1)	(2)	(3)	(4)	(5)
Cu:O <sub>2</sub> 2:1	yes	yes	yes	yes	yes
Solid, stable O <sub>2</sub> adduct at room temp	no	no	no	yes	yes
Cu-Cu 3.6Å	no	no	no	no	yes
Heterocyclic N-ligands	yes	yes	yes	no	yes
X-ray structure	no	yes	no	no	yes
Reversible Cu(II)/Cu(I)	no	no	no	yes	no
UV-Vis similar to Hc	yes	no	no	no	yes
EPR silent	yes	yes	no	no	yes
Peroxo O <sub>2</sub> bridge	yes	yes	no	yes	yes

Table 1.10: Comparison of No Endogenous Bridge Models Against Oxyhemocyanin (Hc)

(1) Karlin NnPy<sub>2</sub><sup>56-60</sup>

(2) Karlin Cu<sub>2</sub>L<sub>2</sub>O<sub>2</sub>,<sup>62-65</sup> L = Mononucleating Ligand

(3) Thompson HB(3,5-Me<sub>2</sub>Pz)<sub>3</sub><sup>66a</sup>

(4) Thompson TEEN<sup>66b</sup>

(5) Kitajima<sup>67</sup>

### 1.5.2 Complexes with an Endogenous Phenolic Oxygen Bridge

A number of research groups have synthesised binuclear copper complexes using ligands containing an endogenous phenolic oxygen bridge. These groups include Sorrel et al.,<sup>75-81</sup> Karlin et al.,<sup>8,82-100</sup> Casella et al.<sup>101-104</sup> and Nishida et al.<sup>105</sup>

Robson et al.<sup>68-74</sup> pioneered the early research of binuclear copper(II) complexes utilizing the disubstituted methylphenol shown in Fig 1.29. Most of the later research groups used the same or similar endogenous bridging in their ligand systems.

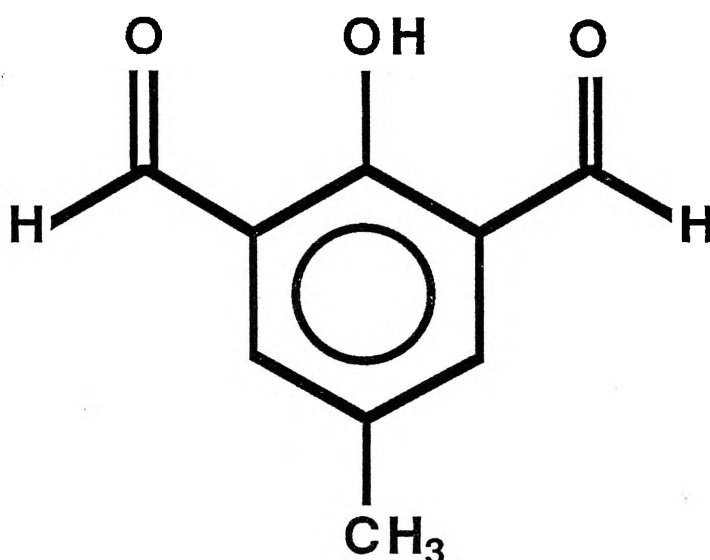
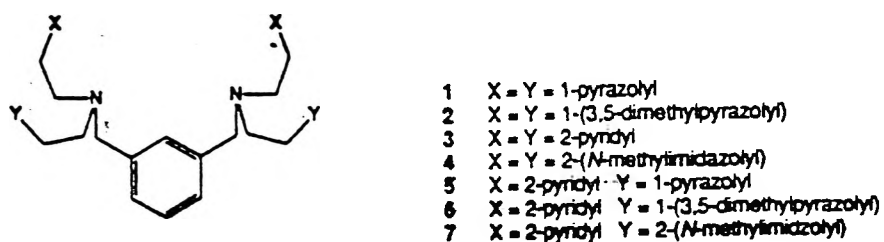
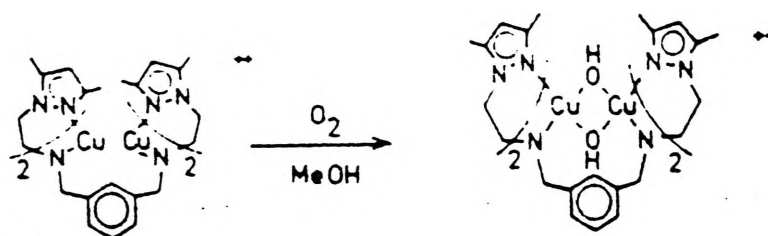


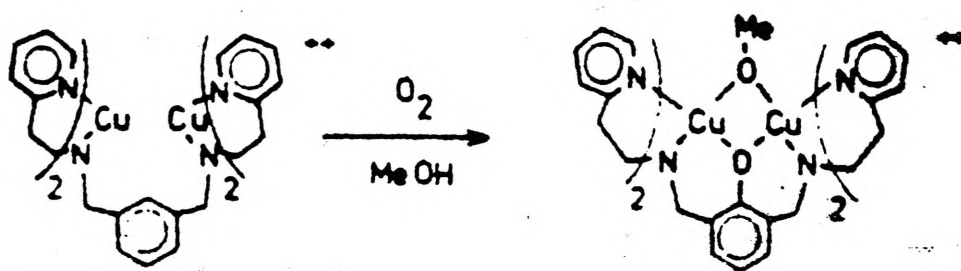
FIG 1.29:<sup>68</sup> Robson et al.'s Substituted Methylphenol Ligand

Sorrel et al.<sup>75-81</sup> have synthesised stable binuclear copper(I) complexes of the ligand shown in Fig1.30.

The ligand which possesses the pyrazole ligand donor groups undergoes a reaction with dioxygen to give a dihydroxide bridged copper(II) complex (Fig1.31).<sup>75</sup>

Fig 1.30:<sup>75</sup> Sorrel et al.'s Disubstituted Xylyl LigandFig 1.31:<sup>75</sup> Sorrel et al.'s Pyrazole Ligands Reaction with Dioxygen

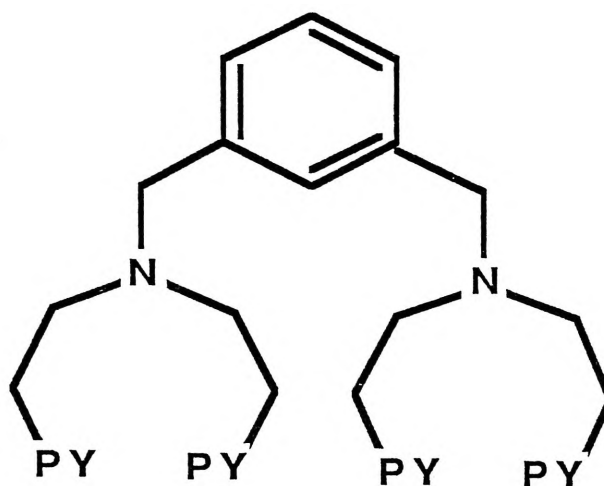
The ligand possessing pyridine ligand donor groups undergoes a reaction with dioxygen to give a phenoxide, methoxide dibridged copper(II) complex (Fig1.32).<sup>75</sup>

Fig 1.32:<sup>75</sup> Sorrel et al.'s Pyridine Ligands Reaction with Dioxygen

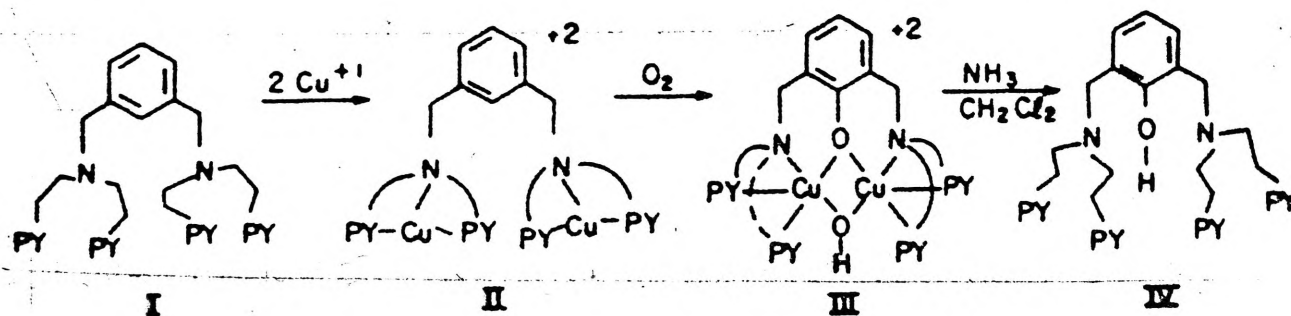


Karlin et al. have published a large number of papers<sup>8,82-100</sup> on model compounds of Type III copper (II) proteins, with a phenolic endogenous bridge. A summary of the majority of the reactions and complexes studied by Karlin et al. is presented in Fig 1.34.<sup>98</sup>

The ligand (a in Fig 1.33)<sup>86</sup> is able to form binuclear copper(I) complexes with no endogenous bridge present (II in Fig 1.33(b)).<sup>86</sup> The hydroxylation of the xyllyl group occurs through the reaction shown in (b) of Fig 1.33.



(a)



(b)

FIG 1.33:<sup>86</sup> Karlin et al.'s Xyllyl Binucleating Ligand

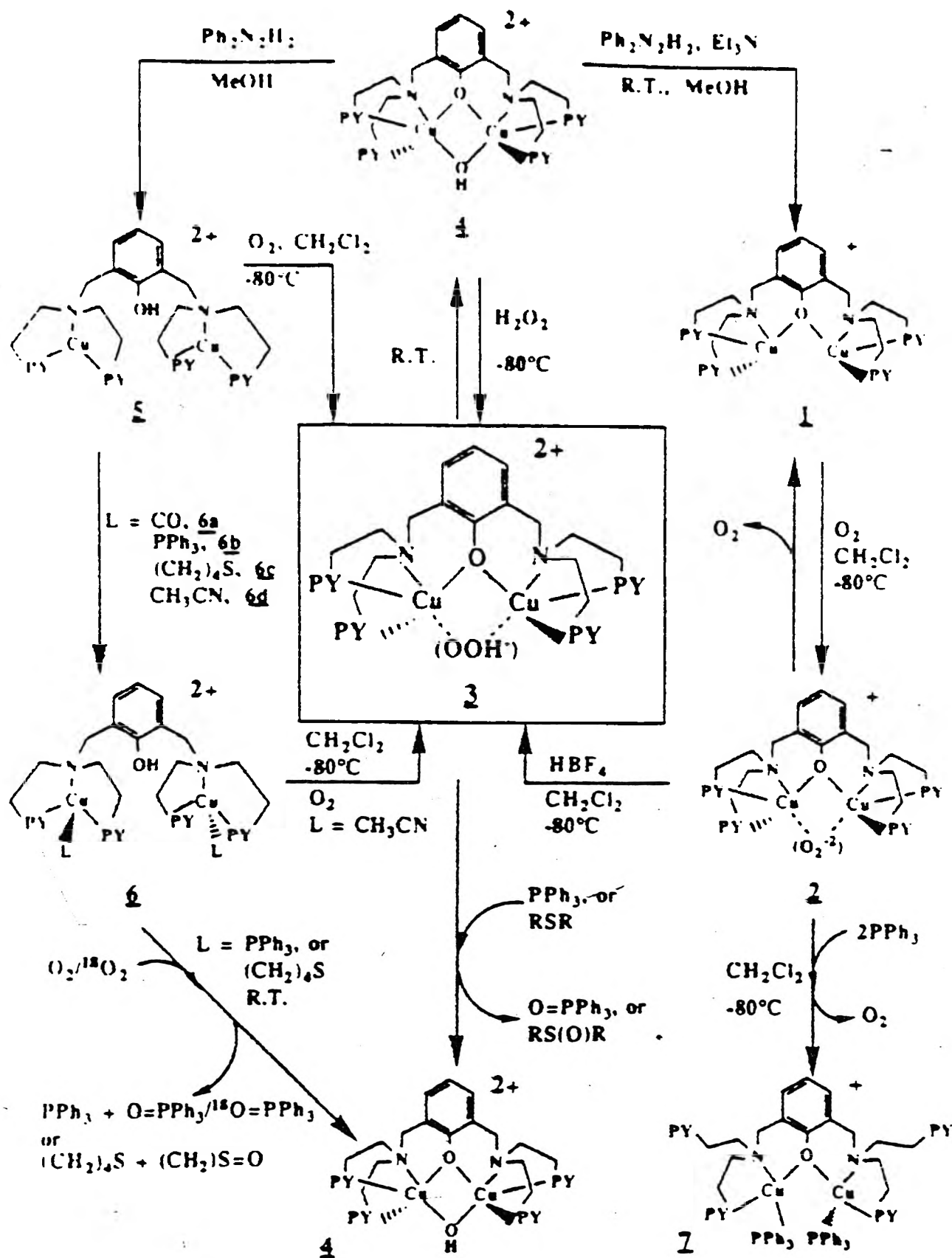


Fig 1.34:98 Reactions of Karlin et al's Substituted Xylyl Ligand

The binuclear copper (I) complex (II in Fig 1.33(b)) reacts with dioxygen to form a binuclear copper (II) complex possessing an endogenous phenoxide bridge and an exogenous hydroxide bridge (III in Fig 1.33(b)).<sup>87</sup> This reaction is similar to the hydroxylation reaction which is catalyzed by Tyrosinase.

The four coordinate binuclear copper (I) phenoxo bridged complex (1 in Fig 1.34)<sup>87,94</sup> has been isolated. The copper atoms are in a pyramidal environment and the complex exhibits a single absorption peak at 380 nm.

The phenoxide bridged binuclear copper (I) complex is able to reversibly bind dioxygen to form a dicopper (II)-peroxo bridged complex (2 in Fig 1.34).<sup>87,94</sup> This reaction occurs in solution at low temperature, the complex being unstable at room temperature.

The UV-Vis spectra for this dicopper(II)-peroxo complex at low temperature is significantly different to that of Hemocyanin (Table 1.11).

TABLE 1.11: UV-Vis Spectra of the Peroxo Complex vs Oxyhemocyanin\*

Oxy Hc <sup>6,61</sup>	Cu <sub>2</sub> LO <sub>2</sub> <sup>87,94</sup>
345 (20,000)	385 (3,000)
425 (sh,400)	505 (6,300)
570 (1,000)	610 (sh 2,500)

\* = Values are in nm(M<sup>-1</sup>cm<sup>-1</sup>)

The spectral differences are attributed to a different mode of peroxo binding (Fig 1.35).<sup>93,94</sup>

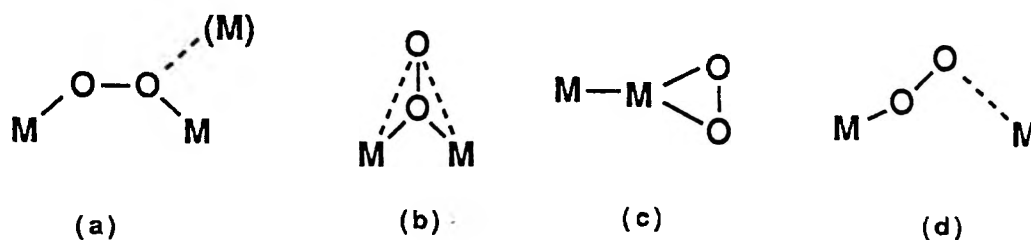


Fig 1.35:<sup>93,94</sup> Possible Modes of Peroxo Binding

EXAFS studies suggest that (d) is the most likely. The copper-copper distance is  $3.31\text{\AA}$ . The binding of dioxygen in this complex is quasi-reversible.

The hydroxo bridged complex (4 in Fig1.34)<sup>99</sup> is able to undergo a number of significant reactions.

1) The first reaction occurs with hydrogen peroxide at low temperature and results in the formation of a hydroperoxo bridged complex (3 in Fig1.34).<sup>99</sup> To date this complex has not been isolated in the solid state. Its formation is based on spectral evidence, its reactivity and also EXAFS studies on frozen solutions.<sup>98</sup> EXAFS data indicates a tetragonal geometry about each copper(II) atom and that the complex is similar in structure to the hydroxide bridged complex which has been isolated and been structurally solved by X-ray crystallography.<sup>86</sup> Therefore  $\mu$ -1,1-bridging is proposed for the complex.<sup>95,98</sup>

2) The second reaction occurs with  $\mu$ -m-ClC<sub>6</sub>H<sub>4</sub>-C(O)OOH at low temperatures in dichloromethane. The  $\mu$ -m-ClC<sub>6</sub>H<sub>4</sub>-C(O)OO bridged complex has been isolated and its crystal structure solved (Fig 1.36).<sup>100</sup> The complex is very similar in structure to the hydroxo bridged complex and the proposed hydroperoxo bridged complex.

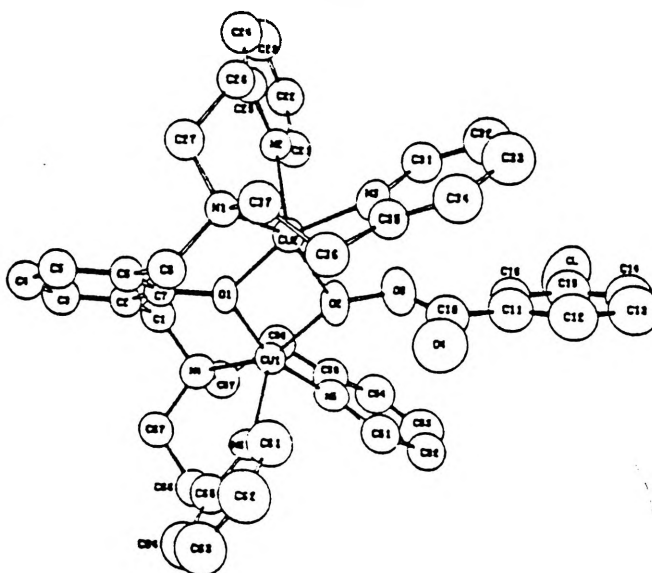


FIG 1.36:<sup>99</sup> Crystal Structure of the Acylperoxy Bridged Complex

Each copper(II) atom has distorted square pyramidal geometry. The acyl peroxy group is  $\mu$ -1,1-bridged.

The UV-Vis spectrum of the acylperoxy bridged complex is very similar to that of hydroperoxide bridged complex, as is the spectra of the hydroxo bridged complex. This data supports the proposition of  $\mu$ -1,1-bridging of the hydroperoxy group in compound 3 of Fig 1.34.

Casella et al.<sup>101-104</sup> have reported the synthesis of binuclear copper (I) complexes similar to Karlin et al.'s xylyl ligand (1 of Fig 1.37). These copper (I) complexes all react with dioxygen at room temperature to form two different complexes with the majority forming a hydroxy, phenoxy bridged binuclear copper (II) complex (Fig 1.37). Spectrally these complexes exhibit a strong absorption peak at  $\sim 350\text{nm}$  ( $1500\text{-}6000\text{M}^{-1}\text{cm}^{-1}$ ) and a weaker absorption peak at  $600\text{-}700\text{nm}$  ( $100\text{-}200\text{M}^{-1}\text{cm}^{-1}$ ). The crystal structure of the pyridine substituted copper (II) complex has been solved (Fig 1.38) and shows the copper atoms to be separated by  $2.99\text{\AA}$  and have a distorted square planar environment. These complexes show no reversibility in the oxygenation, although the copper (II) complexes show some catalytic activity to the reduction of hydroquinone.<sup>104</sup>

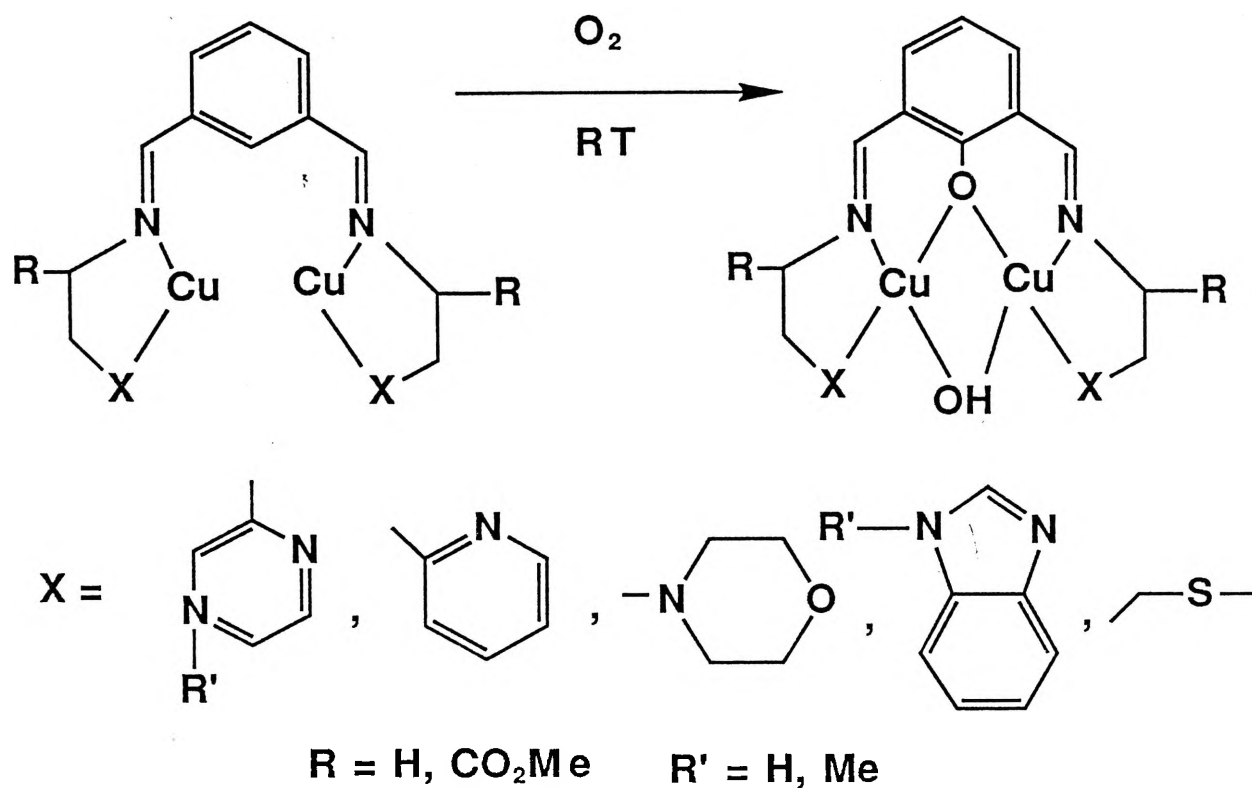


Fig 1.37: Casella et al.'s ligand and its Reaction with Oxygen

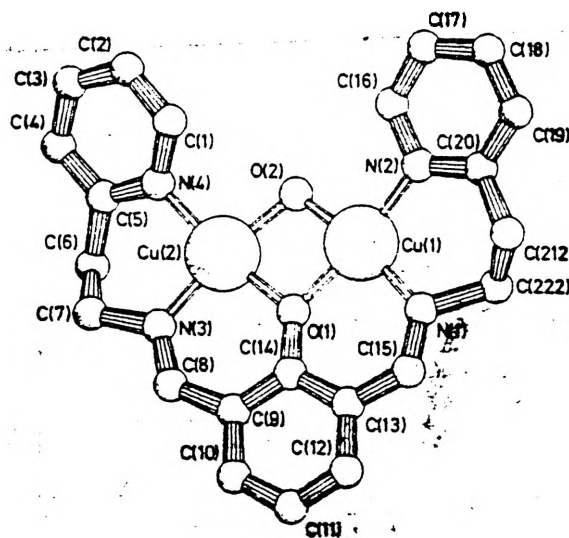


Fig 1.38: Crystal Structure of the Pyridine Copper (II) Complex

Nishida et al.<sup>105</sup> have synthesised a number of binuclear copper(II) complexes using the ligand shown in Fig1.39.

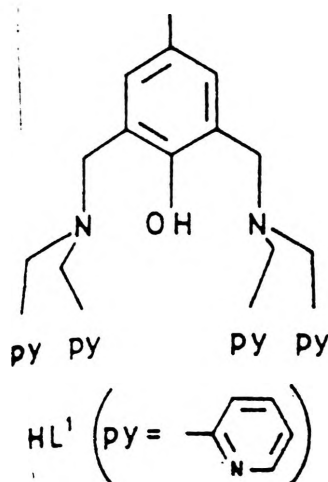


Fig 1.39:<sup>101</sup> Nishida et al.'s Disubstituted Phenol Bridging Ligand

The copper(II) atoms are in five coordinate geometry bridged by the exogenous bridging group X, (X= CH<sub>3</sub>COO<sup>-</sup>, Cl<sup>-</sup> and OH<sup>-</sup>).

These complexes show some catalytic activity in the presence of dioxygen which will be discussed later.

A comparison of the various model compounds in regard to their similarity to Hemocyanin can indicate which compounds are the best models of the four main groups. The results are found in Table 1.12. From this table it appears that the complexes of Karlin et al. are the best models of hemocyanin as these complexes have the most features in common with hemocyanin.

	(1)	(2)	(3)	(4)
Cu:O <sub>2</sub> 2:1	yes	yes	no	no
Solid, stable O <sub>2</sub> adduct at room temp	no	no	no	no
Cu-Cu 3.6Å	no	no	no	no
Heterocyclic N-ligands	yes	yes	yes	yes
X-ray structure	no	no	no	no
Reversible Cu(II)/Cu(I)	no	yes	no	no
UV-Vis similar to Hc	no	no	no	no
EPR silent	no	no	no	no
Peroxo O <sub>2</sub> bridge	yes	yes	no	no

**Table 1.12:** Comparison of Phenolic Bridged Models Against Hemocyanin (Hc)

(1) Sorrel et al.<sup>75-81</sup>

(2) Karlin et al.'s Xylyl Complex<sup>8,82-100</sup>

(3) Nishida et al.<sup>105</sup>

(4) Casella et al.<sup>101-104</sup>



### 1.5.3. Complexes with an Endogenous Alcohol Oxygen Bridge

A number of research groups have synthesised binuclear copper complexes using ligands containing an endogenous alcohol oxygen bridge.

These groups include Reed et al,<sup>106-107</sup> Kida et al,<sup>108-111</sup> Murray et al<sup>112-114</sup> and Mockler et al,<sup>115-120</sup>

Reed et al have studied binuclear complexes based on the benzimidazole ligand shown in Fig 1.40.<sup>106</sup>

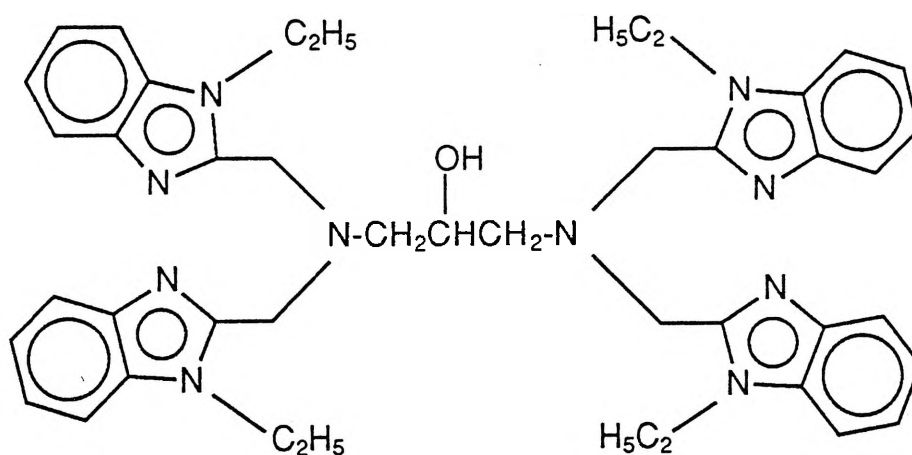


FIG 1.40:<sup>106</sup> Reed et al's Benzimidazole Ligand

Binuclear copper(II) complexes utilizing this ligand possess an exogenous bridging group, X (X= OAc<sup>-</sup>, N<sub>3</sub><sup>-</sup>, NO<sub>2</sub><sup>-</sup>).

The structure of the azide bridged complex (1) is shown in Fig 1.41.<sup>106</sup>

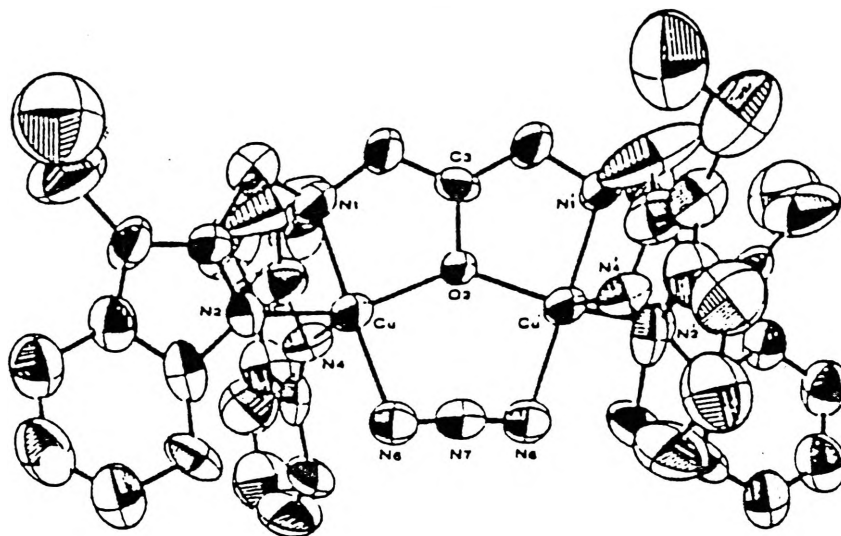


Fig 1.41:<sup>106</sup> Crystal Structure of the Azide Bridged Benzimidazole Ligand

The azide is  $\mu$ -1,3-bound and the complex is diamagnetic. The azide bridged complex has a similar spectrum to that of azidomethemocyanin (Table 1.13)

Table 1.13: Comparison of UV-Vis Spectra of  $\text{Cu}_2\text{LAz}$  and Azidomethemocyanin\*

azidomethemocyanin <sup>28c, 106</sup>	$\text{Cu}_2\text{LAz}$ (1) <sup>106</sup>
360(1500 $\text{M}^{-1}\text{cm}^{-1}$ )nm	364(2380 $\text{M}^{-1}\text{cm}^{-1}$ )nm
710(200 $\text{M}^{-1}\text{cm}^{-1}$ )nm	695(195 $\text{M}^{-1}\text{cm}^{-1}$ )nm

\* azidomethemocyanin from *Busycon caniculatum*.<sup>19,28c</sup>

Based on this spectral data the complex is quite a good model for azidomethemocyanin.

Kida et al.<sup>108-111</sup> have synthesised a number of binuclear copper(II) complexes utilizing the Schiff base ligands shown in Fig 1.42.

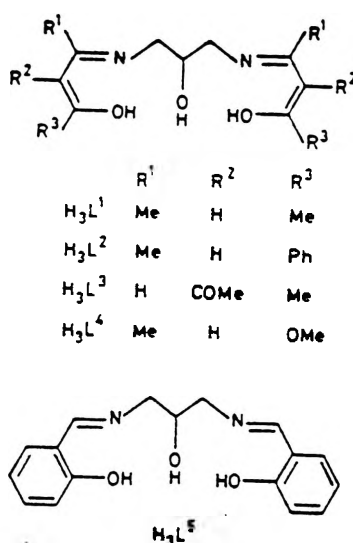


Fig 1.42:<sup>110</sup> Schiff Base Ligands of Kida et al.

These complexes have been studied structurally, magnetically and spectroscopically.

These complexes contain a number of exogenous groups, X (X= O<sub>2</sub>CCH<sub>3</sub><sup>-</sup>, PhCO<sub>2</sub><sup>-</sup>, OMe-, Pyrazolato ion) (Fig 1.43).<sup>108</sup> The copper atoms in the complexes are all antiferromagnetically coupled.

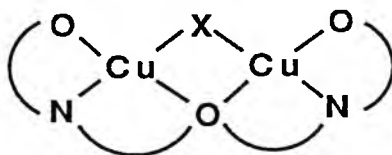


Fig 1.43:<sup>108</sup> Binuclear Copper (II) Complex of Kida et al.'s Ligands

All the complexes have been found to be basically planar and exhibit four or five coordinate copper (II) spectra.

Murray et al.<sup>112-114</sup> have synthesised a number of Schiff base ligands. These consist of a diamino hydroxy alkyl chain coupled to either salicylaldehyde, pyridine-2-aldehyde or imidazole-2-aldehyde (Fig 1.44).

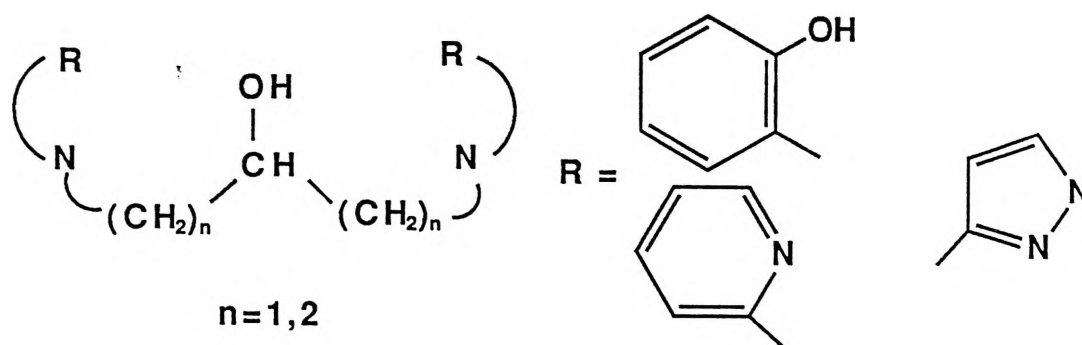


Fig 1.44:<sup>112</sup>Murray et al.'s Schiff Base Ligands

These ligands are able to form binuclear copper(II) complexes containing a number of exogenous bridging groups, X (X= OH<sup>-</sup>, Cl<sup>-</sup>, Br<sup>-</sup>, OMe<sup>-</sup>, OEt<sup>-</sup> and Pyrazolato ion).

The binuclear copper(II) complexes have been studied spectrally, structurally, magnetically and electrochemically. The UV-Vis spectra of these complexes indicates that the copper (II) atoms could be either four or five coordinate.

The structure of both a pyrazolato bridged complex and an acetate bridged complex have been solved and are shown in Figs 1.45,<sup>114</sup> and 1.46.<sup>113</sup>

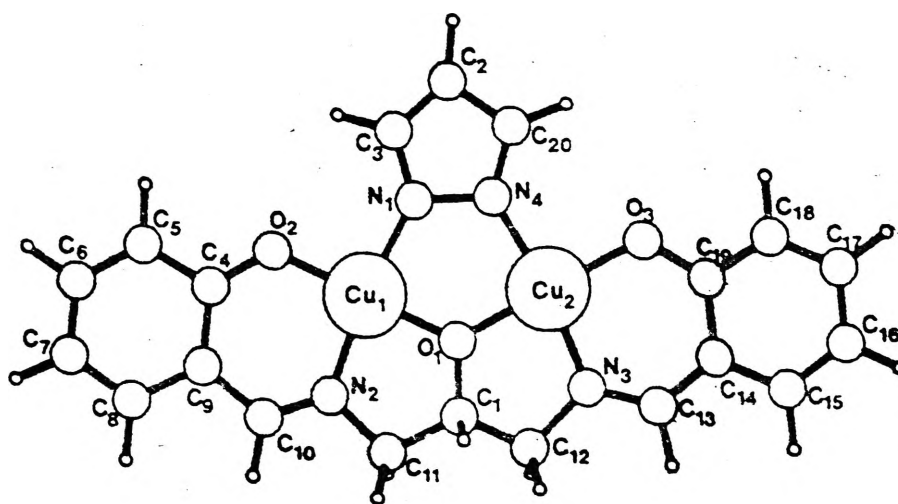


Fig 1.45:<sup>114</sup> Crystal Structure of the Pyrazolato Bridged Complex

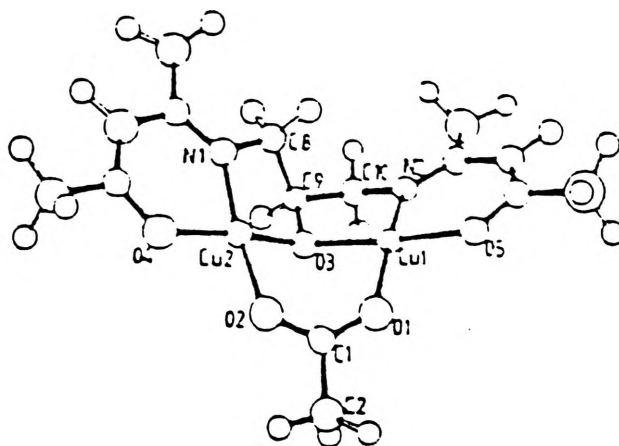


Fig 1.46:<sup>113</sup> Crystal Structure of the Acetate Bridged Complex

The pyrazolato bridged complex is strongly antiferromagnetic and has square planar geometry around both copper atoms.

The acetato bridged complex has square planar geometry around the copper atoms but is weakly ferromagnetic. This compares with an isomer of this complex prepared by Kida et al.<sup>108</sup> which is antiferromagnetic (Fig 1.47).

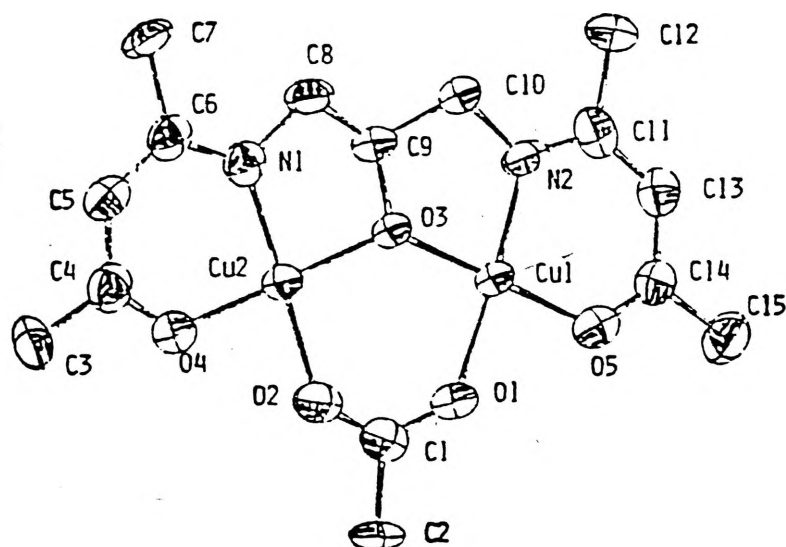


Fig 1.47:<sup>108</sup> Crystal Structure of Kida et al.'s Acetate Bridged Complex

The differences in the magnetism is attributed to the bending of the copper planes away from coplanarity in Murray et al.'s complex. This results in decreased superexchange between the copper (II) atoms.

Mockler et al.<sup>115-120</sup> have utilized Schiff base ligands comprised of 1,3-diaminopropan-2-ol and either salicylaldehyde (abbreviated as SAL-DPLH<sub>3</sub>) or 3-ethoxysalicylaldehyde (ESAL-DPLH<sub>3</sub>) (Fig 1.48).<sup>116</sup>

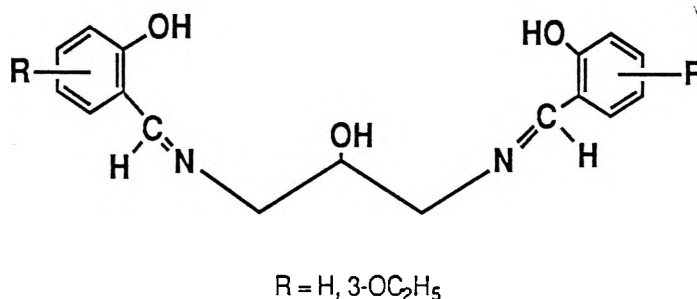


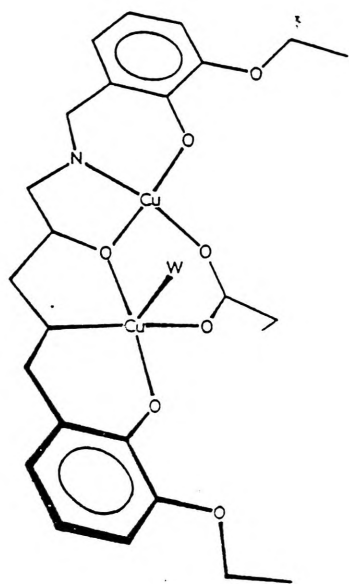
Fig 1.48:<sup>116</sup> Schiff Base Ligand of Mockler et al.

The structure of a number of these complexes have been solved (Figs 1.48a-d).

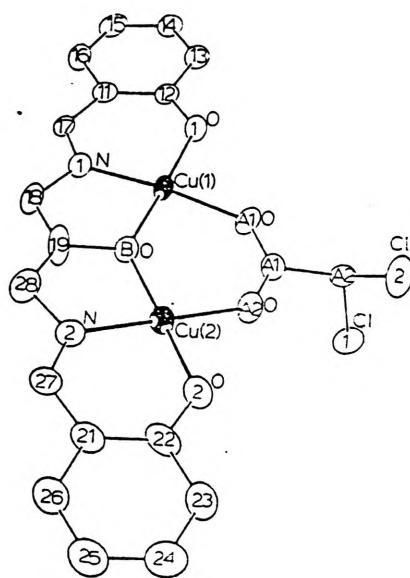
The propionate bridged (Fig 1.49a)<sup>117</sup> and dichloroacetate bridged (Fig 1.49b)<sup>117</sup> complexes are essentially planar complexes and have d-d spectra characteristic of four and five coordinate copper (II). There is antiferromagnetic interaction between the copper atoms.

The pyrazole complex (Fig 1.49c)<sup>117</sup> has a four coordinate square planar environment for each copper atom and is similar in structure to the related compound of Murray et al.<sup>114</sup> They differ mainly in the copper-oxygen-copper angle ( $122.5^\circ$  to  $125.1^\circ$ ) and the dihedral angle ( $7.4^\circ$  to  $3.6^\circ$ ).

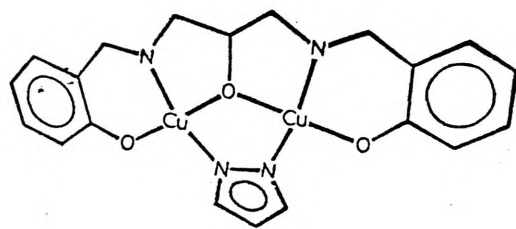
The pivalate bridged complex (Fig 1.49d)<sup>117</sup> is distorted from planarity. This difference in structure is reflected in the magnetism of the complexes with the pivalate being weakly antiferromagnetic below 80K.



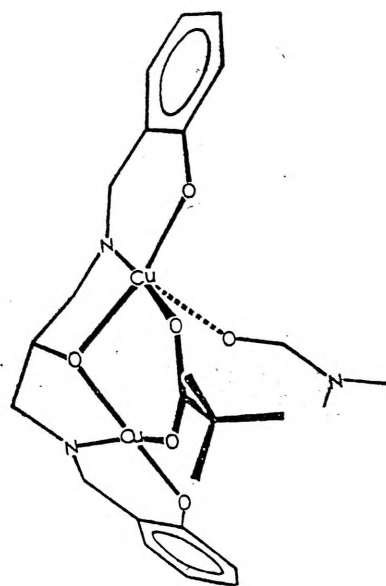
a



b



c



d

Fig 1.49:117-120 Crystal Structure of Mockler et al.'s Complexes

Erickson<sup>120</sup> has synthesised a variety of compounds using the ligand SAL-DPLH<sub>3</sub> utilizing a number of exogenous bridging groups, X (X= Y-Pyrazolato ion (Y= H, 5-NO<sub>2</sub>, 3-CH<sub>3</sub>), Triazolato ion, Benzoato ion and substituted Benzoato ions, (Pyridine-N-Oxides, Phenol and catechol adducts of the phenylacetate bridged complex) and also a dioxygen bridged complex.

The dioxygen bridged complex exhibits a peak at 1051cm<sup>-1</sup> in the infra-red spectra. This position is indicative of a bridging superoxo (O<sub>2</sub><sup>-</sup>) ion. The visible spectra of this complex exhibits a peak at 620-630nm (400M<sup>-1</sup>cm<sup>-1</sup>). The complex has weak antiferromagnetic interaction between the copper (II) atoms. Unfortunately no suitable crystals have yet been produced for X-ray crystallography.

A comparison of the various model compounds in regard to their similarity to Hemocyanin can indicate which compounds are the best models of the three main groups. The results are found in Table 1.14. From this table it appears that the complexes of Reed et al are the best models of hemocyanin using an endogenous alcohol bridge.



	(1)	(2)	(3)	(4)
Cu:O <sub>2</sub> 2:1	no	no	no	yes
Solid, stable O <sub>2</sub> adduct at room temp	no	no	no	yes
Cu-Cu 3.6Å	no	no	no	no
Heterocyclic N-ligands	yes	no	yes	no
X-ray structure	yes*	no	no	no
Reversible Cu(II)/Cu(I)	no	no	no	no
UV-Vis similar to Hc	yes	no	no	no
EPR silent	yes	yes	yes	no
Peroxo O <sub>2</sub> bridge	no	no	no	no

**Table 1.14:** Comparison of Alcohol Bridged Models Against Hemocyanin (Hc)

\* Crystal structure of the similar azide bridged complex

(1) Reed et al.<sup>106-107</sup>

(2) Kida et al.<sup>108-111</sup>

(3) Murray et al.<sup>112-114</sup>

(4) Mockler / Erickson et al.<sup>115-120</sup>

Looking at the three different types of model compounds described in sections 1.5.1 to 1.5.3 (Table 1.15) as models of Hemocyanin it appears clear that the complexes of Kitajima et al. are the best reported in the literature.

	(1)	(2)	(3)
Cu:O <sub>2</sub> 2:1	yes	yes	no
Solid, stable O <sub>2</sub> adduct at room temp	yes	no	no
Cu-Cu 3.6Å	yes	no	no
Heterocyclic N-ligands	yes	yes	yes
X-ray structure	yes	no	no
Reversible Cu(II)/Cu(I)	no	yes	no
UV-Vis similar to Hc	yes	no	yes
EPR silent	yes	no	yes
Peroxo O <sub>2</sub> bridge	yes	yes	no

**Table 1.15:** Comparison of the Different Types of Models Against Hemocyanin (Hc)

(1) Kitajima et al.<sup>67</sup>

(2) Karlin et al.<sup>8,82-100</sup>

(3) Reed et al.<sup>106-107</sup>

#### 1.5.4. Multi-Copper Oxidase Models

There have been reports of models of the Type II/Type III copper centre in the multi-copper oxidases recently by Adams et al.,<sup>121</sup> Karlin et al.<sup>122</sup> and Werakso et al.<sup>123</sup>

Adams et al.<sup>121</sup> have synthesised a trinuclear copper (II) complex which consists of a Type III copper centre and a Type II copper centre. The ligand used is a macrocycle (Fig 1.50)

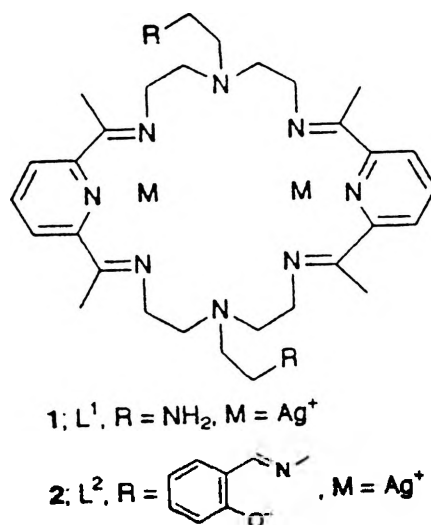


Fig 1.50:<sup>121</sup> Adams' Macrocycle Ligand

The Type II centre is 4.9 and 5.9 Å from the Type III copper atoms. The two copper atoms in the Type III centre are 3.6 Å apart, bridged by a hydroxy group (Fig 1.51).

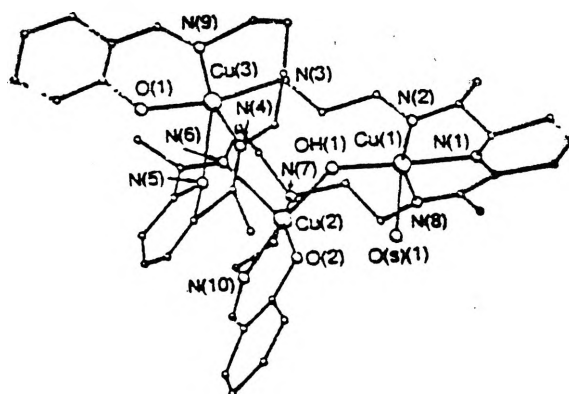
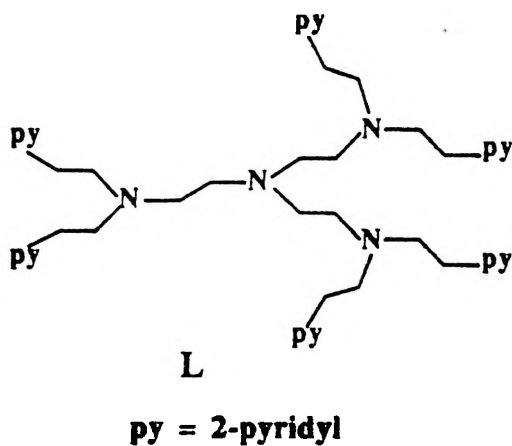


Fig 1.51:<sup>121</sup> Trinuclear Copper Complex

The complex is weakly antiferromagnetic. All three copper atoms have a distorted square pyramidal geometry and are each bound to three nitrogen ligands.

Karlin et al.<sup>122</sup> have reported recently work involving the trinucleating ligand below (Fig 1.52) which they have used to synthesise a trinuclear copper (I) complex (Fig 1.53).



**Fig 1.52:**<sup>121a</sup> Trinucleating Ligand

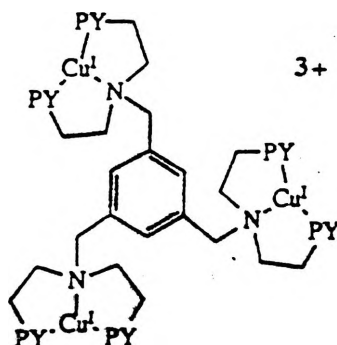


**Fig 1.53:**<sup>121b</sup> Trinuclear Copper (I) Complex

Reaction of this complex with dioxygen at  $-80^{\circ}\text{C}$  followed by warming to room temperature gives a trinuclear copper (II) complex (Fig 1.54). This complex consists of a Type III copper pair bridged by phenoxo and hydroxo groups. The other copper is a Type II copper site which is pentacoordinate through the hydroxy group shown in 2 in Fig 1.54 being bound to another Type II copper atom as shown in Fig 1.54, i.e. there are two trinuclear complexes bound together by the Type II copper atoms.

The Type III copper atoms are EPR silent while the Type II site gives an EPR signal. The oxygen uptake ratio is 6:3 Cu:O<sub>2</sub> (i.e 2:1).

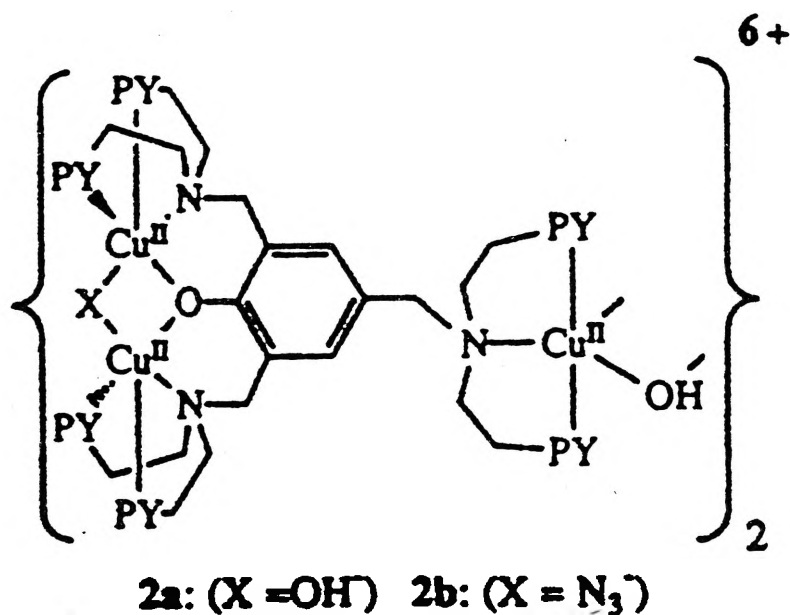


Fig 1.54: <sup>121</sup>C Trinuclear Copper (II) Complex

Werakso et al.<sup>123</sup> have synthesised a number of pentanuclear copper complexes which contain two Type III copper (II) sites and one Type II copper (II) bridging group between the two Type III sites.

The Type III sites use the ligand of Mockler et al. (Fig 1.48) in combination with varying exogenous bridges (e.g 6-Aminoindazole, 4-aminobenzoic acid, 4-aminobutyric acid, etc). The free amino group on these exogenous bridges are reacted with salicylaldehyde and copper (II) ions to give a pentanuclear copper (II) complex (Fig 1.55). The x-ray crystal structure of the 6-aminoindazole bridged compound is shown in Fig 1.56.

All the copper atoms are distorted square planar with the Type III copper atoms having  $\text{NO}_3$  coordination and the Type II  $\text{N}_2\text{O}_2$  coordination. All the complexes are antiferromagnetic with the Type III sites tending towards diamagnetism. The binuclear Type III copper atoms have a copper-copper separation of  $3.36\text{\AA}$ .

To date there has been little work done on models of the multi-copper oxidases and so there is considerable potential for more work especially in regards to synthesising complexes containing models of the Type I copper centre with models of the Type II copper centre, the Type III copper centre or the Type II and Type III copper centres. Out of the currently reported work the model system of Adams et al appear the most relevant as it possesses copper atom separations closest to those reported for Ascorbate Oxidase.

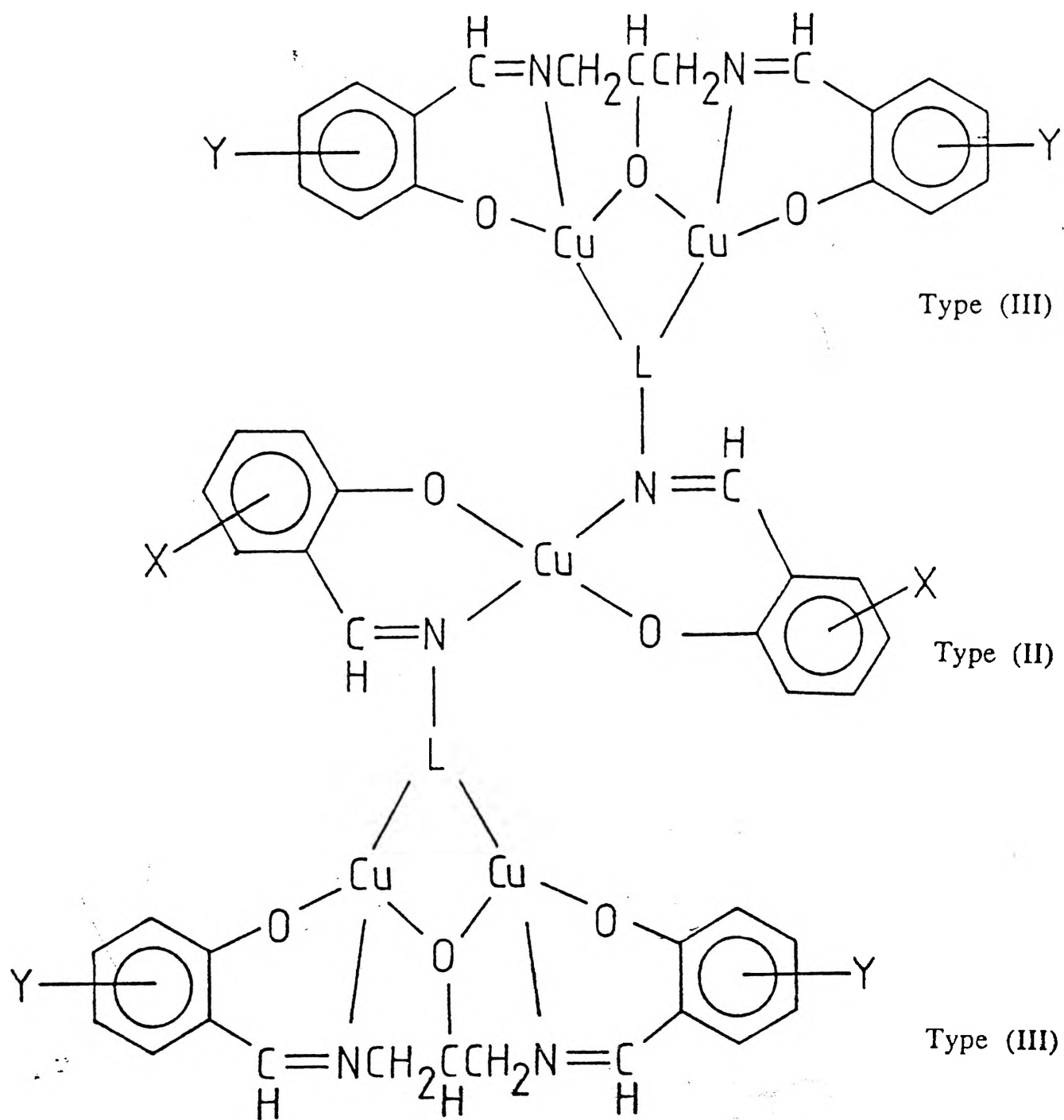
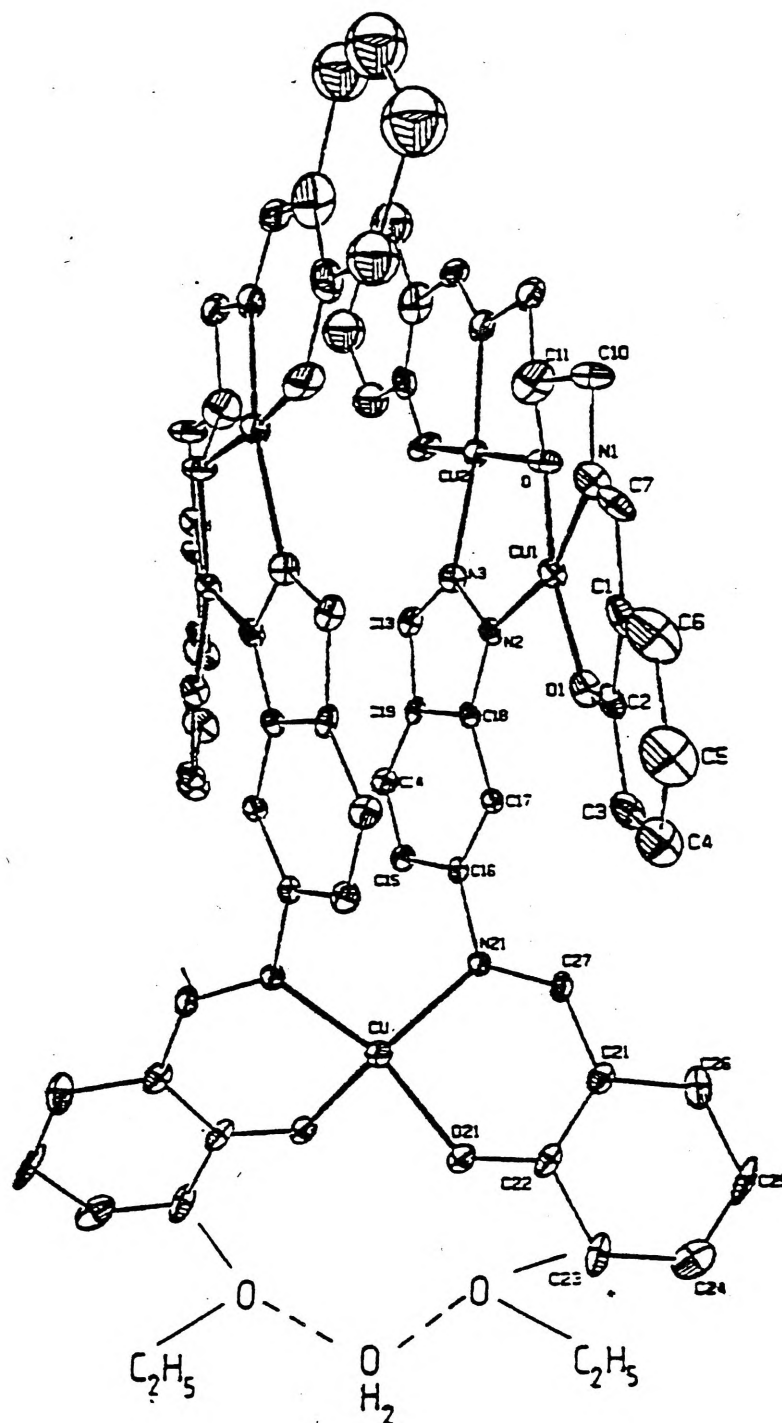


Fig 1.55:123 Schematic of Werakso et al.'s Complexes



**Fig 1.56:**<sup>123</sup> Crystal Structure of  $\text{Cu}_5(\text{ESAL-DPL.6Al.ESAL})_2 \cdot 2\text{H}_2\text{O}$



### 1.5.5 Reactions of Model Compounds with Phenols and Catechols

There have been a number of research groups who have tested various Type III model copper compounds for their reactions with phenols and catechols. These groups include Vigee et al.,<sup>124</sup> Davies et al.,<sup>125</sup> Cabras et al.,<sup>126</sup> Thompson et al.,<sup>127</sup> Karlin et al.,<sup>89</sup> Erickson<sup>120</sup> and Casella et al.<sup>128</sup>

Vigee et al.<sup>124</sup> have synthesised a number of binuclear copper(II) complexes utilizing the disubstituted methylphenol bridge first used by Robson et al. (Fig 1.57).<sup>124c</sup>

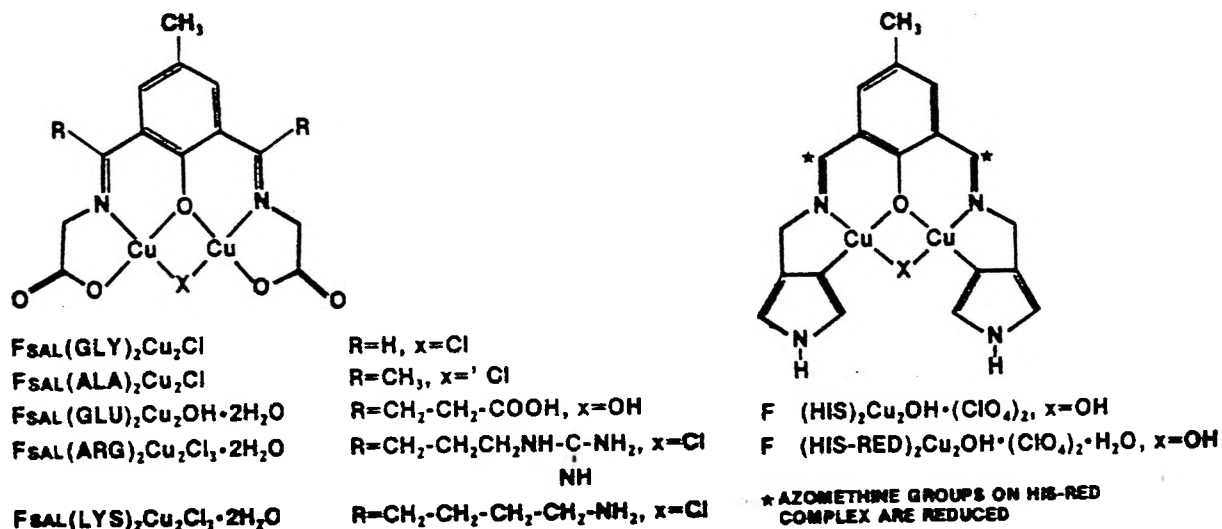


Fig 1.57:<sup>124c</sup> Ligand Utilized by Vigee et al.

These copper (II) complexes have been found to catalyse the air oxidation of substituted catechols. Studies of the oxidation rates show that tyrosinase is 1000 to 2000 times more active than the synthetic copper(II) complexes. The study indicates that the oxidation mechanism is more complicated than previously believed due to the reaction using four moles of dioxygen for every mole of catechol oxidised.

Davies et al.<sup>125</sup> have synthesised a copper (I) dimer (Fig 1.58) utilizing tetraethylenediamine (TEED).

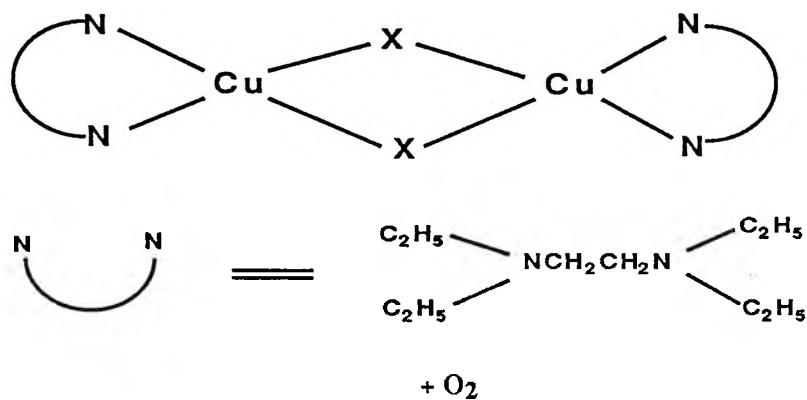


Fig 1.58:<sup>125</sup> Copper(I) Dimer of Davies et al.

(X = Cl, Br)

The complex in Fig 1.58 reacts with dioxygen to give an oxo bridged copper(II) complex (Fig 1.59).<sup>125</sup>

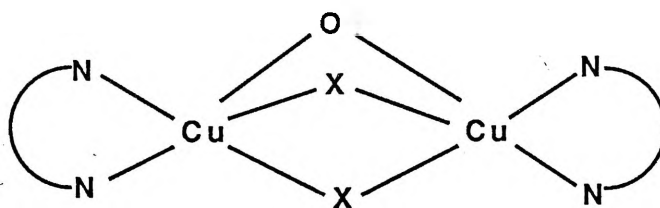


Fig 1.59:<sup>125</sup> Oxocopper(II) Complex of Davies et al.

This binuclear copper (II) oxy bridged complex has been found to catalyze the reaction of 2,6-dimethylphenol to give diphenoquinone or polymeric products (Fig 1.60)<sup>125</sup> depending on the temperature of reaction.

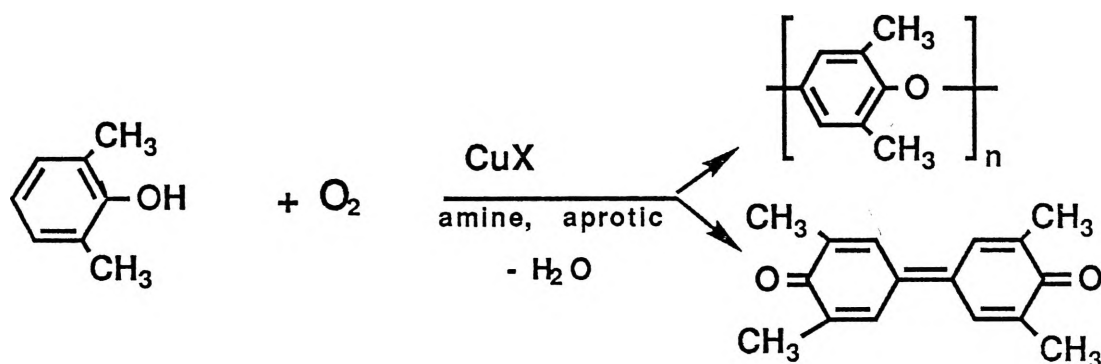


Fig 1.60:<sup>125</sup> Phenol Reaction of Davies et al.'s Oxocopper (II) Complex

Cabras et al.<sup>126</sup> have studied the reaction of  $Cu(o-CACOO)_2$  ( $o-CACOOH$  = ortho-hydroxycinnamic acid) (Fig 1.61) with catechol.

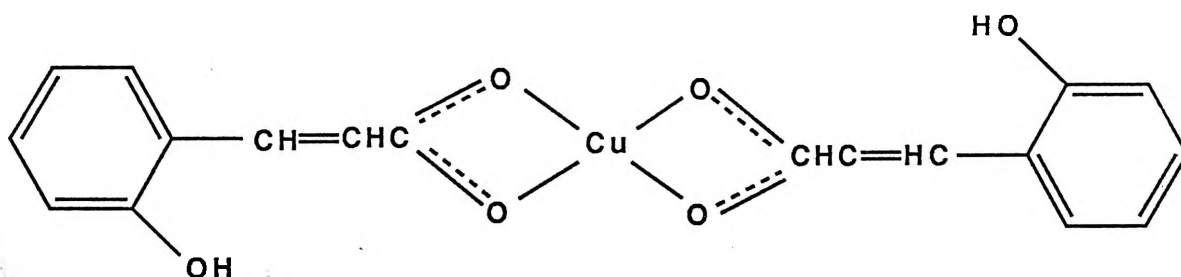


Fig 1.61:<sup>126</sup> Copper Complex of Orthohydroxycinnamic Acid

The complex was found to catalyse the oxidation of catechol to quinone in the presence of dioxygen, with the reaction stopping at the production of the quinone. This is the first reported case of a synthetic copper (II) complex not catalyzing the catechol to a polymer.

Thompson et al.<sup>127</sup> have synthesised a series of copper(II)-3,5-di-*tert*-butyl-o-semiquinone complexes (Fig 1.62).

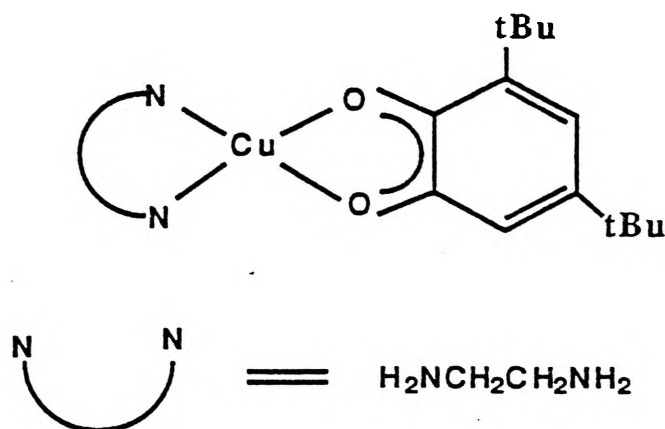


Fig 1.62:<sup>127</sup> Complex of Copper (II) en + 3,5-di-*tert*-butylcatechol

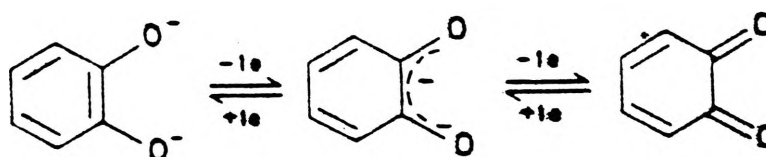
The basic copper (II) dimer-catechol reaction (Scheme III)<sup>127</sup> is proposed as a critical step in the oxidation of catechol to quinone.



Scheme III:<sup>127</sup> Proposed Reaction

R = H or CH<sub>3</sub>; DTBSQ = 3,5-di-*tert*-butyl-o-semiquinone; DTBC = 3,5-di-*tert*-butyl-catechol

The reaction involves a one-electron oxidation of the catechol or a one-electron reduction of the benzoquinone to give the copper(II)-semiquinone complex (Scheme IV).<sup>127</sup>



Scheme IV:<sup>127</sup> Semiquinone Reduction Pathway

The structure of one of the complexes (Fig 1.63) shows that the di-*tert*-butyl-o-semiquinone is  $\mu$ -1,2-bound to a single copper(II) atom.

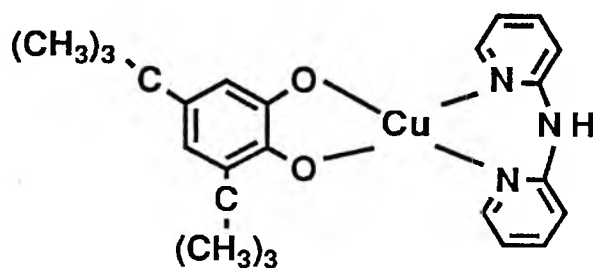


Fig 1.63:<sup>127</sup> Structure of Semiquinone Complex Showing  $\mu$ -1,2-Bridging

Karlin et al.<sup>89</sup> have synthesised a catechol bridged binuclear copper (II) complex (Fig 1.64).

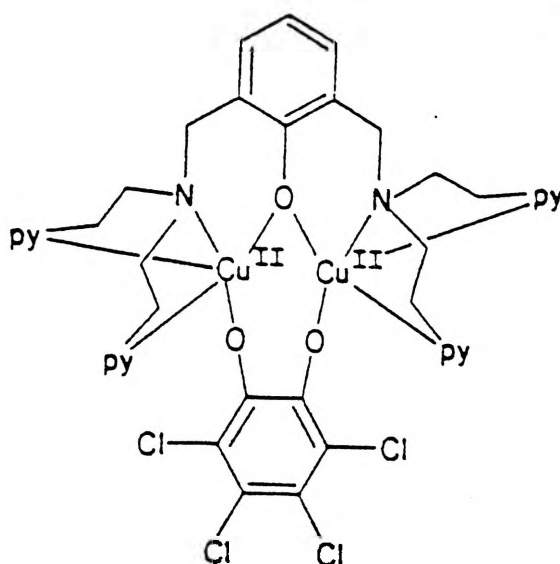


Fig 1.64:<sup>89</sup> Catechol Bridged Binuclear Copper (II) Complex

This complex was synthesised by reaction of the binuclear copper (I) phenoxo bridged complex and tetrachloro-o-benzoquinone.

The catechol is  $\mu$ -1,2-bridged across the two copper (II) atoms. This binding is the same as that proposed for the tyrosinase intermediate in the oxidation of catechols.

Erickson<sup>120</sup> has synthesised a number of phenol and catechol adducts of the complex  $\text{Cu}_2(\text{SAL-DPL})\text{PhAc}$  (Fig 1.65).

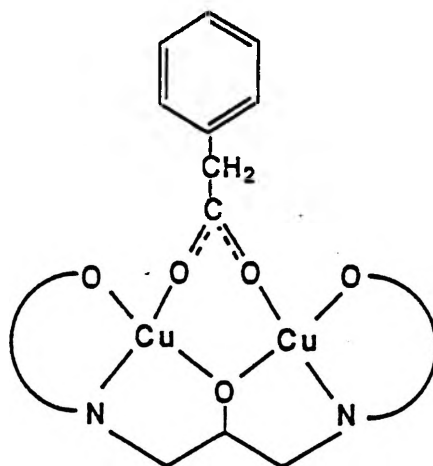


Fig 1.65:<sup>120</sup> Copper (II) (SAL-DPL) Phenylacetate Complex

The crystal structure of the 4-ethylphenol adduct (Fig 1.66) shows that the phenol is hydrogen bonded to the non-bridging oxygen of the ligand backbone.

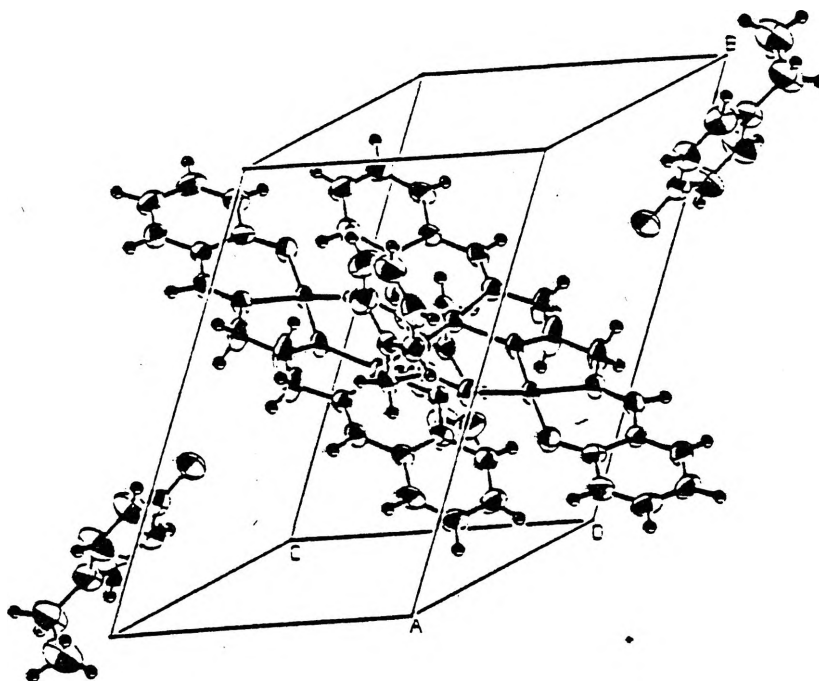


Fig 1.66:<sup>120</sup> Crystal Structure of the Copper(II)(SAL-DPL)Phenylacetate.4-Ethylphenol Complex

It is proposed that the catechol complexes possess similar bonding of the catechol to the copper-phenylacetate complex. It is suggested by Erickson that the first step in the tyrosinase oxidation of catechols involves the hydrogen bonding of catechol to the peptide chain, followed by deprotonation and then binding to the copper atoms and oxidation of the catechol.

Casella et al.<sup>128</sup> have reported the reaction of their binuclear copper (I) complex 101-104 with both methyl-4-hydroxybenzoate and 3,5-dibutylcatechol. They report the isolation of methyl-4-hydroxycatechol from the reaction of their complex with methyl-4-hydroxybenzoate and claim evidence for the presence of 3,5-dibutylquinone from the 3,5-dibutylcatechol adduct formed by the oxygenation of the phenol. They propose a scheme for the reaction involving a  $\mu$ -1,2-catechol bridged complex (Fig 1.67).

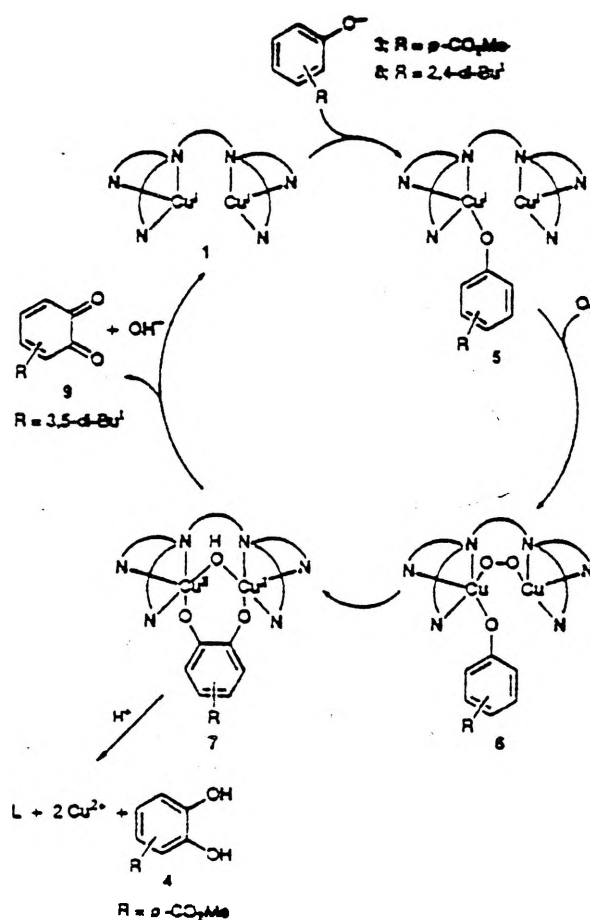


Fig 1.67:<sup>128</sup> Reaction of Phenol with Binuclear Copper (I) Complex of Casella et al.

### 1.5.6. The Electrochemistry of Model Compounds of Type (III) Copper Proteins

A number of groups have studied the electrochemistry of model compounds of Type III copper proteins. These groups include Gryzbowski et al.,<sup>129</sup> Gagne et al.,<sup>130</sup> Li et al.,<sup>131</sup> Sorrel et al.<sup>75</sup> and Bond et al.<sup>132</sup>

Gryzbowski et al.<sup>129</sup> have studied the electrochemistry of complexes based on Robson et al.'s ligand (Fig 1.68).

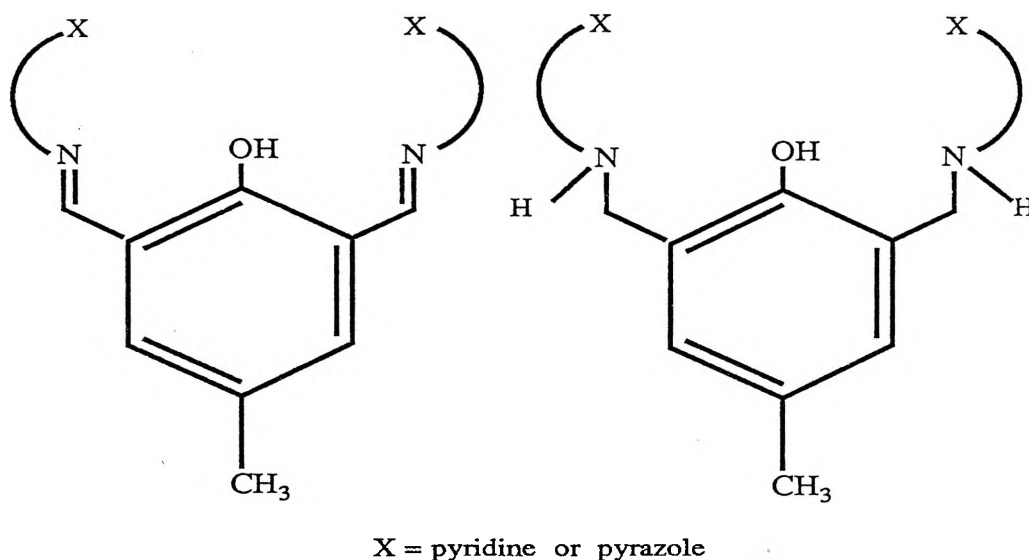
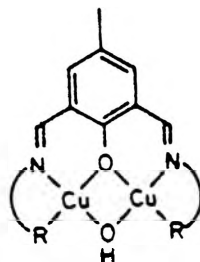


Fig 1.68:<sup>129</sup> Ligand Utilized by Gryzbowski et al.

These complexes have been found to undergo a single two-electron reduction ( $2\text{Cu (II)} + 2e^- \leftrightarrow 2\text{Cu (I)}$ ) at negative potentials. The exact potential is dependent on the nature of the exogenous bridging group, X ( $\text{X} = \text{OH}^-$ ,  $E_{1/2} = -0.60\text{V}$  to  $-0.70\text{V}$ ;  $\text{X} = \text{Cl}^-$ ,  $E_{1/2} = -0.20\text{V}$  to  $-0.25\text{V}$ ). This reduction is irreversible and leads to complex breakdown due to the instability of the mixed valence  $\text{Cu (II) Cu (I)}$  and the binuclear copper (I) complexes.



Gagne et al.<sup>130</sup> have also used the disubstituted methylphenol used by Robson et al. to synthesise binuclear copper (II) complexes (Fig 1.69) for electrochemical studies.



	R	$\lambda$ (e)	$\mu_{\text{eff}}/\text{Cu}$
3		630 (160)	1.4
4		645 (120)	1.2
5		630 (100)	0.96

Fig 1.69:<sup>130</sup> Copper (II) Complex of Gagne et al.'s

These complexes have been found to undergo two quasi- or irreversible one electron reductions ( $E_1 = -0.211$  to  $+0.24\text{V}$   $2\text{Cu (II)} \leftrightarrow \text{Cu (II) Cu (I)}$ ,  $E_2 = -0.91$  to  $+0.008\text{V}$   $\text{Cu (II) Cu (I)} \leftrightarrow 2\text{Cu (I)}$ ). As with the complexes of Gryzbowski et al.,<sup>128</sup> the binuclear copper (I) complexes are unstable, causing the irreversible reduction.

The  $\text{Cu}_2(\text{EDTB})(\text{ClO}_4)_2$  complex prepared by Li et al. (Fig 1.70)<sup>131</sup> was found to undergo two quasi-reversible reductions, both involving a one electron transfer ( $E_1 = +0.25\text{V}$   $2\text{Cu (II)} \leftrightarrow \text{Cu (II) Cu (I)}$ ,  $E_2 = -0.04\text{V}$   $\text{Cu (II) Cu (I)} \leftrightarrow 2\text{Cu (I)}$ ).

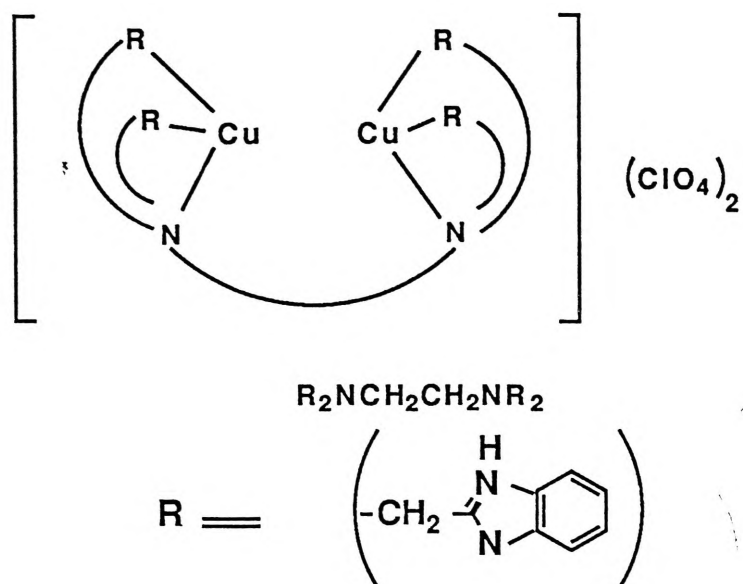


Fig 1.70:<sup>131</sup> Binuclear Copper (I) (EDTB)(ClO<sub>4</sub>)<sub>2</sub> Prepared by Li et al.

In the presence of dioxygen the cathodic and anodic peaks disappear, in the scan region, probably due to the formation of a dioxygen adduct (Fig 1.71).

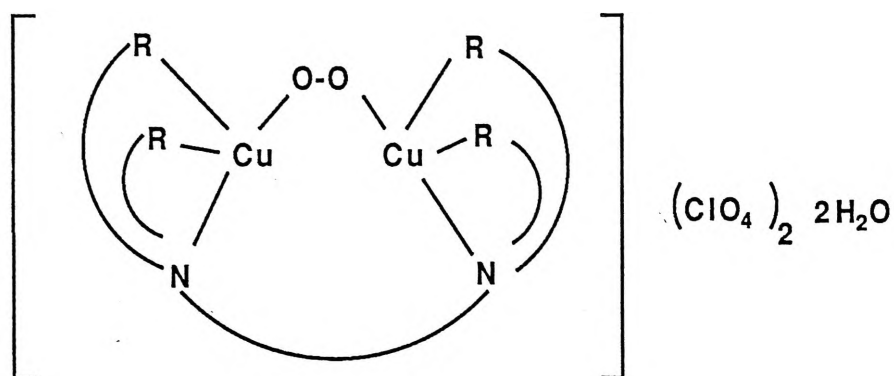


Fig 1.71:<sup>131</sup> Dioxygen Adduct of Copper (II) (EDTB)(ClO<sub>4</sub>)<sub>2</sub>

Sorrel et al.<sup>75</sup> in their work with the pyrazole and pyridine terminal ligands (Fig 1.72) studied the electrochemistry of the binuclear copper (I) complexes.

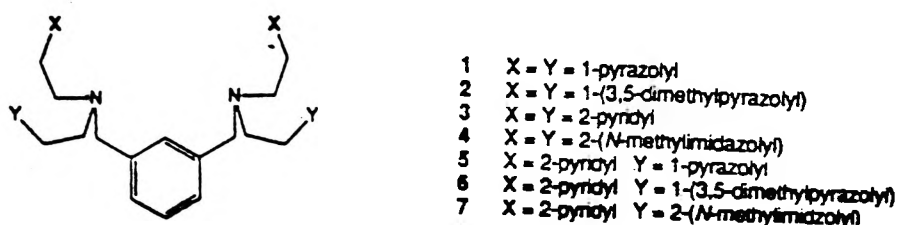


Fig 1.72: Pyridine and Pyrazole Terminal Ligands of Sorrel et al.<sup>75</sup>

The results were, in both cases, a single, reversible, two electron oxidation ( $2\text{Cu(I)} \leftrightarrow 2\text{Cu(II)} + 2e^-$ ).

The half potentials are  $E_{1/2} = +0.48\text{V}$  for the pyrazole terminal complex and  $E_{1/2} = +0.33\text{V}$  for the pyridine terminal complex.

Bond et al.<sup>132</sup> have investigated the electrochemistry of a number of complexes synthesised by Murray et al.<sup>112-114</sup> The complexes containing the phenol endogenous bridge (Fig 1.73) have been found to contain two well separated reduction peaks. The first is a reversible ( $E_{1/2} = -0.79\text{V}$ ) ( $2\text{Cu(II)} \leftrightarrow \text{Cu(II)Cu(I)}$ ) one electron peak, while the second is a quasi-reversible one electron peak ( $E_{1/2} = -1.03\text{V}$ ) ( $\text{Cu(II)Cu(I)} \leftrightarrow 2\text{Cu(I)}$ ).

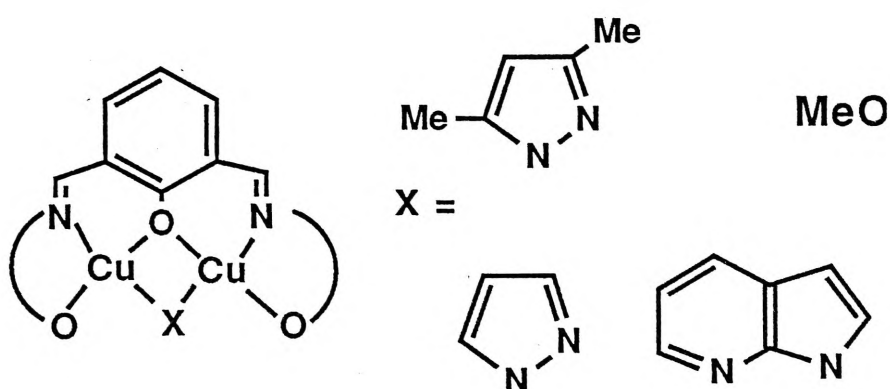


Fig 1.73:<sup>132a</sup> Phenol Bridging Complexes of Murray et al.'s

For complexes containing the hydroxide endogenous bridge (Fig 1.74)<sup>131</sup> the complexes have been found to undergo a single quasi-reversible reduction ( $E_{1/2} = -1.007\text{V}$  to  $-1.012\text{V}$ ) corresponding to  $2\text{Cu(II)} \leftrightarrow \text{Cu(II)Cu(I)}$  and a second irreversible reduction peak ( $E_{1/2} = -1.58\text{V}$  to  $-1.60\text{V}$ ) corresponding to  $\text{Cu(II)Cu(I)} \leftrightarrow 2\text{Cu(I)}$ .

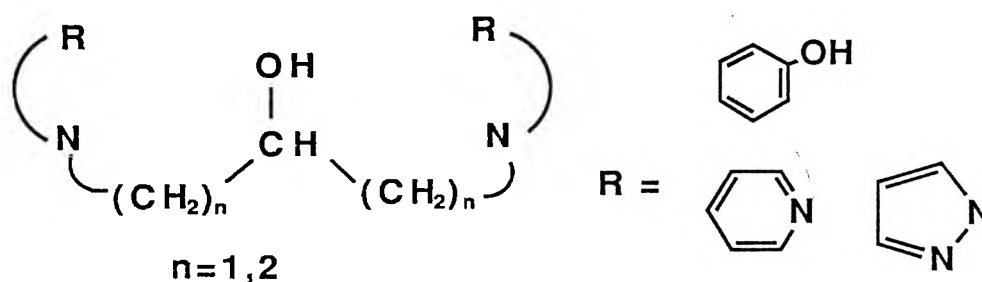


Fig 1.74:<sup>131b</sup> Hydroxide Bridging Complexes of Murray et al.'s

Based upon the characteristics of the Type III copper centre in proteins, to be a good electrochemical model, the model complex needs to undergo a single, fully reversible, two electron transfer at positive reduction potentials.

Gryzbowski et al.'s complexes fail as models by being reduced at negative potentials, Gagne et al. and Li et al.'s complexes both undergo two one electron transfers and Bond et al.'s complexes fail on both aspects.

In this regard only Sorrel et al.'s complexes are good models for the electrochemistry of the Type (III) copper centres of copper proteins.

**2:**

**Empirical Formulae**

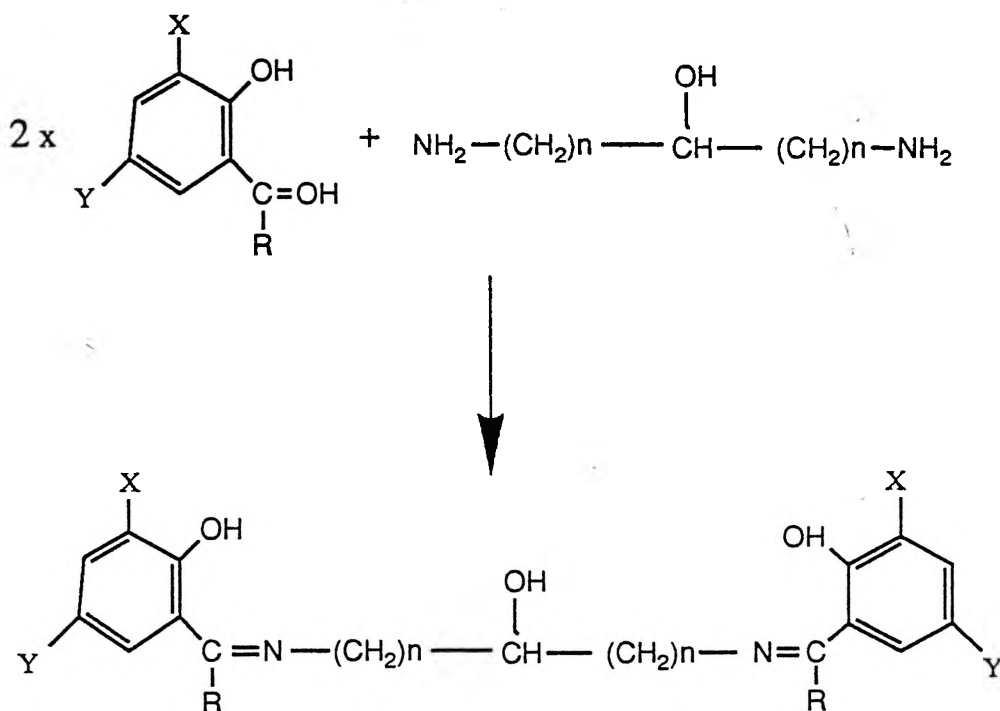
## 2: Empirical Formulae

The empirical formulae of the complexes were determined from the elemental analyses of carbon, hydrogen and nitrogen. Gravimetric analyses identified the percentage of water. The analyses data is collected in Table 2.2. Fig 2.1 shows the schiff base ligand synthesis and the nomenclature used for the various schiff bases used in this study. Table 2.1 gives a list of the abbreviations used for the exogenous bridges and their meaning.

<u>Abbreviation</u>	<u>Bridging Group</u>
OH <sup>-</sup>	Hydroxide
MeOEtO <sup>-</sup>	2-Methoxyethanolate
O <sub>2</sub> <sup>-</sup>	Superoxo
O <sub>2</sub> H <sup>-</sup>	Hydroperoxo
4-OHBzCOO <sup>-</sup>	4-Hydroxybenzylacetate
CAT <sup>2-</sup>	Catecholate (C <sub>6</sub> H <sub>4</sub> O <sub>2</sub> <sup>2-</sup> )
CATH <sup>-</sup>	Catecholate (C <sub>6</sub> H <sub>5</sub> O <sub>2</sub> <sup>-</sup> )
3-MeOCAT <sup>-</sup>	3-Methoxycatecholate
3-MeCAT <sup>-</sup>	3-Methylcatecholate
4-NO <sub>2</sub> CAT <sup>-</sup>	4-Nitrocatecholate
Pz <sup>-</sup>	Pyrazolate
3,5-Me <sup>2</sup> Pz <sup>-</sup>	3,5-Dimethylpyrazolate
3-MePz <sup>-</sup>	3-Methylpyrazolate
5-NO <sub>2</sub> Ind <sup>-</sup>	5-Nitroindazolate
2-OHBzImid <sup>-</sup>	2-Hydroxybenzimidazolate
NH <sub>2</sub> O <sup>-</sup>	Hydroxylamine
2-PyO <sup>-</sup>	2-Hydroxypyridine
5-ClPyO <sup>-</sup>	5-Chloro-2-hydroxypyridine

Table 2.1: Exogenous Bridge Abbreviations

The Schiff base was formed by refluxing two moles of salicylaldehyde or other ortho-hydroxyaldehyde or ketone with one mole of the diamino alcohol. The yellow crystals precipitated out of solution upon cooling and were recrystallized from an appropriate solvent.



X= H, Y= H, R= H, n= 1

SAL-DPL

X= H, Y= H, R= H, n= 2

SAL-DPE

X= 3-OC<sub>2</sub>H<sub>5</sub>, Y= H, R= H, n= 1

ESAL-DPL

X= 3-OC<sub>2</sub>H<sub>5</sub>, Y= H, R= H, n= 2

ESAL-DPE

X= H, Y= CH<sub>3</sub>, R= p-CH<sub>3</sub>-C<sub>6</sub>H<sub>4</sub>, n= 1

M<sup>2</sup>BP-DPL

X= H, Y= CH<sub>3</sub>, R= p-CH<sub>3</sub>-C<sub>6</sub>H<sub>4</sub>, n= 2

M<sup>2</sup>BP-DPE

Fig 2.1: Schiff Base Ligand Synthesis

The binuclear complexes of this study were synthesised by refluxing, in methanol, two molar equivalents of either copper acetate or copper salicylaldehyde with one mole of the desired schiff base ligand and one molar equivalent of the appropriate exogenous bridge and two molar equivalents of piperidine. The complex precipitated out of solution upon cooling and was then recrystallized. A general reaction equation is shown in Fig 2.2.

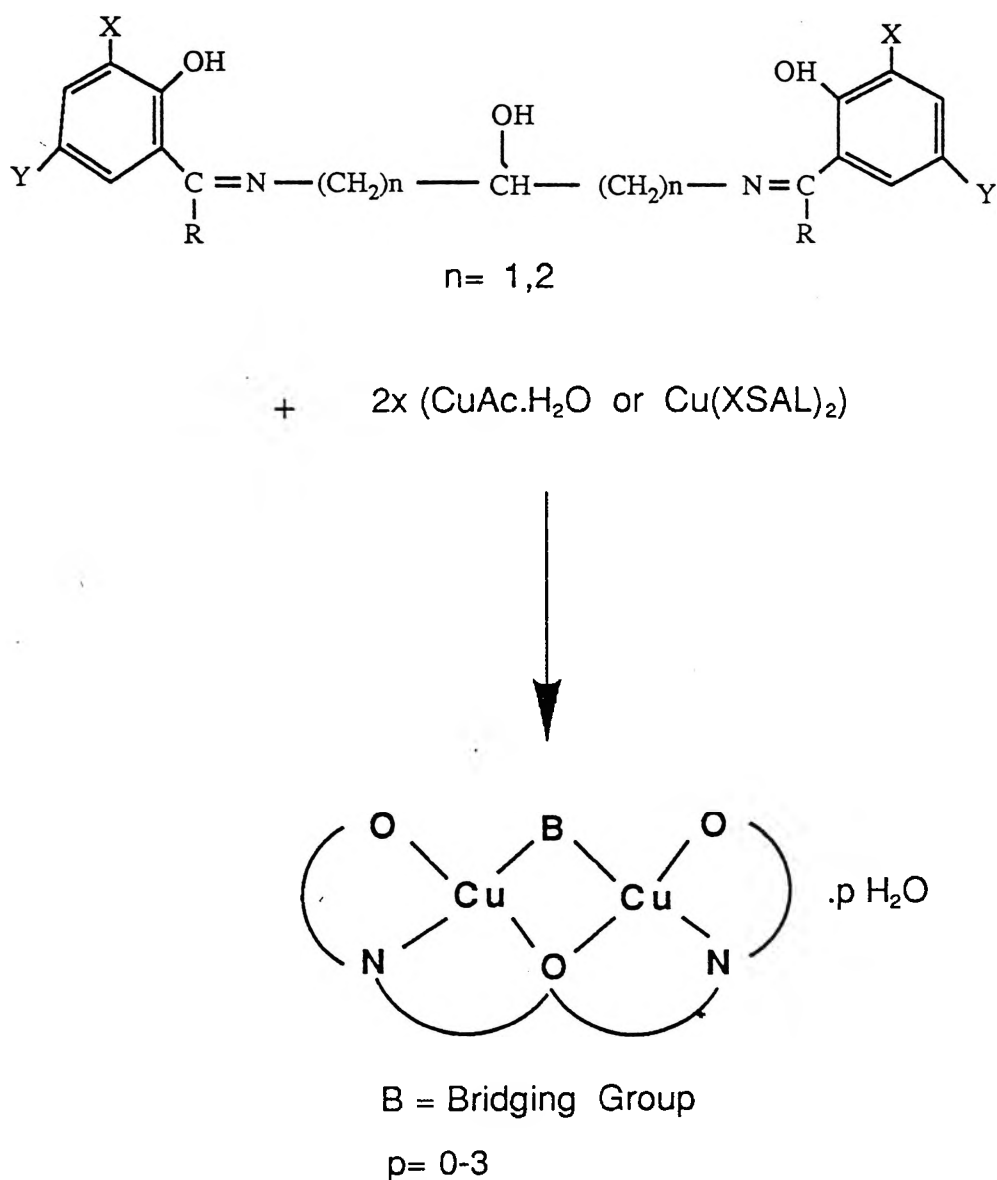


Fig 2.2: General Reaction Showing Formation of the Binuclear Complexes



Compound		%C	%H	%N	%H <sub>2</sub> O
Cu(SAL-DPL)H	Calculated	56.74	4.48	7.78	—
	Found	56.53	4.40	7.62	—
Cu <sub>2</sub> (SAL-DPL)OH.3H <sub>2</sub> O	C	41.38	4.49	5.68	10.95
	F	41.35	4.32	5.56	10.56
Cu <sub>2</sub> (SAL-DPE)OH.H <sub>2</sub> O	C	47.01	4.57	5.7	3.71
	F	46.58	4.63	5.59	3.68
Cu <sub>2</sub> (SAL-DPL)2-MeOEtO	C	48.29	4.46	5.63	—
	F	48.10	4.80	6.10	—
Cu <sub>2</sub> (SAL-DPL)O <sub>2</sub> .2H <sub>2</sub> O	C	41.63	3.90	5.71	—
	F	41.32	3.94	5.80	—
Cu <sub>2</sub> (SAL-DPL)O <sub>2</sub> H.(H <sub>2</sub> O) <sub>0.5</sub>	C	43.97	3.69	6.03	—
	F	44.00	3.70	6.30	—
Cu <sub>2</sub> (SAL-DPL)4-OHBzCOO	C	51.52	3.60	5.01	—
	F	51.53	3.59	4.90	—
<hr/>					
Cu <sub>2</sub> (SAL-DPL)(CAT) <sub>0.5</sub> (H <sub>2</sub> O) <sub>0.5</sub>	C	49.48	3.74	5.77	—
	F	49.65	3.59	5.80	—
Cu <sub>2</sub> (SAL-DPL)(3-MeOCAT) <sub>0.5</sub>	C	50.10	3.69	5.70	—
	F	50.20	3.74	5.74	—
Cu <sub>2</sub> (SAL-DPL)(3-MeCAT) <sub>0.5</sub>	C	50.93	3.75	5.79	—
	F	51.09	3.84	5.87	—
Cu <sub>2</sub> (SAL-DPL)(4-MeCAT) <sub>0.5</sub> (H <sub>2</sub> O) <sub>0.5</sub>	C	50.00	3.89	5.69	—
	F	49.73	3.57	5.45	—
Cu <sub>2</sub> (SAL-DPE)CATH.0.5H <sub>2</sub> O	C	52.81	4.43	4.93	—
	F	52.67	4.31	4.80	—
Cu <sub>2</sub> (SAL-DPE)4-NO <sub>2</sub> CATH	C	49.67	3.83	6.95	—
	F	49.65	4.22	7.35	—
Cu <sub>2</sub> (SAL-DPE)3-MeOCATH.0.5H <sub>2</sub> O	C	52.17	4.55	4.68	—
	F	52.34	4.33	4.57	—
<hr/>					
Cu <sub>2</sub> (SAL-DPL)Pz	C	49.08	3.71	11.45	—
	F	49.88	3.76	10.95	—
Cu <sub>2</sub> (ESAL-DPL)Pz	C	49.91	4.54	9.70	—
	F	49.56	4.82	9.99	—

Cu <sub>2</sub> (SAL-DPE)Pz	C	51.06	4.28	10.83	—
	F	51.12	4.15	10.84	—
Cu <sub>2</sub> (ESAL-DPE)Pz.H <sub>2</sub> O	C	50.07	5.17	8.98	—
	F	50.54	5.39	9.16	—
Cu <sub>2</sub> (SAL-DPL)3,5-Me <sup>2</sup> Pz	C	50.86	4.66	10.78	—
	F	52.10	4.55	9.90	—
Cu <sub>2</sub> (SAL-DPE)3,5-Me <sup>2</sup> Pz.0.5H <sub>2</sub> O	C	51.97	4.91	10.10	—
	F	52.30	4.82	9.11	—
Cu <sub>2</sub> (M <sup>2</sup> BP-DPL)3,5-Me <sup>2</sup> Pz.H <sub>2</sub> O	C	61.36	5.42	7.53	—
	F	60.97	5.40	7.34	—
Cu <sub>2</sub> (SAL-DPE)3-MePz	C	51.97	4.55	10.54	—
	F	51.53	4.66	7.91	—
Cu <sub>2</sub> (SAL-DPL)5-NO <sub>2</sub> Ind	C	50.98	3.78	11.43	—
	F	50.97	3.82	11.87	—
Cu <sub>2</sub> (SAL-DPE)6-NO <sub>2</sub> Ind	C	50.98	3.78	11.43	—
	F	50.91	3.69	11.70	—
Cu <sub>2</sub> (SAL-DPL)0.5(2-OHBzImid). 2H <sub>2</sub> O	C	49.90	3.99	8.31	—
	F	49.57	3.62	8.41	—
<hr/>					
"Cu <sub>2</sub> (SAL-DPL)NH <sub>2</sub> O.H <sub>2</sub> O"	C	43.62	4.70	8.71	—
	F	43.85	4.05	8.79	—
Cu <sub>2</sub> (SAL-DPL)2-PyO.(H <sub>2</sub> O) <sub>0.5</sub>	C	50.28	3.84	8.00	—
	F	50.57	4.22	7.79	—
Cu <sub>2</sub> (SAL-DPL)5-ClPyO.1.5H <sub>2</sub> O	C	45.72	3.66	7.27	—
	F	45.81	3.39	6.41	—
<hr/>					
Cu <sub>5</sub> (ESAL-DPL.6AIESAL) <sub>2</sub> .2H <sub>2</sub> O	C	52.88	4.56	8.34	2.15
	F	52.93	4.28	8.39	2.33
Cu <sub>5</sub> (SAL-DPL.4ABA.SAL) <sub>2</sub> .2H <sub>2</sub> O	C	49.64	4.17	6.20	—
	F	49.94	3.98	6.21	—
Cu <sub>5</sub> (SAL-DPL.PAB.SAL) <sub>2</sub> .3H <sub>2</sub> O	C	51.68	3.78	5.83	—
	F	51.58	3.89	5.65	—

Table 2.2: Empirical Formulae of Binuclear Copper Complexes

**3:**

**Infra-red Spectra**

### 3: Infra-Red Spectra of the Binuclear Copper Complexes

Selected infra-red stretching frequencies are given in Table 3.1 and FTIR results for selected compounds are given in Table 3.2. The spectra of all the complexes were measured in the range 4000-600 $\text{cm}^{-1}$  as Nujol mulls. Selected complexes were measured as potassium bromide disks over the range 4000 to 250 $\text{cm}^{-1}$  using a FTIR spectrophotometer.

#### Interpretation of Infra-Red Spectra

The imine band was readily identifiable by absorption peaks in the range 1600-1650 $\text{cm}^{-1}$  in all the complexes. The compounds containing water have a broad band in the 3450-3300 $\text{cm}^{-1}$  region.

Dioxygen bound to a metal ion has three possible forms and each has an O-O stretch in a distinctive position in the infra-red region of the spectrum.

These forms and the  $\nu_{\text{O-O}}$  stretching frequencies are:-

I) $\text{O}_2$ (molecular oxygen)	~1555 $\text{cm}^{-1}$ 133
II) $\text{O}_2^-$ (superoxo)	~1100 $\text{cm}^{-1}$ 133
III) $\text{O}_2^{2-}$ (peroxo)	900-800 $\text{cm}^{-1}$ 133

Examples of these types of bonding in metalloproteins are:-

Hemoglobin ( $O_2^-$ ) 1155 and 1107  $cm^{-1}$  \*,133

Hemerythrin ( $O_2^{2-}$ ) 844  $cm^{-1}$  \*,133

Hemocyanin ( $O_2^{2-}$ ) 747  $cm^{-1}$  \*,133

Both Hemoglobin and Hemerythrin possess non-symmetrically bound oxygen. This is shown by substituting  $O^{16}O^{18}$  for  $O^{16}_2$  resulting in the frequency being shifted and split, while there is no split in the oxygen frequency of Hemocyanin, by this substitution, indicating that the oxygen molecule is symmetrically bound to the metal atoms in Hemocyanin (Fig 3.1).<sup>133</sup>

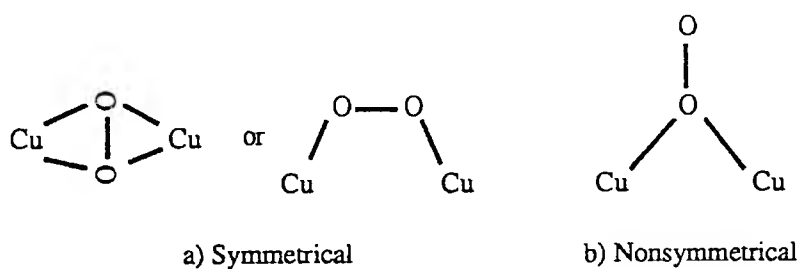


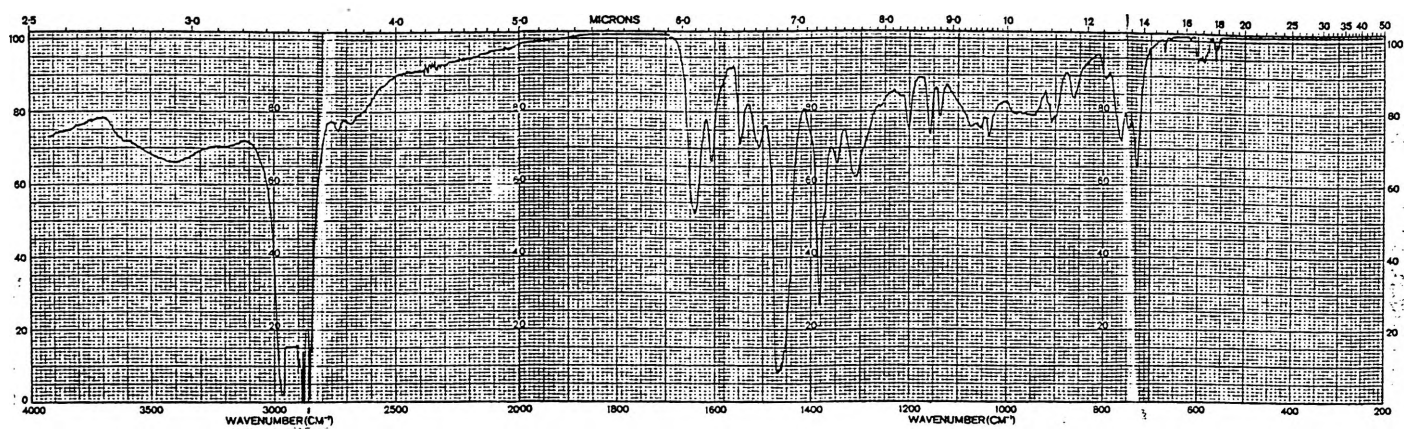
Fig 3.1: Symmetrical and Nonsymmetrical Oxygen Binding to Copper

FTIR results reveal that for  $Cu_2(SAL-DPL)O_2H.(H_2O)_{0.5}$  there is a peak at  $868cm^{-1}$  while in  $Cu_2(SAL-DPL)O_2.2H_2O$  there is a single peak at  $1067cm^{-1}$  which may be assigned to  $\nu_{O-O}$ . If the  $1067cm^{-1}$  band is due to  $\nu_{O-O}$  then it would have to be present as a superoxide bridging ion. This is in agreement with the formula of the complex,  $Cu(II)_2SAL-DPL^3-O_2^-$ . The  $868cm^{-1}$  band may be the  $\nu_{O-O}$  of the hydroperoxo bridge in  $Cu(II)_2SAL-DPL^3-O_2H^-$ .

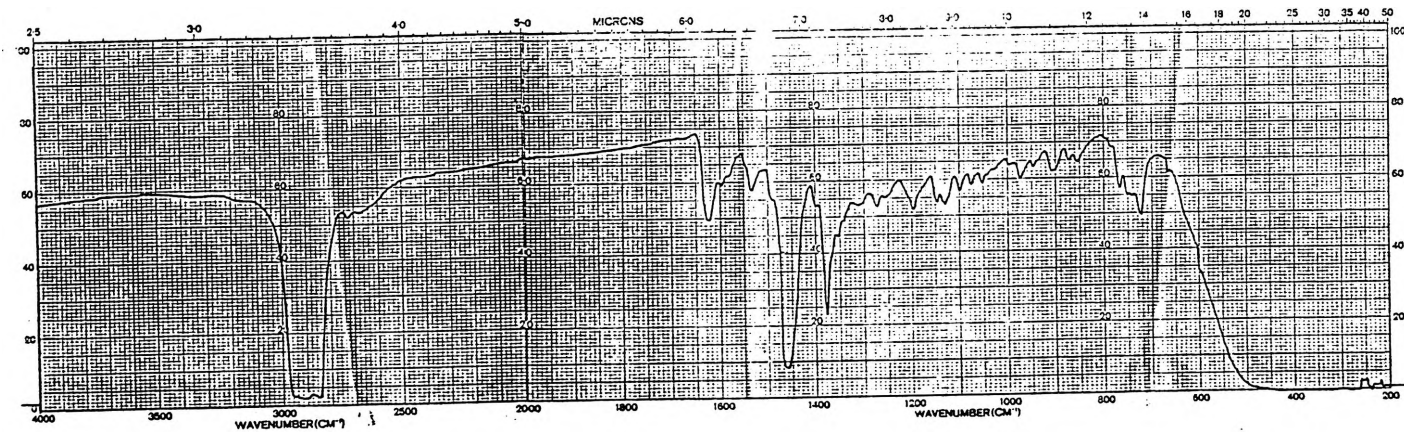
$O^{16}$ - $O^{18}$  isotope substitution experiments would be needed to confirm these assignments. Unfortunately due to the method of preparation<sup>120</sup> (which consists of passing oxygen gas through a suspension of copper powder and piperidine for a number of hours), these experiments would be too expensive to run (as a large amount of  $O_2^{18}$  would be required).

In the complex formed by reacting hydroxylamine with the ligand backbone and copper acetate. $H_2O$ , the presence of an N-H bond is shown in a peak at  $3150\text{cm}^{-1}$ . However the crystal structure indicates that hydroxylamine is not present in the complex and that the band is the result of a R-C-NH-Cu group (see Fig 6.1 crystal structure).

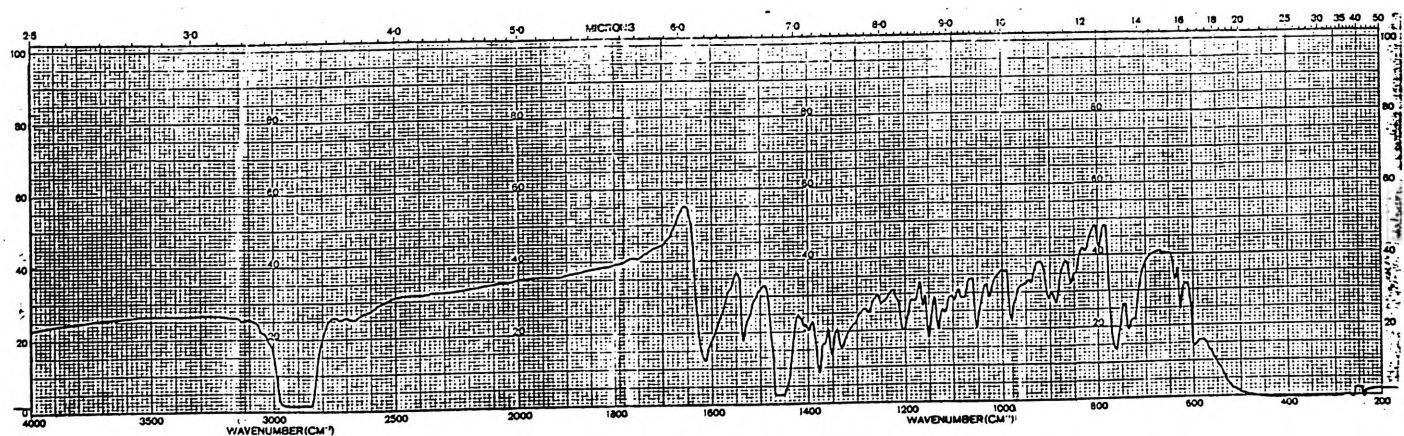
Selected IR spectra are shown in Fig 3.2 a) =  $\text{Cu}_2(\text{SAL-DPL})(\text{CAT})_{0.5}(\text{H}_2\text{O})_{0.5}$ , b) =  $\text{Cu}_2(\text{SAL-DPE})\text{CATH}(\text{H}_2\text{O})_{0.5}$  and c) =  $\text{Cu}_2(\text{SAL-DPE})\text{Pz}$ . Figs 3.3 to 3.5 show the FTIR spectra of  $\text{Cu}_2(\text{SAL-DPL})\text{OH}.3\text{H}_2\text{O}$ ,  $\text{Cu}_2(\text{SAL-DPL})\text{O}_2.2\text{H}_2\text{O}$  and  $\text{Cu}_2(\text{SAL-DPL})\text{O}_2\text{H}.(\text{H}_2\text{O})_{0.5}$



a)



b)



c)

Fig 3.2: Representative IR Spectrum of the Binuclear Complexes

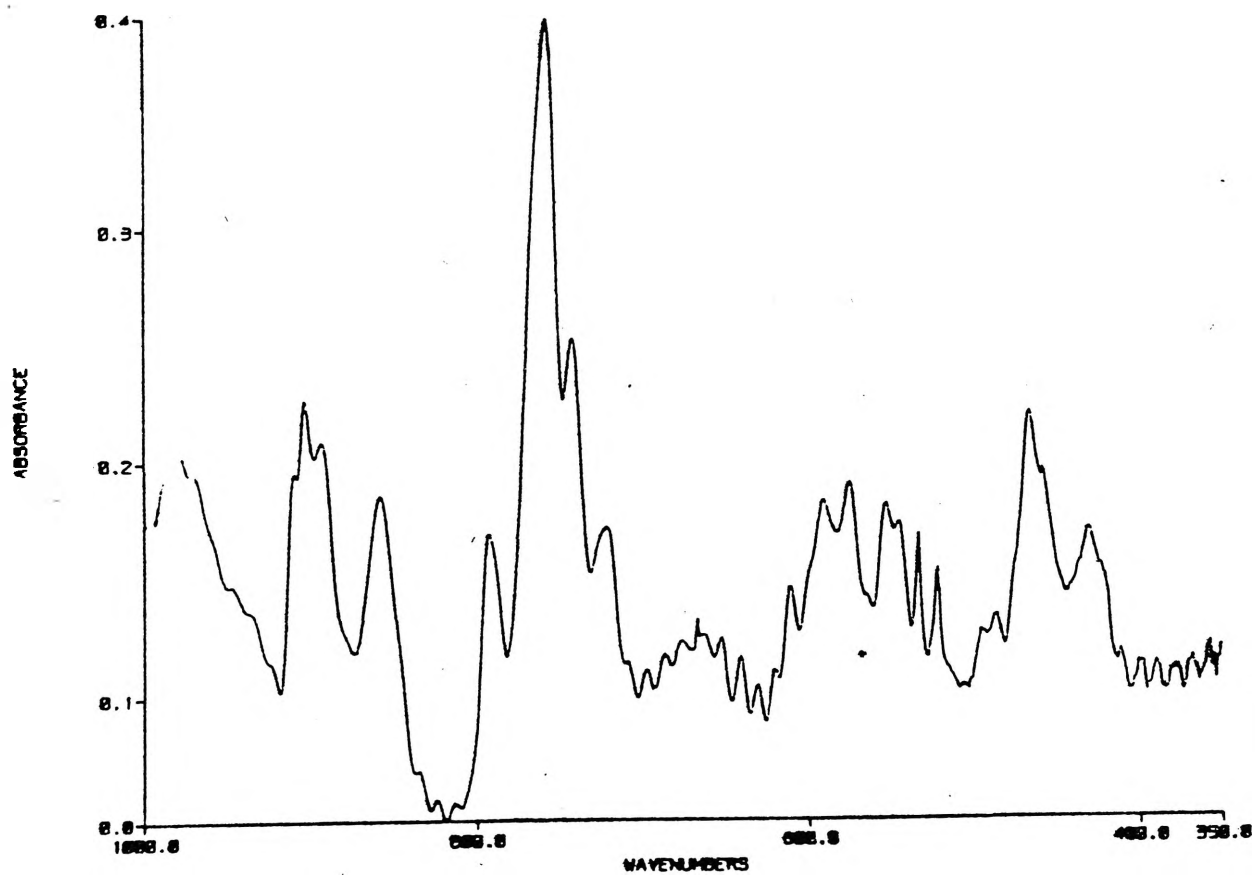
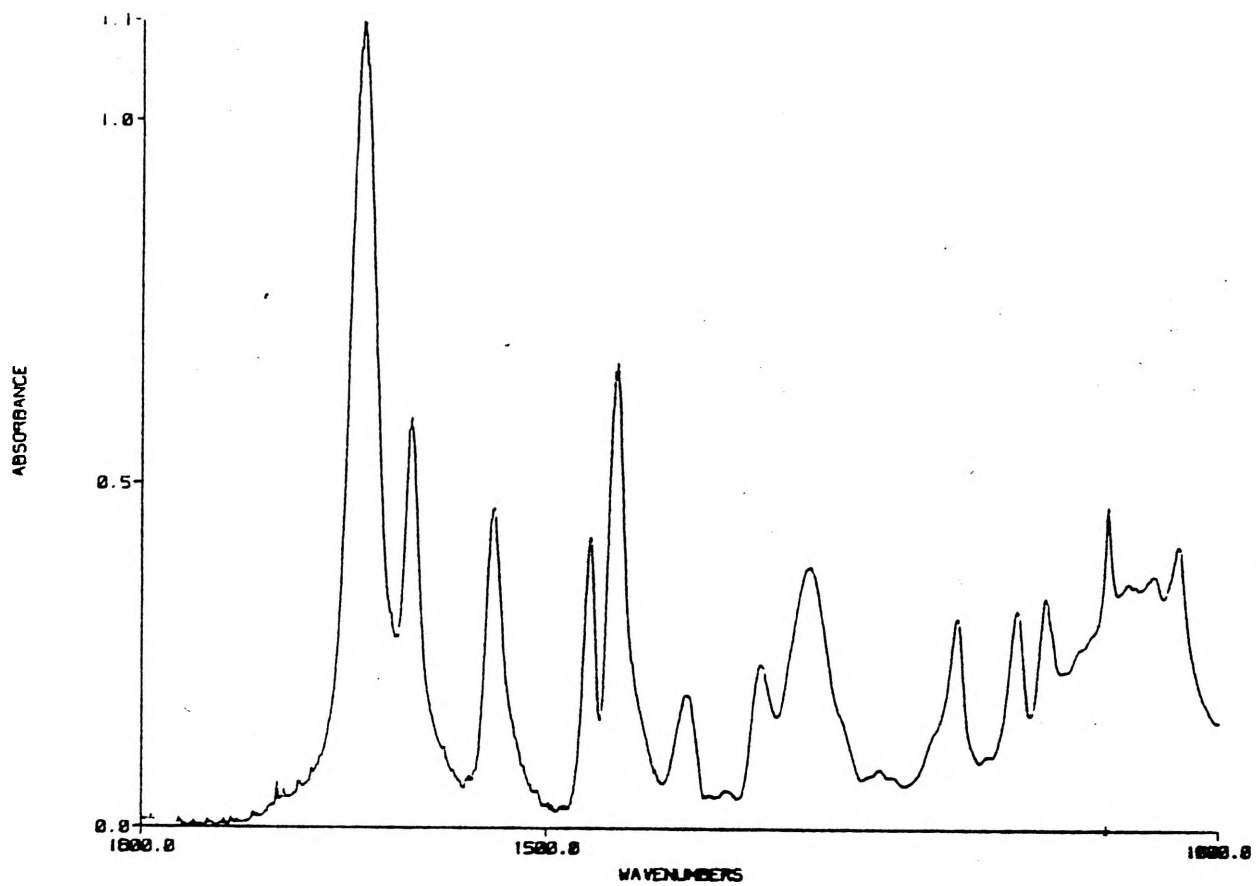


Fig 3.3: FTIR Spectra of  $\text{Cu}_2(\text{SAL-DPL})\text{OH}\cdot 3\text{H}_2\text{O}$



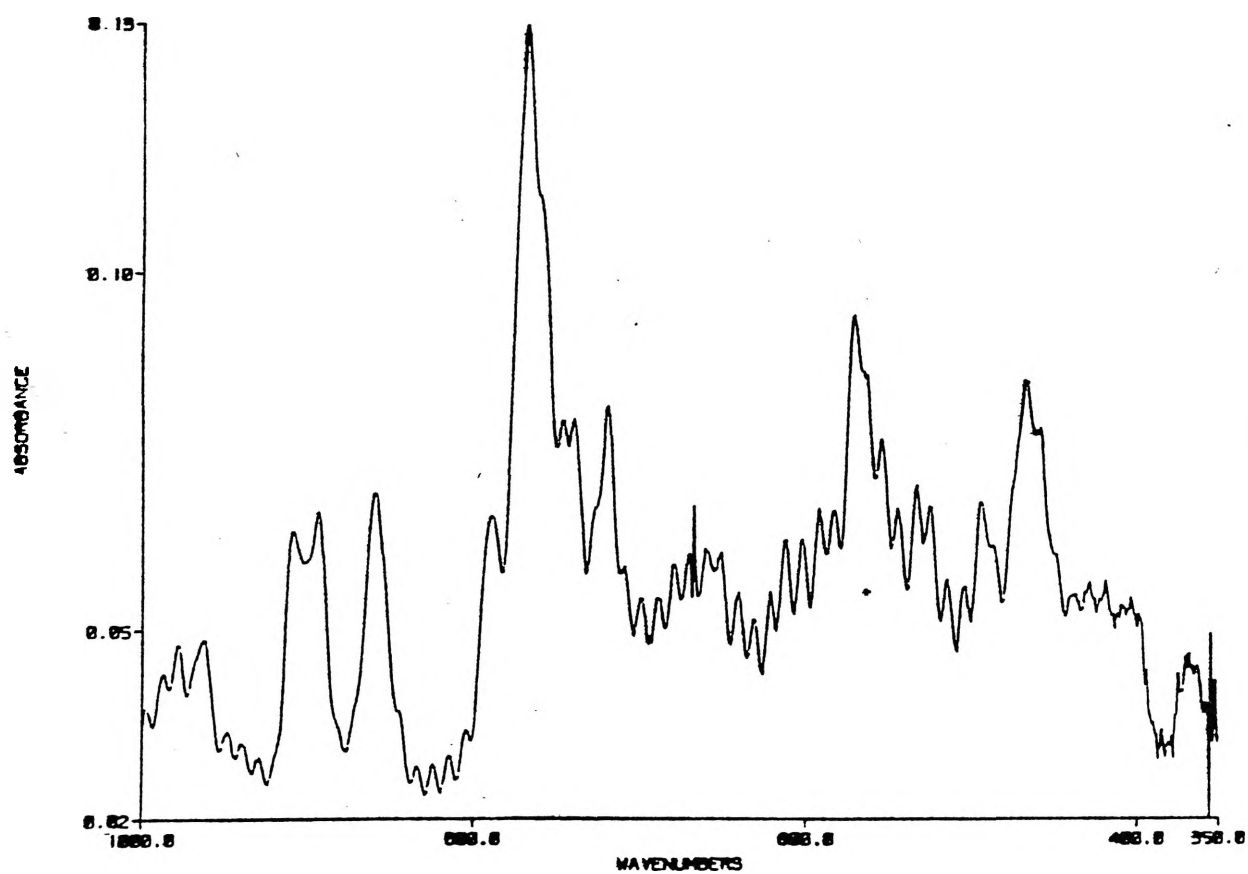
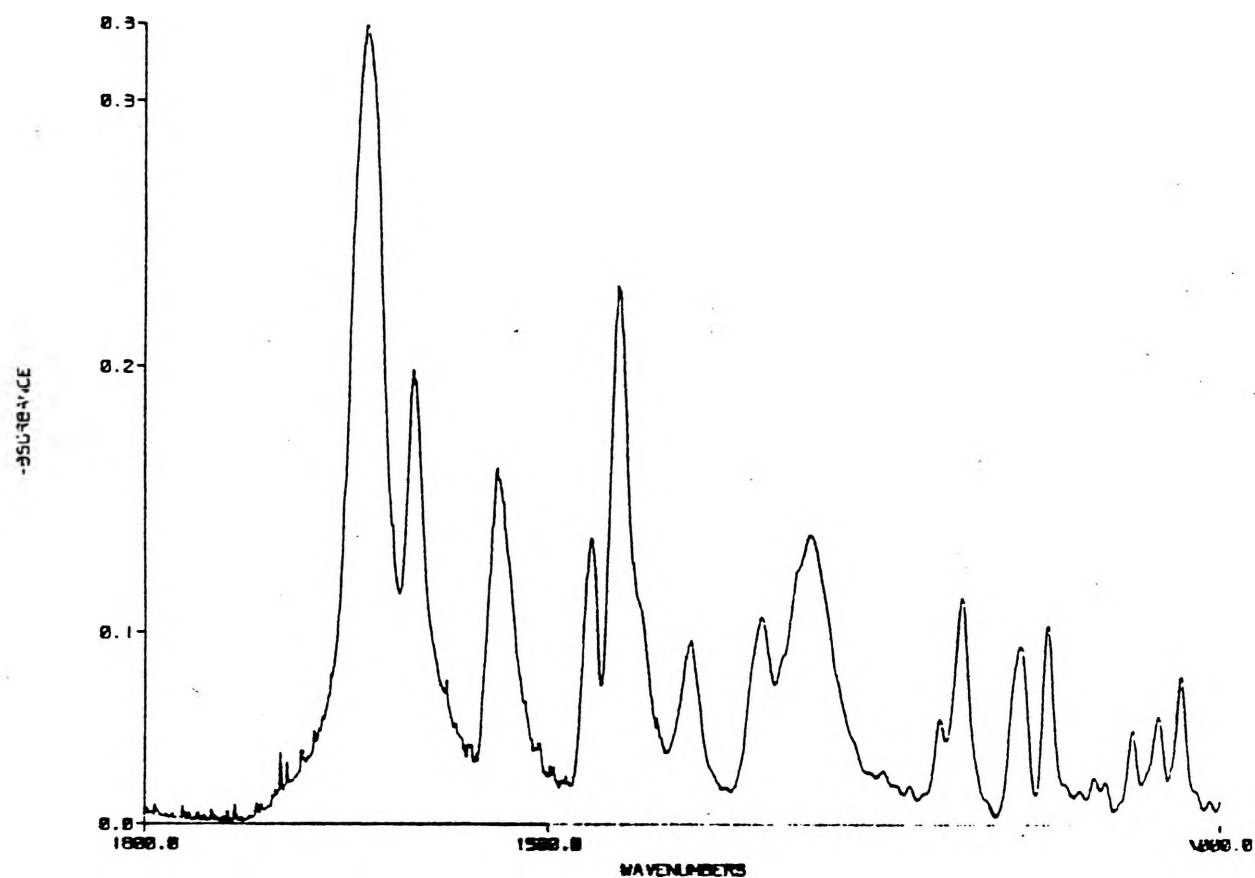


Fig 3.4: FTIR Spectra of  $\text{Cu}_2(\text{SAL-DPL})\text{O}_2 \cdot 2\text{H}_2\text{O}$

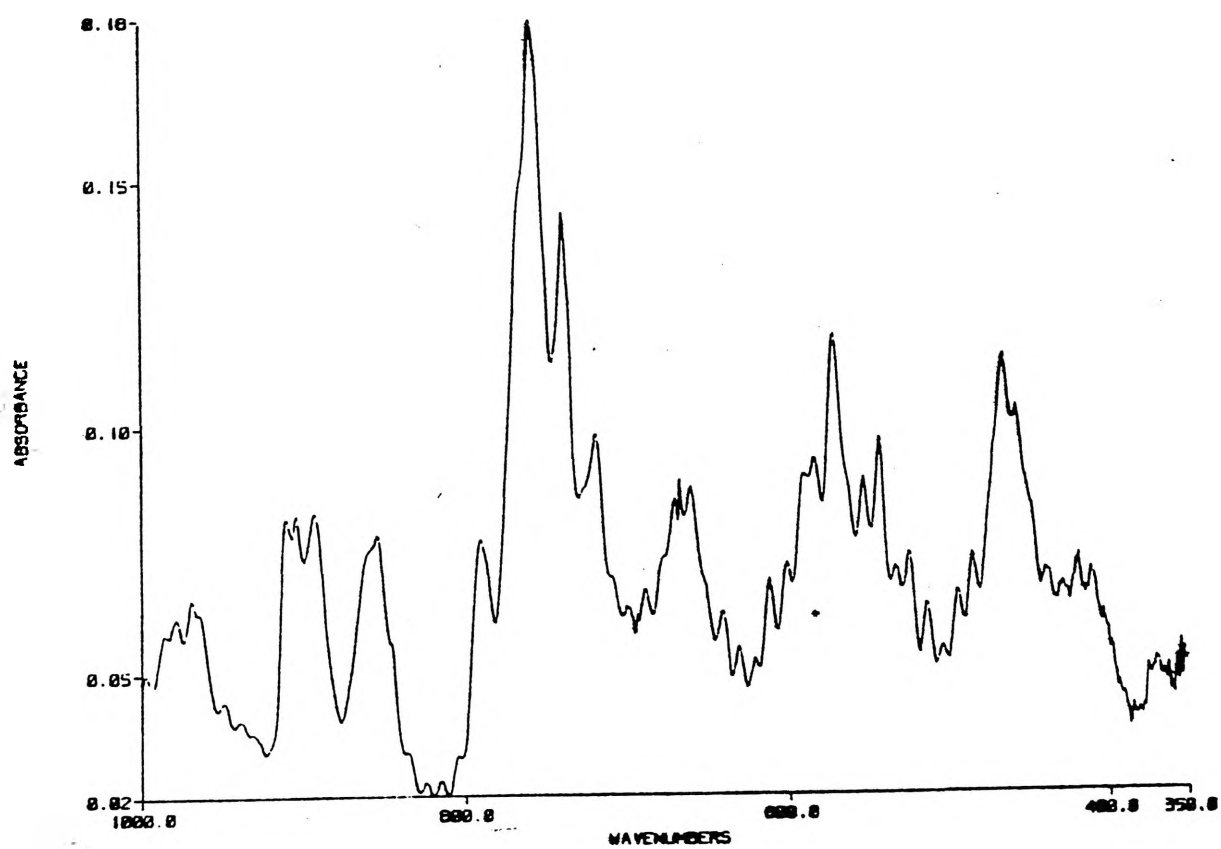
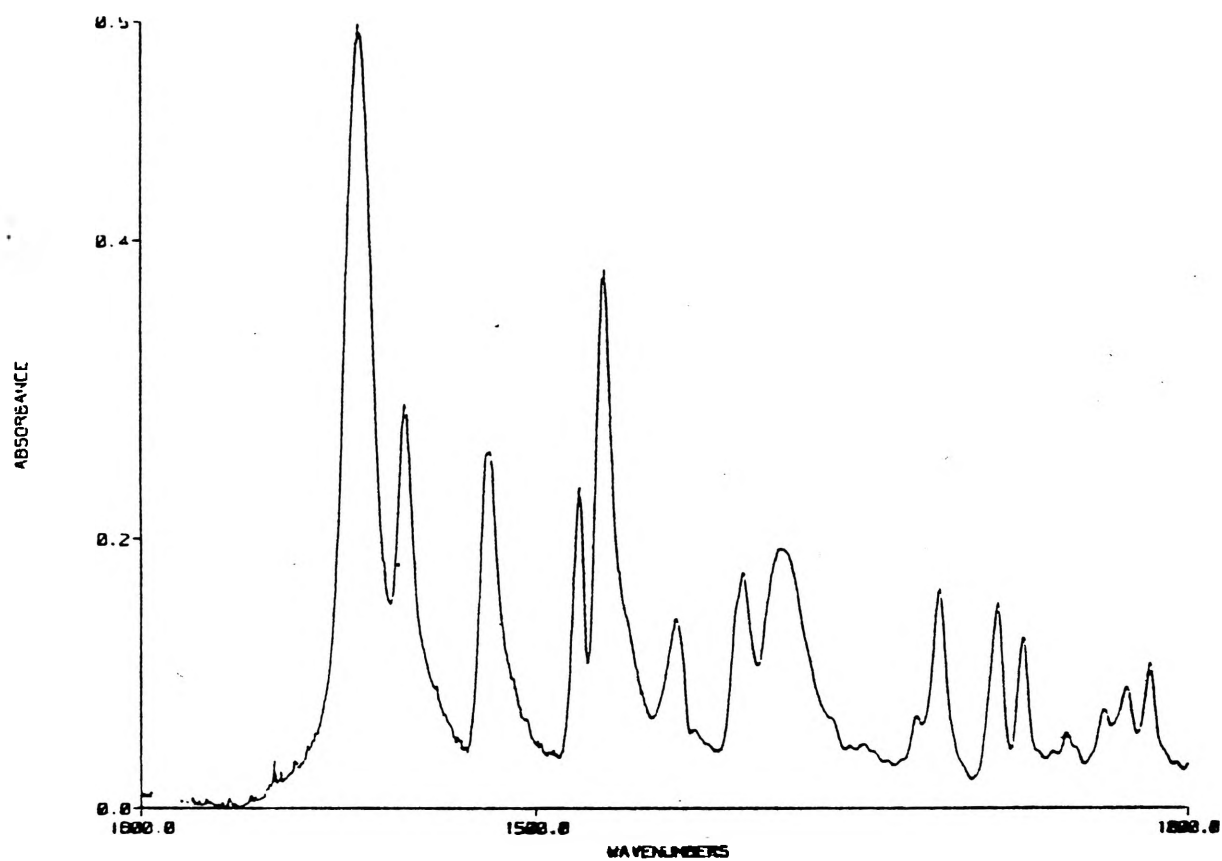


Fig 3.5: FTIR Spectra of  $\text{Cu}_2(\text{SAL-DPL})\text{O}_2\text{H} \cdot (\text{H}_2\text{O})_{0.5}$

COMPOUND	$\nu_{\text{C=N}}$	$\nu_{\text{O-H}}$	$\nu_{\text{N-H}}$
$\text{Cu}_2(\text{SAL-DPL})\text{O}_2 \cdot 2\text{H}_2\text{O}$	1640	3340	—
$\text{Cu}_2(\text{SAL-DPL})\text{O}_2 \cdot \text{H}_2\text{O} \cdot 0.5\text{H}_2\text{O}$	1630	3345	—
$\text{Cu}_2(\text{SAL-DPL})\text{CAT}_{0.5}(\text{H}_2\text{O})_{0.5}$	1635	—	—
$\text{Cu}_2(\text{SAL-DPL})(3\text{-MeCAT})_{0.5}$	1622	—	—
$\text{Cu}_2(\text{SAL-DPL})(4\text{-MeCAT})(\text{H}_2\text{O})_{0.5}$	1622	3310	—
$\text{Cu}_2(\text{SAL-DPL})(3\text{-MeOCAT})_{0.5}$	1630	—	—
$\text{Cu}_2(\text{SAL-DPE})\text{CATH}(\text{H}_2\text{O})_{0.5}$	1625	—	—
$\text{Cu}_2(\text{SAL-DPE})3\text{-MeOCATH}(\text{H}_2\text{O})_{0.5}$	1622	3315	—
$\text{Cu}_2(\text{SAL-DPE})4\text{-NO}_2\text{CATH}$	1615	—	—
<hr/>			
$\text{Cu}_2(\text{SAL-DPL})\text{OH} \cdot 3\text{H}_2\text{O}$	1632	3400	—
$\text{Cu}_2(\text{SAL-DPE})\text{OH} \cdot \text{H}_2\text{O}$	1634	3385	—
$\text{Cu}_2(\text{SAL-DPL})2\text{-MeOEtO}$	1635	—	—
$\text{Cu}_2(\text{SAL-DPL})4\text{-OHBzCOO}$	1640	—	—
<hr/>			
$\text{Cu}_2(\text{SAL-DPL})\text{Pz}$	1635	—	—
$\text{Cu}_2(\text{SAL-DPE})\text{Pz}$	1630	—	—
$\text{Cu}_2(\text{ESAL-DPL})\text{Pz}$	1630	—	—
$\text{Cu}_2(\text{ESAL-DPE})\text{Pz} \cdot \text{H}_2\text{O}$	1628	—	—
$\text{Cu}_2(\text{SAL-DPL})3,5\text{Me}_2\text{Pz}$	1612	—	—
$\text{Cu}_2(\text{SAL-DPE})3,5\text{Me}_2\text{Pz}$	1620	—	—
$\text{Cu}_2(\text{M}^2\text{BP-DPL})3,5\text{Me}_2\text{Pz} \cdot \text{H}_2\text{O}$	1630	3410	—
$\text{Cu}_2(\text{SAL-DPE})3\text{-MePz}$	1622	—	—
$\text{Cu}_2(\text{SAL-DPL})5\text{-NO}_2\text{InD}$	1612	—	—
$\text{Cu}_2(\text{SAL-DPE})6\text{-NO}_2\text{InD}$	1615	—	—
$\text{Cu}_2(\text{SAL-DPL})(2\text{-OBzIMID})_{0.5}(\text{H}_2\text{O})_2$	1630	—	—
<hr/>			
$\text{Cu}_2(\text{SAL-DPL})2\text{-PyO} \cdot (\text{H}_2\text{O})_{0.5}$	1640	3425	—
$\text{Cu}_2(\text{SAL-DPL})5\text{-ClPyO} \cdot 1.5\text{H}_2\text{O}$	1630	—	—
" $\text{Cu}_2(\text{SAL-DPL})\text{NH}_2\text{O} \cdot \text{H}_2\text{O}$ "	1645	3400	3150

Table 3.1: I.R. Results for the Binuclear Copper Complexes

Cu(SAL-DPL)H	Cu <sub>2</sub> (SAL-DPL) O <sub>2</sub> H.(H <sub>2</sub> O) <sub>0.5</sub>	Cu <sub>2</sub> (SAL-DPL) O <sub>2</sub> .2H <sub>2</sub> O	Cu <sub>2</sub> (SAL-DPL) OH.3H <sub>2</sub> O
—	495	—	488
521	518	—	—
—	586	—	—
608	602	—	—
647	—	—	—
—	667	660	667
—	674	—	671
700	699	—	707
—	741	721	740
—	765	766	—
—	791	—	793
851	852	845	—
—	868	—	—
931	932	—	—
945	—	—	—
965	970	964	968
985	981	989	985
—	1035	—	—
—	1059	1056	—
1065	—	1067	—
1078	1094	1089	1086
1240	1250	1249	—
1264	—	1263	—
1283	1277	—	—
1318	1325	1326	—

Table 3.2: Selected FTIR Data

**4:**

**UV-Vis Spectra**

#### 4: UV-Vis Spectra of the Copper Complexes

Type III copper proteins exhibit a number of charge transfer and d-d transition spectral bands in the UV-Visible region. The d-d bands can be accounted for by assigning four and/or five coordination to the copper(II) atoms.<sup>134</sup>

The precise assignment of structure and coordination around the copper(II) atom based solely upon spectral evidence is made more difficult due to the overlap of the three available d-d transitions in tetragonally distorted copper(II) complexes, Fig 4.1.<sup>135</sup>

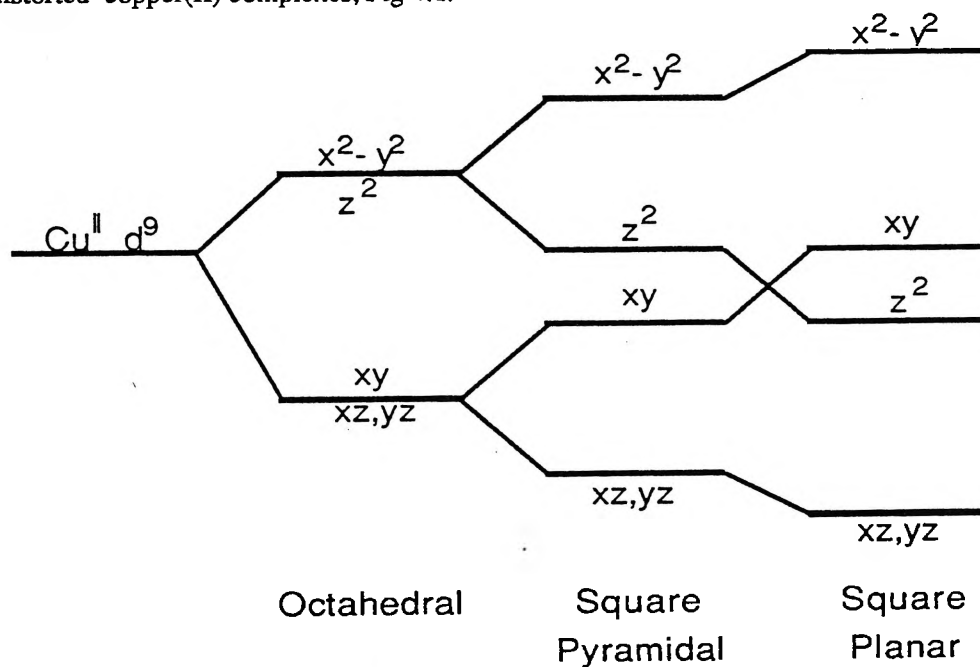


FIG 4.1:<sup>135</sup> d Orbital Splitting for Copper (II) in Different Stereochemistries

Knowledge of a complex's structure allows tentative correlation of structure to spectral data. Generally square planar copper (II) spectra exhibit the highest energy bands with a broad band between 500-900 nm (Table 4.1)<sup>136</sup> which may be resolved into two or three bands. These transitions are from  $(dxz, dyz)$ ,  $dz^2$  and  $dxy$  to the  $dx^2-y^2$  level. Square pyramidal copper (II) also shows a broad absorption band, though at slightly higher wavelengths, between 700-900 nm (Table 4.1). This band exhibits maximum intensity at lower wavelengths.

The d-d spectra of trigonal bipyramidal copper (II) is similar to that of square pyramidal copper (II), although only two transitions are available. The broad band occurs between 700-1000 nm (Table 4.1) with the maximum intensity occurring at higher wavelengths.

Tetrahedral copper (II) has the highest wavelengths, with a broad band occurring between 700 nm and 1400 nm (Table 4.1).

Copper (I) complexes have no d-d transitions due to their full  $d^{10}$  configuration, so structural assignment is even more difficult for copper (I) complexes.

The position of the peaks is dependent upon the ligand field strength of the ligand as shown by the spectrochemical series.

Copper Configuration	Wavelength (nm)	Comment
Square Planar	500-900	broad, 2-3 bands possible
Square Pyramidal	700-900	broad, maximum intensity at lower wavelengths
Trigonal Bipyramidal	700-1000	broad, maximum intensity at higher wavelengths
Tetrahedral	700-1400	broad

Table 4.1:<sup>136</sup> Optical Properties of Copper (II) Geometries

Table 4.2 lists the optical properties of the hemocyanin and multi-copper oxidases along with their extinction coefficients where known.

Copper Protein	Wavelength (nm)	$\epsilon$ (M <sup>-1</sup> cm <sup>-1</sup> )
<u>Hemocyanin</u>		
Molluscan		
<i>Busycon</i> <sup>25</sup>	350	20000
	570	1180
Arthropod		
<i>Cancer</i> <sup>25</sup>	350	20000
	430	1700
	570	1090
	680	890
<u>Blue Oxidases</u>		
Laccase <sup>137-139</sup>		
<i>Rhus</i>	330	3000
	450	
	~600	4000-6000
	700	
	800	
	1000	
	1700	
Ceruloplasmin <sup>140-141</sup>		
	330	
	450	
	~600	4000-6000
	750	
	850	
	1000	
Ascorbate Oxidase <sup>142-144</sup>		
	330	
	~600	4000-6000
	750	

Table 4.2: Optical Properties of Copper Proteins



The UV-Vis spectra data is collected in Table 4.3. The spectra were recorded between 450 and 750nm in the solid state (as nujol mulls on filter paper) and in solution (between  $1 \times 10^{-3}$  and  $1 \times 10^{-4}$ M) in dichloromethane and DMF.

Murray et al.<sup>114</sup> synthesised  $\text{Cu}_2(\text{SAL-DPL})\text{Pz}$  and solved its crystal structure. It was found that the two copper atoms are in a square planar configuration with each copper atom bound to two nitrogen and two oxygen atoms. This complex exhibits a single peak in the solid state at 560nm and in solution at 570nm with an intensity of 587 to  $680 \text{ M}^{-1} \text{ cm}^{-1}$  in solvents including chloroform, acetonitrile, DMF, methanol and water. Murray et al. assigned this peak as representing a d-d square planar geometry around the copper centres.

Erickson<sup>120</sup> also synthesised  $\text{Cu}_2(\text{SAL-DPL})\text{Pz}$  and solved the crystal structure of this complex, and as with Murray et al.,<sup>114</sup> the copper atoms were found to be square planar in geometry. In the solid state the peak at 560nm was assigned as a d-d transition indicating square planar geometry. This peak shifts to 570nm in solution with an intensity of 632 in dichloromethane and  $748 \text{ M}^{-1} \text{ cm}^{-1}$  in DMF.

The similarity of the spectra of  $\text{Cu}_2(\text{SAL-DPL})\text{Pz}$  to that of molluscan oxyhemocyanin suggests that the copper atoms in molluscan oxyhemocyanin may be in a similar environment to that of the model complex  $\text{Cu}_2(\text{SAL-DPL})\text{Pz}$  i.e.  $\text{Cu}_2\text{N}_2\text{O}_2$ . This possibility is consistent with the EAXFS data of oxyhemocyanin which indicates that each copper atom is bound to two or three histidine nitrogens, a dioxygen oxygen atom and a hydroxide oxygen atom. While there may be a charge transfer contribution to the band at 570nm in molluscan oxyhemocyanin, it would seem more likely that the band is a d-d band indicating square planar copper.

a) Pyrazole-Type Bridged Complexes ( $\text{CuN}_2\text{O}_2$ )

1)  $\text{Cu}_2(\text{SAL-DPL})\text{X}$ , X= Pyrazoles and Indazoles

In the solid state spectra of these complexes the d-d transitions are assigned to peaks in the range 550 to 600nm, the same as Murray et al.<sup>114</sup> and Erickson<sup>120</sup> in regards to  $\text{Cu}_2(\text{SAL-DPL})\text{Pz}$ . As was the case for Murray et al.<sup>114</sup> and Erickson<sup>120</sup> this probably indicates that the copper atoms are in a square planar environment in these complexes. In dichloromethane and DMF this peak is found at 570 to 610nm and 570 to 625nm respectively. The only complex that shows a significant shift in peak position on dissolution is  $\text{Cu}_2(\text{ESAL-DPL})\text{Pz}$  which shifts from 560nm in the solid state to 625nm in dichloromethane and 640nm in DMF. This may indicate formation of a DMF adduct in DMF solution. It is unlikely that dichloromethane would also act as a coordinating solvent.<sup>136</sup>

All the complexes have peak intensities similar to that of the  $\text{Cu}_2(\text{SAL-DPL})\text{Pz}$  complex and as a result of the peak positions and intensities these peaks are assigned to a d-d transition for square planar copper (II).

11)  $\text{Cu}_2(\text{SAL-DPE})\text{X}$

X= Pyrazoles and Indazoles

The  $\text{Cu}_2(\text{SAL-DPE})\text{X}$  complexes exhibit a single peak at 570 to 600nm in the solid state and a peak at 585nm in dichloromethane and 585 to 595nm in DMF. The peak intensities of these complexes in solution are similar to those of the  $\text{Cu}_2(\text{SAL-DPL})\text{X}$  complexes. This peak is assigned, in all the complexes, as a d-d transition indicating a square planar geometry around each of the copper atoms.

Both the  $\text{Cu}_2(\text{SAL-DPL})\text{X}$  and  $\text{Cu}_2(\text{SAL-DPE})\text{X}$  complexes possess an  $\text{N}_2\text{O}_2$  environment around each copper atom which results in these complexes having a strong ligand field around each copper atom which influences the peak position. There is no obvious difference in spectral properties between the SAL-DPL complexes and the SAL-DPE complexes.

#### b) Oxygen-Type Bridged Complexes ( $\text{CuNO}_3$ )

##### 1. Catechol Bridged Complexes

##### 1.1 $\text{Cu}_2(\text{SAL-DPL})(\text{XCAT})_{0.5}$

The  $\text{Cu}_2(\text{SAL-DPL})(\text{XCAT})_{0.5}$  complexes exhibit a single peak in the range 620 to 655nm in the solid state and a peak at 590 to 625nm in dichloromethane and 600 to 630nm in DMF. As these complexes only differ from the pyrazole-type bridged complexes in the nature of the exogenous bridge it would seem, given the similarity in peak position, that this peak is indicative of a square planar geometry around each copper atom. The peak intensities of these complexes ( $265$  to  $368\text{M}^{-1}\text{cm}^{-1}$  in dichloromethane and  $210$  to  $391\text{M}^{-1}\text{cm}^{-1}$  in DMF) are, on average, lower than found in the pyrazole complexes. The shift to higher wavelengths of the peaks indicates the presence of a slightly weaker ligand field which is consistent with the  $\text{CuNO}_3$  versus the  $\text{CuN}_2\text{O}_2$  environment.

##### 1.2 $\text{Cu}_2(\text{SAL-DPE})\text{XCATH}$

The  $\text{Cu}_2(\text{SAL-DPE})\text{XCATH}$  complexes exhibit a single peak at 540 to 615nm in the solid state, a peak at 530 to 630nm in dichloromethane and 570 to 620nm in DMF. As for the  $\text{Cu}_2(\text{SAL-DPL})(\text{XCAT})_{0.5}$  complexes, this peak can be assigned as a d-d transition indicating square planar geometry around each copper atom. In solution the peak occurs as a shoulder on a very intense charge transfer band of maxima below 400nm in wavelength. This charge transfer band was not investigated as it reveals nothing about the stereochemistry surrounding the copper atoms. It is difficult to draw any conclusions about the relative ligand field strength of these complexes because most of these bands were present as shoulders on the side of the intense charge transfer band.

## 2. $\text{Cu}_2(\text{SAL-DPL})\text{O}_2$ , $\text{Cu}_2(\text{SAL-DPL})\text{O}_2\text{H}$ and $\text{Cu}_2(\text{SAL-DPL})\text{p-OHBzCOO}$

The complexes exhibit a single peak at 620 to 635nm in the solid state, 625 to 630nm in dichloromethane and 625nm in DMF. This peak is assigned to a d-d transition indicating a square planar geometry around each copper atom. Given the peak intensity of these peaks ( $310$  to  $343\text{M}^{-1}\text{cm}^{-1}$  in dichloromethane and  $237$  to  $394\text{M}^{-1}\text{cm}^{-1}$ ) it would seem unlikely that the peak is representative of a charge transfer band. There is no shift in the peak wavelength in DMF compared to dichloromethane and the solid state spectra. This indicates that in these complexes there is no DMF coordination upon dissolving in this solvent.

## 3. $\text{Cu}_2(\text{SAL-DPL})2\text{-MeOEtO}$ , $\text{Cu}_2(\text{SAL-DPL})\text{OH}$ and $\text{Cu}_2(\text{SAL-DPE})\text{OH}$

These complexes exhibit a single peak at 610 to 635nm in the solid state and at 585 to 630nm in dichloromethane and 585 to 635nm in DMF. This result again suggests square planar copper (II) in both the solid state and in solution.

## c) $\text{Cu}_2(\text{SAL-DPL})\text{XPyO}$

These complexes exhibit a single peak at 590 to 610nm in the solid state and at 610 to 615nm in dichloromethane and 625 to 630nm in DMF. This peak suggests that the copper (I) is square planar in configuration in the solid state and shifts to five coordinate in DMF solution.

Some examples of the solid state, dichloromethane and DMF solution UV-Vis spectras of selected complexes are shown in Figs 4.1, 4.2 and 4.3.

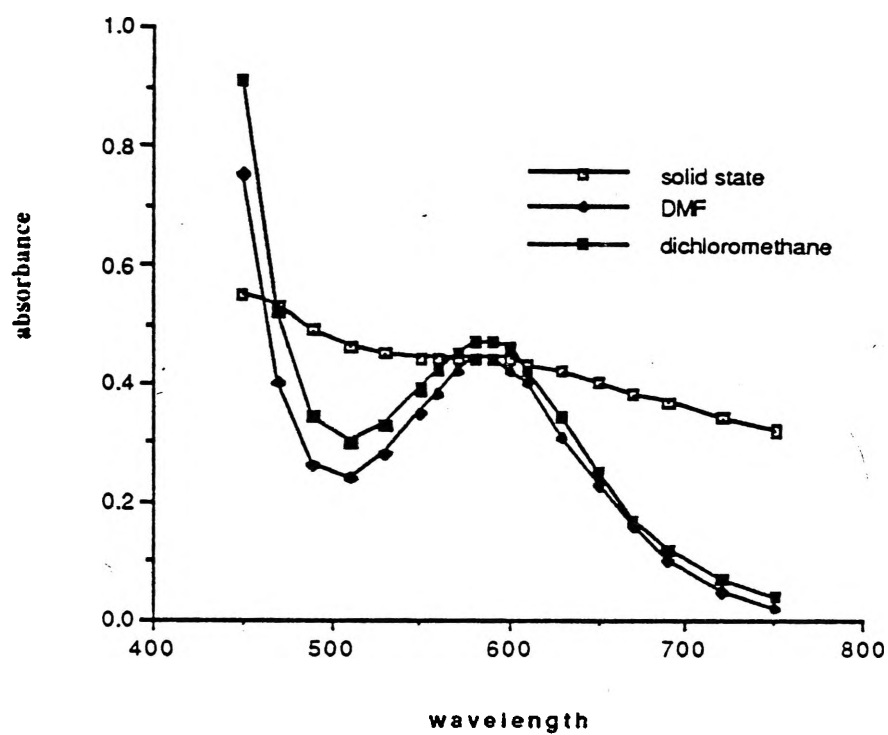


Fig 4.1: UV-Vis Spectra of  $\text{Cu}_2(\text{SALDPE})\text{Pz}$

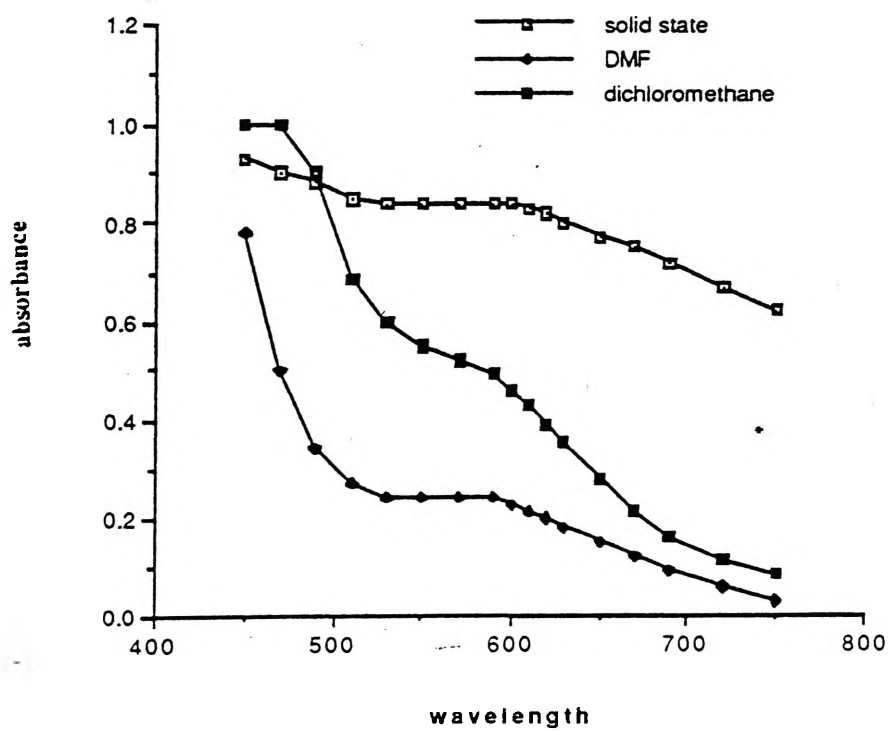


Fig 4.2: UV-Vis Spectra of  $\text{Cu}_2(\text{SALDPE})\text{CATH}$

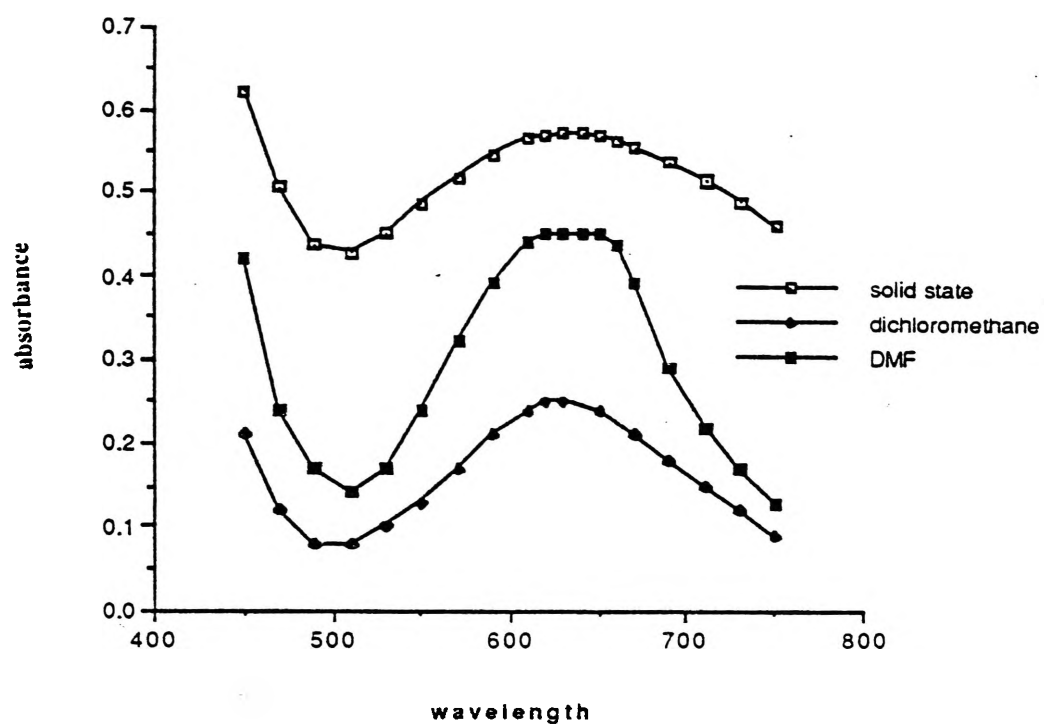


Fig 4.3: UV-Vis Spectra of  $\text{Cu}_2(\text{SALDPL})\text{MeOEtO}$

Compound	S.S*	DCM			DMF		
		$\lambda$	$\epsilon$	$10^{-3}M$	$\lambda$	$\epsilon$	$10^{-3}M$
		nm			nm		
Cu(SAL-DPL)H**	610	—	—	—	620	152	0.58
Cu <sub>2</sub> (SAL-DPL)Pz	560	570	748	0.82	570	632	0.77
Cu <sub>2</sub> (ESAL-DPL)Pz	560	570	632	0.9	570	711	0.81
Cu <sub>2</sub> (SAL-DPE)Pz	580	585	443	1.1	590	422	1.04
Cu <sub>2</sub> (ESAL-DPE)Pz	570	585	233	0.61	585	311	0.39
Cu <sub>2</sub> (SAL-DPE)3-MePz	600	585	303	0.96	595	346	1.1
Cu <sub>2</sub> (SAL-DPL)3,5-Me <sub>2</sub> Pz	600	610	427	0.60	610	477	0.91
Cu <sub>2</sub> (SAL-DPE)3,5-Me <sub>2</sub> Pz.0.5H <sub>2</sub> O	590	585	251	0.96	585	296	1.1
Cu <sub>2</sub> (M <sup>2</sup> BP-DPL)3,5-Me <sub>2</sub> Pz.H <sub>2</sub> O	600	610	635	0.56	610	520	0.71
Cu <sub>2</sub> (SAL-DPL)5-NO <sub>2</sub> Ind	580	585	451	1.1	595	400	0.95
Cu <sub>2</sub> (SAL-DPE)6-NO <sub>2</sub> Ind	590	585	491	1.01	595	414	1.01
Cu <sub>2</sub> (SAL-DPL)(2-OHBzImid) <sub>0.5</sub> .2H <sub>2</sub> O	610	615	425	0.99	625	420	1.01
Cu <sub>2</sub> (SAL-DPL)(CAT) <sub>0.5</sub> (H <sub>2</sub> O) <sub>0.5</sub>	630	620	265	0.91	630	391	0.97
Cu <sub>2</sub> (SAL-DPL)(3-MeCAT) <sub>0.5</sub>	655	590	330	0.91	600	210	0.9

Table 4.1: UV-Vis Data For Copper Complexes

\* S.S = solid state, \*\* Cu(SAL-DPLH) is insoluble in DCM

Compound	S.S*	DCM			DMF		
		$\lambda$	$\epsilon$	$10^{-3}M$	$\lambda$	$\epsilon$	$10^{-3}M$
		nm			nm		
$Cu_2(SAL-DPL)(3-MeOCAT)_{0.5}$	620	625	368	1.1	610	300	1.01
$Cu_2(SAL-DPL)(4-MeCAT)_{0.5}$ ( $H_2O$ ) <sub>0.5</sub>	625	610	310	0.94	620	210	1.1
$Cu_2(SAL-DPE)CATH(H_2O)_{0.5}$	590	570	sh***	1.01	570	sh	0.95
$Cu_2(SAL-DPE)3-MeOCATH$ ( $H_2O$ ) <sub>0.5</sub>	540	530 630	sh sh	1.01	590	sh	1.01
$Cu_2(SAL-DPE)4-NO_2CATH$	615	605	299	0.73	620	173	0.38
$Cu_2(SAL-DPL)O_2.2H_2O$	630	625	310	1.33	625	342	1.53
$Cu_2(SAL-DPL)O_2H(H_2O)_{0.5}$	620	630	325	0.72	625	394	0.94
$Cu_2(SAL-DPL)4-OHBzCOO$	635	630	343	2.86	625	237	2.31
$Cu_2(SAL-DPL)MeOEtO$	635	630	247	1.02	635	469	0.97
$Cu_2(SAL-DPL)OH.3H_2O$	620	590	373	2.63	595	485	1.96
$Cu_2(SAL-DPE)OH.H_2O$	610	585	434	0.94	585	325	0.93
$Cu_2(SAL-DPL)2-PyO$ ( $H_2O$ ) <sub>0.5</sub>	600	610	489	0.94	630	386	1.01
$Cu_2(SAL-DPL)5-ClPyO$ 1.5 $H_2O$	590	610	483	1.14	630	436	0.99

Table 4.1: UV-Vis Data For Copper Complexes

\* S.S = solid state, \*\*\* sh = shoulder



**5:**

**Magnetism**

### 5: Magnetism of the Binuclear Copper (II) Complexes

Investigation of the magnetic properties of Type III copper proteins indicates that the binuclear copper II atoms undergo antiferromagnetic interaction via a superexchange pathway.<sup>145</sup>

The degree of interaction can be determined through the magnetic susceptibility ( $\chi$ ) defined by the equation:<sup>146</sup>

$$\chi = \frac{-N}{H} \frac{\sum_{i=1}^n \left( -\frac{\partial e^i}{\partial H} \right) e^{-E_i/kT}}{\sum_{i=1}^n e^{-E_i/kT}}$$

N = Avagadros number

H = applied magnetic field

$E_i$  = energy of level i expressed as a convergent series in H ( $E_i = E_i + E_i H + E_i H^2 + \dots$ )

k = Boltzman's Constant

T = Temperature (absolute)

This can be modified through a series of steps<sup>146-148</sup> to give the Bleaney-Bowers equation.<sup>149</sup>

$$\chi = \frac{2N g^2 \beta^2}{3kT} [1 + (1/3)e^{-2J/kT}]^{-1}$$

$\chi$  is expressed here as per copper ion.

This equation satisfactorily explains the observed magnetic behaviour in a number of binuclear copper II complexes.

There are a number of factors which affect the degree of interaction between the copper II atoms:150

- 1) the copper- $\theta$ -copper and copper- $\omega$ -copper angles, where x and y are bridging groups (Fig 5.1)
- 11) the dihedral angle ( $\tau$ ) of the complex, i.e. the planarity of the complex (Fig 5.2)
- 111) the nature of the bridging groups and binding method.

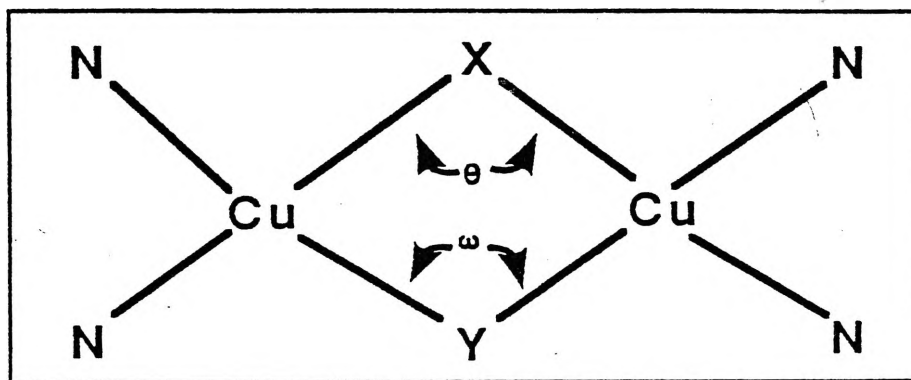


FIG 5.1: Copper- $\theta$ -Copper and Copper- $\omega$ -Copper Angles

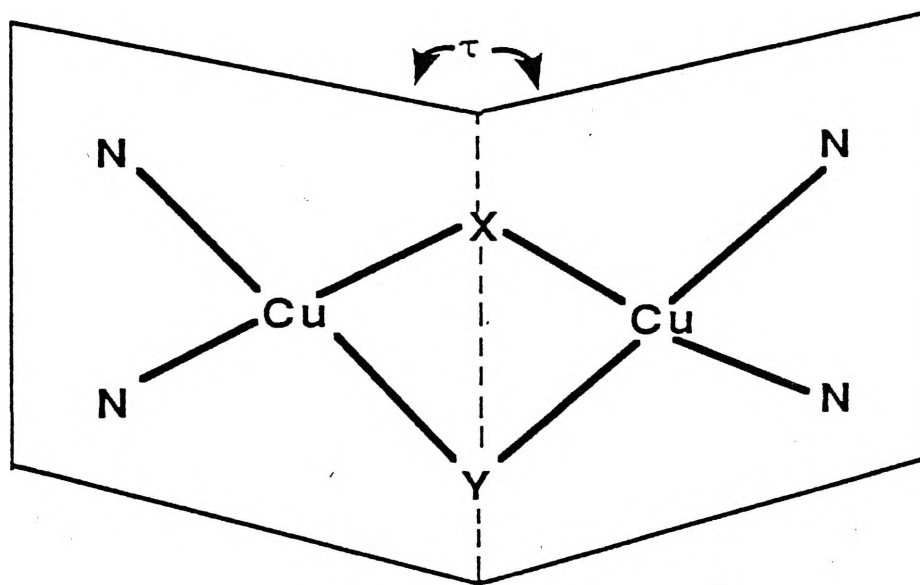


FIG 5.2: Dihedral Angle ( $\tau$ )

It has been established from studies by Hatfield and Hodgson<sup>151</sup> and Kahn et al.,<sup>152-153</sup> on di-hydroxy bridged complexes, that if the copper-oxygen-copper angle is less than  $97.5^\circ$  and the copper-copper separation great enough to prevent direct metal-metal interaction then the compound exhibits ferromagnetic interaction.

Decreasing the dihedral angle from  $180^\circ$  to  $130^\circ$  increases the stability of the antibonding orbital in relation to the bonding orbital thereby decreasing the energy separation between the molecular orbitals. The closer to  $130^\circ$  the dihedral angle the greater the degeneracy of the orbitals resulting in decreased interaction (Fig 5.3).<sup>152a</sup> Angles smaller than  $130^\circ$  can give rise to ferromagnetic interaction.

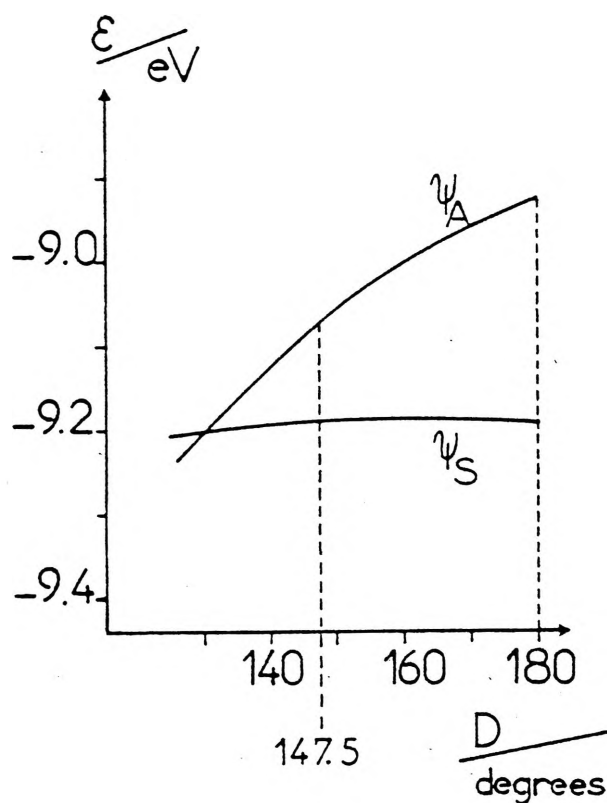


FIG 5.3:<sup>152a</sup> Degeneracy of d Orbitals with Decreasing Dihedral Angle

Kahn and others<sup>106-107</sup> have found that the method of azide bridging in binuclear copper II complexes (Fig 5.4) and also the use of halogens as bridges can result in severely decreased interaction and in some cases even ferromagnetic interaction.

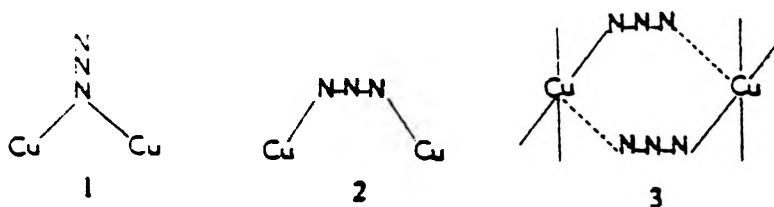


FIG 5.4:<sup>154</sup> Types of Azide Bridging 1) end on,  
2) symmetrical end-to-end, 3) unsymmetrical end-to-end

In the case of the multi-copper oxidases,<sup>154-156</sup> the magnetism is a mixture of the magnetic properties of the different types of copper. The Type III centres are diamagnetic in all cases so that the observed magnetism of the oxidised complexes is due to the Type I and Type II centres which are magnetically dilute non-interacting copper atoms with a value of  $\sim 1.70$  B.M. per copper. The reduced oxidases are diamagnetic.

The magnetic data of the copper complexes is collated in Table 5.1.

The two most important factors in determining the degree of antiferromagnetism exhibited by binuclear complexes are:

- 1) the nature of the exogenous bridge (X) (Fig 5.5), and
- 2) the copper-endogenous oxygen-copper angle.

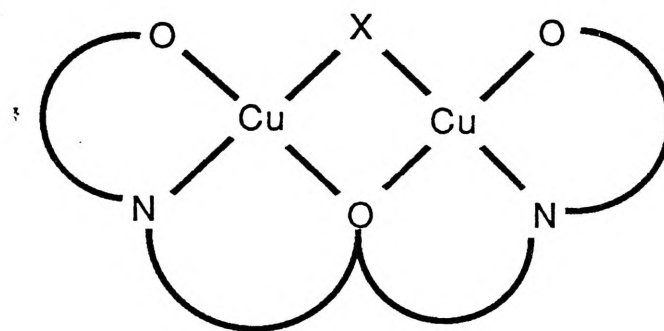


**Fig 5.5:** Schematic Diagram of the Binuclear Complexes showing the Exogenous and Endogenous Bridges

The importance of the first factor on the complexes' antiferromagnetism is that the exogenous bridge governs the energy separation between the symmetrical (Ds) and antisymmetrical (Da) orbitals of the copper atoms.

According to Hoffman et al.<sup>157</sup> the highest occupied molecular orbitals of the copper atoms are the symmetric (Ds) and antisymmetric (Da) energy levels of the  $dx^2-dy^2$  orbital. The greater the degree of the separation between these levels the stronger the antiferromagnetism. According to Kida et al.<sup>110</sup> in the endogenous alkoxide bridge the  $p_x$  orbital of the oxygen interacts with the antisymmetric level of the copper atoms raising the energy of this level in relation to the symmetric level resulting in stronger antiferromagnetism (Fig 5.6). This interaction does not vary in our complexes.

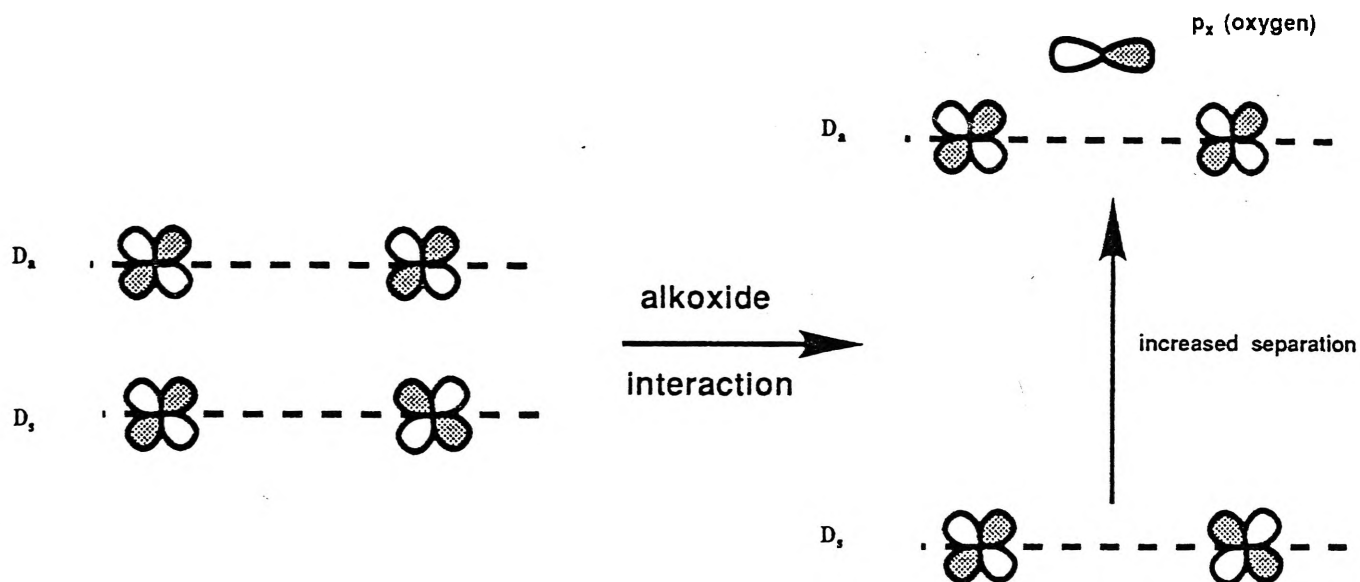


Fig 5.6: Alkoxide Interaction with the  $dx^2-dy^2$  Copper(II) Orbital

The exogenous bridge can act in two ways, it can interact with the symmetric configuration to reduce its energy in relation to the antisymmetric configuration thus increasing the energy separation and hence the antiferromagnetism of the complexes. This is known as the complementary effect (Fig 5.7). It can increase the energy of the symmetric level in relation to the antisymmetric configuration causing a decrease in the energy separation and thus lowering the antiferromagnetic interaction. This is known as the counter-complementary effect (Fig 5.8).

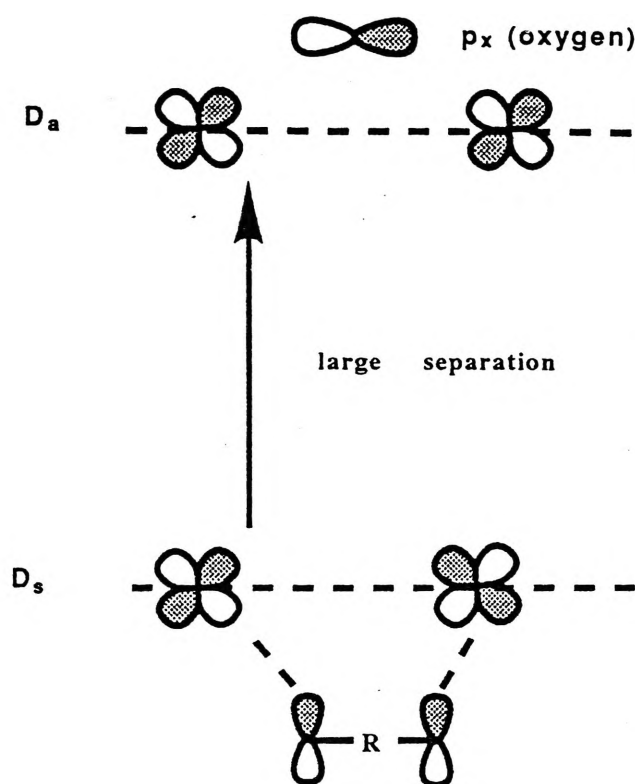


Fig 5.7: Complementary Effect,  $R = \text{odd numbers}$

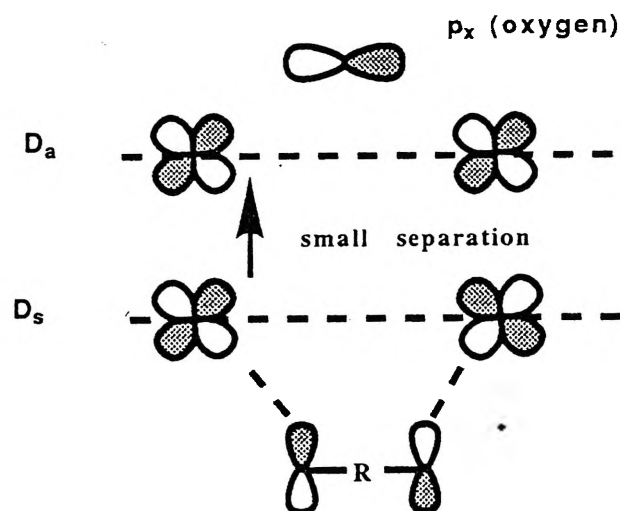
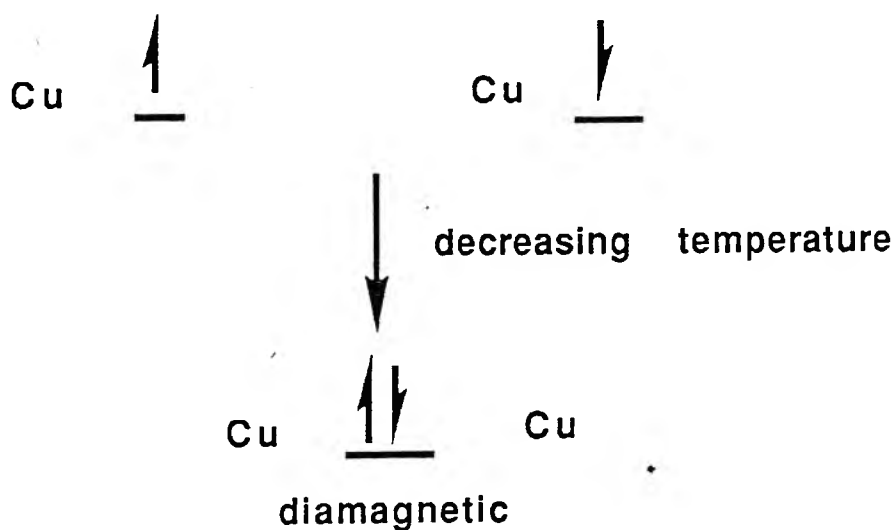


Fig 5.8: Counter-complementary Effect,  $R = 0$  or even numbers



The second important factor is the copper-endogenous oxygen-copper angle, called the dihedral angle. It has been found by Hodgson and co-workers<sup>151</sup> that this angle plays a major role in the amount of copper-copper interaction in binuclear copper complexes. The closer this angle is to  $180^\circ$  the greater the interaction. As the angle approaches  $90^\circ$  the interaction decreases due to disruption of the superexchange pathway existing between the copper atoms and the endogenous oxygen. Thus the closer the dihedral angle is to  $180^\circ$  the lower the magnetic moment of the complex will be.

When, for complexes which undergo antiferromagnetic interaction, the ambient temperature surrounding the complexes is lowered the two unpaired electrons possessed by the copper atoms, one electron for each copper atom, begin to pair up resulting eventually in the complexes becoming diamagnetic. The upper magnetic limits for the complexes under study will approach the spin only value of 1.73 B.M. per Cu, while at liquid helium temperatures the complexes should approach diamagnetism, plus any paramagnetic impurity (Fig 5.9).



**Fig 5.9: Effect of Temperature on a  $d^9$  Electron of Copper(II)**

The variable temperature data for all the binuclear complexes is Tabulated in Section 13.4 in the appendix. In Table 5.1 the temperature range and magnetic moment ranges are given. The variable temperature data was used to examine whether the complexes were antiferromagnetically coupled and the strength of this interaction even when the room temperature moments were above the spin only values, e.g. the SAL-DPL catechol bridged complexes.

The complexes under investigation can be placed, generally, into two categories with regard to their magnetic behaviour:

- 1) strongly interacting, and;
- 2) weakly interacting compounds.

#### 5.1) Strongly Interacting Complexes

These complexes can be divided into two sections.

##### 5.1.1 $\text{Cu}_2(\text{SAL-DPL})\text{X}$ and $\text{Cu}_2(\text{SAL-DPE})\text{X}$ , X= pyrazoles and indazoles.

The pyrazole-type bridged complexes all possess an aromatic ring containing two nitrogen atoms with the nitrogen atoms exogenously bridging the two copper atoms (Fig 5.10). As a result of this arrangement the dihedral angle of the complexes should be close to  $180^\circ$  as a result of the stereochemical constraints imposed by the ring. Also the  $\pi$  electron cloud of the pyrazole interacts complementarily with the symmetrical  $\text{dx}^2\text{-y}^2$  configuration of the copper atoms (Fig 5.11).

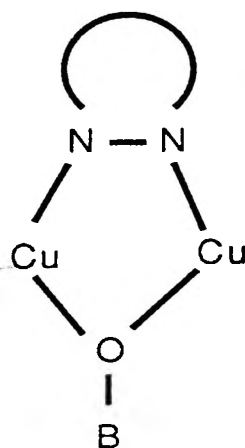


Fig 5.10: B= Ligand Backbone

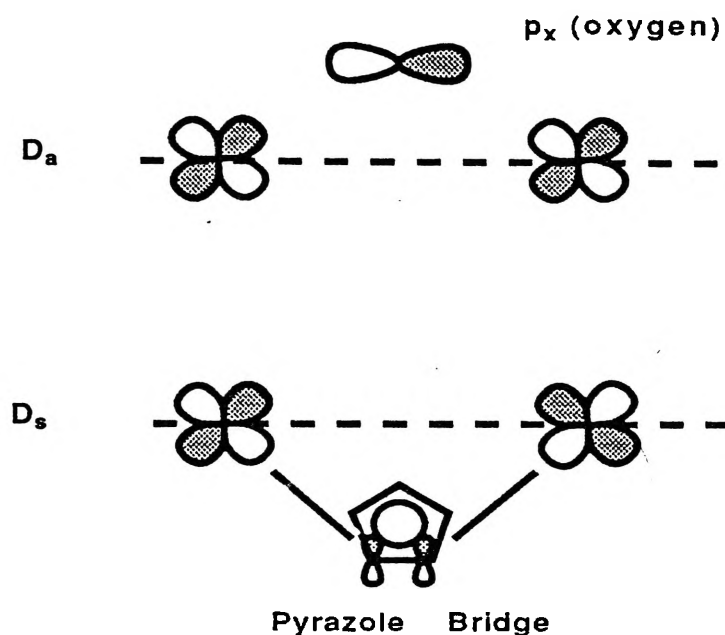


Fig 5.11: Pyrazole-Type Bridges

These two factors combined should result in the pyrazole-type bridged complexes exhibiting very low magnetic moments, which they do (0.75 to 1.10 B.M./Cu atom) with the SAL-DPE complexes being at the low end of this range (see Table 5.1). When the temperature is lowered the complexes rapidly approach diamagnetism and the strongest interacting complexes are almost diamagnetic even at liquid nitrogen temperatures.  $\text{Cu}_2(\text{M}_2\text{BP-DPL})3,5\text{-Me}_2\text{Pz}$  is the exception to this as it has a room temperature magnetic moment of 1.75 B.M. This weaker interaction implies that the complex is not as planar as the other pyrazoles, to examine this the crystal structure for this complex was examined (see Chapter 6).

### 5.1.2: Cu<sub>2</sub>(SAL-DPE)XCATH

These complexes possess a catechol bridge between the two copper atoms (Fig 5.12). The presence of the catechol bridge should confer a dihedral angle close to 180° for these complexes as a result of stereochemical constraints imposed by the aromatic ring. The bonding through the two oxygen atoms should result in a slightly increased copper-copper separation while the oxygen atoms of the catechol bridge will interact complementarily with the copper  $dx^2-y^2$  orbitals (Fig 5.13). This interaction is the same as for the pyrazole-type bridged complexes. As the temperature is lowered the SAL-DPE catechol bridged complexes interact strongly as expected ( $\mu = 0.81-1.08$  B.M. at room temperature) and approach diamagnetism at liquid nitrogen temperatures. The results are similar to those of the pyrazole bridged complexes as was expected given their similar interactions as mentioned earlier.

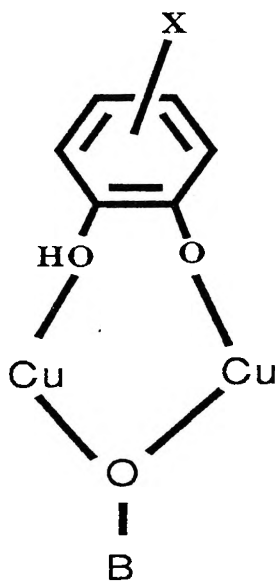


Fig 5.12: B= Ligand Backbone

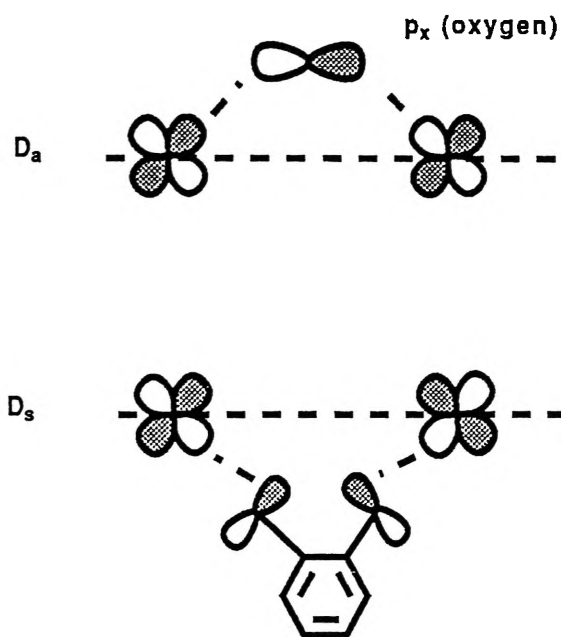


Fig 5.13:  $\text{Cu}_2(\text{SAL-DPE})\text{XCAT}$ -Type Bridges

## 5.2: Weakly Interacting Complexes

These complexes can be divided into four sections:

### 5.2.1: $\text{Cu}_2(\text{SAL-DPL})(\text{XCAT})_{0.5}$

These complexes exhibit a single oxygen-type bridge (Fig 5.14) with magnetic moments in the range 1.98 to 2.06 B.M./Cu atom. The reason for these higher magnetic moments is that the two copper atoms are probably bridged by only a single exogenous oxygen atom. In this situation the unoccupied orbital of the bridging group will readily interact complementarily with the symmetrical  $\text{dx}^2\text{-y}^2$  orbitals of the copper atoms (Fig 5.15). This interaction is offset by the fact that due to this single oxygen bond the dihedral angle will be considerably distorted from  $180^\circ$  and so the two important factors in lowering magnetic interaction tend to cancel each other out.

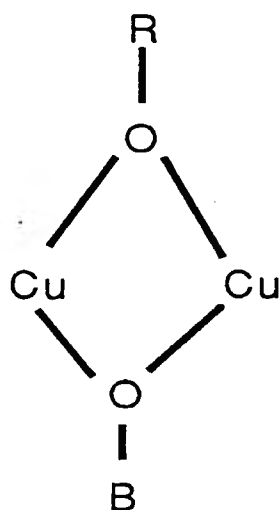


Fig 5.14: B= Ligand Backbone, R= (XCAT)<sub>0.5</sub>

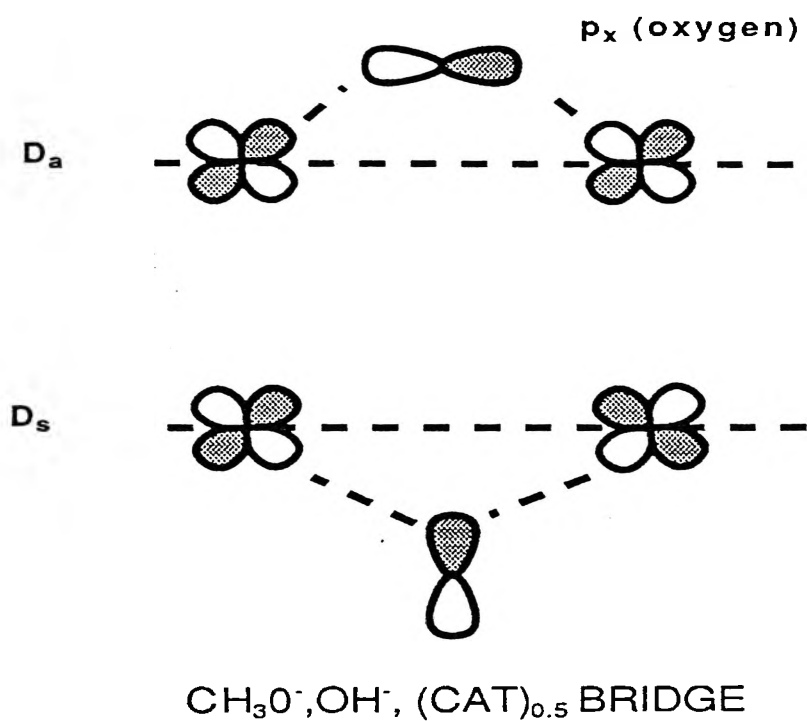


Fig 5.15: Single Oxygen-Type Bridge Interaction with the  $dx^2-dy^2$  Copper (II) Orbital

As the temperature is lowered the SAL-DPL(CAT)<sub>0.5</sub> type bridged complexes are not as strongly interacting as the pyrazole bridged and Cu<sub>2</sub>(SAL-DPE)XCATH complexes as would be expected with the predicted greater dihedral angle distortion of these complexes disrupting the superexchange pathway of these complexes.

### 5.2.2: Cu<sub>2</sub>(SAL-DPL)X and Cu<sub>2</sub>(SAL-DPE)OH, X= OH, 2-MeOEtO

These complexes have magnetic moments ranging from 1.55B.M. for Cu<sub>2</sub>(SAL-DPE)OH to 2.02B.M. for the methoxyethanol bridged complex. The reason for these higher magnetic moments is that the two copper atoms are bridged by only a single oxygen atom (Fig 5.16) and so it behaves in a similar manner to Cu<sub>2</sub>(SAL-DPL)(CAT)<sub>0.5</sub>.

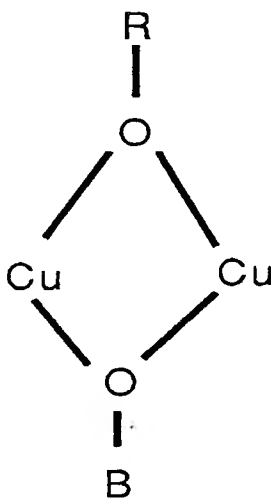


Fig 5.16: B= Ligand Backbone, R= (XCAT)<sub>0.5</sub>

As the temperature is lowered the SAL-DPL single oxygen-type bridged complexes are not as strongly interacting as the pyrazole bridged and Cu<sub>2</sub>(SAL-DPE)XCATH complexes. This was expected as these complexes would probably have a greater dihedral angle distortion, due to the single atom bridge drawing the copper atoms out of the plane of the molecule, this would disrupt the superexchange pathway of these complexes. As was observed in the pyrazole complexes (5.1.1) the SAL-DPE hydroxy bridged complex has the lowest magnetic moment of these complexes, this may be due to the greater flexibility of the SAL-DPE ligand causing less disruption of the superexchange pathway.

### 5.2.3 $\text{Cu}_2(\text{SAL-DPL})\text{X}$ , $\text{X} = \text{O}_2, \text{O}_2\text{H}, \text{p-OHBzCOO}$

In these complexes the two copper atoms are bridged by two oxygen atoms either directly joined (O-O) or carboxylate-type (O-R-O) (Fig 5.17). In the case of the directly joined oxygen bridged complexes the exogenous bridge can be orientated in two fashions these being end-on or end-to-end (Fig 5.18). The magnetism of these complexes does not indicate which method occurs. In either case the bridge will not interact with the symmetrical configuration resulting in higher magnetic moments than observed for pyrazole-type bridged complexes.

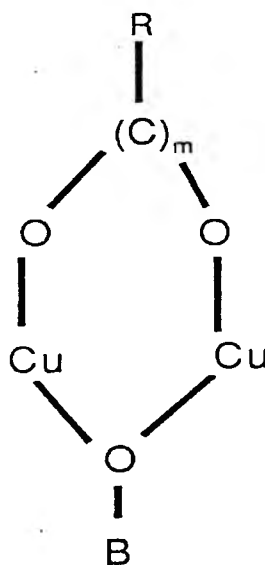


Fig 5.17: B= Ligand Backbone,  $m=0$  or 1



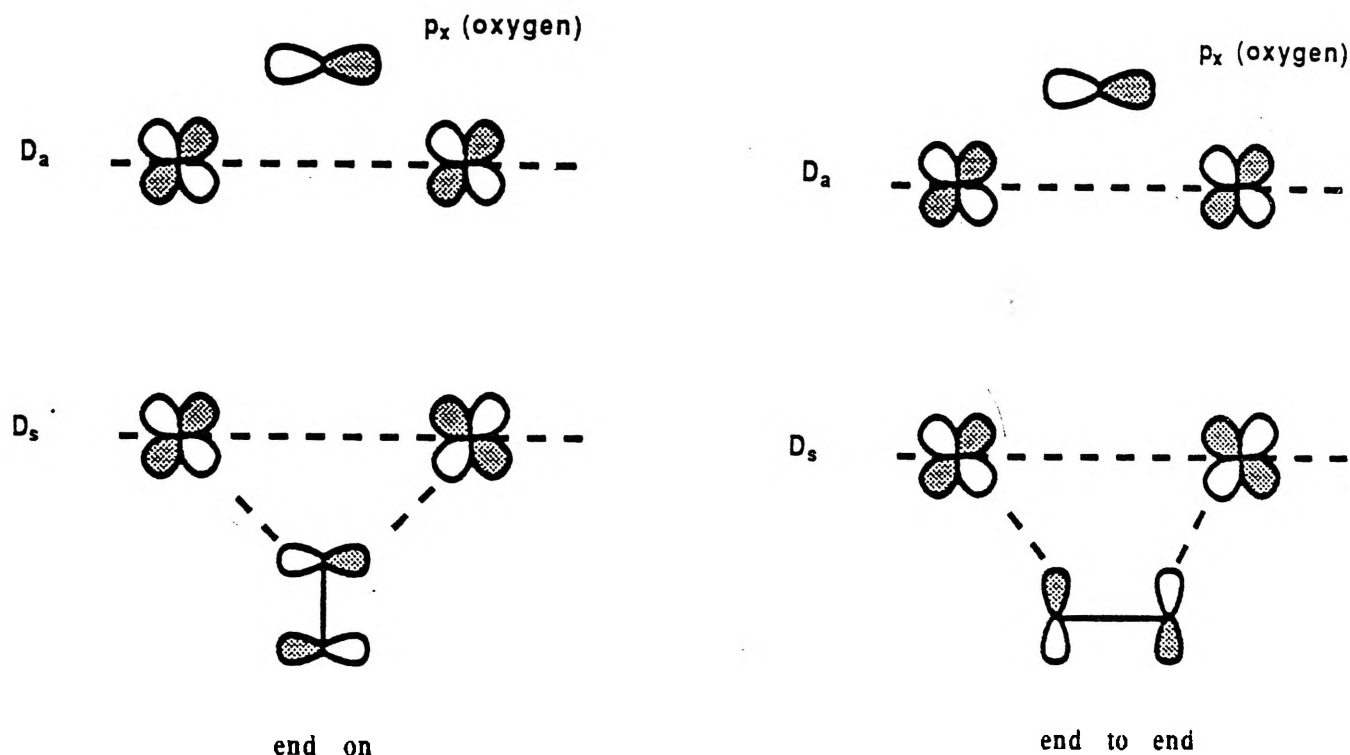


Fig 5.18: Two Methods of Dioxygen Binding

IR spectra and empirical formula data indicates that  $\text{Cu}_2(\text{SAL-DPL})\text{O}_2 \cdot 2\text{H}_2\text{O}$  possesses a single electron on the superoxo oxygen atom. Due to the presence of the superoxo oxygen there will be one unpaired electron in the complex which means that the complex is unable to achieve diamagnetism upon lowering the temperature.

This means that in the case of ferromagnetic coupling the upper temperature limit would be  $\mu = \sqrt{3}g\sqrt{\{1/2(1/2+1)\}} = 1.5g$  (3.0 B.M. if  $g = 2$ ) and the low temperature limit would be  $\mu = g/2\sqrt{15} = 1.94g$  (3.87 B.M. if  $g = 2$ ).

For antiferromagnetic interaction the limits would be  $\mu = \sqrt{3}g\sqrt{\{1/2(1/2+1)\}} = 1.5g$  (3.0 B.M. if  $g = 2$ ) for the high temperature limit and either  $\sqrt{3}$  (1.73 B.M.) or  $(g/2)\sqrt{3}$  (1.73 B.M. if  $g = 2$ ) for the low temperature limit depending on the position of the residual electron of the superoxo complex (i.e. whether the electron is associated with the dioxygen bridge or one of the Cu(II) atoms).

As the temperature is lowered the  $\text{Cu}_2(\text{SAL-DPL})\text{O}_2 \cdot 2\text{H}_2\text{O}$  complex exhibits low and high temperature values which approach those of the antiferromagnetic limits above agreeing with the possibility that the oxygen occurs in the superoxo form.

In the carboxylate-type bridged complexes the bridging group will interact with the symmetrical configuration (Fig 5.19) in a complementary manner, while in the directly joined oxygen-type bridged complexes the interaction will be counter complementary (Fig 5.18).

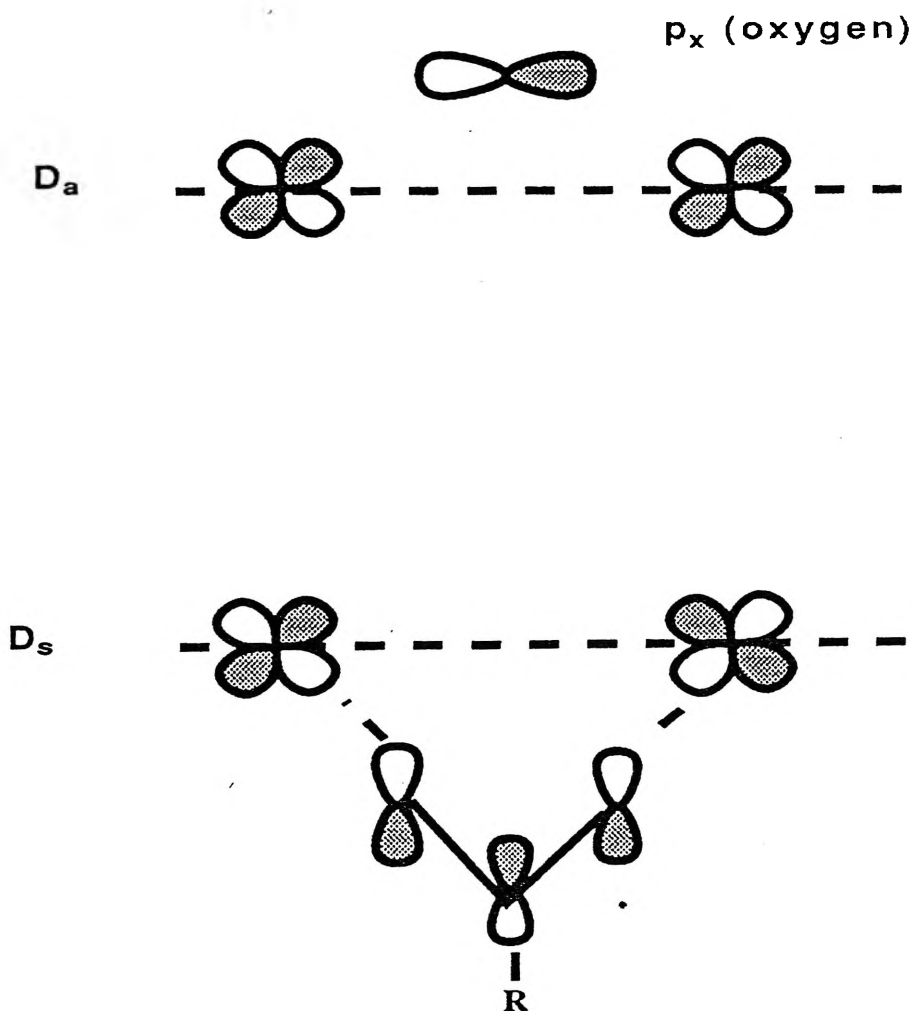


Fig 5.19: Carboxylate-Type Bridges

In these complexes the exogenous bridge will produce some dihedral distortion from  $180^\circ$  as there is no stereochemical constraints caused by an aromatic/heterocyclic ring resulting in the oxygen-type bridged complexes having higher magnetic moments than the pyrazole-type bridged complexes. As the temperature is lowered the SAL-DPL oxygen-type bridged complexes are not as strongly interacting as the pyrazole bridged and  $\text{Cu}_2(\text{SAL-DPE})\text{XCATH}$  complexes.

#### 5.2.4: $\text{Cu}_2(\text{SAL-DPL})\text{X}$ , $\text{X} = \text{PyO}$ , 2-OHBzImid

The pyridine-N-oxide type bridged complexes are also only weakly interacting (1.61 to 1.93 B.M/Cu atom). As in the pyrazole bridged complexes the heterocyclic ring enforces stereochemical constraints upon the complexes resulting in dihedral angles closer to  $180^\circ$  than in the oxygen bridged complexes although slightly less than for the pyrazoles (Fig 5.20).

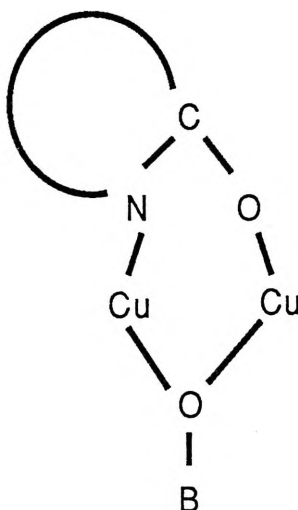
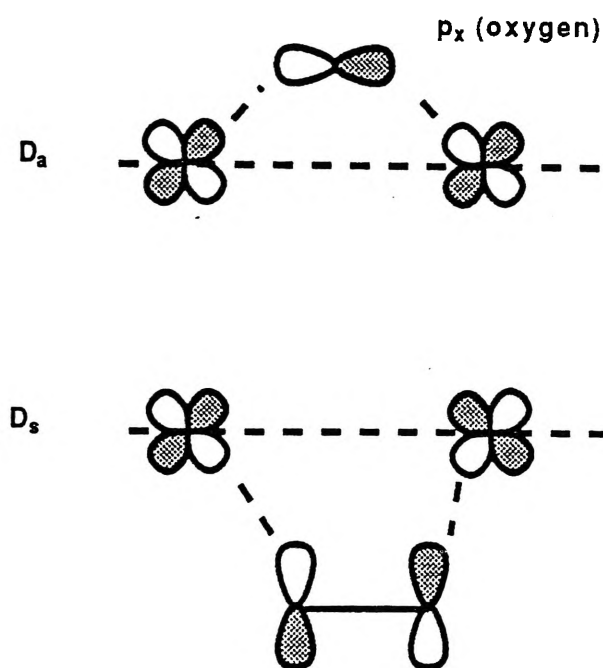


Fig 5.20: B= Ligand Backbone

However these exogenous bridges are unable to interact complementarily with the  $dx^2-y^2$  symmetrical orbital (Fig 5.21) which will result in these complexes having magnetic moments close to the spin only value as the above two factors cancel each other out. A notable feature of this group of complexes is that the  $\text{Cu}_2(\text{SAL-DPL})2\text{-PyO}(\text{H}_2\text{O})_{0.5}$  complex is the only complex to exhibit Curie-Weiss behaviour down to liquid nitrogen temperatures. This result is somewhat surprising given that the other complexes with this type of bridging are antiferromagnetic but may indicate the strength of counter complementary interaction.



### PYRIDINE-N-OXIDE TYPE BRIDGE

**Fig 5.21:** Pyrdine-N-oxide Type Bridges

Selected graphs of the variable temperature data versus the magnetic moments of both strongly interacting and weakly interacting complexes are presented in Figs 5.22 to 5.26

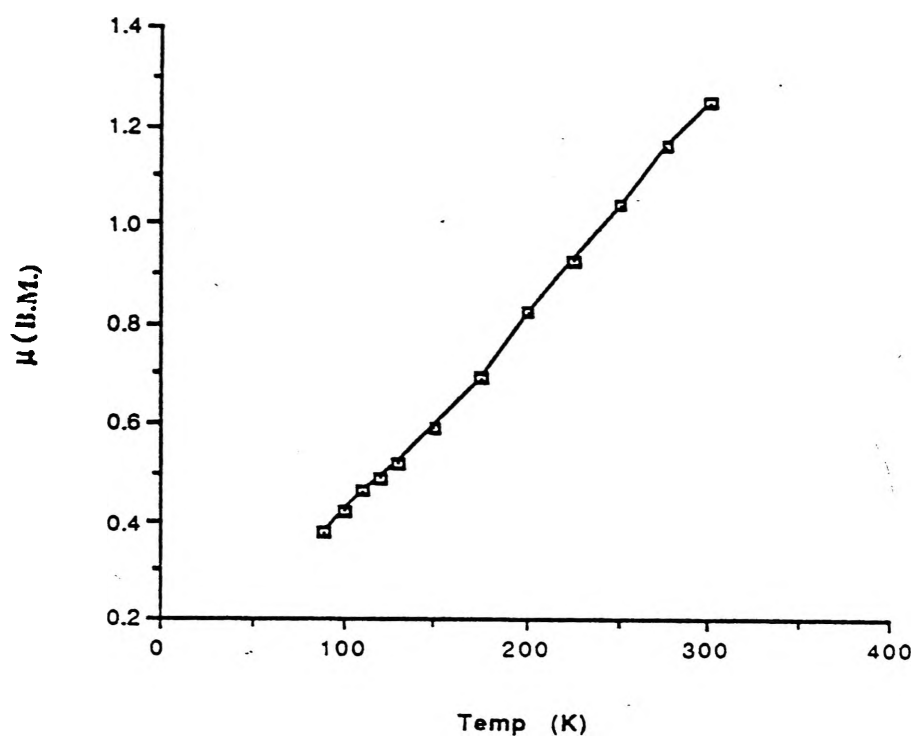


Fig 5.22: Temperature versus Magnetic Moment for  $\text{Cu}_2(\text{SAL-DPL})\text{Pz}$

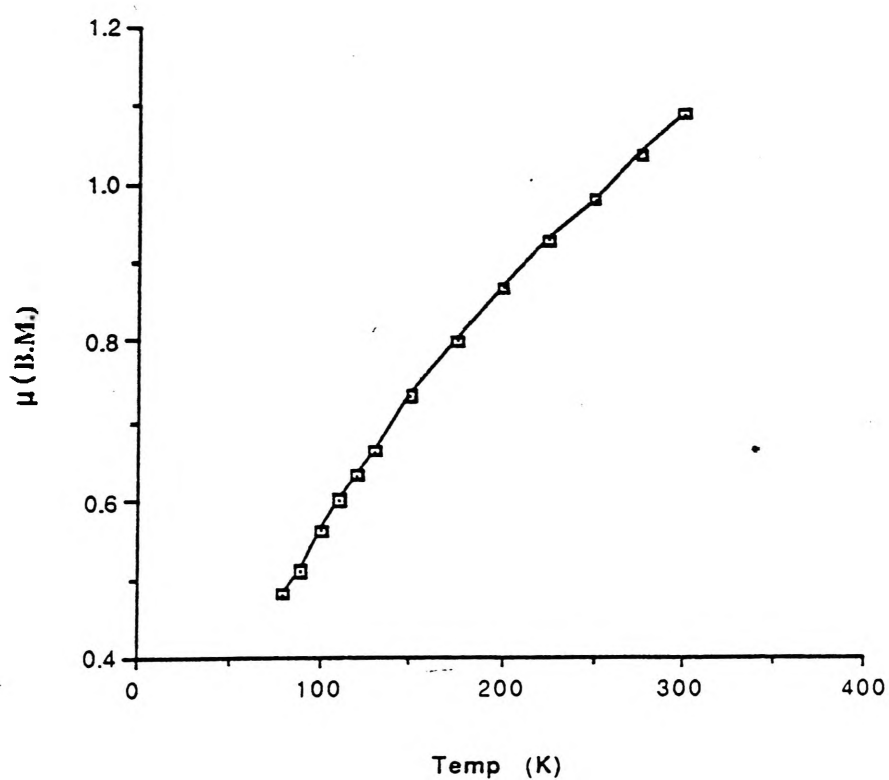


Fig 5.23: Temperature versus Magnetic Moment for  $\text{Cu}_2(\text{SAL-DPE})_4\text{-NO}_2\text{CATH}$

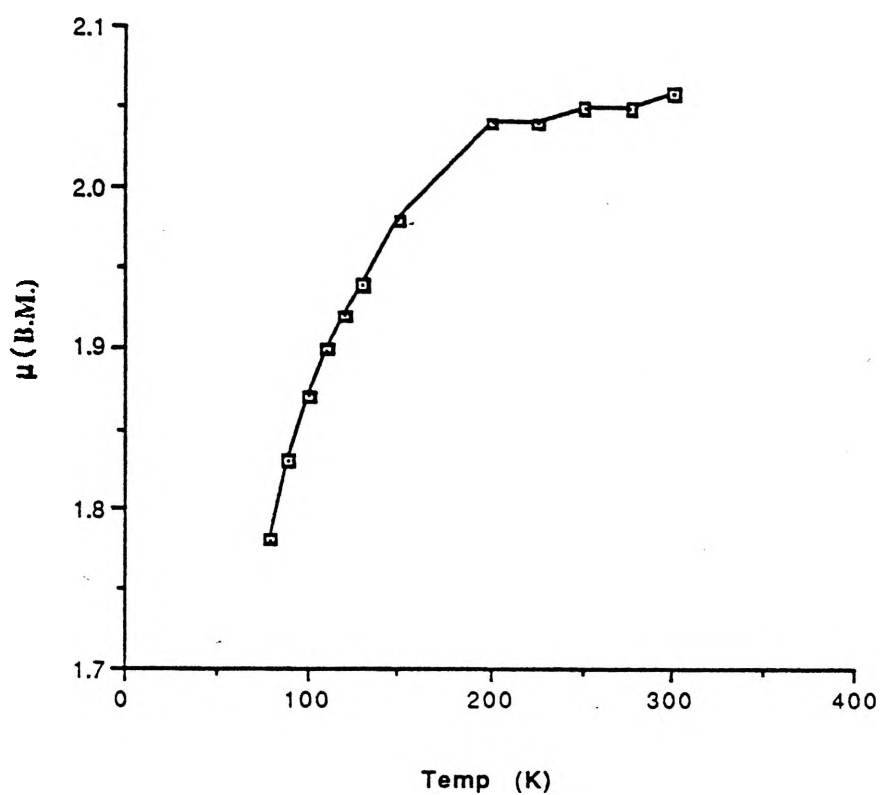


Fig 5.24: Temperature versus Magnetic Moment for  $\text{Cu}_2(\text{SAL-DPL})(\text{CAT})_{0.5}(\text{H}_2\text{O})_{0.5}$

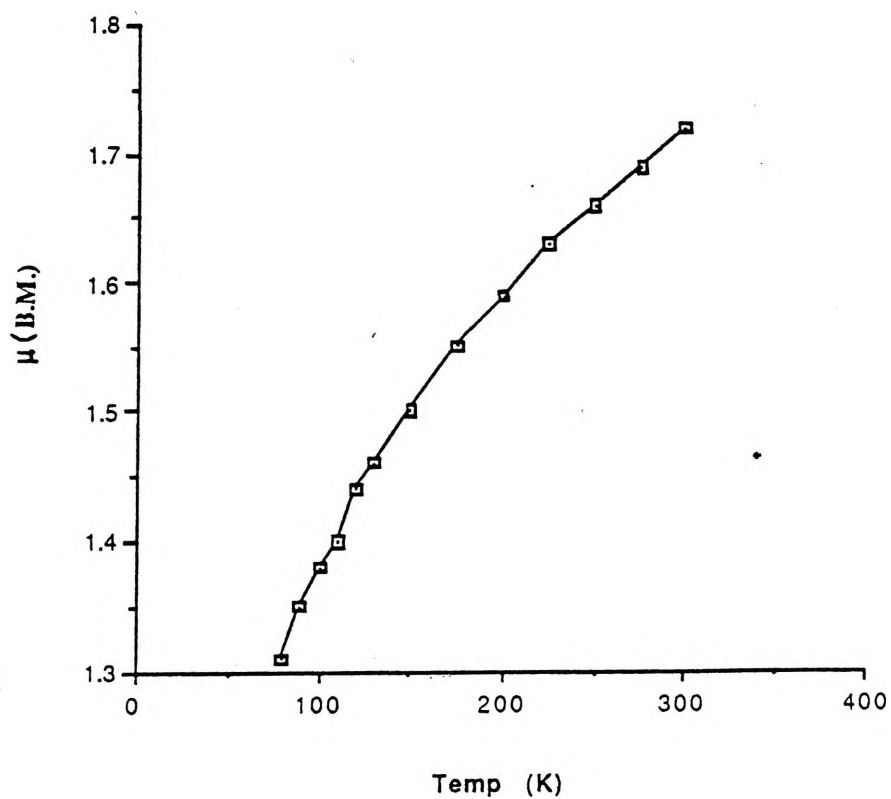


Fig 5.25: Temperature versus Magnetic Moment for  $\text{Cu}_2(\text{SAL-DPL})\text{OH} \cdot 3\text{H}_2\text{O}$

Compound	Temp K	$\chi_g$ x10 <sup>-6</sup>	m/Cu B.M.	m(T)-m(T) B.M.
Cu(SAL-DPL)H	297	3.33	1.79	
Cu <sub>2</sub> (SAL-DPL)Pz	300	1.70	1.25	0.38(90)-1.25(300)
Cu <sub>2</sub> (ESAL-DPL)Pz	301	1.09	1.04	0.29(90)-1.03(300)
Cu <sub>2</sub> (SAL-DPE)Pz	297	0.46	0.75	0.32(80)-0.73(300)
Cu <sub>2</sub> (ESAL-DPE)Pz.H <sub>2</sub> O	290	0.51	0.83	0.36(80)-0.85(300)
Cu <sub>2</sub> (SAL-DPE)3-MePz	295	0.83	0.90	0.43(90)-0.91(300)
Cu <sub>2</sub> (SAL-DPL)3,5-Me <sub>2</sub> Pz	296	1.48	1.08	0.47(80)-1.09(300)
Cu <sub>2</sub> (SAL-DPE)3,5-Me <sub>2</sub> Pz.0.5H <sub>2</sub> O	294	1.2	1.05	0.56(90)-1.04(300)
Cu <sub>2</sub> (M <sup>2</sup> BP-DPL)3,5-Me <sub>2</sub> Pz.H <sub>2</sub> O	294	2.97	1.75	1.06(85)-1.76(300)
Cu <sub>2</sub> (SAL-DPL)5-NO <sub>2</sub> Ind	297	0.8	0.95	0.43(80)-0.95(300)
Cu <sub>2</sub> (SAL-DPE)6-NO <sub>2</sub> Ind	295	0.77	0.94	0.42(90)-0.94(300)
Cu <sub>2</sub> (SAL-DPL)(CAT) <sub>0.5</sub> (H <sub>2</sub> O) <sub>0.5</sub>	297	6.95	2.06	1.78(80)-2.06(300)
Cu <sub>2</sub> (SAL-DPL)(3-MeOCAT) <sub>0.5</sub>	297	6.69	2.03	1.73(80)-2.03(300)
Cu <sub>2</sub> (SAL-DPL)(3MeCAT) <sub>0.5</sub>	296	6.43	1.98	1.62(80)-1.99(300)
Cu <sub>2</sub> (SAL-DPL)(4-MeCAT) <sub>0.5</sub> (H <sub>2</sub> O) <sub>0.5</sub>	295	3.26	1.96	1.55(90)-1.96(300)
Cu <sub>2</sub> (SAL-DPE)(CATH)(H <sub>2</sub> O) <sub>0.5</sub>	297	0.52	0.81	0.40(80)-0.82(300)
Cu <sub>2</sub> (SAL-DPE)(4NO <sub>2</sub> CATH)	297	1.19	1.08	0.48(80)-1.09(300)

Compound	Temp K	$\chi_g$ $\times 10^{-6}$	$\mu/\text{Cu}$ B.M.	$\mu(T)-\mu(T)$ B.M.
$\text{Cu}_2(\text{SAL-DPL})\text{OH}\cdot 3\text{H}_2\text{O}$	296.6	5.01	1.71	1.31(80)-1.72(300)
$\text{Cu}_2(\text{SAL-DPE})\text{OH}\cdot \text{H}_2\text{O}$	296	2.08	1.57	1.48(90)-1.57(300)
$\text{Cu}_2(\text{SAL-DPL})2\text{-MeOETO}$	296	6.51	2.02	1.82(85)-2.02(300)
$\text{Cu}_2(\text{SAL-DPL})\text{O}_2\cdot 2\text{H}_2\text{O}$	300	5.93	1.93	1.77(90)-1.93(300)
$\text{Cu}_2(\text{SAL-DPL})\text{O}_2\text{H}\cdot 0.5\text{H}_2\text{O}$	296	3.83	1.57	1.38(85)-1.57(300)
$\text{Cu}_2(\text{SAL-DPL})4\text{-OHBzCOO}$	294	3.46	1.64	0.98(90)-1.65(300)
$\text{Cu}_2(\text{SAL-DPL})2\text{-PyO}\cdot (\text{H}_2\text{O})_{0.5}$	297	5.51	1.91	1.96(85)-1.90(300)
$\text{Cu}_2(\text{SAL-DPL})5\text{-ClPyO}\cdot 1.5\text{H}_2\text{O}$	295	4.66	1.87	1.33(90)-1.87(300)
$\text{Cu}_2(\text{SAL-DPL})(2\text{-OBenzImid})_{0.5}\cdot 2\text{H}_2\text{O}$	297	3.81	1.61	0.77(90)-1.66(300)

Table 5.1: Magnetic Data for the Binuclear Complexes



**6:**  
**Crystal Structures**

## 6: Crystal Structure of the Binuclear Copper (II) Complexes

### 6.1: Hydroxylamine Complex

Due to our lack of success over a period of two years to grow suitable crystals of the dioxygen bridged binuclear copper complex first synthesised by Erickson<sup>120</sup>, it was decided to synthesise complexes containing an N-O exogenous bridge in an attempt to better elucidate the structure and properties of the dioxygen bridged complexes than is possible with the pyrazole bridged complexes. It was hoped that the N-O bridged complexes would produce suitable crystals for X-ray analysis.

Given the many similarities in properties between nitrogen and oxygen it should have been possible to base conclusions regarding the dioxygen bridged complexes upon the results found for the two atom N-O bridged complexes.

SAL-DPLH<sub>3</sub> and copper tetrafluoroborate were reacted with hydroxylamine and pyridine-N-oxides. Of these only the hydroxylamine complex produced crystals suitable for X-ray analysis.

The crystal structure of the hydroxylamine bridged complex gave an unexpected result. The crystal structure of " $\text{Cu}_2(\text{SAL-DPL})\text{NH}_2\text{O} \cdot \text{H}_2\text{O}$ " (this nomenclature will be used for the sake of convenience although it is incorrect) is shown in Fig 6.2. Crystal structure data is tabulated in Section 13.1 in the appendix. Relevant structural data is tabulated in Table 6.1. A schematic diagram of the area surrounding the copper atoms is shown in Fig 6.1.

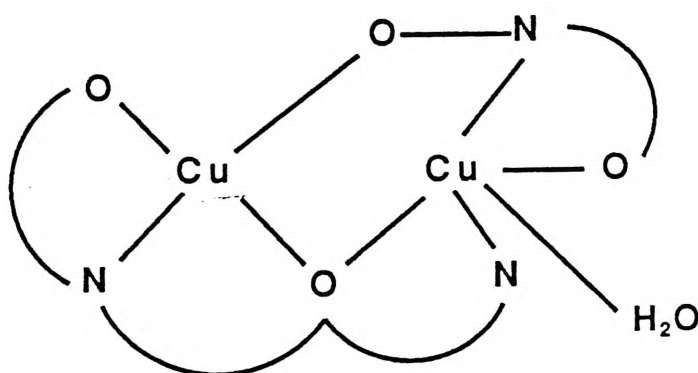


Fig 6.1: Schematic Diagram of the Copper Centre of " $\text{Cu}_2(\text{SAL-DPL})\text{NH}_2\text{O} \cdot \text{H}_2\text{O}$ "

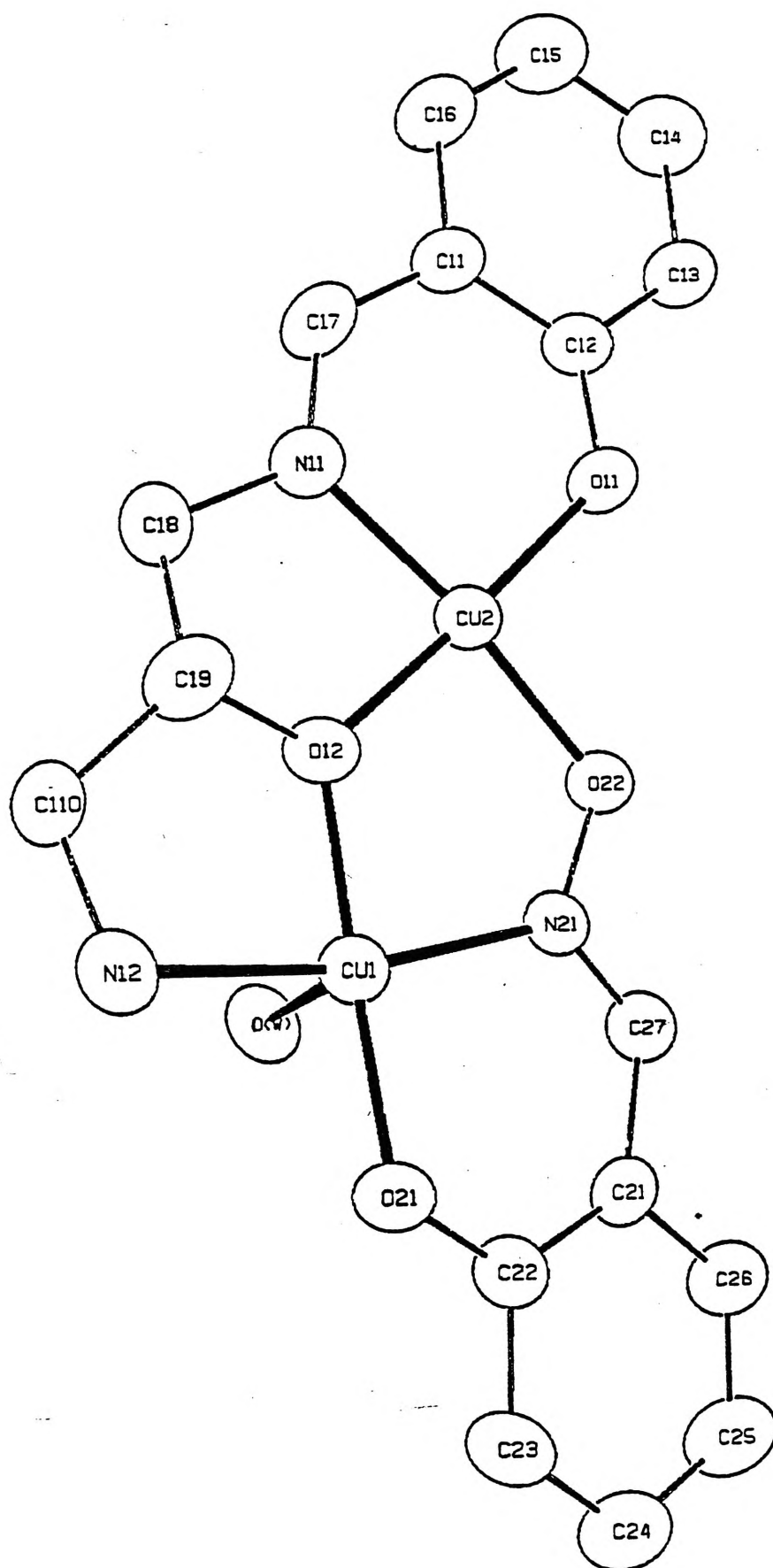


Fig 6.2: Crystal Structure of " $\text{Cu}_2(\text{SAL-DPL})\text{NH}_2\text{O}\cdot\text{H}_2\text{O}$ "

<u>Bond Distances (Å)</u>			<u>Bond Angles (°)</u>			
Cu1	O(W)	2.483	O11	Cu2	N11	93.8
Cu1	O21	1.899	O11	Cu2	O22	93.4
Cu1	N21	1.984	O11	Cu2	O12	175.5
Cu1	N12	2.055	N11	Cu2	O12	82.6
Cu1	O12	1.877	N11	Cu2	O22	172.1
Cu2	O22	1.936	O12	Cu2	O22	90.3
Cu2	O12	1.865	Cu2	O12	Cu1	124.4
Cu2	N11	1.951	Cu2	O22	N21	116.3
Cu2	O11	1.900	O12	Cu1	N12	83.3
Cu1	Cu2	3.31	O12	Cu1	N21	86.1
			O12	Cu1	O21	170.7
			O12	Cu1	O(W)	96.7
			O21	Cu1	N21	96.1
			N12	Cu1	O21	93.8
			N12	Cu1	O(W)	95.7
			N12	Cu1	N21	168.6
			O21	Cu1	O(W)	92.4
			N21	Cu1	O(W)	89.5
			Cu1	N21	O22	125.0

TABLE 6.1: Relevant Bond Distances and Bond Angles of "Cu<sub>2</sub>(SAL-DPL)NH<sub>2</sub>O.H<sub>2</sub>O"

It was expected that the hydroxylamine group would simply bridge exogenously between the copper atoms in a  $\mu$ -1,2 fashion.

The crystals obtained were not those of the hydroxylamine bridged binuclear complex. It appears that the imino group of one of the salicylaldehyde groups has been hydrolysed with this bond having been broken (Fig 6.3). The free salicylaldehyde group has then reacted with hydroxylamine to form the schiff base salicylaldoxine and this schiff base then bridges the two copper atoms (Fig 6.3). The remaining part of the SAL-DPLH<sub>3</sub> ligand also bridges the two copper atoms. The following reaction sequence probably occurs.

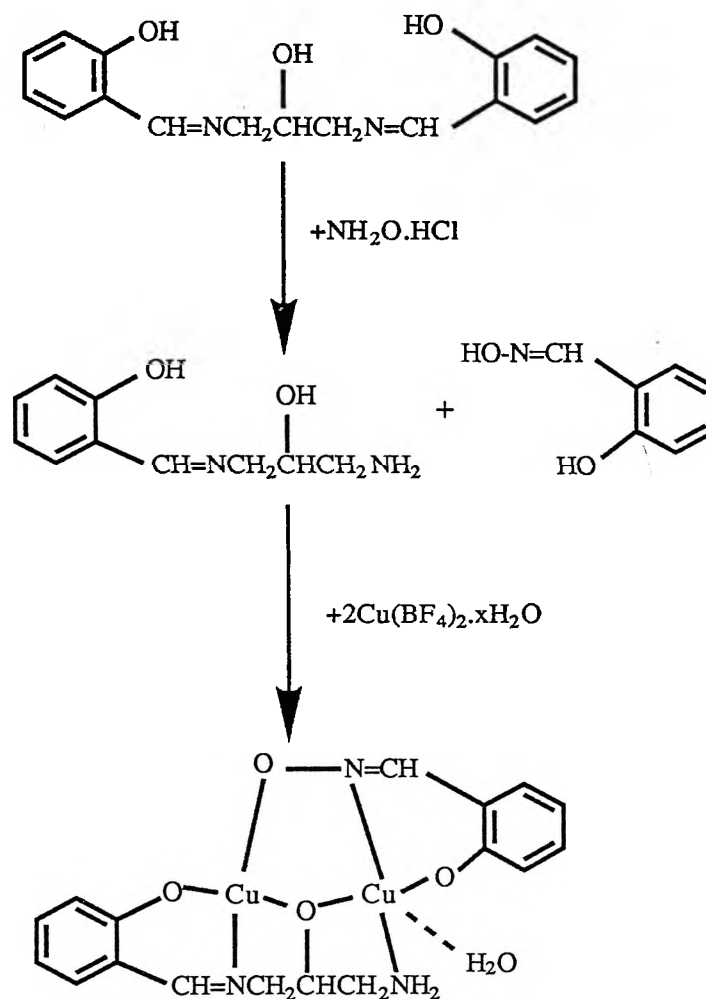


Fig 6.3: Possible Reaction Pathway for " $\text{Cu}_2(\text{SAL-DPL})\text{NH}_2\text{O}\cdot\text{H}_2\text{O}$ " Synthesis

This reaction was not expected, however upon consideration, it is only moderately surprising given that hydroxylamine itself readily forms schiff base ligands. It is surprising, however, that complete hydrolysis did not occur to form copper(salicylaldehyde)<sub>2</sub>. If excess hydroxylamine had been used, this product may have been formed.

The " $\text{Cu}_2(\text{SAL-DPL})\text{NH}_2\text{O}$ " complex was found to have one of the copper atoms in a slightly distorted square planar environment. This copper atom has a copper-nitrogen bond distance of  $1.95\text{\AA}$  and the copper-oxygen bond distances are  $1.94$ ,  $1.90$  and  $1.87\text{\AA}$  for each of the three copper-oxygen bonds. The bond angles vary from  $93.8$  to  $82.6^\circ$ . All these bond angles and bond lengths indicate distorted square planar geometry.

The second copper atom is five coordinate having a water molecule bound to it in addition to the other bonds. The two copper-oxygen bonds for this copper are shorter than the two copper nitrogen bonds ( $1.88$  and  $1.90\text{\AA}$  compared to  $1.98$  and  $2.01\text{\AA}$ ). The water molecule, as is expected, is further displaced from the copper atom ( $2.5\text{\AA}$ ) than the other atoms. The endogenous oxygen-copper-nitrogen bond angles are below  $90^\circ$  while the salicylaldehyde oxygen-copper-nitrogen bond angles are over  $90^\circ$ . The water molecule is approximately perpendicular to the plane of the copper atom-schiff base ligand group. The bond lengths and bond angles all indicate that the copper atom is in a square pyramidal environment. We can conclude that both copper atoms are in a distorted environment.

It was found that the copper atoms are  $3.31\text{\AA}$  apart which is shorter than the distance found for oxyhemocyanin. The dihedral angle was found to be  $169.7^\circ$  meaning that there is only slight distortion from planarity for the overall molecule.

Attempts were then made to prepare complexes bridged by  $\text{NH}(\text{CH}_3)\text{O}^-$  and  $\text{N}(\text{CH}_3)_2\text{O}^-$  which cannot form schiff bases with salicylaldehyde. Green products were obtained which gave unsatisfactory analysis.

## 6.2: $\text{Cu}_2(\text{SAL-DPL})_6\text{AI}$

The crystal structure of  $\text{Cu}_5(\text{ESAL-DPL}_6\text{ALESAL})_2 \cdot 2\text{H}_2\text{O}$  has been determined by Werakso<sup>123</sup>. It was decided to solve the structure of the binuclear precursor type complex ( $\text{Cu}_2(\text{SAL-DPL})_6\text{AI}$ ) to examine whether there were any differences in the environment around each Type III copper (II) atom upon being incorporated into a pentanuclear copper II complex containing different types of copper centres.

Crystal structure data of  $\text{Cu}_2(\text{SAL-DPL})_6\text{-AI}$  is tabulated in Section 13.2 in the appendix. The crystal structure is shown in Fig 6.4. Relevant crystal data is located in Table 6.2. A schematic diagram of the copper-copper centre and atom numbering scheme is shown in Fig 6.5.

<u>Bond Distances (<math>\text{\AA}</math>)</u>			<u>Bond Angles (<math>^\circ</math>)</u>			
Cu1	Cu2	3.391	O11	Cu1	O	175.7
Cu1	O	1.901	O11	Cu1	N1	96.9
Cu1	O11	1.902	O11	Cu1	N11	93.6
Cu1	N1	1.976	N11	Cu1	N1	168.7
Cu1	N11	1.945	N11	Cu1	O	82.3
Cu2	O	1.887	O	Cu1	N1	87.3
Cu2	O21	1.913	Cu1	O	Cu2	124.4
Cu2	N2	1.954	O21	Cu2	N21	94.4
Cu2	N21	1.941	O21	Cu2	N2	95.8
			O21	Cu2	O	174.7
			N21	Cu2	N2	169.8
			N21	Cu2	O	82.7
			O	Cu2	N2	87.1

TABLE 6.2: Relevant Bond Distances and Bond Angles of  $\text{Cu}_2(\text{SAL-DPL})_6\text{-AI}$

It was found that both copper atoms are in a slightly distorted square planar environment with the bond distances being shorter between the copper atoms and the oxygen atoms in comparison to the copper-nitrogen bond distances. The average copper-oxygen bond distance is  $1.90\text{\AA}$  while that of copper-nitrogen is  $1.95\text{\AA}$ .

The bond angles also show this slight distortion from a perfect square planar environment, with the bond angles between the endogenous bridging oxygen, the two copper atoms and the different nitrogen groups are all below  $90^\circ$  ( $82.3$  to  $87.3^\circ$ ). The bond angles for the salicylaldehyde oxygens, the two copper atoms and the nitrogen groups are all over  $90^\circ$  ( $93.6$  to  $96.9^\circ$ ).

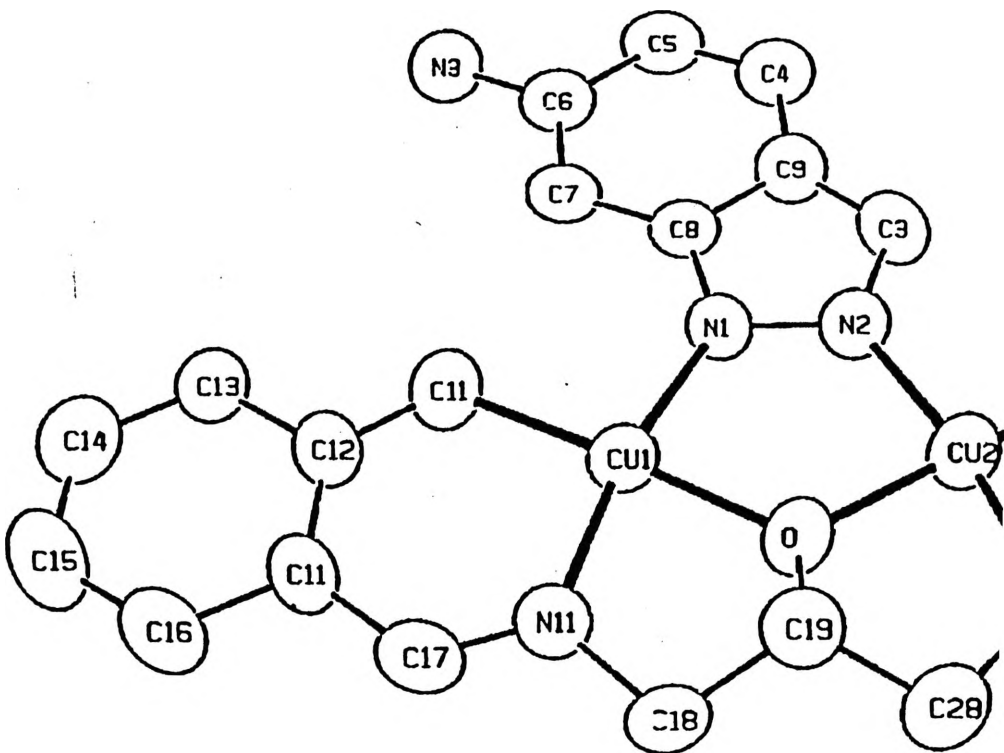
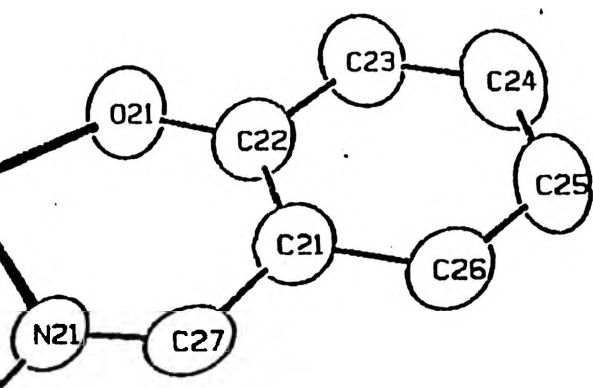


Fig 6.4: Crystal Structure of  $\text{Cu}_2(\text{SAL-DPL})_6 \cdot \text{Al}$





The two copper atoms were found to be separated by 3.39Å and the dihedral angle was found to be 165.2° indicating that the complex is reasonable flat.

If we compare these results with those for the Type III copper atoms in the pentanuclear complex first synthesised by Werakso<sup>123</sup> we find that there are only minor differences in the copper environments. Some of the small differences in the bond lengths and angles may be due to the presence of the 3-ethoxy groups on  $\text{Cu}_5(\text{ESAL-DPL.6AIESAL})_2 \cdot 2\text{H}_2\text{O}$ . Tables 6.3 and 6.4 compares the bond distances and bond angles of  $\text{Cu}_2(\text{SAL-DPL})_6\text{-AI}$  and the Type III centre of  $\text{Cu}_5(\text{ESAL-DPL.6AIESAL})_2 \cdot 2\text{H}_2\text{O}$ . The addition of a Type II copper centre to this binuclear complex appears to have little affect on the Type III copper centre.

a) Bond Distances (Å)

Cu1	Cu2	3.391
Cu1	O	1.901
Cu1	O11	1.902
Cu1	N1	1.976
Cu1	N11	1.945
Cu2	O	1.887
Cu2	O21	1.913
Cu2	N2	1.954
Cu2	N21	1.941

b) Bond Distances (Å)

Cu1	Cu2	3.36
Cu1	O	1.925
Cu1	O1	1.876
Cu1	N1	1.926
Cu1	N2	1.965
Cu2	O	1.862
Cu2	O1'	1.872
Cu2	N1'	1.937
Cu2	N3	1.966

**TABLE 6.3:** Relevant Bond Distances a)  $\text{Cu}_2(\text{SAL-DPL})_6\text{-AI}$  and b)  $\text{Cu}_5(\text{ESAL-DPL.6AIESAL})_2 \cdot 2\text{H}_2\text{O}$

a) <u>Bond Angles (°)</u>				b) <u>Bond Angles (°)</u>			
O11	Cu1	O	175.7	O	Cu1	O1	169.8
O	Cu1	N11	82.3	O	Cu1	N1	83.7
O	Cu1	N1	87.3	O	Cu1	N2	86.2
N11	Cu1	N1	168.7	N1	Cu1	N2	163.8
O11	Cu1	N11	93.6	O1	Cu1	N1	93.8
O11	Cu1	N1	96.9	O1	Cu1	N2	98.3
Cu1	O	Cu2	124.4	Cu1	O	Cu2	124.9
O21	Cu2	N21	94.4	O1'	Cu2	N1'	95.2
O21	Cu2	N2	95.8	O1'	Cu2	N3	94.7
O21	Cu2	O	174.7	O	Cu2	O1'	173.4
N21	Cu2	N2	169.8	N1'	Cu2	N3	162.9
N21	Cu2	O	82.7	O	Cu2	N3	86.4
O	Cu2	N2	87.1	O	Cu2	N1'	85.5

TABLE 6.4: Relevant Bond Angles of a)  $\text{Cu}_2(\text{SAL-DPL})_6\text{-Al}$  and b)  
 $\text{Cu}_5(\text{ESAL-DPL}, 6\text{AIESAL})_2 \cdot 2\text{H}_2\text{O}$

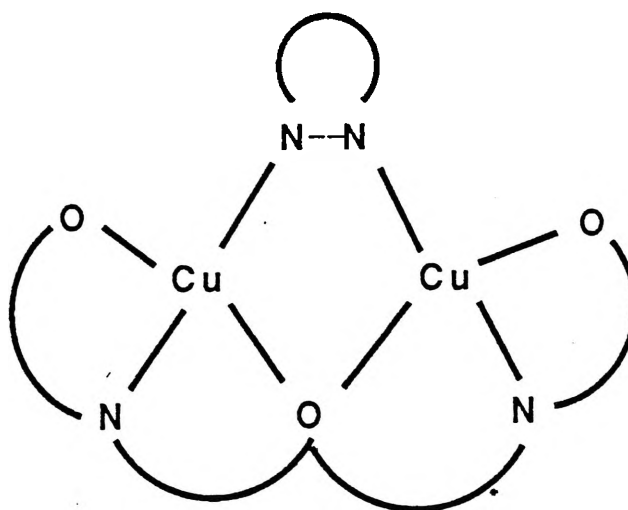


Fig 6.5: Schematic Diagram of the Copper Centre of  $\text{Cu}_2(\text{SAL-DPL})_6\text{-Al}$  and  
 $\text{Cu}_2(\text{M}^2\text{BP-DPL})_3 \cdot 5\text{M}^2\text{Pz}$

### 6.3: $\text{Cu}_2(\text{M}^2\text{BP-DPL})3,5\text{-Me}^2\text{Pz}$

In studying the binuclear complexes synthesised to aid our study of the electrochemistry of the catechol bridged complexes it was found  $\text{Cu}_2(\text{M}^2\text{BP-DPL})3,5\text{-Me}^2\text{Pz}$  had a substantially higher magnetic moment (1.75B.M.) than was usually found for the other pyrazole bridged complexes (0.75 to 1.11B.M.). To try to explain this anomalous result, the crystal structure of  $\text{Cu}_2(\text{M}^2\text{BP-DPL})3,5\text{-Me}^2\text{Pz}$  was determined.

Crystal structure data of  $\text{Cu}_2(\text{M}^2\text{BP-DPL})\text{Me}^2\text{Pz}$  is tabulated in Section 13.3 in the appendix. Relevant data on the area surrounding the copper-copper centre is collected in Table 6.5. The crystal structure is shown in Fig 6.6 and a schematic diagram of the area surrounding the copper-copper centres is shown in Fig 6.5.

<u>Bond Distances (Å)</u>			<u>Bond Angles (°)</u>			
Cu1	O	1.890	O	Cu1	O1	174.85
Cu1	O1	1.897	O	Cu1	N1	83.42
Cu1	N1	1.988	O	Cu1	N3	86.03
Cu1	N3	1.999	O1	Cu1	N1	91.46
Cu2	O	1.885	O1	Cu1	N3	98.86
Cu2	O2	1.870	N1	Cu1	N3	164.03
Cu2	N2	1.979	CU1	N3	N4	119.0
Cu2	N4	1.984	O	Cu2	O2	172.8
N3	N4	1.398	O	Cu2	N2	83.77
Cu1	Cu2	3.372	O	Cu2	N4	86.04
			O2	Cu2	N2	91.61
			O2	Cu2	N4	99.40
			N2	Cu2	N4	166.0
			Cu1	O	Cu2	126.54

TABLE 6.5: Relevant Bond Distances and Bond Angles of  $\text{Cu}_2(\text{M}^2\text{BP-DPL})\text{M}^2\text{Pz}$

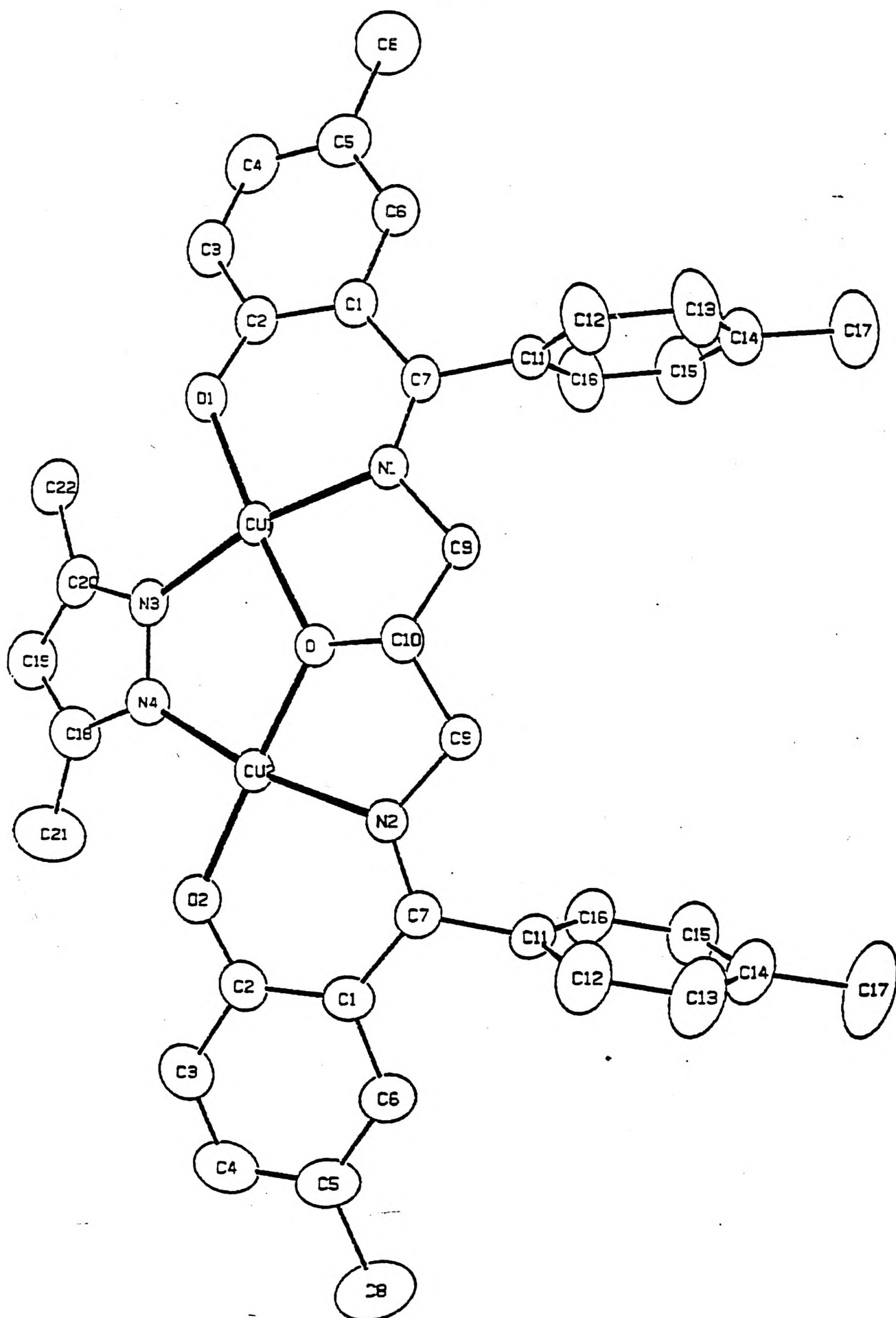


Fig 6.6: Crystal Structure of  $\text{Cu}_2(\text{M}^2\text{BP-DPL})_3,5\text{M}^2\text{Pz}$

There is no significant difference in the copper environments between  $\text{Cu}_2(\text{SAL-DPL})6\text{Al}$ ,  $\text{Cu}_2(\text{SAL-DPL})\text{Pz}^{120}$  and  $\text{Cu}_2(\text{M}^2\text{BP-DPL})3,5\text{-Me}^2\text{Pz}$ . Tables 6.6 and 6.7 compare the bond distances and bond angles of  $\text{Cu}_2(\text{M}^2\text{BP-DPL})3,5\text{-Me}^2\text{Pz}$  and  $\text{Cu}_2(\text{SAL-DPL})\text{Pz}^{120}$  and as can be seen the values are similar.

Given that there is little structurally different between  $\text{Cu}_2(\text{M}^2\text{BP-DPL})3,5\text{-Me}^2\text{Pz}$  and  $\text{Cu}_2(\text{SAL-DPL})\text{Pz}$  there is no obvious explanation, based on crystal structure evidence, as to why the magnetic moment of this complex is so much higher than is normal for the binuclear complexes containing a pyrazole type bridge. Despite satisfactory elemental analysis, it would appear that the original sample of  $\text{Cu}_2(\text{M}^2\text{BP-DPL})3,5\text{-Me}^2\text{Pz}$  contained a substantial amount of paramagnetic impurity.

a) Bond Distances (Å)

Cu1	Cu2	3.372
Cu1	O	1.890
Cu1	O1	1.897
Cu1	N1	1.988
Cu1	N3	1.999
Cu2	O	1.885
Cu2	O2	1.870
Cu2	N2	1.979
Cu2	N4	1.984

b) Bond Distances (Å)

Cu1	Cu2	3.351
Cu1	O2	1.917
Cu1	O1	1.889
Cu1	N1	1.930
Cu1	N2	1.952
Cu2	O2	1.905
Cu2	O1'	1.874
Cu2	N1'	1.936
Cu2	N3	1.950

**TABLE 6.6:** Relevant Bond Distances of a)  $\text{Cu}_2(\text{M}^2\text{BP-DPL})3,5\text{-Me}^2\text{Pz}$  and b)  $\text{Cu}_2(\text{SAL-DPL})\text{Pz}$

<u>Bond Angles (°)</u>				<u>Bond Angles (°)</u>			
O	Cu1	O1	174.9	O2	Cu1	O1	176.7
O	Cu1	N1	83.4	O2	Cu1	N1	83.2
O	Cu1	N3	86.0	O2	Cu1	N2	88.0
O1	Cu1	N1	91.5	O1	Cu1	N1	94.6
O1	Cu1	N3	98.9	O1	Cu1	N2	94.6
N1	Cu1	N3	164.0	N1	Cu1	N2	164.0
Cu1	O	Cu2	126.5	Cu1	O	Cu2	122.5
O	Cu2	O2	172.8	O2	Cu2	O1'	173.6
O	Cu2	N2	83.8	O2	Cu2	N1'	83.2
O	Cu2	N4	86.0	O2	Cu2	N3	88.1
O2	Cu2	N2	91.6	O1'	Cu2	N1'	*
O2	Cu2	N4	99.4	O1'	Cu2	N3	88.1
N2	Cu2	N4	166.0	N1'	Cu2	N3	166.8

TABLE 6.7: Relevant Bond Angles of a) Cu<sub>2</sub>(M<sup>2</sup>BP-DPL)3,5-Me<sup>2</sup>Pz and b) Cu<sub>2</sub>(SAL-DPL)Pz

\* Data not available

**7:**

**Mass Spectra**



## 7: Mass Spectra of The Copper Complexes

The mass spectral data is collected in the appendix. Some of the mass signals appear to correspond to the molecular ions. Table 7.1 lists the masses of these ions and their assignments. The other complexes show only fragmentation masses with some unusual fragments apparently occurring. Some of the complexes give mass signals greater than the mass of the molecular ion and these masses and their possible assignments are given in Table 7.3, while the masses of the exogenous bridges, where they occur, the common positive ions and common negative ions along with their possible assignments are given in Tables 7.2, 7.4 and 7.5 respectively. The other binuclear complexes were not studied due to our inability to find suitable media in which to dissolve these complexes.

<u>Mass Weight</u>	<u>Assignment</u>
612	$\text{Cu}_2(\text{SAL-DPE})_6\text{NO}_2\text{IND}$
516	$\text{Cu}_2(\text{SAL-DPL})\text{PyO}$
487	$\text{Cu}_2(\text{SAL-DPL})(\text{CAT})_{0.5}(\text{H}_2\text{O})_{0.5}$
360	$\text{Cu}(\text{SAL-DPLH})$

**Table 7.1: Mass Signals Corresponding to Molecular Ions**

<u>Mass Weight</u>	<u>Assignment</u>
122	$3\text{-MeCAT}^{2-}$
107	$\text{CAT}^{2-}$
162	$6\text{NO}_2\text{IND}^-$
94	$\text{PyO}^-$

**Table 7.2: Mass Signals of The Exogenous Bridges**

<u>Mass Weight</u>	<u>Assignment</u>
937	$\text{Cu}_4(\text{SAL-DPL})_2\text{PyO}^+$
845	$\text{Cu}_4(\text{SAL-DPL})_2\text{H}_3^+$
781	$\text{Cu}_3(\text{SAL-DPL})_2\text{H}_2^+$
647	$\text{Cu}_4(\text{SAL-DPL})\text{PyO}$
580	$\text{Cu}_3(\text{SAL-DPL})\text{PyO}$
<hr/>	
782	$\text{Cu}_2(\text{SAL-DPE})6\text{NO}_2\text{IND} + \text{C}_8\text{H}_6\text{NOCu}$
776	$\text{Cu}_2(\text{SAL-DPE})6\text{NO}_2\text{IND} + \text{C}_5\text{H}_{11}\text{NOCu}$
757	$\text{Cu}_2(\text{SAL-DPE})6\text{NO}_2\text{IND} + \text{C}_7\text{H}_7\text{OCu}$
<hr/>	
422	$\text{Cu}(\text{SAL-DPLH}) + \text{Cu}$
<hr/>	
844	$\text{Cu}_4(\text{SAL-DPL})_2$ or $\text{Cu}_2(\text{SAL-DPL})(\text{CAT})_{0.5}(\text{H}_2\text{O})_{0.5} + \text{Cu}(\text{SAL-DPLH})$
<hr/>	
845	$\text{Cu}_4(\text{SAL-DPL})_2$

Table 7.3: Mass of the Associated Ions

<u>Mass Weight</u>	<u>Assignment</u>
450	$\text{Cu}_2(\text{SAL-DPE})$
422	$\text{Cu}_2(\text{SAL-DPL})$
360	$\text{Cu}(\text{SAL-DPLH})$
307	$\text{C}_{10}\text{H}_{16}\text{N}_2\text{OCu}_2^*$
288	$\text{C}_9\text{H}_7\text{NO}_2\text{Cu}_2^*$
196	$\text{C}_8\text{H}_6\text{NOCu}_2^*$
154	$\text{C}_3\text{H}_{10}\text{N}_2\text{OCu}^*$
136	$\text{C}_3\text{H}_7\text{NOCu}^*$
121	$\text{C}_7\text{H}_6\text{NO}^*$
107	$\text{C}_7\text{H}_7\text{O}^*$
89	$\text{C}_6\text{OH}^*$
77	$\text{C}_6\text{H}_5^*$
65	$\text{Cu}$

Table 7.4: Positive Common Ion Mass Signals

\* Possible structures for these common ions are shown in Table 7.6

<u>Mass Weight</u>	<u>Assignment</u>
421	$\text{Cu}_2(\text{SAL-DPL})$
305	$\text{C}_{16}\text{H}_{12}\text{NO}_2\text{Cu}_2^{**}$
224	$\text{C}_9\text{H}_8\text{NO}_2\text{Cu}^{**}$
199	$\text{C}_8\text{H}_9\text{NOCu}^{**}$
168	$\text{C}_7\text{H}_5\text{OCu}^{**}$
151	$\text{C}_3\text{H}_8\text{N}_2\text{OCu}^{**}$
136	$\text{C}_3\text{H}_7\text{NOCu}^{**}$
120-122	$\text{C}_7\text{H}_7\text{NO}^{**}$

**Table 7.5: Negative Common Ion Masses**

**\*\* Possible structures of these common ions are shown in Table 7.7**

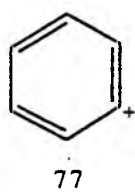
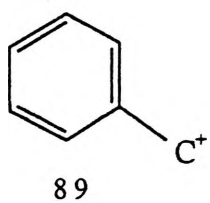
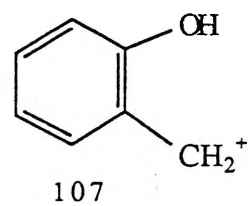
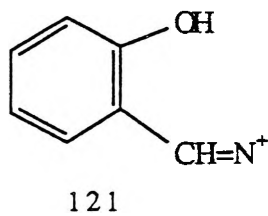
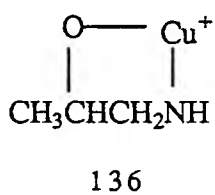
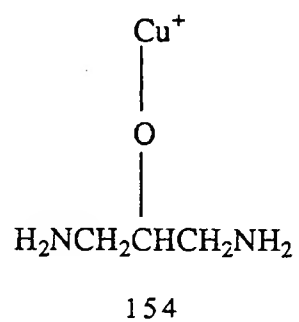
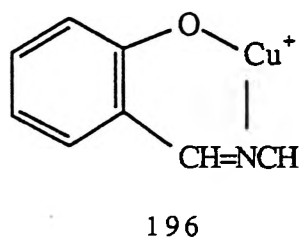
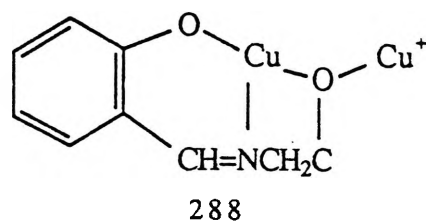
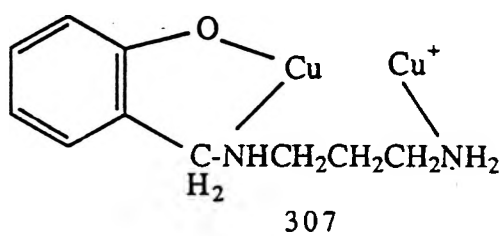


Table 7.6: Possible Positive Common Ion Structures

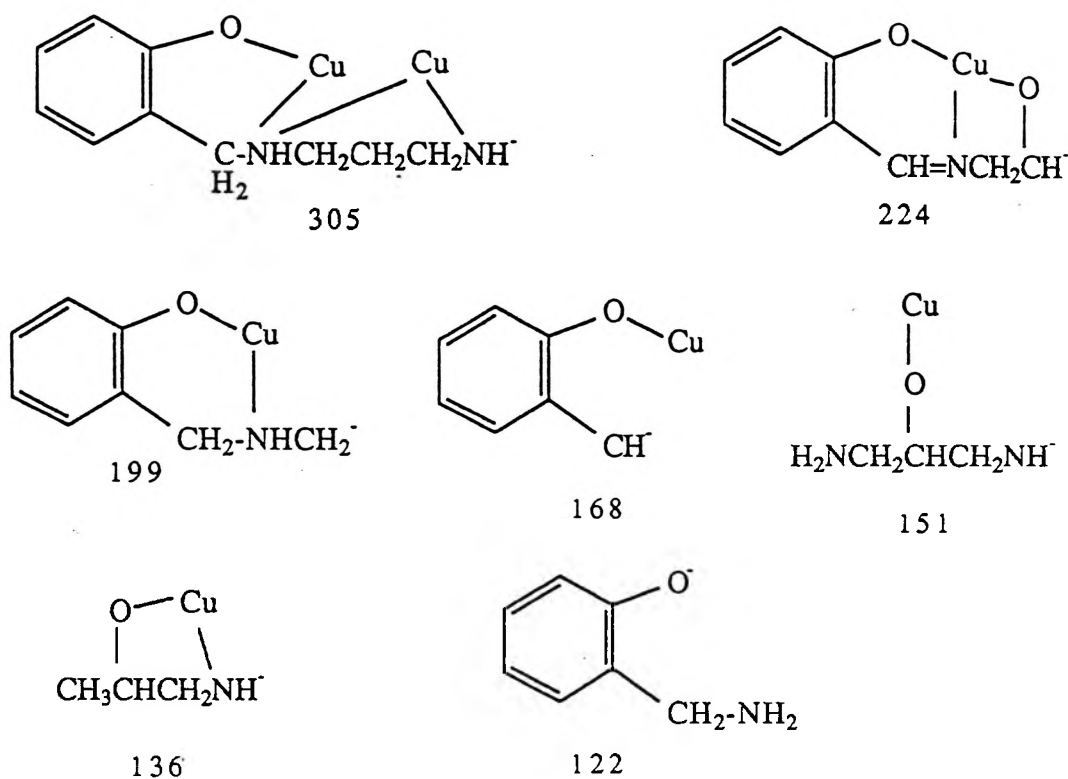


Table 7.7: Possible Negative Common Ion Structures

In conclusion mass spectral studies are not a particularly useful diagnostic tool for these complexes, although common ions and associated ions were found for some complexes.

**8:**

## **Electrochemistry**

## 8: Electrochemistry

A study of the electrochemical behaviour of copper proteins is important, as the proposed modes of function of these proteins involves the oxidation/reduction of the copper centre between the +1 and +2 oxidation states.

Electrochemical studies of model copper complexes provides data on the potential of the oxidation/reduction couple, the number of electrons transferred in an oxidation/reduction couple and whether the couple is reversible. Electrochemistry also provides information on the stability of the complex at any given potential. The electrochemical data of some copper proteins and the copper centre involved in the reduction/oxidation are given in Table 8.1.

<u>Copper Protein</u>	<u>E<sub>1/2</sub></u>	<u>Type of Copper Centre</u>
Tyrosinase <sup>158</sup>	360mV	III
<u>Multi-copper Oxidases</u>		
Laccase <sup>159-168</sup>	415mV	I
	434mV, 782mV	III
Ceruloplasmin <sup>169-170</sup>	490mV	I
	580mV	III
Ascorbate Oxidase <sup>171-172</sup>	344mV	I
	slightly higher	III

Table 8.1: Electrochemical Data of Copper Proteins

There are a number of techniques available to investigate the electrochemistry of the copper proteins and model compounds. The most useful techniques are cyclic voltammetry, differential pulse voltammetry, polarography and coulometry.



### 8.1. Cyclic Voltammetry

The main use of cyclic voltammetry is to provide a preliminary mechanistic investigation of the system under study. The technique allows the rapid determination of potentials at which electrochemical processes occur.<sup>173-174</sup>

Its mode of action is the application of a steadily changing potential, to a designated potential limit at which point the potential scan reverses direction and steadily reverts to the other limit, at which it can be stopped or cycled back again. This results in a triangular excitation signal (Fig 8.1).

The cell current is recorded as a function of the applied potential and gives a voltammogram similar to that shown in Fig 8.2. The data available is the cathodic and anodic peak potential,  $E_{pc}$  and  $E_{pa}$ , the anodic and cathodic peak currents,  $I_{pa}$  and  $I_{pc}$ , and the half peak potentials  $E_{p/2c}$  and  $E_{p/2a}$  (Fig 8.2).<sup>173</sup>

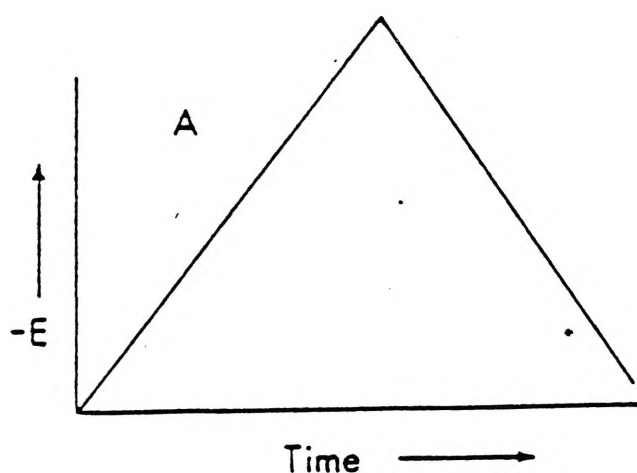


FIG 8.1:<sup>174</sup> Excitation Signal in Cyclic Voltammetry

One important piece of data available from cyclic voltammetry is the reversibility of the process, i.e. does e.g. copper (II) reduce to copper (I) and reoxidise back completely (reversible) or does the copper reduce without reoxidising (irreversible) or does only some of the copper reoxidise (quasi-reversible). A reversible system is important in copper proteins, otherwise with time the protein will cease to function unless it is constantly renewed by the production of new protein.

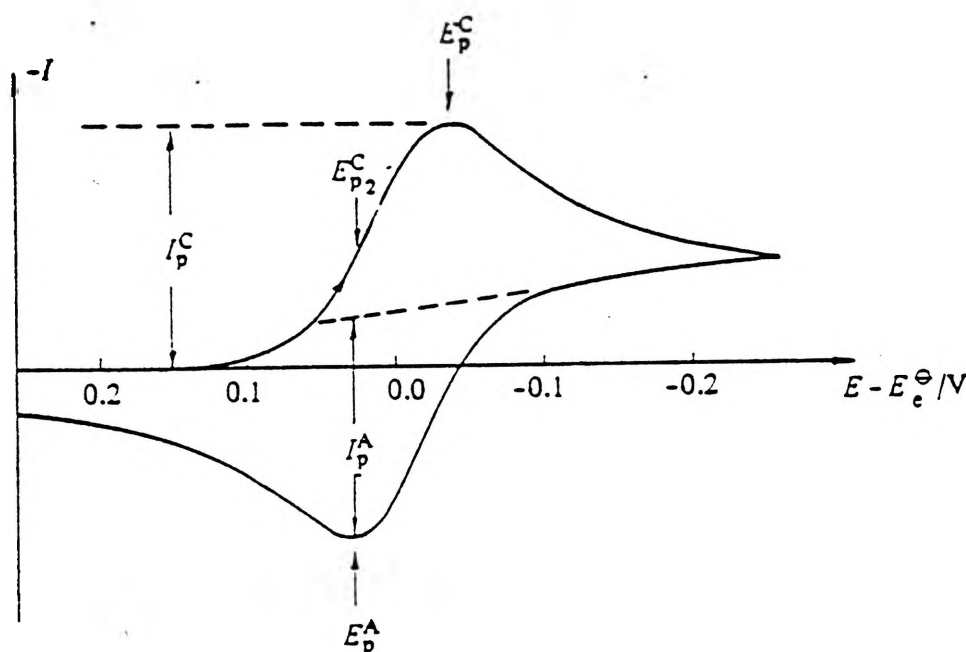


FIG 8.2: 173-174 Kinetic Data from a Typical Cyclic Voltammogram

One test of reversibility is a plot of  $I_p$  versus  $V^{1/2}$ , where  $V$  is the scan rate in mV/s. Linearity passing through the origin implies a reversible system. There are other tests available for reversibility, irreversibility and quasi-reversibility.<sup>173</sup>

## 8.2. Differential Pulse Voltammetry (DPV)<sup>173-176</sup>

This method involves the use of a slow D.C. voltammetric sweep over which is superimposed a series of square wave pulses (Fig 8.3).<sup>173</sup> The current is measured just prior to the beginning and just before the end of the pulse. The difference between these two values is then recorded as a function of the potential. The voltammogram is peak shaped (Fig 8.4).<sup>173</sup>

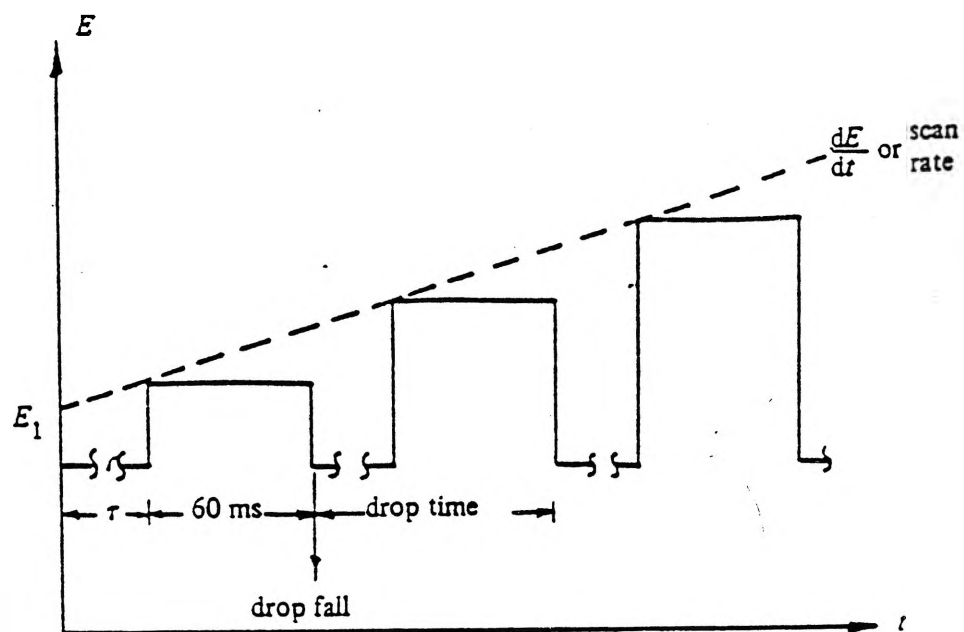


FIG 8.3:173 Applied DPV Sweep

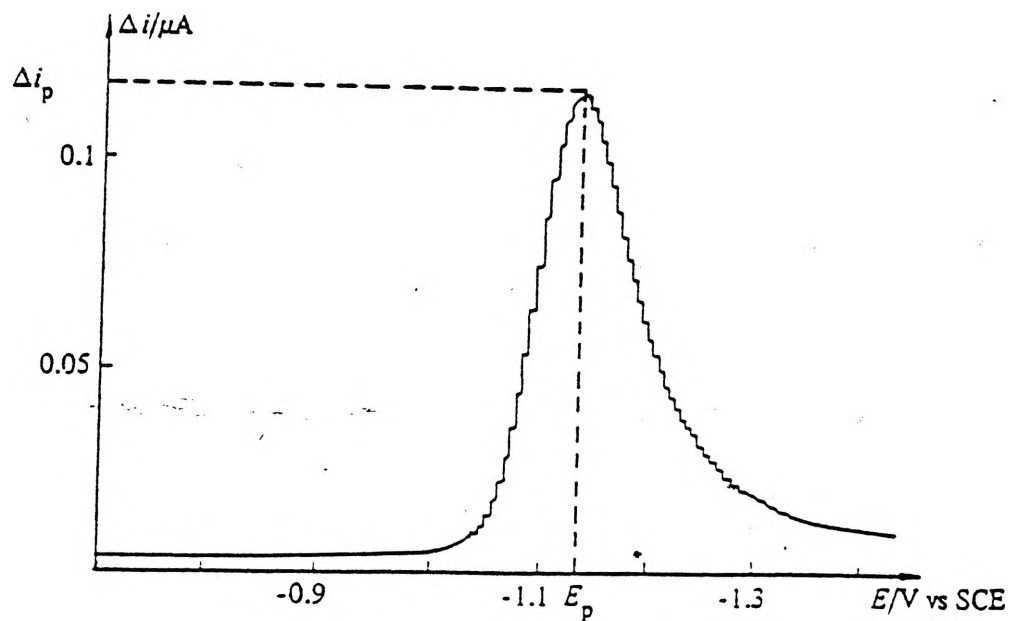


FIG 8.4:173 Typical DPV Response

From the differential pulse voltammetry a variety of information can be determined, e.g. the number of electrons involved in a reduction can be determined from the equation below. Greef et al.<sup>173</sup> state that the diffusion coefficient typically has the value  $10^{-5} \text{ cm}^2 \text{ s}^{-1}$ .

$$I_p = 2.72 \cdot 10^5 n^{3/2} D^{1/2} A V^{1/2} C^0$$

$I_p$  = peak current (A)

$C^0$  = concentration of bulk solution (moles  $\text{L}^{-1}$ )

$D$  = diffusion coefficient ( $10^{-5} \text{ cm}^2 \text{ s}^{-1}$ )

$A$  = area of electrode surface ( $\text{mm}^2$ )

$n$  = number of electrons

$V$  = scan rate ( $\text{mVs}^{-1}$ ).

### 8.3. Coulometry

Coulometry is also called constant potential electrolysis. In this technique the potential is held steady and the current (Amperes) and charge (coulombs) are measured as a function of time.<sup>173</sup>

This method allows a direct determination of the number of electrons being passed for any one process as indicated by cyclic voltammetry.<sup>176</sup>

The limiting current  $I_t$  should fall according to the equation of Lingane et al.<sup>178</sup>

$$I_t = I_0 \exp(-bt)$$

$I_0$  = initial current

$b$  = constant related to the mass transfer coefficient ( $DA/V\partial$ ) ( $\partial$  = thickness of diffusion layer).

The reason for the decrease in current is that the limiting current is a function of the mass transfer coefficient and the concentration of the sample. As the reaction proceeds the concentration of the sample decreases and so the limiting current decreases.<sup>177</sup>

A plot of  $\log I$  with time is linear, while a plot of the charge passed ( $Q_D$ ) versus  $I_t$  should be linear for a simple reaction mechanism.<sup>173</sup> From this plot  $Q^B$  (the total charge) can be determined by extrapolation back to  $I_t = 0$ .

The total charge passed is also equal to  $nFCV$ ; i.e.

$$Q^B = nFCV$$

$n$  = number of electrons

$F$  = Faraday constant

$C$  = concentration of species

$V$  = volume of solution.

#### 8.4 Polarography

Polarography is a technique which uses a dropping mercury electrode and its mode of function is based on determining the change in the average current for the mercury drop measured over time (Fig 8.5).<sup>179</sup> The current is controlled by diffusion processes and this gives rise to the alternate name of DC Polarography for this technique.

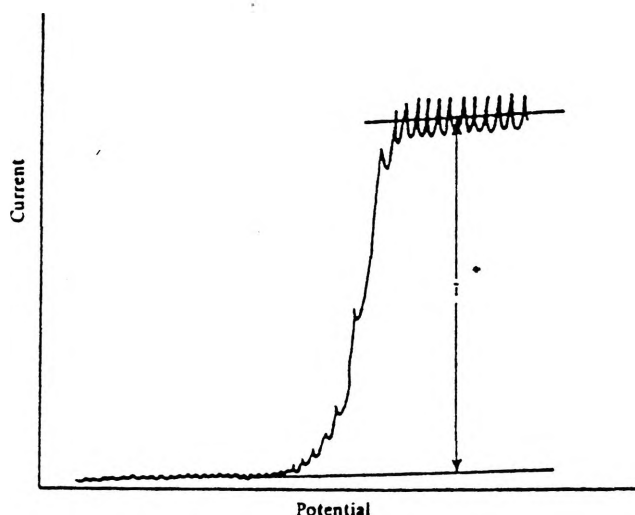


Fig 8.5: Typical Polarogram

The change in the current of the drop with changing potential can be measured to give a plot as shown in Fig 8.6.<sup>179</sup>

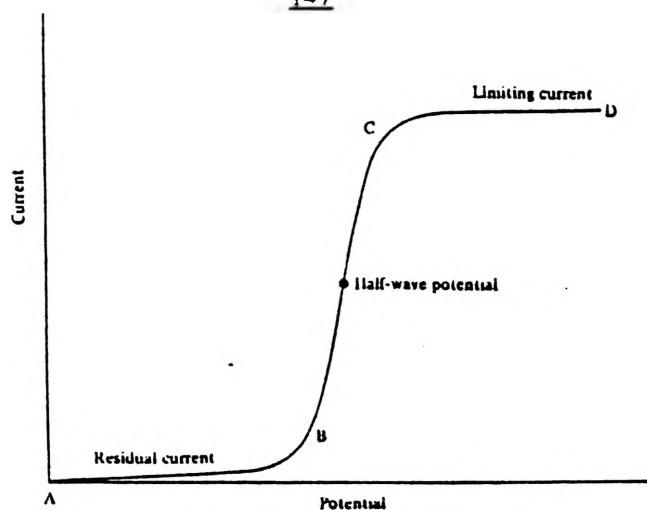


Fig 8.6: Changing Drop Potential

It can be seen from this that at low potentials the current is small (A-B). This is known as the residual current. As the reduction potential of the species under study is reached the current rises exponentially for only a small change in potential (B-C). This occurs until the current is limited by mass transfer (C-D). This area is known as the mean limiting current and is proportional of the bulk concentration of the reducible species.

The halfwave potential is representative of the reducible species and represents the point where the ratio of oxidised and reduced species represents unity.<sup>180</sup>

As can be seen from Fig 8.7<sup>181</sup> the nature of the polarogram changes for a reversible system as compared to an irreversible system with the reversible process being clean and sharp and the irreversible process having more a gradual rise in current rather than a sharp rise.

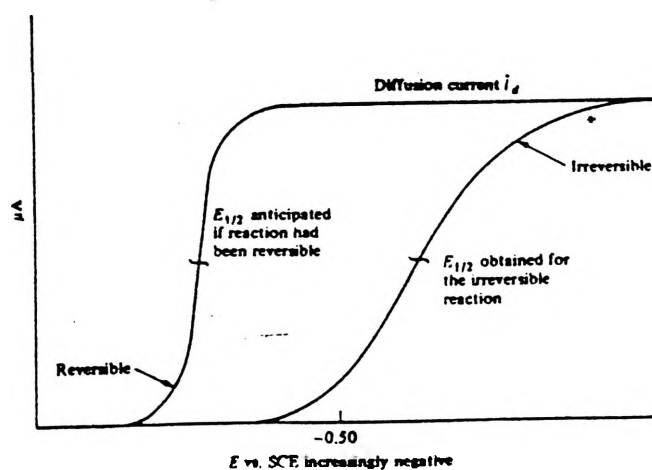


Fig 8.7: Change in Polarogram for Reversible and Irreversible Systems

### 8.5. Summary

The use of cyclic voltammetry and differential pulse voltammetry allows the reversibility of the system to be investigated. Coulometry allows a very accurate determination of the number of electrons being transferred at any one potential.

All four techniques have limitations to their accuracy or convenience. Cyclic voltammetry and differential pulse voltammetry have the following limitations:-

- I) limited potential range available.
- II) below +1.6V the surface of the platinum electrode becomes roughened and blackened altering the electrode response.
- III) oxidised and reduced states need to be stable otherwise the electrode is easily contaminated with the decomposition products of the sample being studied.
- IV) both cyclic voltammetry and differential pulse voltammetry require the presence of a supporting electrolyte thereby introducing impurities to the system.
- V) in cyclic voltammetry a number of scan rates need to be used to give meaningful results.
- VI) in differential pulse voltammetry the height and shape of the peak is sensitive to the systems reversibility.

The limitations of coulometry are:<sup>177</sup>

- I) the equipment is relatively complicated.
- II) the integration of the current time is difficult and is of limited precision.
- III) as the length of time at low current increases the effect of background and impurity currents becomes more significant.
- IV) sources of efficiency loss are:-
  - a) unwanted reactions.
  - b) electromigration in divided cells.

V) the current efficiency must be 100%.

VI) solution stirring is required.

VII) coulometry is only successful for processes that are kinetically moderate or fast.

The limitations of polarography are:

I) the electrode set up is complicated.

II) polarography maxima occur.

III) a supporting electrolyte is required.

IV) the sloping baseline makes identification of kinetically slow processes very difficult.

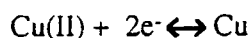
The last limitation which applies to all four techniques and is that the cells need to be oxygen free so as to eliminate secondary reactions involving oxygen.

### 8.6 Coulometry of the Copper Complexes

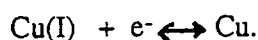
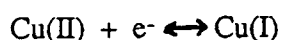
#### a) Cu(SAL-DPLH)

Coulometry measurements of Cu(SAL-DPLH) indicate that, at -1600mV, a 2.19 electron reduction per mole of complex occurs. At -300mV 2.10 electrons are involved in the reoxidation of the reduced complex (Table 8.2). This redox process can occur in two ways;

(1) in a single process involving the transfer of both electrons at the same potential



or (11) the electrons could be transferred in two one electron processes

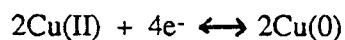




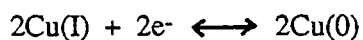
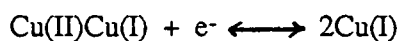
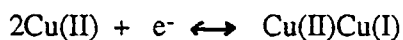
## b) Binuclear Copper Complexes

Coulometry measurements of  $\text{Cu}_2(\text{SAL-DPL})\text{X}$  indicate that, at -1600mV, a 4 electron reduction per mole of complex occurs. At -300mV 4 electrons are involved in the reoxidation of the reduced complexes (Table 8.2). There are a number of ways these four electrons could be transferred;

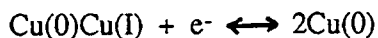
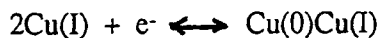
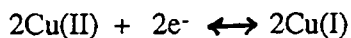
(1) a single four electron reduction/oxidation



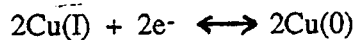
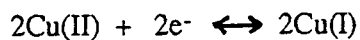
(II) two one electron reductions followed by a two electron reduction



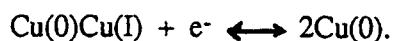
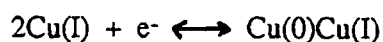
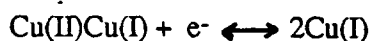
(III) a two electron reduction followed by two one electron reductions



(IV) two two electron reductions



(V) four one electron reductions



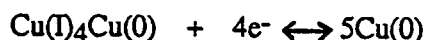
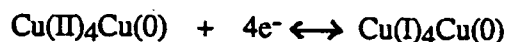
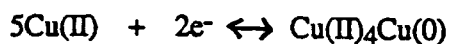
Given the similarities of the copper environments around each copper atom it would seem that either the single four electron reduction or two two electron reductions are the most likely methods of reduction. Coulometry does not indicate which method occurs and consequently other techniques are used.

#### c) Pentanuclear Copper Complexes

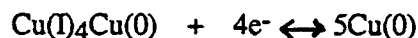
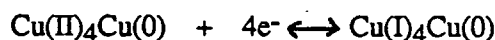
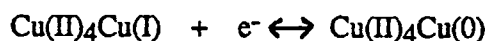
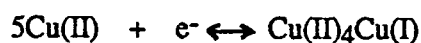
Coulometric measurements of  $\text{Cu}_5$  complexes at -1600mV gives a result of 10 electrons per mole of complex for the reduction. At -300mV the complexes undergo a reoxidation using 10 electrons per mole of complex (Table 8.2). In the case of  $\text{Cu}_5(\text{SAL-DPL.PAB.SAL})_2 \cdot 3\text{H}_2\text{O}$ , a coulometry measurement was also run at -1100mV with a result of a clear cut endpoint indicating two electrons transferred per mole of complex below -1100mV. After the endpoint was established the coulometer was adjusted to -1600mV and a further eight electrons were measured as having been transferred. This gives a total of ten electrons per mole of complex with two electrons per mole transferring below -1100mV.

In the pentanuclear complexes in general these ten electrons can be transferred in a number of ways. The most likely ways based on the earlier results and those of  $\text{Cu}_5(\text{SAL-DPL.PAB.SAL})_2 \cdot 3\text{H}_2\text{O}$  are

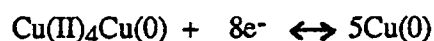
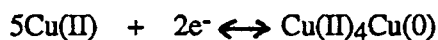
I) one two electron reduction followed by two four electron reductions



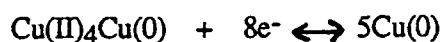
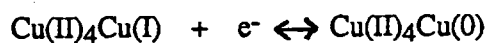
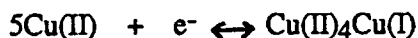
or, II) two one electron reductions followed by two four electron reductions



or, III) a single two electron reduction followed by a single eight electron reduction



or, IV) two one electron reductions followed by a single eight electron reduction



The other pentanuclear complexes could undergo a single ten electron reduction or two five electron reductions or other combinations, although these are less likely given the results found for



	-1600mV	-300mV		
Cu(SAL-DPLH)	2.19 electrons	2.10 electrons		
Cu <sub>2</sub> (SAL-DPL)OH.3H <sub>2</sub> O	4.07	3.90		
Cu <sub>2</sub> (SAL-DPE)OH	4.10	4.07		
Cu <sub>2</sub> (SAL-DPL)(CAT) <sub>0.5</sub> (H <sub>2</sub> O) <sub>0.5</sub>	3.93	4.02		
Cu <sub>2</sub> (SAL-DPE)CATH	4.23	4.20		
Cu <sub>2</sub> (SAL-DPL)4-OHBzCOO	3.86	3.92		
Cu <sub>2</sub> (SAL-DPL)Pz	3.85	3.97		
Cu <sub>2</sub> (SAL-DPE)Pz	3.84	4.02		
Cu <sub>2</sub> (SAL-DPL)PyO(H <sub>2</sub> O) <sub>0.5</sub>	3.73	4.07		
			-1100mV	-300mV
Cu <sub>5</sub> (SAL-DPL.SAL.PAB) <sub>2</sub> .3H <sub>2</sub> O	9.82	10.15	2.04	2.01
Cu <sub>5</sub> (SAL-DPL.4ABA.SAL) <sub>2</sub> .2H <sub>2</sub> O	9.91	9.80		
Cu <sub>5</sub> (ESAL-DPL.6AIESAL) <sub>2</sub> .2H <sub>2</sub> O	10.50	10.21		

Table 8.2: Coulometry Results

Coulometry cannot distinguish between the different possibilities so additional electrochemical techniques were used. These techniques were DC Polarography, differential pulse voltammetry and cyclic voltammetry.

Reduction/oxidation of the copper atoms in all the solutions was confirmed by UV-Vis spectrophotometry, Fig 8.8a shows this for Cu(SAL-DPLH). As reduction occurs, the copper(II) d-d transition peak at 625nm disappears confirming that the copper(II) atom of Cu(SAL-DPLH) is being reduced to a species which has no d-d spectra, e.g. copper(I) or copper(0). Copper metal is seen to precipitate out of solution onto the mercury pool surface. Reoxidation of this suspension at -300mV is accompanied by the reappearance of a copper(II) d-d transition peak at 640nm (Fig 8.8b).

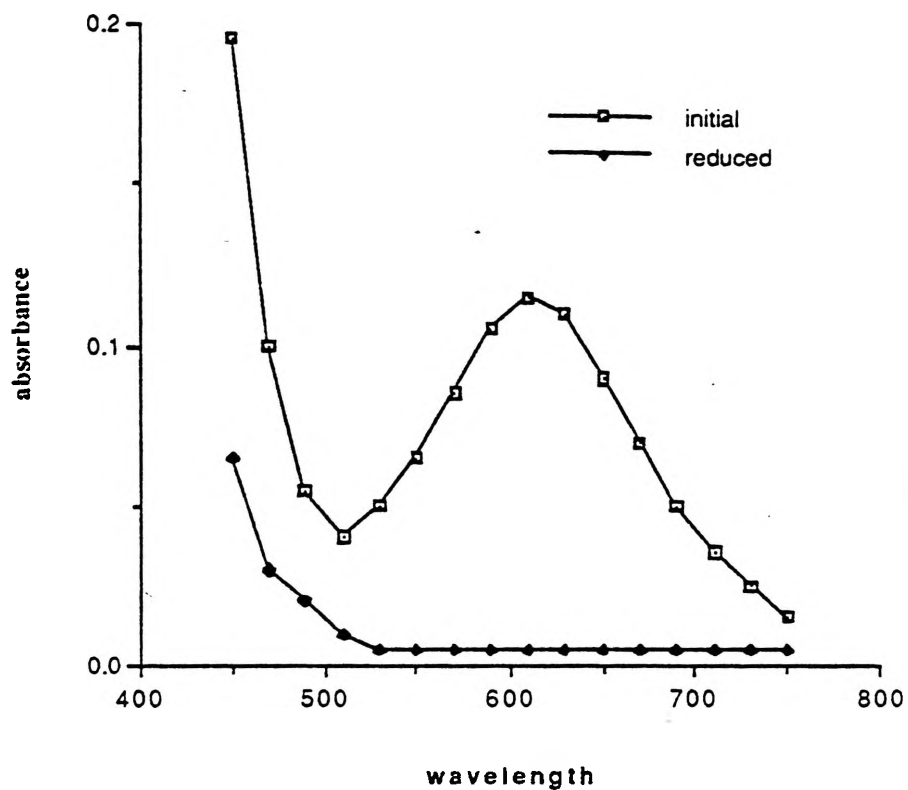


Fig 8.8a: Initial and Reduced UV-Vis Spectra of Cu(SAL-DPLH)

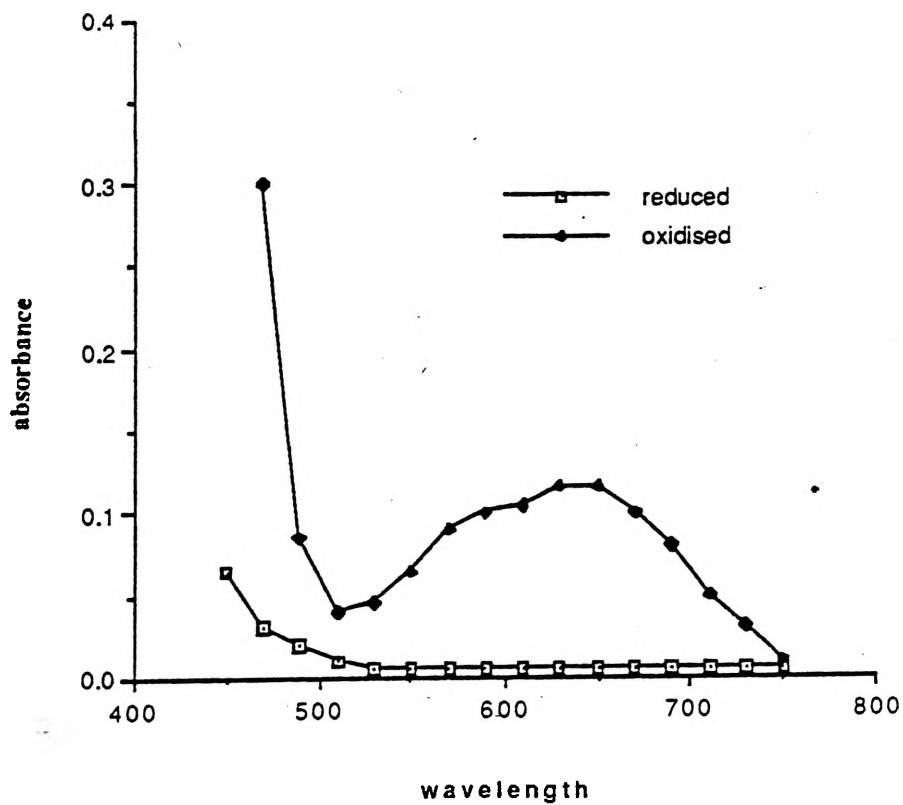


Fig 8.8b: Reduced and Oxidised UV-Vis Spectra of Cu(SAL-DPLH)

### 8.7 Cu(SAL-DPLH)

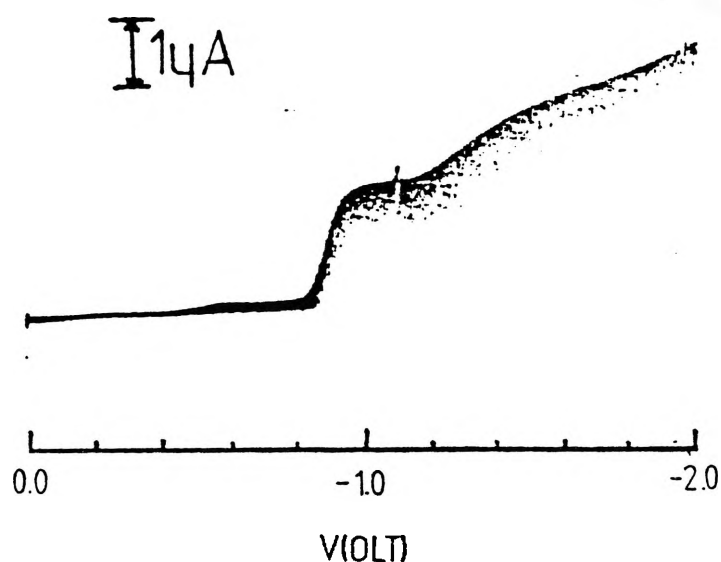
#### a) DC Polarography.

DC Polarography has two features which help in the understanding of the electrochemical processes of these copper complexes and both are related to the nature of the electrode surface. In polarography the electrode surface consists of a mercury drop which is constantly renewed, in this case every second. This means that the electrode surface is not subject to the contamination problems which can affect solid electrode surfaces. This is important in these complexes as the copper (II) reduces to copper metal and deposits upon the electrode surface thereby fouling the surface and interfering with the accuracy of the results. Due to the clean electrode surface in DC Polarography, the potential at which electrochemical processes occur can be more accurately determined. Each redox process is separately shown and the relative peak heights are indicative of the current involved in each process; e.g. two processes with a peak height ratio of 1:1 indicate two one electron steps where coulometry indicates a total of two electrons being transferred.

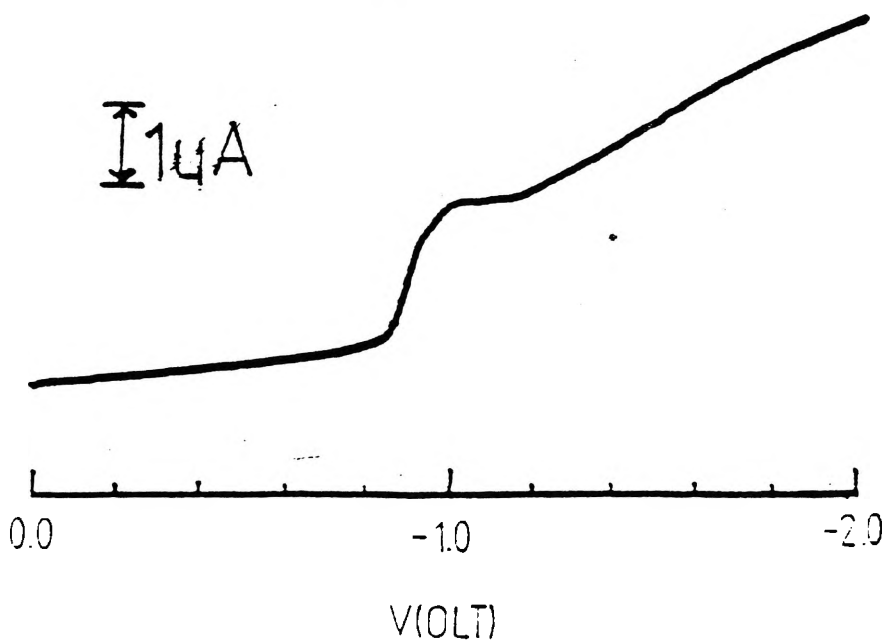
During the DC Polarographic investigation of Cu(SAL-DPLH) it was initially found that there were two peaks at  $E_{1/2} = -1090\text{mV}$  and  $E_{1/2} = -1400\text{mV}$  with a peak height ratio of 7:1 (Table 8.3). This ratio was considered unusual in view of the other electrochemical data for Cu(SAL-DPLH) and the fact that there is only one copper atom as the source of electrons. Initially it was believed that the second peak may have been the result of an impurity and consequently the sample of Cu(SAL-DPLH) was recrystallized.

The DC Polarography was rerun and gave a result of two peaks at  $E_{1/2} = -1135\text{mV}$  and  $E_{1/2} = -1385\text{mV}$  with a peak height ratio of 1:1 (Table 8.3). This seemed reasonable on its own but was inconsistent with the differential pulse voltammetry results. Further studies of Cu(SAL-DPLH) revealed that contamination of the sample was occurring through incomplete exclusion of oxygen (to which the techniques are very sensitive and consequently the cell was redesigned to rigorously exclude oxygen.

The redesigned cell gave a DC Polarography result of one process at  $E_{1/2} = -970\text{mV}$  (Table 8.3, Fig 8.9). This result indicates that the two electrons are transferred in a single step which is accompanied with the complex breakdown as copper metal is formed. The upward sloping trend of the polarogram after the reduction is a common effect and due to the gradual increase of the residual current. This current is seen also in coulometry where after the rapid electron exchange of the reduction, the coulometry cell reaches a 'steady state' where a small number of coulombs flow for whatever period the potential is continued to be applied.



a) Raw Data



b) Redrawn Data

Fig 8.9: DC Polarogram of Cu(SAL-DPLH)

## b) Differential Pulse Voltammetry

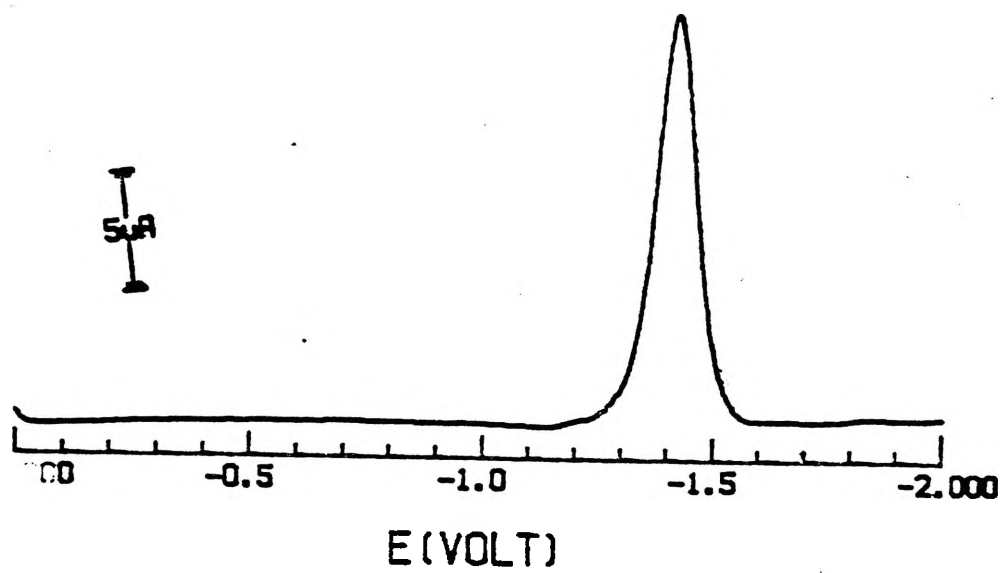
Differential pulse voltammetry indicates the potential at which redox processes occur. If the diffusion coefficient for a system is known accurately the number of electrons involved in a process can be calculated by utilizing the equation of Greef et al.<sup>173</sup> This means that differential pulse voltammetry along with cyclic voltammetry are useful techniques for initially gaining insight into any redox processes occurring in complexes. However both differential pulse voltammetry using a solid surface electrode and cyclic voltammetry suffer from some problems which diminish their usefulness in an indepth study of Cu(SAL-DPLH). These problems are related to the fact that they utilise a solid electrode surface. The electrode surface can become fouled by precipitation of copper while the scan is being carried out. This results in the diffusion coefficient being indeterminate as the thickness and diameter of the electrode surface is continually changing making the above equation unuseable for these complexes. This problem can be avoided in differential pulse voltammetry by using a dropping mercury electrode.

As with polarography the number of peaks can reflect the number of redox processes occurring in a system, the potential at which each process occurs and the current flowing as a result of the reactions.

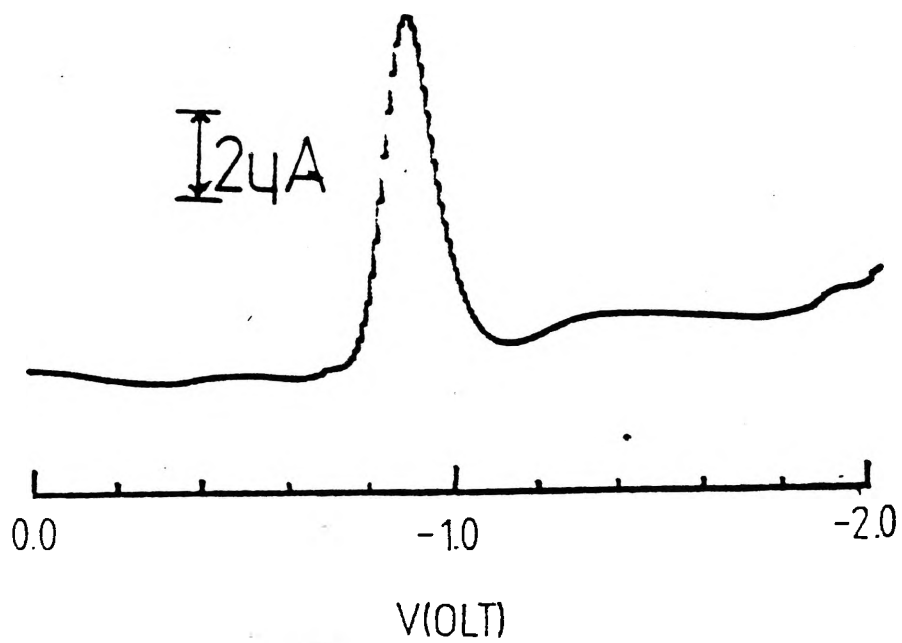
The recrystallized sample of Cu(SAL-DPLH) in the redesigned cell shows, in differential pulse voltammetry using a glassy carbon electrode, one major process at  $E_{1/2} = -1420\text{mV}$  (Table 8.3, Fig 8.10a). This result is consistent with the DC Polarography result which also shows one process. Using a dropping mercury electrode gave a result of one peak at  $E_{1/2} = -935\text{mV}$ , which is also consistent with the DC Polarography result (Table 8.3, Fig 8.10b).

The reason for the shift in potential between a mercury electrode surface and a glassy carbon surface is due to the difference in electrode material and indicates that the Cu(SAL-DPLH) is easier to reduce on a mercury electrode than it is on glassy carbon.





a) Glassy Carbon



b) Dropping Mercury

Fig 8.10: Differential Pulse Voltammogram of Cu(SAL-DPLH)

### c) Cyclic Voltammetry

Cyclic voltammetry is a useful technique for investigating reduction/oxidation processes occurring in these complexes as it is able to easily give an indication of the number of reduction/oxidation processes occurring in the scan range, the potential at which each reduction and oxidation process occurs and the reversibility of these processes. For a fully reversible system the peak current ratio ( $I_R^P/I_F^P$ ) should be 1:1 and have a reduction peak-oxidation peak separation ( $E_A^P/E_C^P$ ) of  $59/n$  mV where  $n$  = the number of electrons (e.g. for a two electron transfer ( $n = 2$ ) the peak to peak separation should be 29-30mV)<sup>137</sup>. For an irreversible system the peak current ratio should be zero as no reverse peak occurs. This gives two quick methods of determining the reversibility of any process.

The recrystallized sample of Cu(SAL-DPLH) again shows one reduction process at  $E_{1/2} = -1490$  mV with the reduction being quasi-reversible ( $I_R^P/I_F^P = 0.62$  and  $E_A^P/E_C^P = 120$  mV) (Table 8.3, Fig 8.11a). This result agrees with all the other results and indicates that the Cu(SAL-DPLH) complex undergoes a single quasi-reversible reduction involving a two electron transfer.

It should be noted that cooling of the Cu(SAL-DPLH) solution results in a decrease in the currents involved in all the processes which implies that all the processes involve the stereochemical rearrangement of the molecule as would be expected for a reduction of copper(II) to copper(I) and/or copper metal as copper(II) prefers a square planar configuration and copper(I) prefers a tetrahedral configuration and cooling restricts this rearrangement causing the current to drop.

Multiple scans of Cu(SAL-DPLH) were conducted (Table 8.3, Fig 8.11b) to examine the stability of the complex. It was found that for up to five scans the complex is reasonably stable with there being a reduction in the current of the reduction process after the first scan. Further scans show little reduction in current nor any shift in potential indicating that Cu(SAL-DPLH) is reasonably stable down to -2000 mV. The reduction in current is believed to be due to fouling of the electrode surface. The reason there is no further decrease in the current is not clear but it is possible that a copper amalgam is forming on the electrode surface. The complex is considered to exhibit quasi-reversible redox properties.

The only previous electrochemical studies of Cu(SAL-DPLH) have been by Bond et al.<sup>132b</sup> and more recently by Nishida et al.<sup>182</sup>

Bond et al.<sup>132b</sup> report in Table VI of their paper, without any discussion, the DC Polarography results for their sample of Cu(SAL-DPLH). They report only one peak at  $E_{1/2} = -1020\text{mV}$  for a half second drop time. This is consistent with the peak observed for our sample at  $E_{1/2} = -970\text{mV}$ . The difference in potential being attributable to experiment differences.

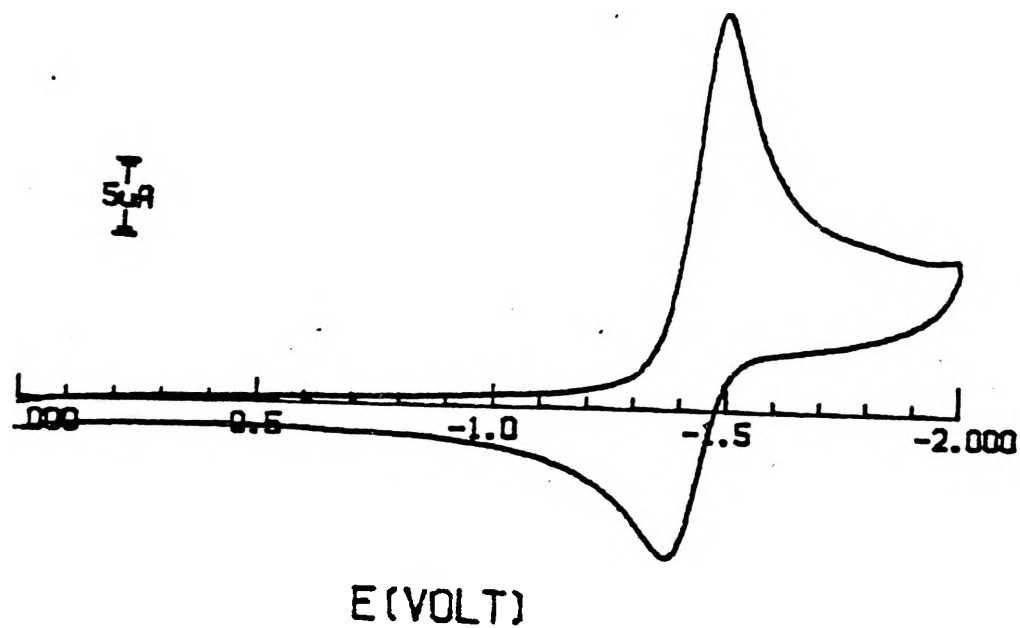
Nishida et al.<sup>182</sup> used Cu(SAL-DPLH) as part of an investigation of superoxide dismutase and reported cyclic voltammetry results for Cu(SAL-DPLH), under argon, with a single quasi-reversible process at  $-970\text{mV}$ .

In summary both Bond et al.<sup>132b</sup> and Nishida et al.<sup>182</sup> report a single process at  $\sim -1000\text{mV}$  for their samples of Cu(SAL-DPLH). The data agrees with our results for Cu(SAL-DPLH). Overall a single two electron reduction from copper(II) to copper metal and SAL-DPL<sup>3-</sup> is observed in our complex while Bond et al.<sup>132b</sup> and Nishida et al.<sup>182</sup> who both conclude that the reduction is from copper (II) to copper (I) based their deductions only on cyclic voltammetry data.

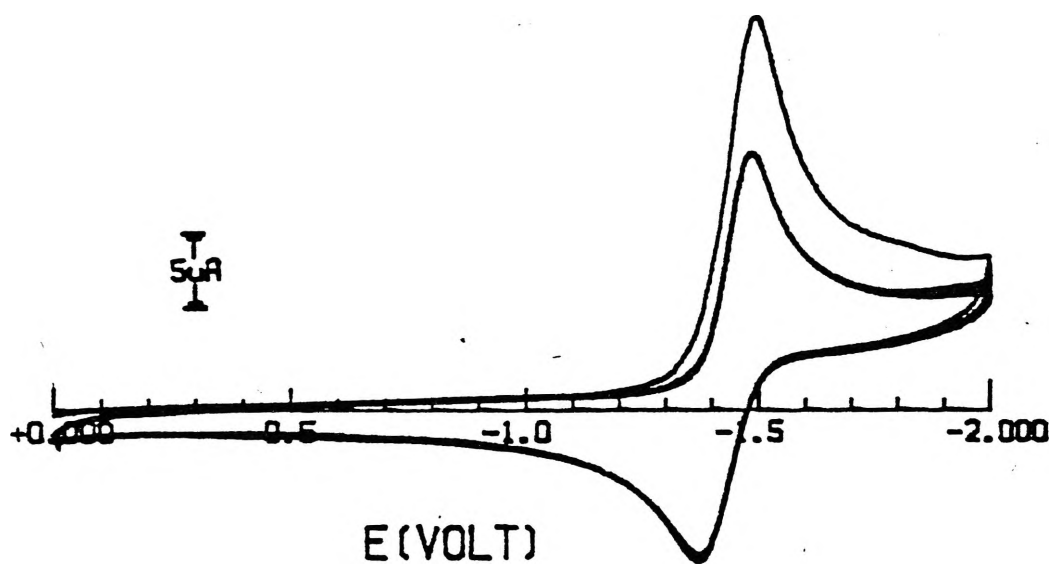
<u>Polarography</u>			Peak 1	Peak 2	Peak Ratio		
			-1090mV	-1400mV	7:1		
Recrystallized			-1135mV	-1385mV	1:1		
New Cell			-970mV	—	—		
<u>DPV</u>	GC	Recrystallized	-1110mV	-1350mV	1:3		
	GC	New Cell	-1420mV	—	—		
	DME		-935mV	—	—		
<u>CV</u>		Reduction	mA	Oxidation	mA	$I_R^P/I_F^P$	$E_A^P/E_C^P$
	Recrys	-1490mV	21.0	-1370mV	13.0	0.62	120mV
	Scan 5	-1490mV	15.0	-1365mV	13.0	0.87	125mV

Table 8.3: Electrochemical Data for Cu(SAL-DPLH)

\* GC = glassy carbon, DME = dropping mercury electrode



a) Initial Scan



b) Multiple Scans

Fig 8.11: Cyclic Voltammograms of Cu(SAL-DPLH)

8.8  $\text{Cu}_2(\text{SAL-DPL})\text{OH}\cdot 3\text{H}_2\text{O}$ 

## a) DC Polarography

DC Polarographic measurements of  $\text{Cu}_2(\text{SAL-DPL})\text{OH}\cdot 3\text{H}_2\text{O}$  in the potential range 0 to -2000mV indicates one reduction process at  $E_{1/2} = -1430\text{mV}$  (Table 8.4, Fig 8.12). This result suggests that the four electrons are transferred in one four electron step.

At slightly higher potential on the residual current a polarographic maximum is observed. These polarographic maxima are a known problem in polarography and also in differential pulse voltammetry using a dropping mercury electrode.

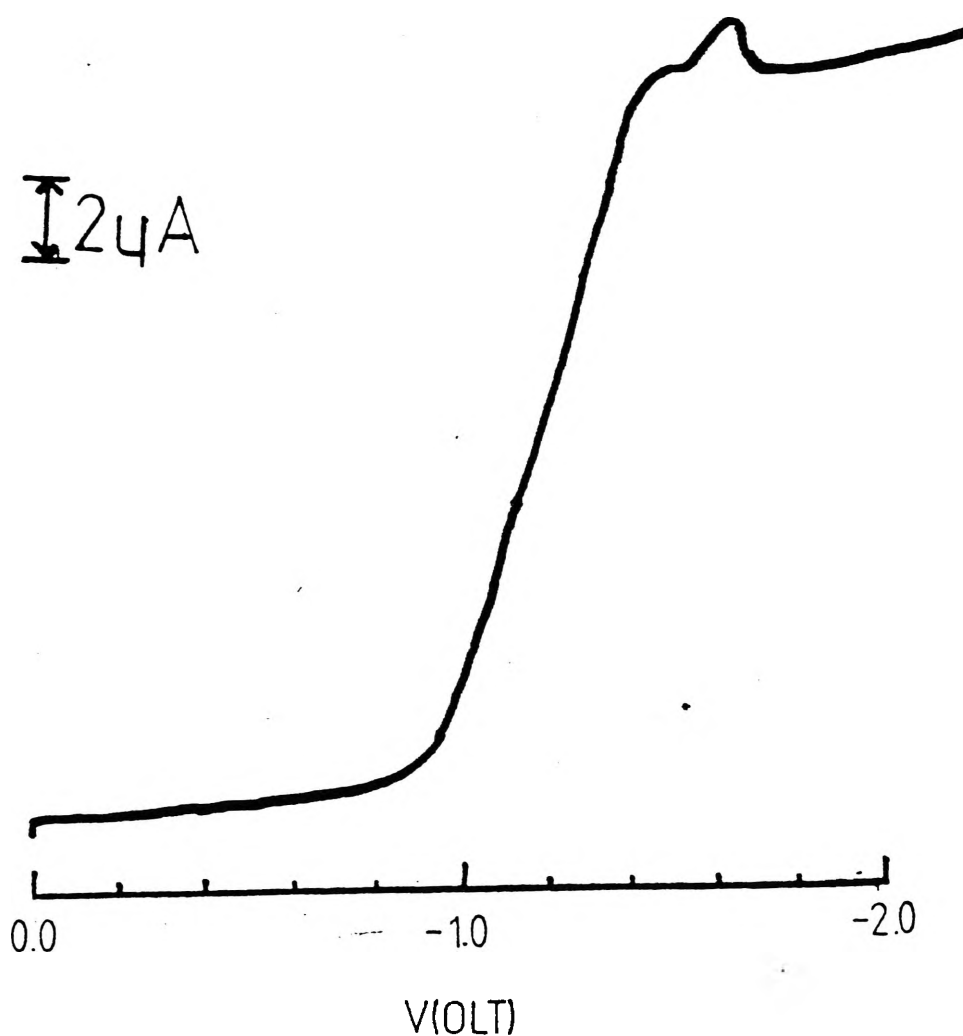


Fig 8.12: DC Polarogram of  $\text{Cu}_2(\text{SAL-DPL})\text{OH}\cdot 3\text{H}_2\text{O}$

## b) Differential Pulse Voltammetry

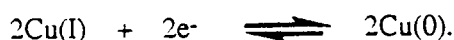
The differential pulse voltammetry investigation of  $\text{Cu}_2(\text{SAL-DPL})\text{OH}\cdot 3\text{H}_2\text{O}$  using a glassy carbon electrode shows only one major reduction process at  $E_{1/2} = -1260\text{mV}$  (Table 8.4, Fig 8.13a). This reduction peak is asymmetric in nature suggesting that there might be two processes very close together in potential. This result agrees with the DC Polarography. There is also a reduction peak at  $E_{1/2} = -1590\text{mV}$  which is significantly smaller. This peak can be considered as some type of background noise because of its current in comparison to the first reduction peak.

Differential pulse voltammetry was also conducted using a dropping mercury electrode which eliminates the problems associated with a glassy carbon solid surface. The result of this experiment was the appearance of two reduction peaks at  $E_{1/2} = -1490\text{mV}$  and  $E_{1/2} = -1650\text{mV}$  (Table 8.4, Fig 8.13b). This result does not agree with the glassy carbon differential pulse voltammetry unless the glassy carbon differential pulse voltammetry result is really two processes as hinted at by its asymmetric nature. The shift in potentials between glassy carbon and dropping mercury indicate that for this complex the compound is more easily reduced on glassy carbon than on mercury. This is the reverse of the situation found for  $\text{Cu}(\text{SAL-DPLH})$  where the reduction is easier on the mercury electrode. The explanation for this is unknown although as they are different compounds there is no reason that they should give the same result.

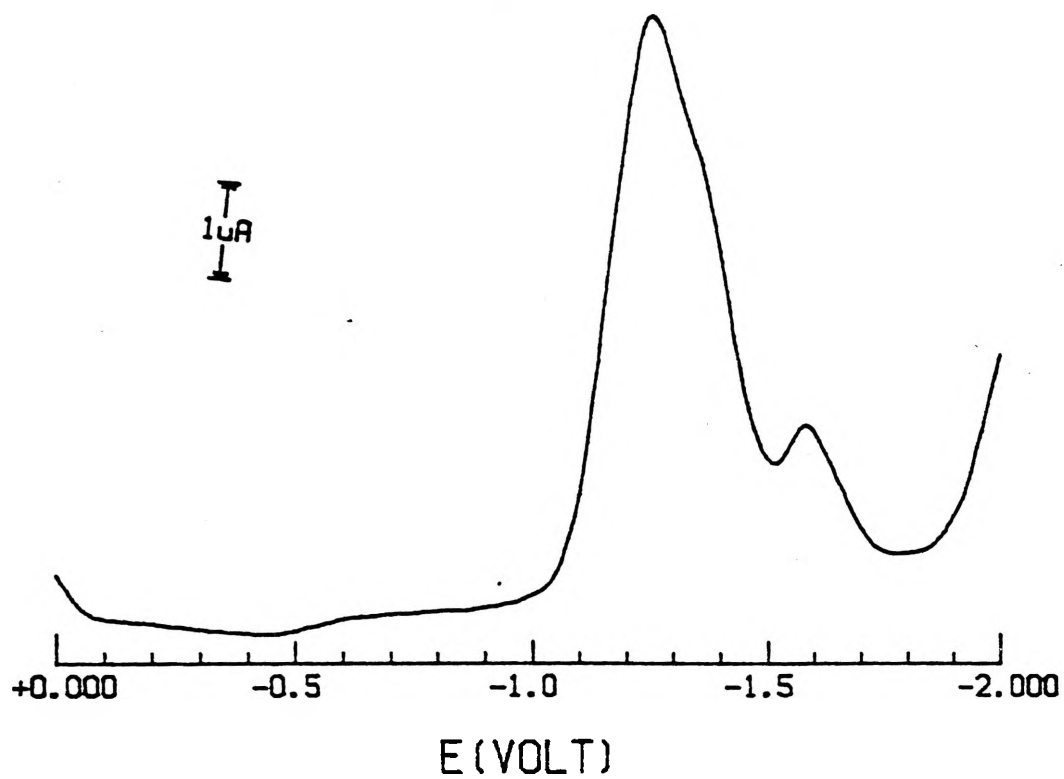
Both differential pulse voltammetry measurements suggest there are possibly two reduction processes occurring so close together as to be difficult to separate. These two processes are probably two two electron reductions



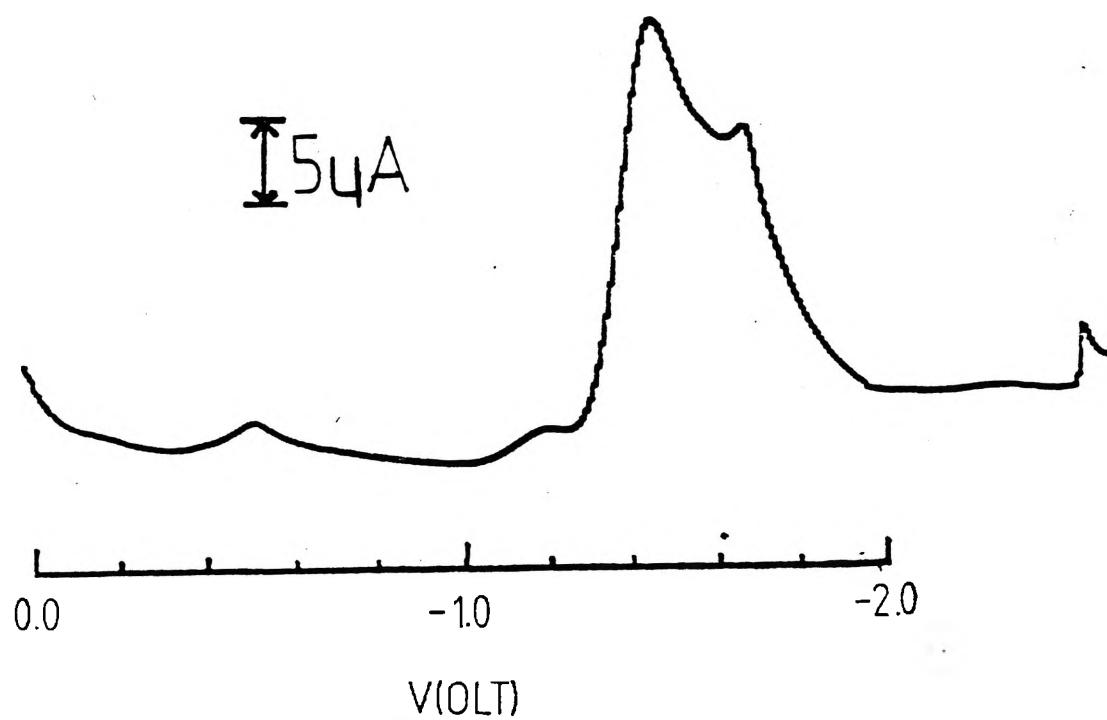
Although the alternative possibility



cannot be ruled out.



a) Glassy Carbon



b) Dropping Mercury

Fig 8.13: Differential Pulse Voltammogram of  $\text{Cu}_2(\text{SAL-DPL})\text{OH} \cdot 3\text{H}_2\text{O}$

### c) Cyclic Voltammetry

The cyclic voltammetry of  $\text{Cu}_2(\text{SAL-DPL})\text{OH}\cdot 3\text{H}_2\text{O}$  using a glassy carbon electrode indicates two reduction processes at  $E_{1/2} = -1340\text{mV}$  and  $E_{1/2} = -1430\text{mV}$ . The voltammogram shows a broad oxidation process at  $E_{1/2} = -450\text{mV}$  (Table 8.4, Fig 8.14a). This oxidation is believed to be that of free copper indicating that the reduction processes are irreversible. The cyclic voltammetry is supported by both of the differential pulse voltammetry measurements which suggest the presence of two reduction processes at close potentials. The DC Polarography only shows one process, however, as the two processes observed for both cyclic voltammetry and differential pulse voltammetry are very close together in terms of their potentials so they could easily appear as a single reduction process for polarography especially when the polarography is affected by a polarographic maxima. Therefore it seems likely that  $\text{Cu}_2(\text{SAL-DPL})\text{OH}\cdot 3\text{H}_2\text{O}$  undergoes two two electron reductions at almost the same potential.

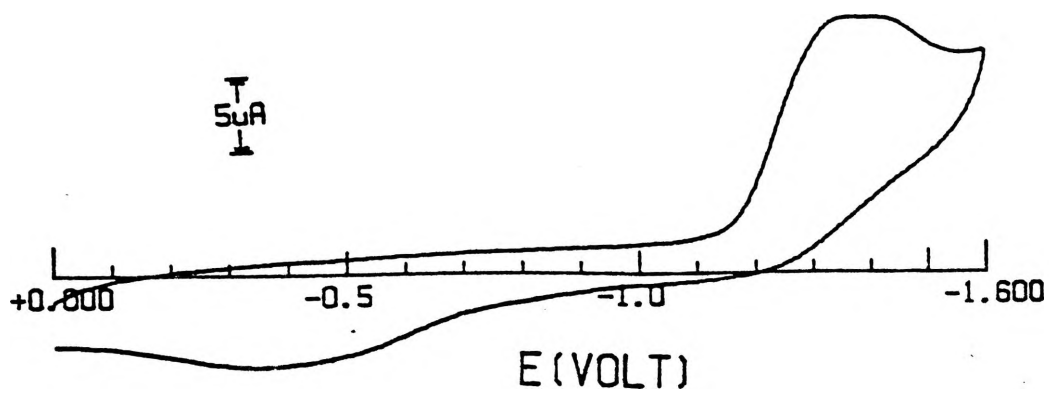
Multiple scans of  $\text{Cu}_2(\text{SAL-DPL})\text{OH}\cdot 3\text{H}_2\text{O}$  indicates that this complex is unstable with there being considerable breakdown over five scans of the complex with the two reduction processes disappearing with repeated scans and the growth of a reduction peak at  $E_{1/2} = -1075\text{mV}$  (Table 8.4, Fig 8.14b). The reduction peak at  $-1075\text{mV}$  is believed to be that of a simple copper salt  $\text{Cu}(\text{DMF})_x^{2+}$ . To test this possibility the cyclic voltammetry of copper acetate was examined using a glassy carbon electrode. The cyclic voltammetry of copper acetate contained a reduction peak at  $E_{1/2} = -1050\text{mV}$  and an oxidation peak at  $E_{1/2} = -435\text{mV}$  indicating free copper ions in the solution (Table 8.4, Fig 8.15) which suggests that the new reduction in  $\text{Cu}_2(\text{SAL-DPL})\text{OH}\cdot 3\text{H}_2\text{O}$  at  $E_{1/2} = -1075\text{mV}$  is most likely that of a simple copper salt.



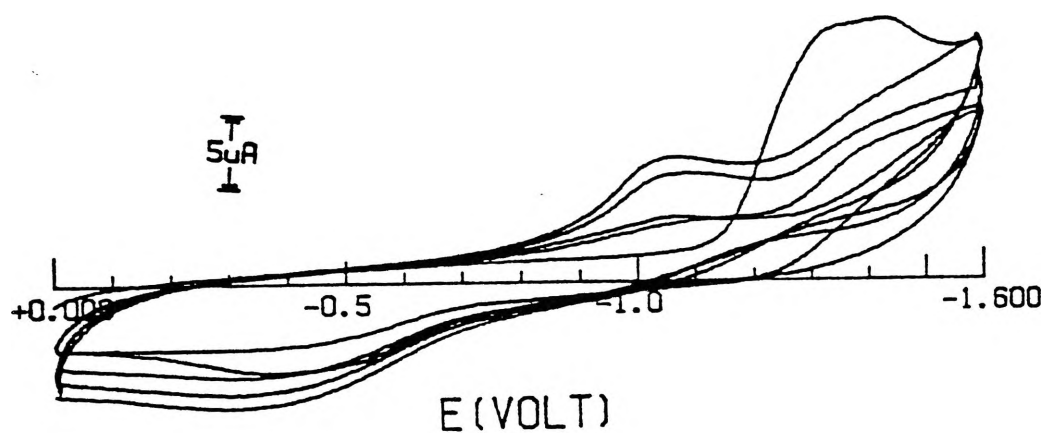
It should be noted that the peak at -1075mV increases in current with repeated scans, i.e. with only the free copper oxidation at  $\sim -450\text{mV}$  occurring, the multiple cyclic voltammetry scans show a breakdown of the complex. Where there is an oxidation process at lower potentials (below  $\sim -1000\text{mV}$ ) in other binuclear complexes the multiple cyclic voltammetry scans show no appearance of the reduction peak at  $\sim -1000\text{mV}$ , e.g. see Cu(SAL-DPLH). This trend is observed for all the complexes studied, i.e. when the complex undergoes irreversible reduction and as a result breaks down, this breakdown is shown by there being only one oxidation process at  $E_{1/2} = \sim -450\text{mV}$ , due to free copper, and a reduction peak appears at  $E_{1/2} = \sim -1000\text{mV}$  on multiple scans for the reduction of the simple copper salt to free copper.

DC Polarography		Peak 1	Peak 2				
		-1430mV					
DPV	GC	-1260mV					
	DME	-1490mV	-1650mV(sh)				
CV		Reduction	$\mu\text{A}$	Oxidation	$\mu\text{A}$	$I_{\text{P}_R}/I_{\text{P}_F}$	$E_{\text{P}_A} - E_{\text{P}_C}$
	Scan 1	-1340mV	7.1	-465mV	2.1	0.3	875mV
		-1430mV	7.1				
	Scan 5	-1075mV	2.0	—	—	—	—
Copper Acetate	CV	-1050mV	75.0	-435mV	75.0	1.0	615mV

Table 8.4: Electrochemical Data for  $\text{Cu}_2(\text{SAL-DPL})\text{OH} \cdot 3\text{H}_2\text{O}$



a) Initial Scan



b) Multiple Scan

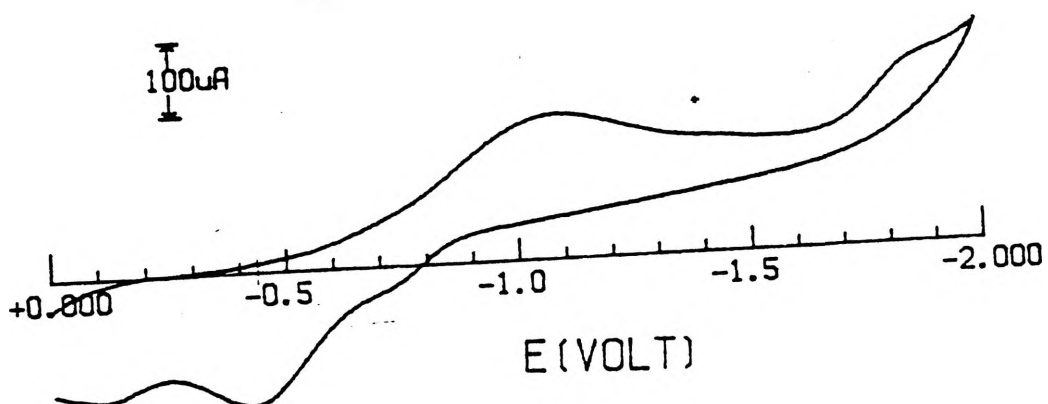
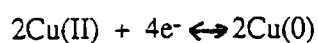
Fig 8.14: Cyclic Voltammogram of  $\text{Cu}_2(\text{SAL-DPL})\text{OH} \cdot 3\text{H}_2\text{O}$ 

Fig 8.15: Cyclic Voltammogram of Copper (II) Acetate

8.9  $\text{Cu}_2(\text{SAL-DPE})\text{OH}\cdot\text{H}_2\text{O}$ 

## a) DC Polarography

DC Polarographic investigation of  $\text{Cu}_2(\text{SAL-DPE})\text{OH}\cdot\text{H}_2\text{O}$  in the potential range 0 to -2000mV reveals a result of one process at  $E_{1/2} = -1110\text{mV}$  (Table 8.5, Fig 8.16). This implies that the four electrons are being reduced in a single step



The DC Polarograph is quite sharp with a small polarographic maxima appearing upon the face of the reduction slope and there is no indication of more than one reduction process.

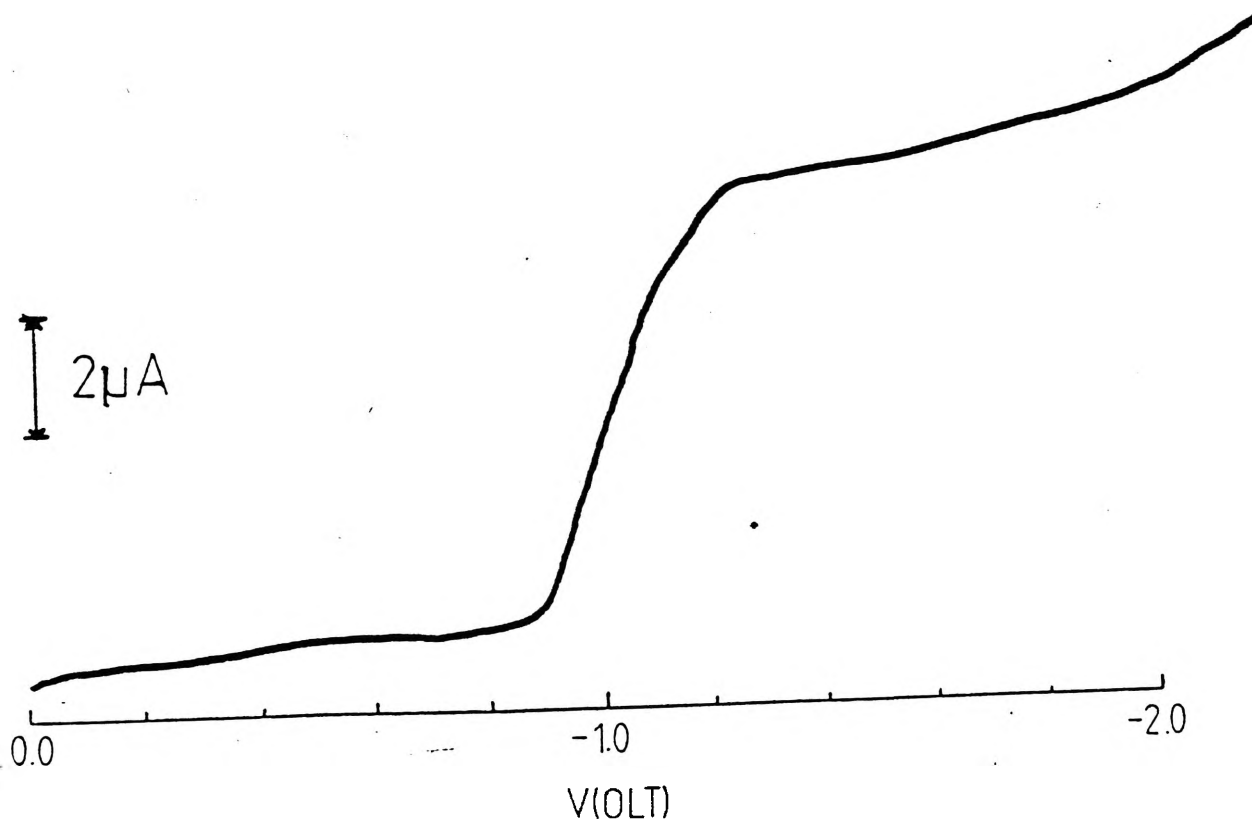
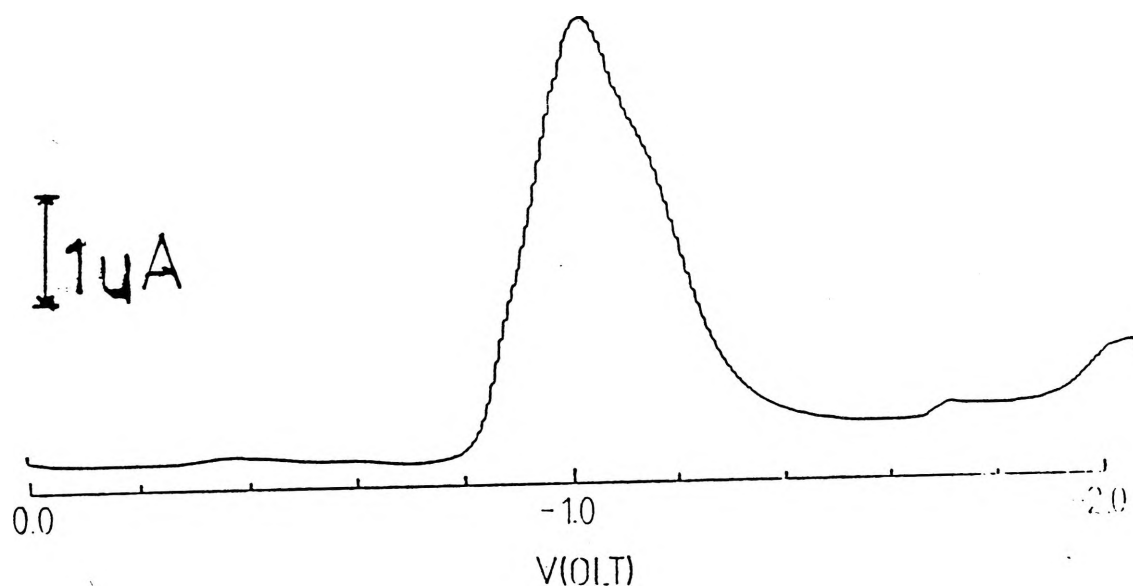


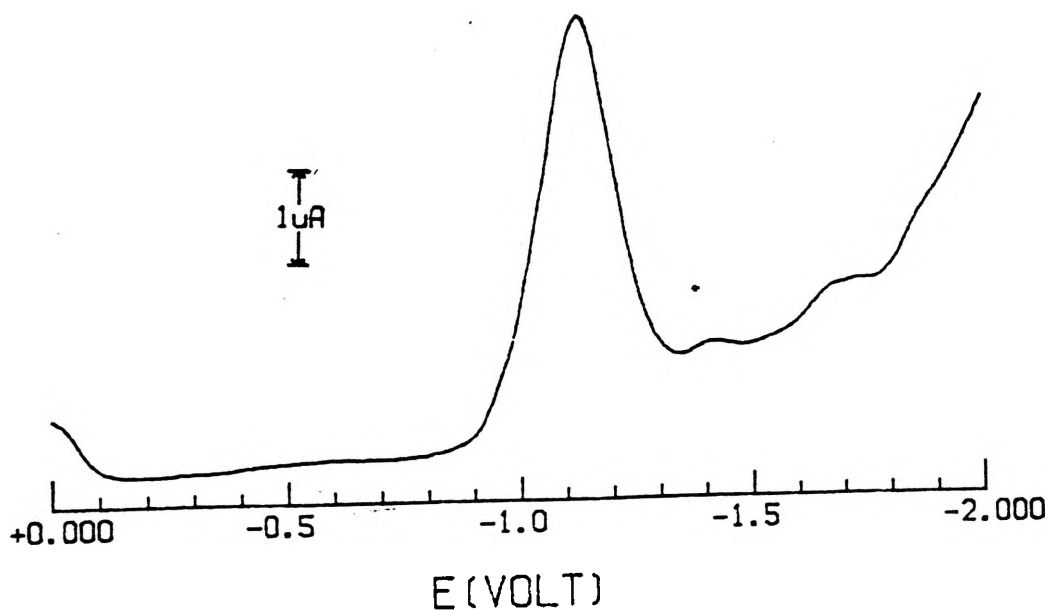
Fig 8.16: DC Polarogram of  $\text{Cu}_2(\text{SAL-DPE})\text{OH}\cdot\text{H}_2\text{O}$

## b) Differential Pulse Voltammetry

The differential pulse voltammetric investigation of  $\text{Cu}_2(\text{SAL-DPE})\text{OH}\cdot\text{H}_2\text{O}$  with a glassy carbon electrode gives a result of a single major peak with this peak occurring at  $E_{1/2} = -1135\text{mV}$  (Table 8.5, Fig 8.17a). Using a dropping mercury electrode to overcome any solid surface effects gives a single peak at  $E_{1/2} = -1045\text{mV}$  (Table 8.5, Fig 8.17b) with the suggestion of a second peak on the lower potential side. This suggests that there are two reduction processes of two electrons very close together.



a) Glassy Carbon



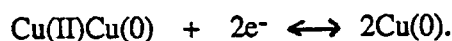
b) Dropping Mercury

Fig 8.17: Differential Pulse Voltammogram of  $\text{Cu}_2(\text{SAL-DPE})\text{OH}\cdot\text{H}_2\text{O}$

## c) Cyclic Voltammetry

The cyclic voltammetry result for  $\text{Cu}_2(\text{SAL-DPE})\text{OH}\cdot\text{H}_2\text{O}$  using a glassy carbon electrode indicates a result of a single reduction process at  $E_{1/2} = -1230\text{mV}$ . An oxidation process is observed at  $E_{1/2} = -420\text{mV}$  (Table 8.5, Fig 8.18a) and this is believed to be due to free copper. It can be concluded that the redox process of  $\text{Cu}_2(\text{SAL-DPE})\text{OH}\cdot\text{H}_2\text{O}$  is irreversible.

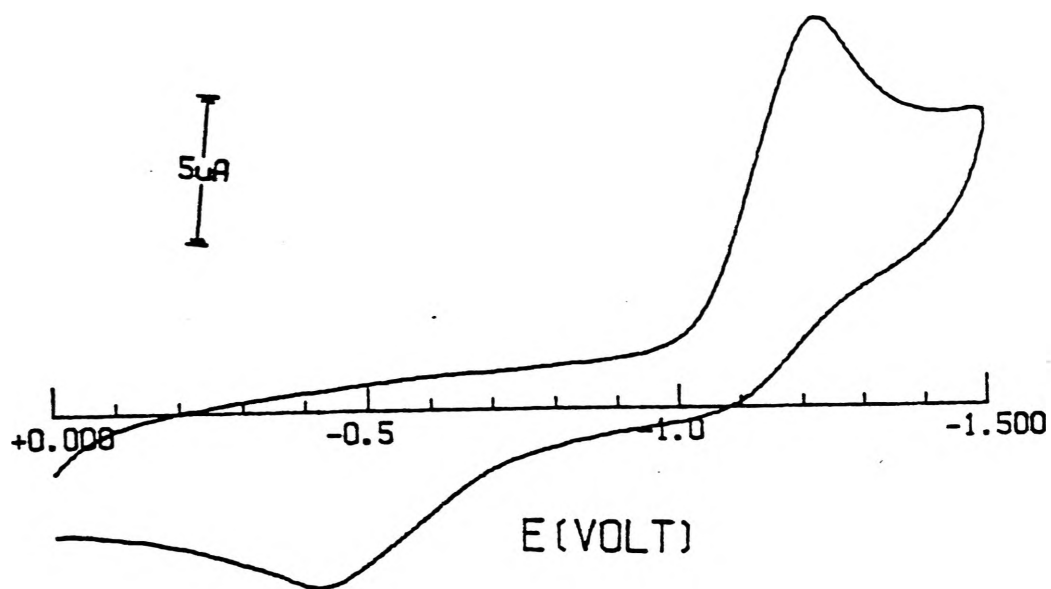
It would appear that  $\text{Cu}_2(\text{SAL-DPE})\text{OH}\cdot\text{H}_2\text{O}$  undergoes two two electron reductions as has been observed for  $\text{Cu}_2(\text{SAL-DPL})\text{OH}\cdot 3\text{H}_2\text{O}$  with these two reductions occurring at potentials which are close together



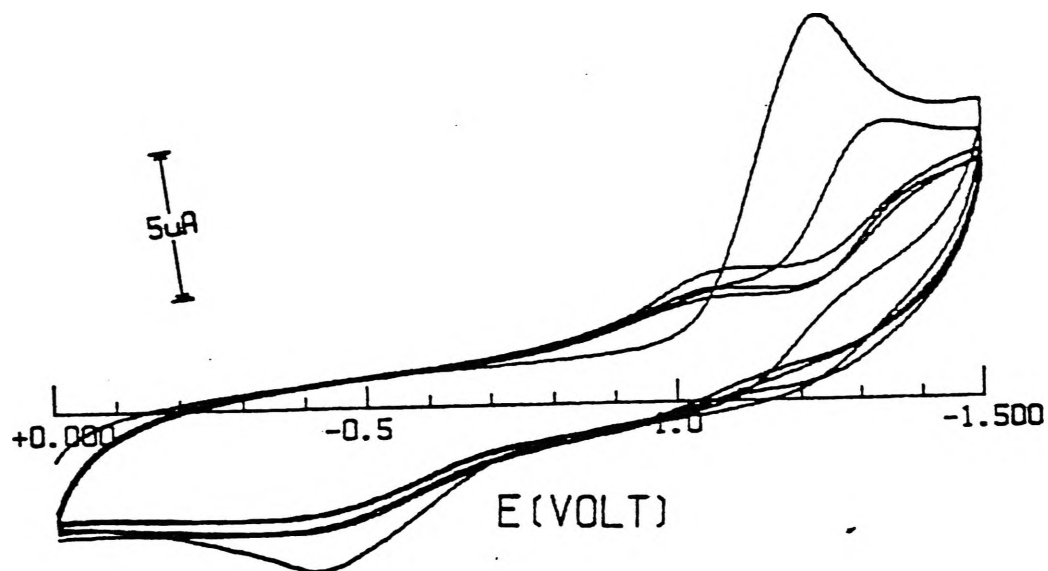
Multiple scans of  $\text{Cu}_2(\text{SAL-DPE})\text{OH}\cdot\text{H}_2\text{O}$  (Table 8.5, Fig 8.18b) show the same effect as for  $\text{Cu}_2(\text{SAL-DPL})\text{OH}\cdot 3\text{H}_2\text{O}$ , i.e. the growth of the  $\sim 1000\text{mV}$  reduction peak and the disappearance of the initial reduction peak, which indicates that the complex undergoes an irreversible redox process.

		Peak 1					
DC Polarography		-1110mV					
DPV	GC	-1135mV					
	DME	-1045mV					
CV		Reduction	mA	Oxidation	mA	$I_R^P/I_F^P$	$E_A^P - E_C^P$
	Scan 1	-1230mV	8.0	-420mV	2.42	0.28	810mV
	Scan 5	—	—	—	—	—	—

Table 8.5: Electrochemical Data for  $\text{Cu}_2(\text{SAL-DPE})\text{OH}\cdot\text{H}_2\text{O}$



a) Initial Scan



b) Multiple Scan

Fig 8.18: Cyclic Voltammogram of  $\text{Cu}_2(\text{SAL-DPE})\text{OH}\cdot\text{H}_2\text{O}$

8.10  $\text{Cu}_2(\text{SAL-DPL})(\text{CAT})_{0.5}(\text{H}_2\text{O})_{0.5}$ 

## a) DC Polarography

DC Polarographic measurements of  $\text{Cu}_2(\text{SAL-DPL})(\text{CAT})_{0.5}(\text{H}_2\text{O})_{0.5}$  in the potential range 0 to -2000mV indicate a single reduction process at  $E_{1/2} = -1440\text{mV}$  (Table 8.6, Fig 8.19). The result suggests that the reduction occurs in a single four electron reduction

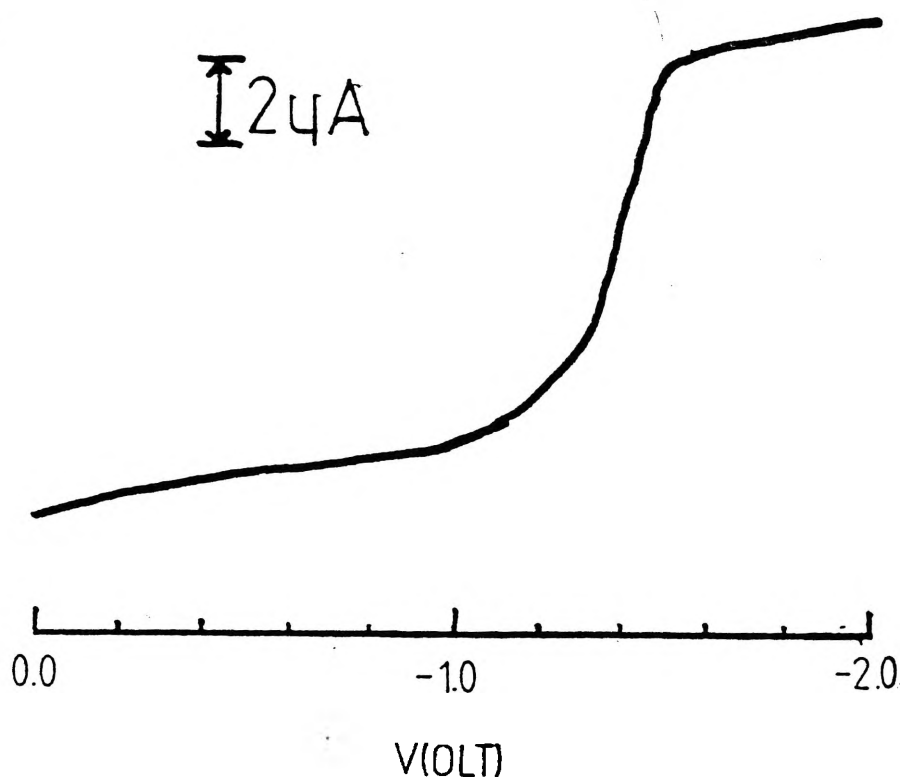
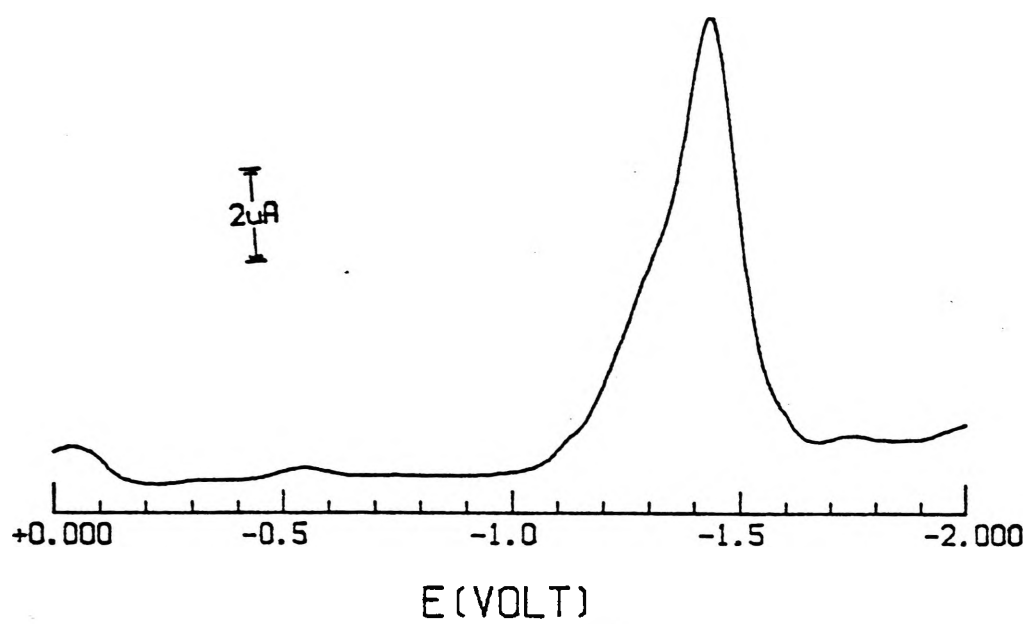


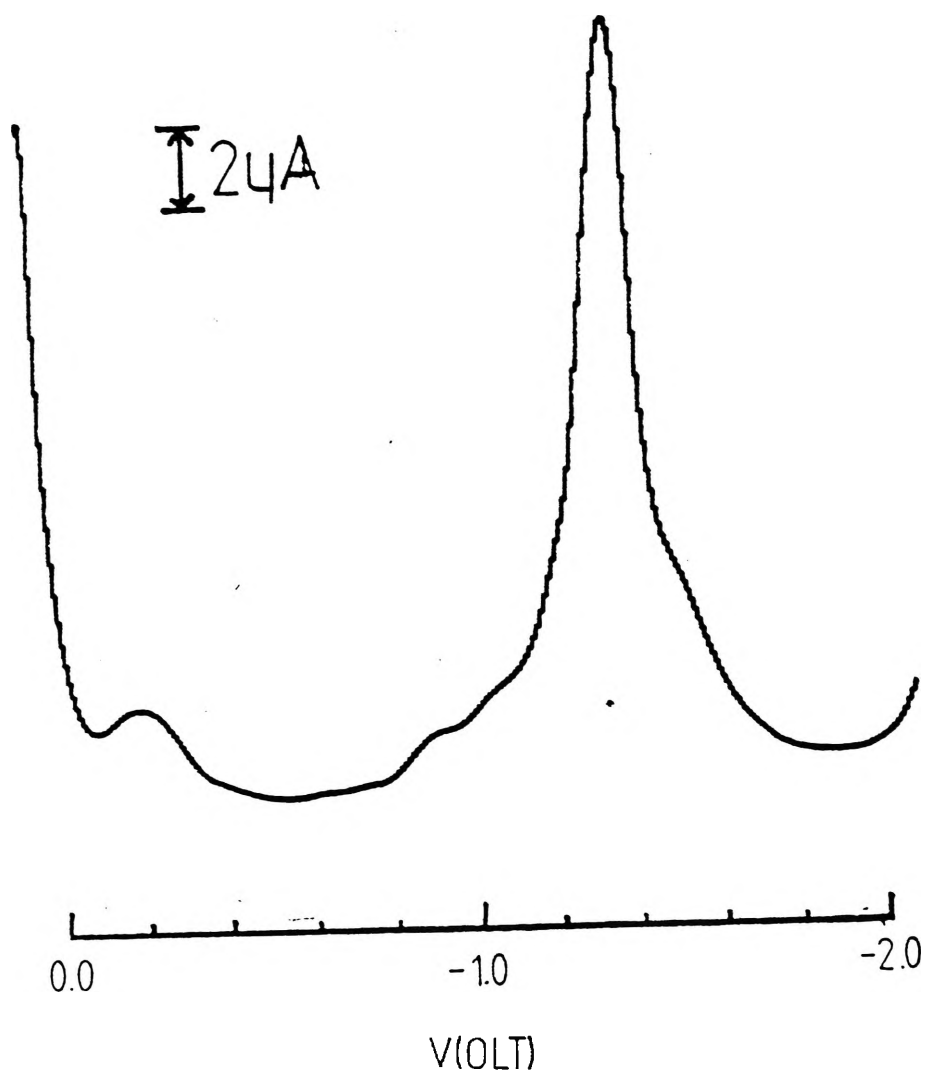
Fig 8.19: DC Polarogram of  $\text{Cu}_2(\text{SAL-DPL})(\text{CAT})_{0.5}(\text{H}_2\text{O})_{0.5}$

## b) Differential Pulse Voltammetry

Differential pulse voltammetric investigation of  $\text{Cu}_2(\text{SAL-DPL})(\text{CAT})_{0.5}(\text{H}_2\text{O})_{0.5}$  using a glassy carbon electrode gives a result of one peak at  $E_{1/2} = -1430\text{mV}$  (Table 8.6, Fig 8.20a). This result agrees with the polarography result. To verify this result the differential pulse voltammetry was rerun using a dropping mercury electrode. The result was again a single reduction peak at  $E_{1/2} = -1420\text{mV}$  confirming the DC Polarography and glassy carbon differential pulse voltammetry results (Table 8.6, Fig 8.20b).



a) Glassy Carbon



b) Dropping Mercury

Fig 8.20: Differential Pulse Voltammogram of  $\text{Cu}_2(\text{SAL-DPL})(\text{CAT})_{0.5}(\text{H}_2\text{O})_{0.5}$

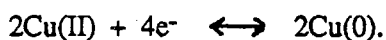


## c) Cyclic Voltammetry

The cyclic voltammetry of  $\text{Cu}_2(\text{SAL-DPL})(\text{CAT})_{0.5}(\text{H}_2\text{O})_{0.5}$  using a glassy carbon electrode gives a result of a single reduction process at  $E_{1/2} = -1530\text{mV}$  and coupled with this is a reoxidation peak at  $E_{1/2} = -1330\text{mV}$  ( $I^{\text{P}}_{\text{R}}/I^{\text{P}}_{\text{F}} = 0.3$ ,  $E^{\text{P}}_{\text{A}} - E^{\text{P}}_{\text{C}} = 200\text{mV}$ ) (Table 8.6, Fig 8.21a). There is also an oxidation peak at  $E_{1/2} = -550\text{mV}$  due to free copper, i.e. the reduction of the complex is a quasi-reversible process.

Multiple scans of  $\text{Cu}_2(\text{SAL-DPL})(\text{CAT})_{0.5}(\text{H}_2\text{O})_{0.5}$  show the same trend as mentioned for  $\text{Cu}(\text{SAL-DPLH})$  (Table 8.6, Fig 8.21b), i.e. the complex appears stable after the initial reduction scan when there is an oxidation peak below  $-1000\text{mV}$ .

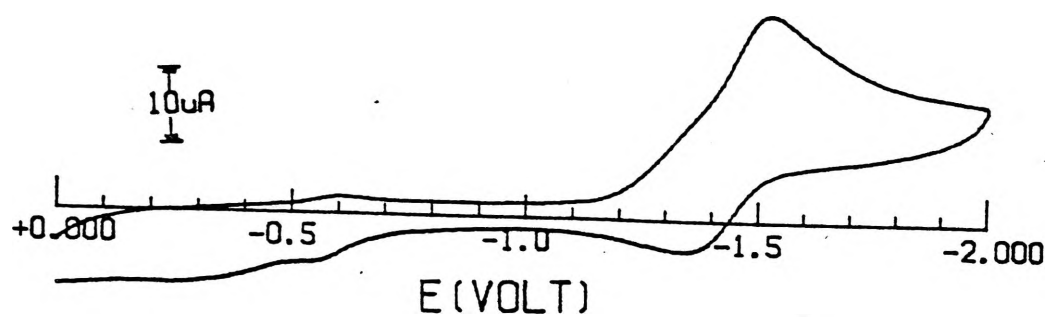
In conclusion it can be said that  $\text{Cu}_2(\text{SAL-DPL})(\text{CAT})_{0.5}(\text{H}_2\text{O})_{0.5}$  undergoes a single four electron reduction/oxidation with the reduction occurring at  $-1430\text{mV}$



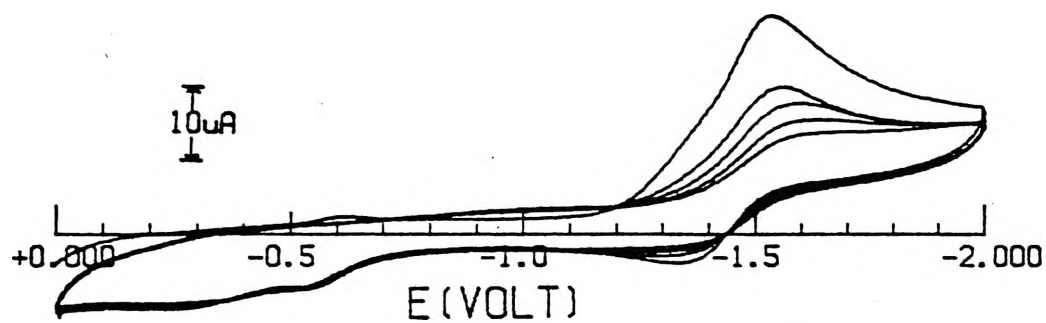
It is probable that like  $\text{Cu}_2(\text{SAL-DPE})\text{OH}\cdot\text{H}_2\text{O}$  there are two two electron reductions occurring but that these processes are so close together in potential that they appear as one reduction process.

		Peak 1					
DC Polarography		-1440mV					
DPV	GC	-1430mV					
	DME	-1420mV					
		Reduction	mA	Oxidation	mA	$I^{\text{P}}_{\text{R}}/I^{\text{P}}_{\text{F}}$	$E^{\text{P}}_{\text{A}} - E^{\text{P}}_{\text{C}}$
CV	Scan 1	-1530mV	29.0	-1330mV	6.9	0.3	200mV
	Scan 5	-1550mV	5.1	—	—	—	—

Table 8.6: Electrochemical Data for  $\text{Cu}_2(\text{SAL-DPL})(\text{CAT})_{0.5}(\text{H}_2\text{O})_{0.5}$



a) Initial Scan



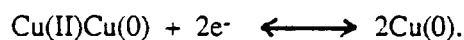
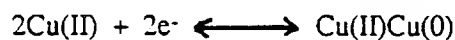
b) Multiple Scan

Fig 8.21: Cyclic Voltammogram of  $\text{Cu}_2(\text{SAL-DPL})(\text{CAT})_{0.5}(\text{H}_2\text{O})_{0.5}$

8.11 Cu<sub>2</sub>(SAL-DPE)CATH.0.5H<sub>2</sub>O

## a) DC Polarography

The DC Polarographic investigation of Cu<sub>2</sub>(SAL-DPE)CATH.0.5H<sub>2</sub>O in the potential range 0 to -2000mV reveals two reduction processes at  $E_{1/2} = -1390\text{mV}$  and  $E_{1/2} = -1570\text{mV}$  (Table 8.7, Fig 8.22). Given the poor separation of the two peaks, no valid peak heights could be determined. The two peaks suggest that the copper atoms are reduced in two steps



It is not possible to confirm this by coulometry as the two processes are too close together to allow a potential to be selected which has a chance of giving an accurate result. A well defined separation of more than 200mV is needed for a coulometry measurements to be conducted on each peak.

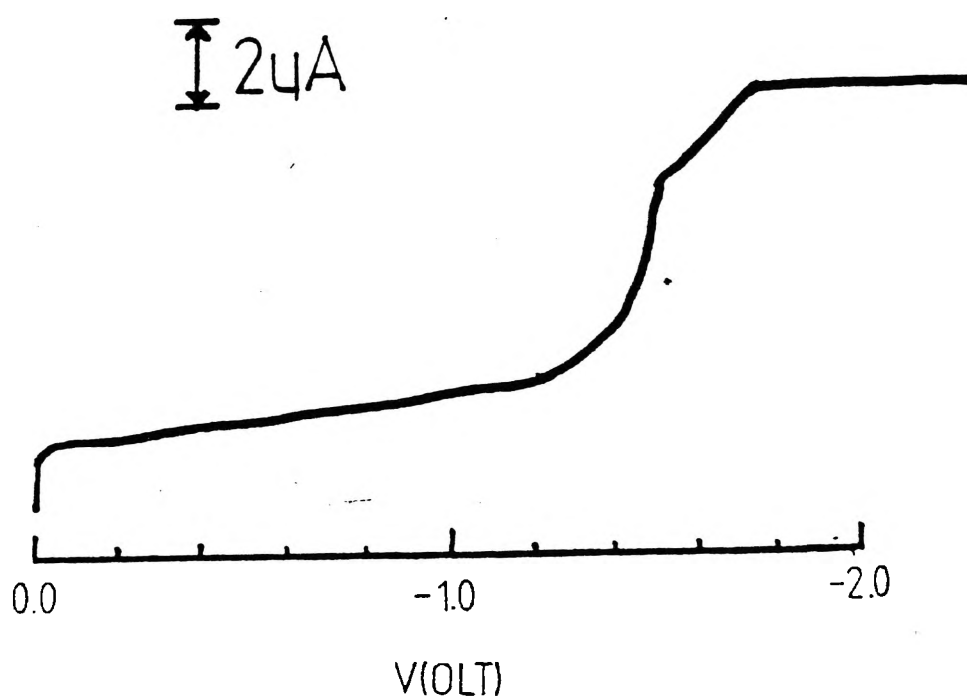


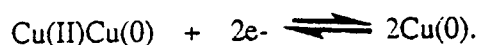
Fig 8.22: DC Polarogram of Cu<sub>2</sub>(SAL-DPE)CATH.0.5H<sub>2</sub>O

### b) Differential Pulse Voltammetry

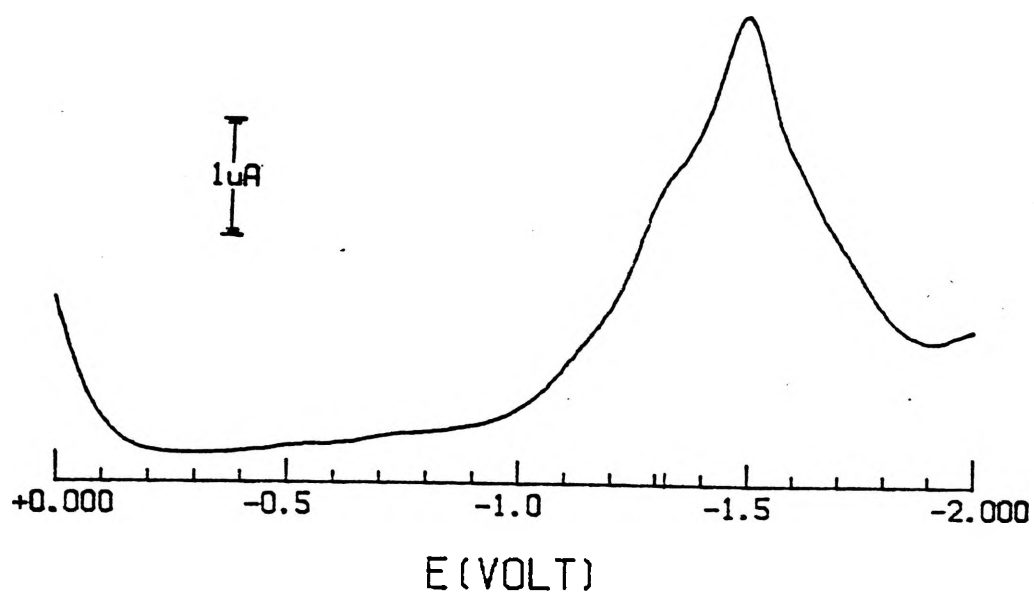
The glassy carbon electrode differential pulse voltammetric investigation of  $\text{Cu}_2(\text{SAL-DPE})\text{CATH.0.5H}_2\text{O}$  indicates a result of one process at  $E_{1/2} = -1500\text{mV}$ . This peak is asymmetric in character with a shoulder on the higher potential side at  $E_{1/2} = -1310\text{mV}$  (Table 8.7, Fig 8.23a). This asymmetric peak result suggests that there are two reduction processes occurring that are very close together in potential. The presence of two reduction processes would agree with the polarography result. The dropping mercury electrode gives a result of  $E_{1/2} = -1430\text{mV}$  and  $E_{1/2} = -1530\text{mV}$  which also agrees with the polarography result (Table 8.7, Fig 8.23b) with these two reductions again being very close together in potential. As for the polarography no valid peak heights could be determined.

### c) Cyclic Voltammetry

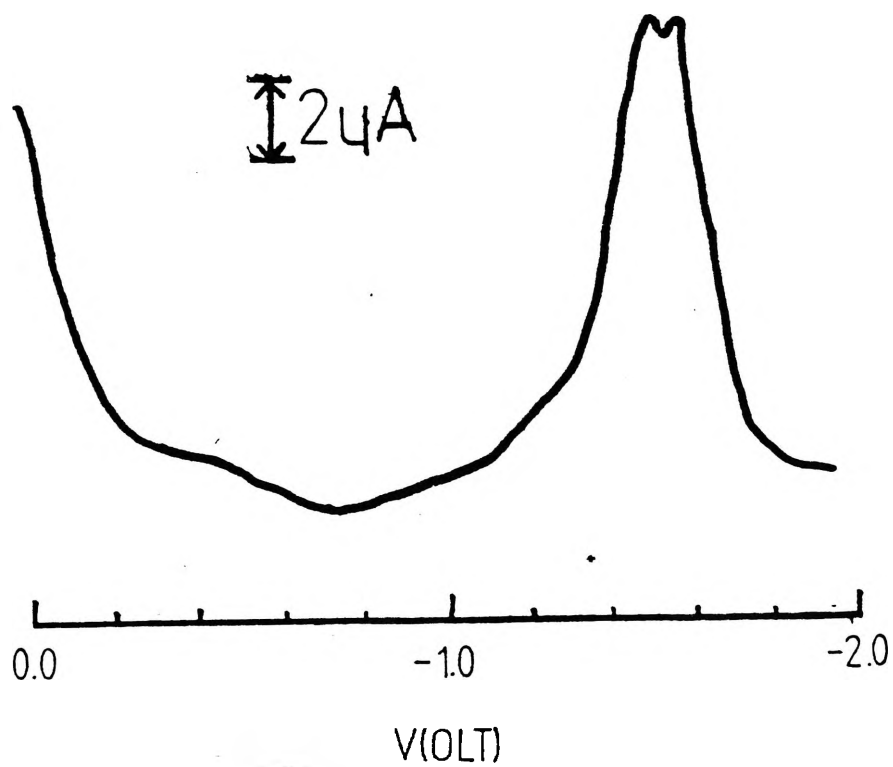
The cyclic voltammetry investigation of  $\text{Cu}_2(\text{SAL-DPE})\text{CATH.0.5H}_2\text{O}$  down to  $-2000\text{mV}$  gives a result of a double reduction process at  $E_{1/2} = -1600\text{mV}$  and  $E_{1/2} = -1670\text{mV}$ . On the oxidative scan there is observed an oxidation process at  $E_{1/2} = -1060\text{mV}$  and the free copper oxidation process at  $E_{1/2} = -375\text{mV}$  (Table 8.7, Fig 8.24a). This double reduction process agrees with the differential pulse voltammetry and polarography result in suggesting that  $\text{Cu}_2(\text{SAL-DPE})\text{CATH.0.5H}_2\text{O}$  undergoes two reduction processes which are very close together in potential. Therefore  $\text{Cu}_2(\text{SAL-DPE})\text{CATH.0.5H}_2\text{O}$  appears to undergo two two electron reduction steps



Multiple scans of  $\text{Cu}_2(\text{SAL-DPE})\text{CAT.0.5H}_2\text{O}$  (Table 8.7, Fig 8.24b) give the same result as for  $\text{Cu}_2(\text{SAL-DPL})(\text{CAT})_{0.5}(\text{H}_2\text{O})_{0.5}$ , i.e. the redox process is quasi-reversible.

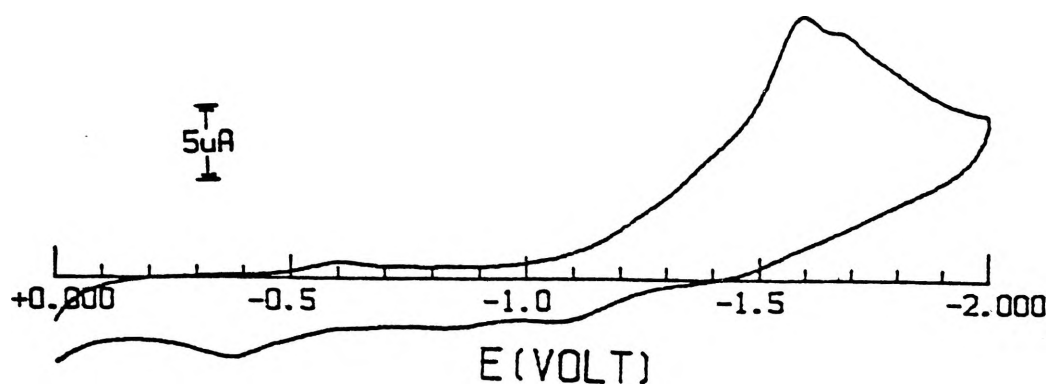


a) Glassy Carbon

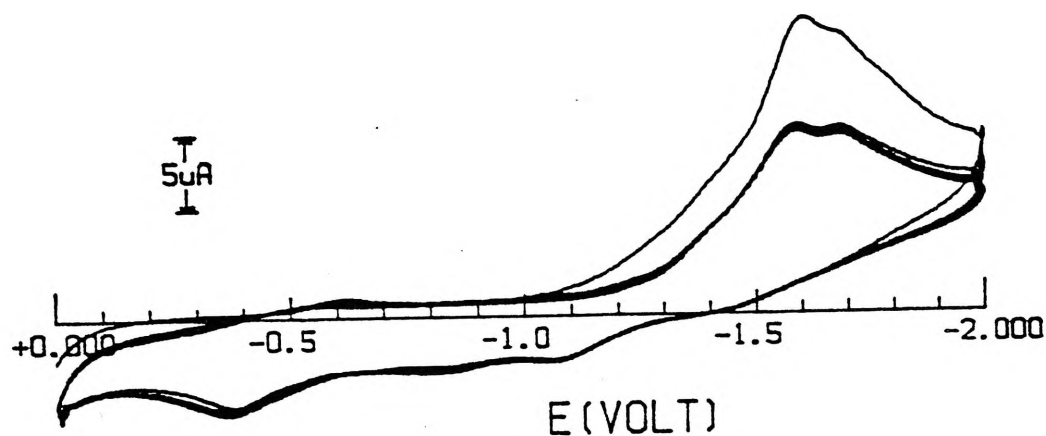


b) Dropping Mercury

Fig 8.24: Differential Pulse Voltammogram of  $\text{Cu}_2(\text{SAL-DPE})\text{CATH} \cdot 0.5\text{H}_2\text{O}$



a) Initial Scan



b) Multiple Scan

Fig 8.25: Cyclic Voltammogram of  $\text{Cu}_2(\text{SAL-DPE})\text{CATH} \cdot 0.5\text{H}_2\text{O}$ 

<u>DC Polarography</u>		Peak 1	Peak 2	Peak Ratio	
		-1390mV	-1570mV	1:1	
<u>DPV</u>	GC	-1310mV	-1500mV	—	
	DME	-1430mV	-1530mV	1:1	
<u>CV</u>	RT	Reduction $\mu\text{A}$	Oxidation $\mu\text{A}$	$I^{\text{P}}_{\text{R}}/I^{\text{P}}_{\text{F}}$	$E^{\text{P}}_{\text{A}}-E^{\text{P}}_{\text{C}}$
		-1600mV 0.72	-375mV 1.75	0.49	1225mV
		-1670mV 0.72	-1060mV 1.1	0.31	610mV
	Scan 5	-1600mV 0.72	-375mV 1.4	1.94	1225mV
		-1665mV 0.72	-1045mV 0.92	1.27	620mV

Table 8.7: Electrochemical Data for  $\text{Cu}_2(\text{SAL-DPE})\text{CATH} \cdot 0.5\text{H}_2\text{O}$

8.12 Cu<sub>2</sub>(SAL-DPL)Pz

## a) DC Polarography

The DC Polarographic investigation of Cu<sub>2</sub>(SAL-DPL)Pz in the potential range 0 to -2000mV shows a result of one reduction peak at  $E_{1/2} = -1450\text{mV}$  (Table 8.8, Fig 8.25) indicating that the complex undergoes a single four electron reduction.

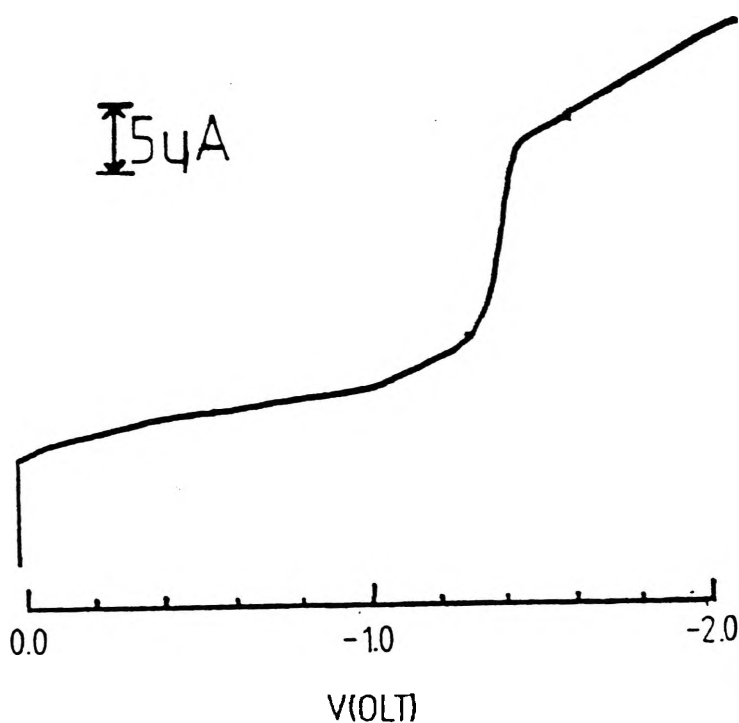
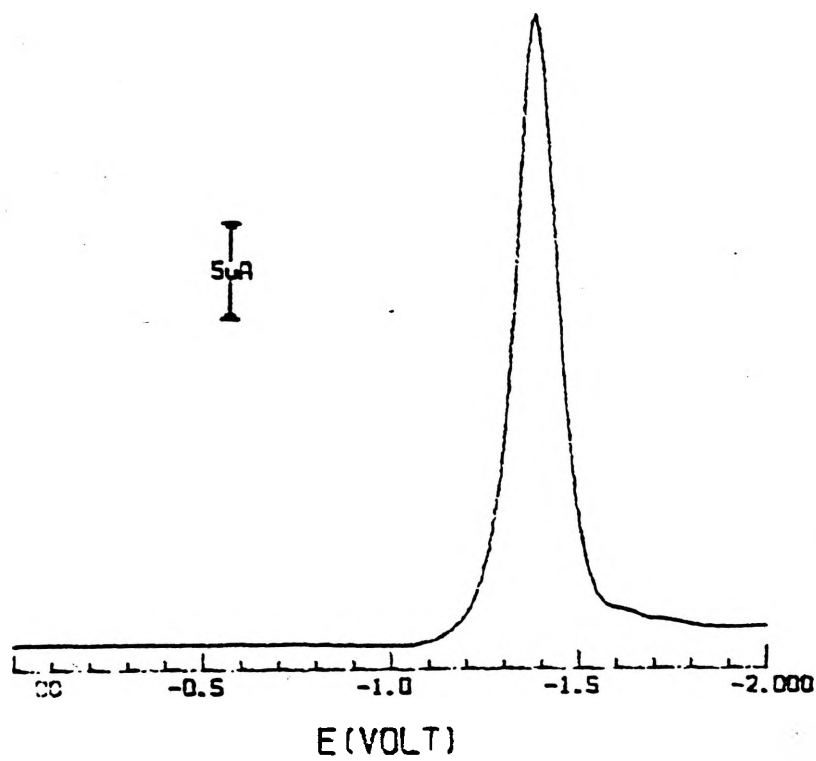


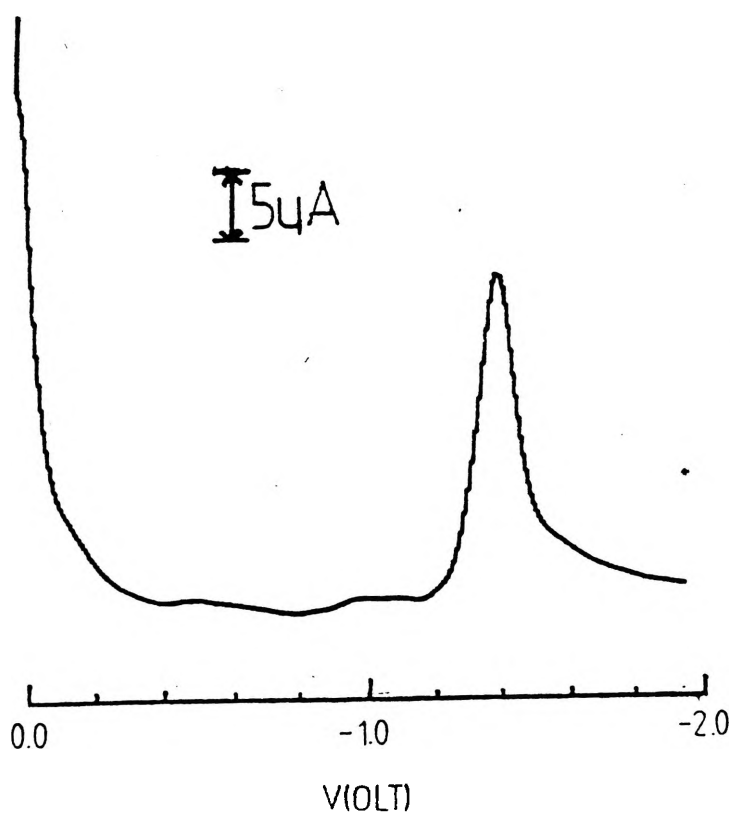
Fig 8.25: DC Polarogram of Cu<sub>2</sub>(SAL-DPL)Pz

## b) Differential Pulse Voltammetry

The glassy carbon differential pulse voltammetry gives a result of a single reduction peak at  $E_{1/2} = -1400\text{mV}$  while the dropping mercury electrode gives a result of one peak at  $E_{1/2} = -1420\text{mV}$  (Table 8.8, Figs 8.26a and 8.26b). These results agree with the DC Polarography result of a single four electron reduction.



a) Glassy Carbon Electrode



b) Dropping Mercury Electrode

Fig 8.26: Differential Pulse Voltammogram of  $\text{Cu}_2(\text{SAL-DPL})\text{Pz}$



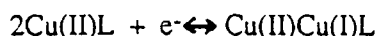
### c) Cyclic Voltammetry

The cyclic voltammetry of  $\text{Cu}_2(\text{SAL-DPL})\text{Pz}$  also produces a result of one reduction peak at  $E_{1/2} = -1475\text{mV}$ . This scan also exhibits two reoxidation peaks at  $E_{1/2} = -670\text{mV}$  and  $E_{1/2} = -1365\text{mV}$  with this second oxidation peak being quasi-reversible with the reduction process ( $I^{\text{P}}_{\text{R}}/I^{\text{P}}_{\text{F}} = 0.38$ ,  $E^{\text{P}}_{\text{A}} - E^{\text{P}}_{\text{C}} = 110\text{mV}$ ) (Table 8.8, Fig 8.27a) and the first oxidation process at  $E_{1/2} = -670\text{mV}$  is attributed to free copper. The oxidation potential is significantly lower for this complex ( $E_{1/2} = -670\text{mV}$  compared to  $E_{1/2} = \sim -400\text{mV}$ ). This may be due to the pyrazole coordinating to the copper atom making the copper easier to oxidise than in the other complexes where no pyrazolate anion is present.

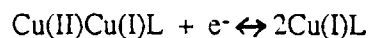
Multiple scans of  $\text{Cu}_2(\text{SAL-DPL})\text{Pz}$  (Table 8.8, Fig 8.27b) shows the same results as for  $\text{Cu}_2(\text{SAL-DPL})(\text{CAT})_{0.5}(\text{H}_2\text{O})_{0.5}$ , i.e. the redox process is quasi-reversible.

Bond et al.<sup>132</sup> have also studied a sample of  $\text{Cu}_2(\text{SAL-DPL})\text{Pz}$  and have found for cyclic voltammetry, two processes on the reductive scan, using a platinum electrode, at  $E_{1/2} = -1155\text{mV}$  and  $E_{1/2} = -1600\text{mV}$  with the first process being coupled with a process on the oxidative scan at  $E_{1/2} = -898\text{mV}$ , i.e. the first process is quasi-reversible and the second is irreversible. The hanging mercury drop electrode cyclic voltammogram of this complex confirmed this result with a quasi-reversible first process at  $E_{1/2} = -1043\text{mV}$  ( $E_{1/2} = -962\text{mV}$  on the oxidative scan) and an irreversible second process at  $E_{1/2} = -1580\text{mV}$ . DC Polarography showed two processes, as well, with  $E_{1/2}$  for the first at  $-996\text{mV}$  and  $E_{1/2}$  for the second at  $-1200\text{mV}$ .

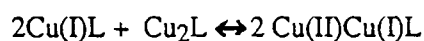
Bond et al. believed that the first process involved a one electron reduction per binuclear complex



and that the second process was the result of a further single electron transfer



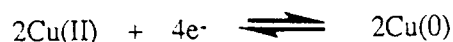
with this dianion undergoing interaction with  $\text{Cu}_2\text{L}$



with there being two possible stereochemical forms of both  $\text{Cu}_2\text{L}$  and  $\text{Cu(II)Cu(I)L}$ .

Using a platinum electrode cyclic voltammetry scan for our sample of  $\text{Cu}_2(\text{SAL-DPL})\text{Pz}$ , only one quasi-reversible process is observed at  $E_{1/2} = -1540\text{mV}$  (Table 8.9) as is the case for the glassy carbon electrode. The hanging mercury drop electrode scan of  $\text{Cu}_2(\text{SAL-DPL})\text{Pz}$  also shows only one reduction process at  $E_{1/2} = -1455\text{mV}$  which is consistent with all the other results for  $\text{Cu}_2(\text{SAL-DPL})\text{Pz}$  (Table 8.10). With both the platinum and hanging mercury drop scans, at varying scan rates, the peak potential becomes more positive as the scan rate slows and the current of the reduction process also decreases as the scan rate slows. Due to noise on the reoxidation scan using the hanging mercury drop electrode the  $\text{IP}_\text{R}/\text{IP}_\text{F}$  ratio could not be determined accurately however the result should be the same as for the platinum scans where the ratio increases as the scan rate decreases. Bond et al.<sup>132</sup> also found this result for their sample of  $\text{Cu}_2(\text{SAL-DPL})\text{Pz}$ .

This sample of  $\text{Cu}_2(\text{SAL-DPL})\text{Pz}$  and that of Bond et al differ considerably in their electrochemistry with Bond observing two processes which he believed comprised two one electron reductions although no coulometry or differential pulse voltammetry work to confirm this conclusion was reported while our sample of  $\text{Cu}_2(\text{SAL-DPL})\text{Pz}$  exhibits only a single reduction process consisting of a four electron transfer



supported by not only cyclic voltammetry and DC polarography work but also coulometry and differential pulse voltammetry studies of the complex. As with the earlier binuclear complexes there may be two two electron reduction steps but they are too close together to be separated.

Bond et al. observed two reduction processes at  $E_{1/2} = -1155\text{mV}$  and  $E_{1/2} = -1600\text{mV}$  with the first reduction being claimed to be quasi-reversible, while we observed only one quasi-reversible process at  $E_{1/2} = -1540\text{mV}$ . The only logical reason for this difference that we can think of would seem to be the presence of oxygen in Bond et al's electrochemical cell. As seen for  $\text{Cu}(\text{SAL-DPLH})$  the  $E_{1/2} = -1155\text{mV}$  reduction seen by Bond could easily be that of oxygen as we observed an oxygen peak at  $E_{1/2} = -1200\text{mV}$  for  $\text{Cu}(\text{SAL-DPLH})$ . There are perhaps other reasons for the differences but they are not immediately apparent.

		Peak 1					
DC Polarography		-1450mV					
DPV	GC	-1400mV					
	DME	-1420mV					
		Red	mA	Oxid	mA	$I^P_R/I^P_F$	$E^P_A - E^P_C$
CV	Scan 1	—	—	-670mV	8.5	—	—
		-1475mV	47.0	-1365mV	17.7	0.38	110mV
	Scan 5	—	—	-650	11.0	—	—
		-1480mV	35.0	-1365mV	16.0	0.46	115mV

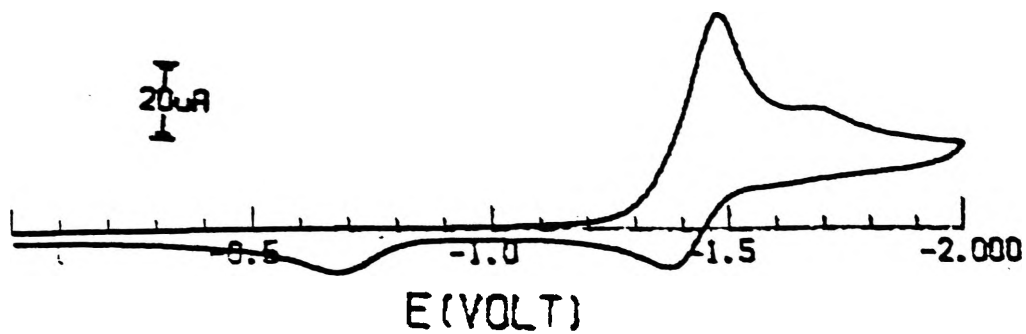
Table 8.8: Electrochemical Data for  $\text{Cu}_2(\text{SAL-DPL})\text{Pz}$

CV	Scan Rate mV/sec	Red	$\mu\text{A}$	Oxid	$\mu\text{A}$	$I^{\text{P}}_{\text{R}}/I^{\text{P}}_{\text{F}}$	$E^{\text{P}}_{\text{A}}-E^{\text{P}}_{\text{C}}$
	10	-1500mV	0.5	-725mV	0.16	3	—
	20	-1510mV	0.6	-685mV	0.27	2.4	—
	50	-1525mV	1.1	-645mV	0.5	2.2	—
	100	-1540mV	1.3	-630mV	0.6	1.8	—
	200	-1555mV	2.9	-540mV	2.5	1.5	—
	500	-1585mV	5.0	-595mV	4.2	1.3	—

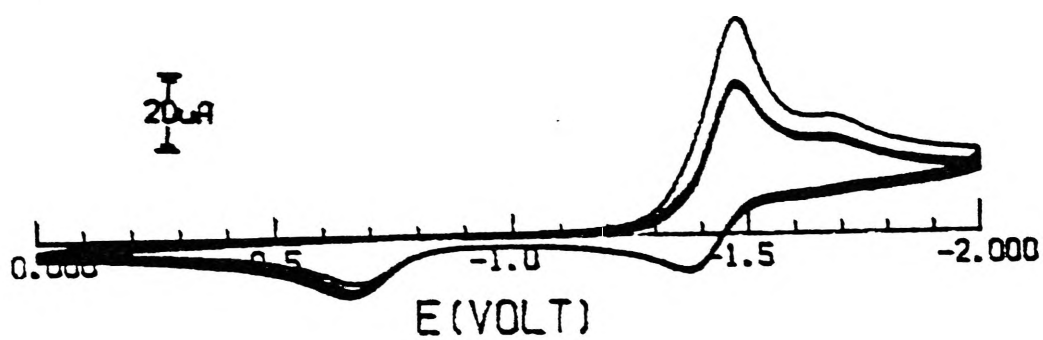
Table 8.9: Platinum Electrode Data for  $\text{Cu}_2(\text{SAL-DPL})\text{Pz}$ 

CV	Scan Rate mV/sec	Red	$\mu\text{A}$	Oxid	$\mu\text{A}$	$I^{\text{P}}_{\text{R}}/I^{\text{P}}_{\text{F}}$	$E^{\text{P}}_{\text{A}}-E^{\text{P}}_{\text{C}}$
	10	-1410mV	0.03	—	—	—	—
	20	-1415mV	0.05	—	—	—	—
	50	-1445mV	0.11	—	—	—	—
	100	-1455mV	0.15	—	—	—	—
	200	-1480mV	0.17	—	—	—	—
	500	-1490mV	0.25	—	—	—	—

Table 8.10: Hanging Mercury Drop Electrode Data for  $\text{Cu}_2(\text{SAL-DPL})\text{Pz}$



a) Initial Scan



b) Multiple Scan

Fig 8.27: Cyclic Voltammogram of  $\text{Cu}_2(\text{SAL-DPL})\text{Pz}$

8.13 Cu<sub>2</sub>(SAL-DPE)Pz

## a) DC Polarography

The DC Polarographic investigation of Cu<sub>2</sub>(SAL-DPE)Pz, in the potential range 0 to -2000mV, shows a result of a single reduction process at  $E_{1/2} = -1430\text{mV}$  (Table 8.9, Fig 8.28) indicating that Cu<sub>2</sub>(SAL-DPE)Pz undergoes a single four electron reduction

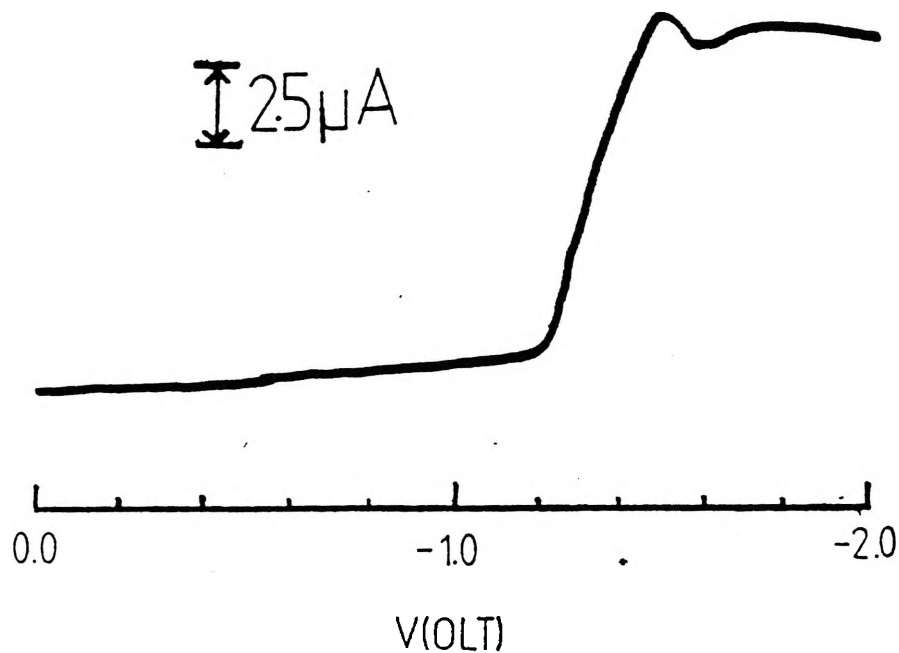
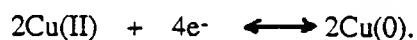


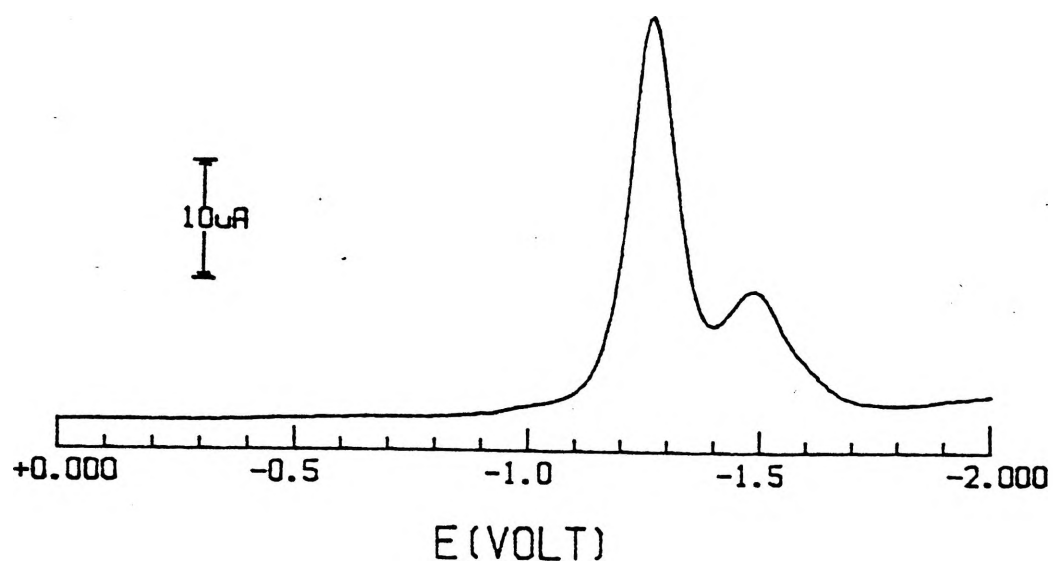
Fig 8.28: DC Polarogram of Cu<sub>2</sub>(SAL-DPE)Pz

## b) Differential Pulse Voltammetry

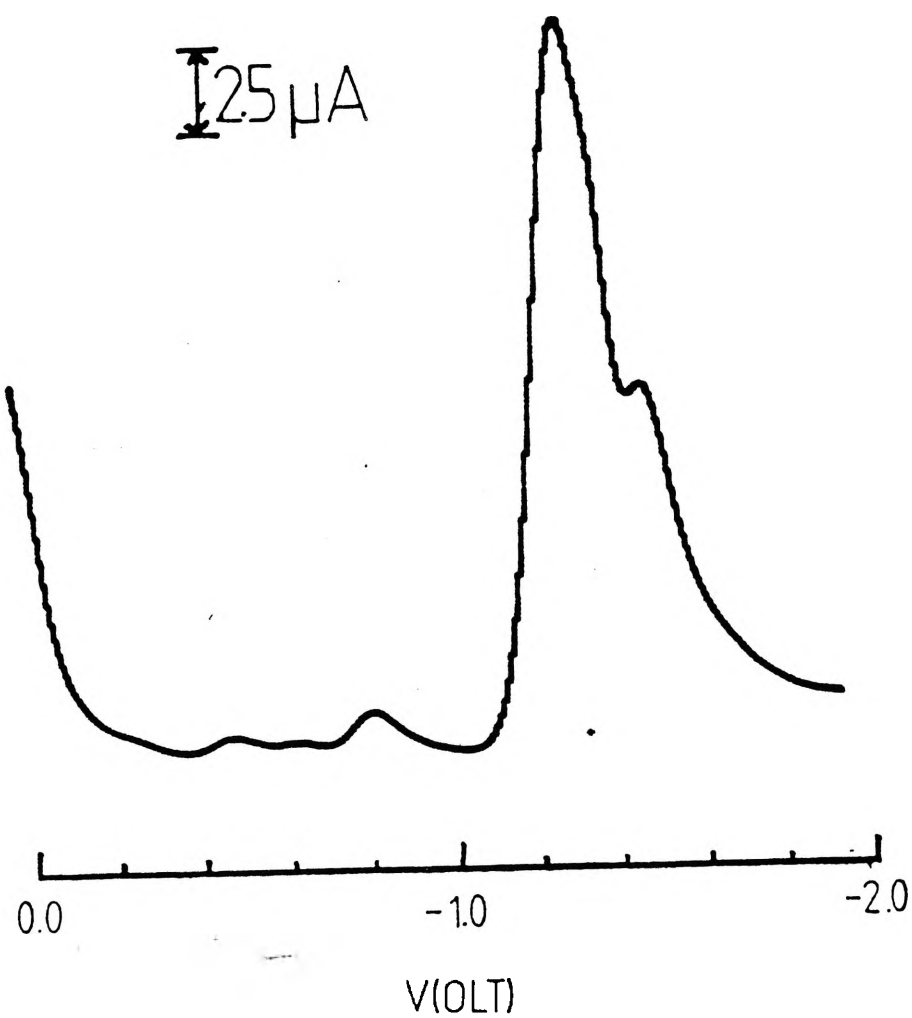
The glassy carbon electrode investigation of  $\text{Cu}_2(\text{SAL-DPE})\text{Pz}$  reveals a result of two reduction processes at  $E_{1/2} = -1300\text{mV}$  and  $E_{1/2} = -1520\text{mV}$  with a peak area ratio of 2:1 (Table 8.9, Fig 8.29a). A peak area ratio of 2:1 is difficult to explain when there are only four electrons transferred above  $-1600\text{mV}$ , therefore the ratio cannot be strictly accurate in terms of representing the number of electrons involved in a process. It should be noted that the peak area or peak height ratios are only accurate for ideal systems which  $\text{Cu}_2(\text{SAL-DPE})\text{Pz}$  is not ideal, therefore we can only look at the glassy carbon differential pulse result as an indication of the number of processes involved while being unsure of the exact number of electrons involved in each process. This result does not agree with the DC Polarography result in that there are two reduction processes against a single reduction process for polarography.

The dropping mercury electrode differential pulse voltammetry investigation of  $\text{Cu}_2(\text{SAL-DPE})\text{Pz}$  shows a result of two reduction processes at  $E_{1/2} = -1380\text{mV}$  and  $E_{1/2} = -1580\text{mV}$  (Table 8.9, Fig 8.29b). This result agrees with the glassy carbon differential pulse voltammetry results in terms of there being two reduction processes. The peak area ratio for the dropping mercury electrode indicates two two electron reduction processes. This is a more reasonable ratio and may be more reliable than the glassy carbon result as the surface of the glassy carbon electrode is easily fouled, while the dropping mercury electrode surface is being constantly renewed.

Often it was found that when fresh solutions of these binuclear complexes were studied the results for a particular technique differed significantly. As a consequence when we had developed what we felt was a reliable system, a fresh solution of  $\text{Cu}_2(\text{SAL-DPE})\text{Pz}$  was made and the glassy carbon and dropping mercury differential pulse voltammetries were remeasured. The result was two peaks of similar potential to those found above. This result confirms that we had a consistent and reliable closed system.



a) Glassy Carbon



b) Dropping Mercury

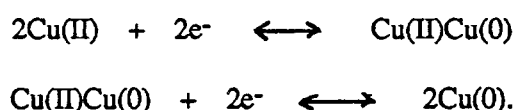
Fig 8.29: Differential Pulse Voltammogram of  $\text{Cu}_2(\text{SAL-DPE})\text{Pz}$



## c) Cyclic Voltammetry

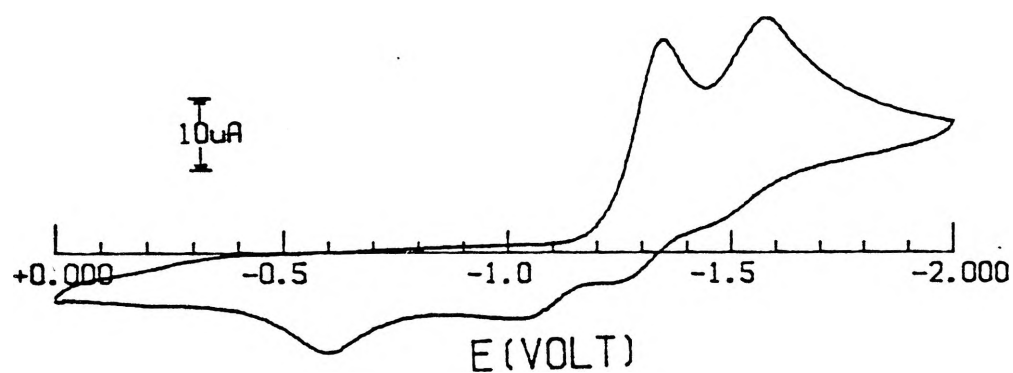
The cyclic voltammetry investigation of  $\text{Cu}_2(\text{SAL-DPE})\text{Pz}$  reveals two reduction processes at  $E_{1/2} = -1355\text{mV}$  and  $E_{1/2} = -1600\text{mV}$ . Associated with these two reduction processes are four oxidation processes at  $E_{1/2} = -665\text{mV}$ ,  $E_{1/2} = -1055\text{mV}$ ,  $E_{1/2} = -1225\text{mV}$  and  $E_{1/2} = -1515\text{mV}$ . The last two could form quasi-reversible couples with the two reduction processes ( $I_{\text{P}_R}/I_{\text{P}_F} = 0.15$ ,  $E_{\text{P}_A} - E_{\text{P}_C} = 80\text{mV}$  and  $I_{\text{P}_R}/I_{\text{P}_F} = 0.17$ ,  $E_{\text{P}_A} - E_{\text{P}_C} = 85\text{mV}$  respectively) (Table 8.9, Fig 8.30a). As was explained earlier the oxidation at  $-665\text{mV}$  is believed to be that of free copper. The nature of the other three oxidation processes ( $E_{1/2} = -1055\text{mV}$ ,  $E_{1/2} = -1225\text{mV}$  and  $E_{1/2} = -1515\text{mV}$ ) is unknown, i.e. we do not fully understand the reoxidation of this complex.

The presence of two reduction processes supports the differential pulse result and given the currents of the two reductions a result of two two electron reductions seems the most likely.

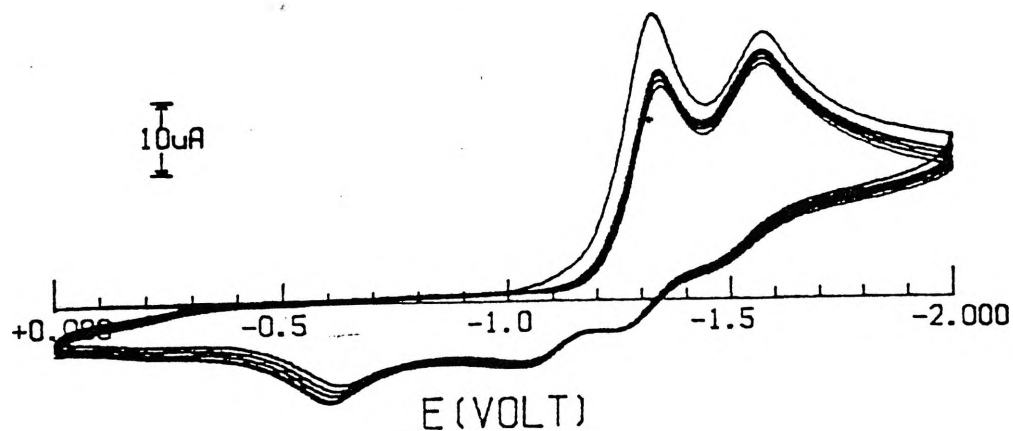


Multiple scans of  $\text{Cu}_2(\text{SAL-DPE})\text{Pz}$  (Table 8.9, Fig 8.30b) gives the same result as observed for  $\text{Cu}_2(\text{SAL-DPL})(\text{CAT})_{0.5}(\text{H}_2\text{O})_{0.5}$ , i.e. the redox process is quasi-reversible.

DC Polarography		Peak 1 -1430mV	Peak 2 —		Peak Ratio —		
DPV	GC	-1300mV	-1520mV		2:1		
	DME	-1380mV	-1580mV		1:1		
CV	Scan 1	Red	μA	Oxid	μA	$I^P_R/I^P_F$	$E^P_A-E^P_C$
		—	—	-665mV	3.2	—	—
		—	—	-1055mV	3.2	—	—
		-1355mV	29.3	-1275mV	4.4	0.15	80mV
	-1600mV	8.8	-1515mV	1.5	0.17	85mV	
	Scan 5	—	—	-655mV	3.3	—	—
		—	—	-1035mV	4.0	—	—
		-1365mV	22.0	-1270mV	4.5	0.21	95mV
		-1600mV	9.3	-1500mV	1.3	0.14	100mV
		—	—	—	—	—	—

Table 8.9: Electrochemical Data for  $\text{Cu}_2(\text{SAL-DPE})\text{Pz}$ 

a) Initial Scan



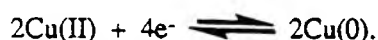
b) Multiple Scan

Fig 8.30: Cyclic Voltammogram of  $\text{Cu}_2(\text{SAL-DPE})\text{Pz}$

8.14  $\text{Cu}_2(\text{SAL-DPL})\text{PyO} \cdot 0.5\text{H}_2\text{O}$ 

## a) DC Polarography

The DC Polarographic investigation of  $\text{Cu}_2(\text{SAL-DPL})\text{PyO} \cdot 0.5\text{H}_2\text{O}$ , in the potential range 0 to -2000mV reveals a one step reduction occurring at  $E_{1/2} = -1245\text{mV}$  (Table 8.10, Fig 8.31) with the polarogram exhibiting a polarographic maxima at this potential. This single reduction suggests that the complex undergoes a single four electron reduction



It should be noted that the slope of the reduction is shallow, i.e. it occurs over a much larger potential range than is the case for some of the other complexes. Also there is a shoulder on its face and the peak itself is affected by a polarographic maxima. All these factors lead to the possibility that there is more going on under this peak than it is possible to determine from the polarogram itself.

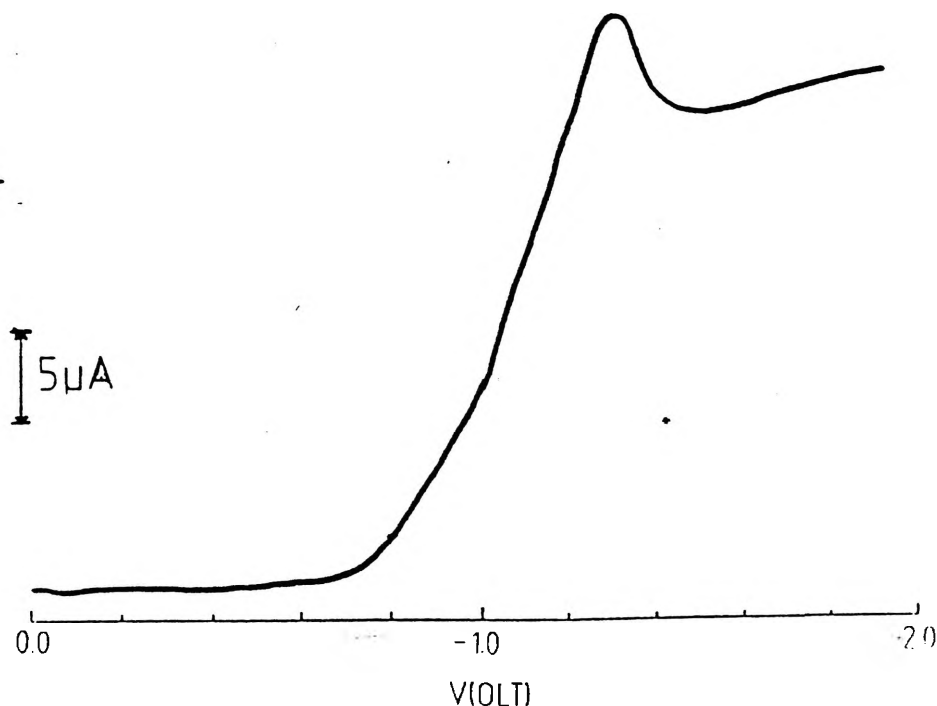


Fig 8.31: DC Polarogram of  $\text{Cu}_2(\text{SAL-DPL})\text{PyO} \cdot 0.5\text{H}_2\text{O}$

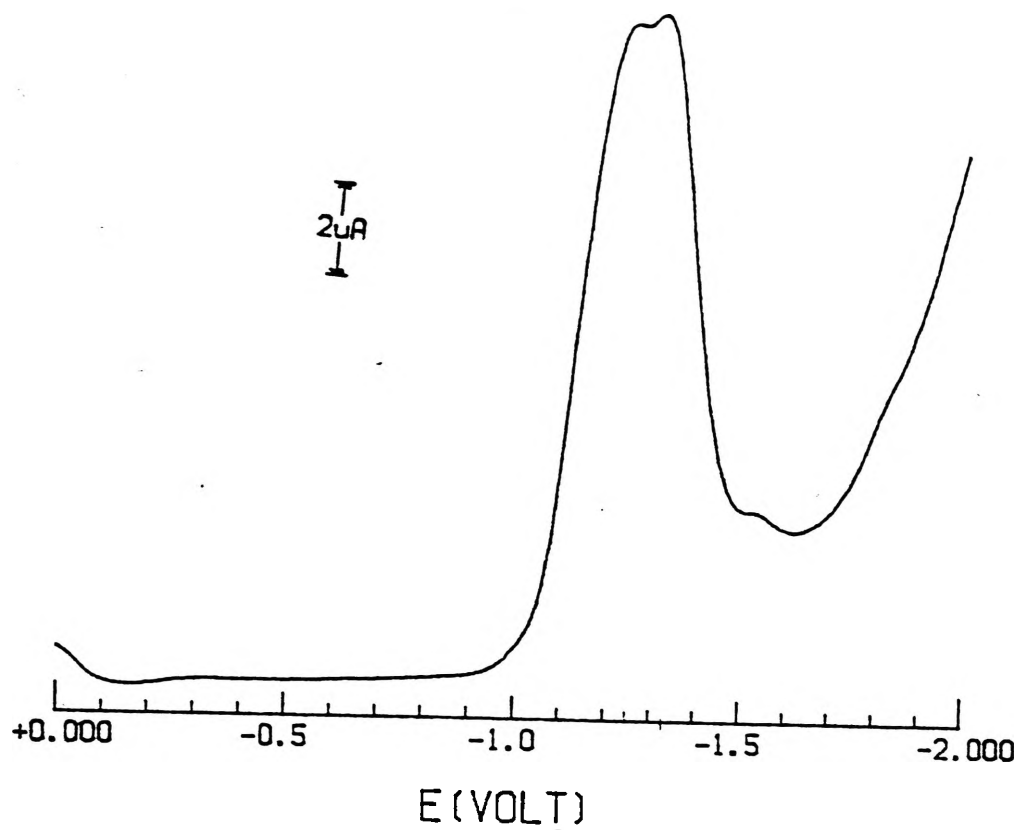
### b) Differential Pulse Voltammetry

The differential pulse voltammetry scan of  $\text{Cu}_2(\text{SAL-DPL})\text{PyO} \cdot 0.5\text{H}_2\text{O}$  using a glassy carbon electrode, shows a double reduction peak. The first peak occurs at  $E_{1/2} = -1250\text{mV}$  and the second at  $E_{1/2} = -1330\text{mV}$  (Table 8.10, Fig 8.32a). It is impossible to determine a peak area ratio as the two peaks are almost close enough to appear as one peak. The same situation applies for the dropping mercury differential pulse voltammetry where there is a broad band consisting of a peak at  $E_{1/2} = -1100\text{mV}$  and a second peak of almost equal height at  $E_{1/2} = -1230\text{mV}$  (Table 8.10, Fig 8.32b), i.e. the peak appears to have two equal humps with it again being impossible to determine any sort of peak area or peak height ratio.

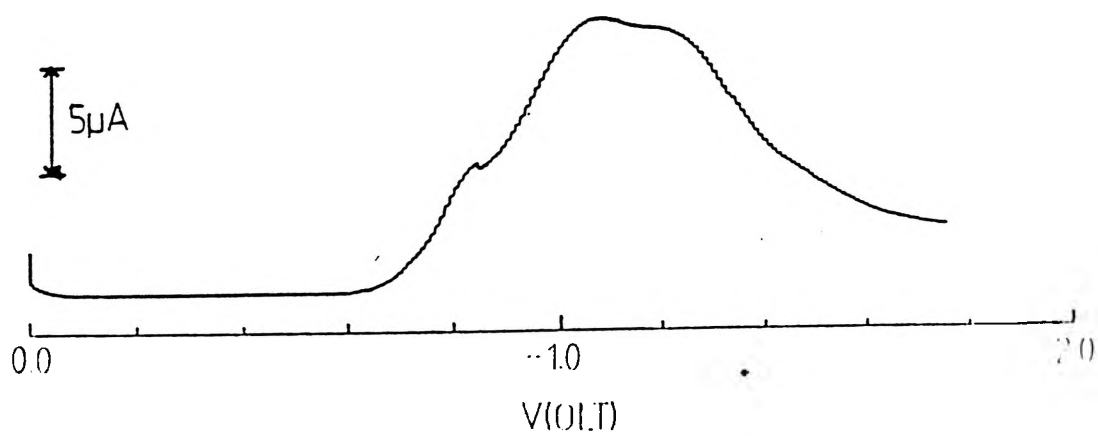
These results disagree with those of the polarography if the polarography suggests just one reduction. This is understandable because differential pulse voltammetry has better resolution than polarography given the nature of their sampling techniques. The two differential pulse voltammetry results indicate that  $\text{Cu}_2(\text{SAL-DPL})\text{PyO} \cdot 0.5\text{H}_2\text{O}$  undergoes two two electron reduction steps so close together as to appear almost as one reduction. There is a slight shift in potential between glassy carbon and mercury which indicates that  $\text{Cu}_2(\text{SAL-DPL})\text{PyO} \cdot 0.5\text{H}_2\text{O}$  is easier to reduce on mercury than on glassy carbon.

### c) Cyclic Voltammetry

The cyclic voltammetric scan of  $\text{Cu}_2(\text{SAL-DPL})\text{PyO} \cdot 0.5\text{H}_2\text{O}$  shows two reduction processes at  $E_{1/2} = -1350\text{mV}$  and  $E_{1/2} = -1430\text{mV}$  and a single oxidation process at  $E_{1/2} = -390\text{mV}$  which is due to free copper (Table 8.10, Fig 8.33a). The two reduction processes support the differential pulse voltammetry results.



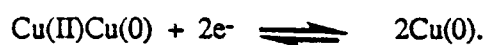
a) Glassy Carbon



b) Dropping Mercury

Fig 8.32: Differential Pulse Voltammogram of  $\text{Cu}_2(\text{SAL-DPL})\text{PyO} \cdot 0.5\text{H}_2\text{O}$

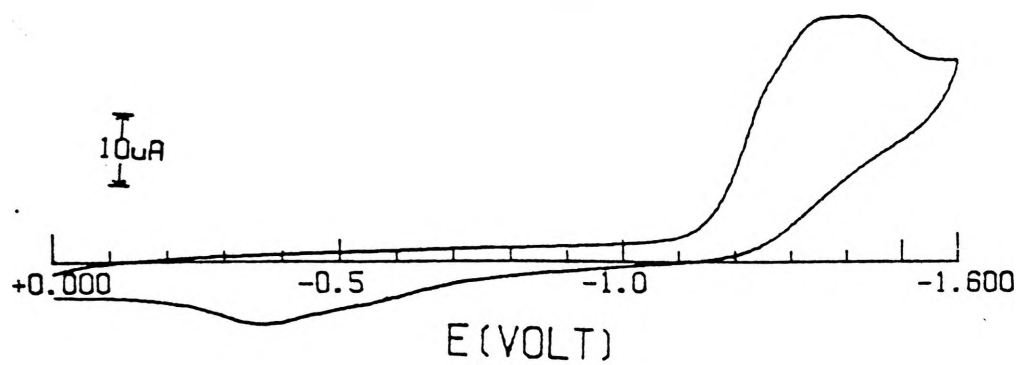
In conclusion  $\text{Cu}_2(\text{SAL-DPL})\text{PyO} \cdot 0.5\text{H}_2\text{O}$  undergoes two two electron reductions that are very close together in potential



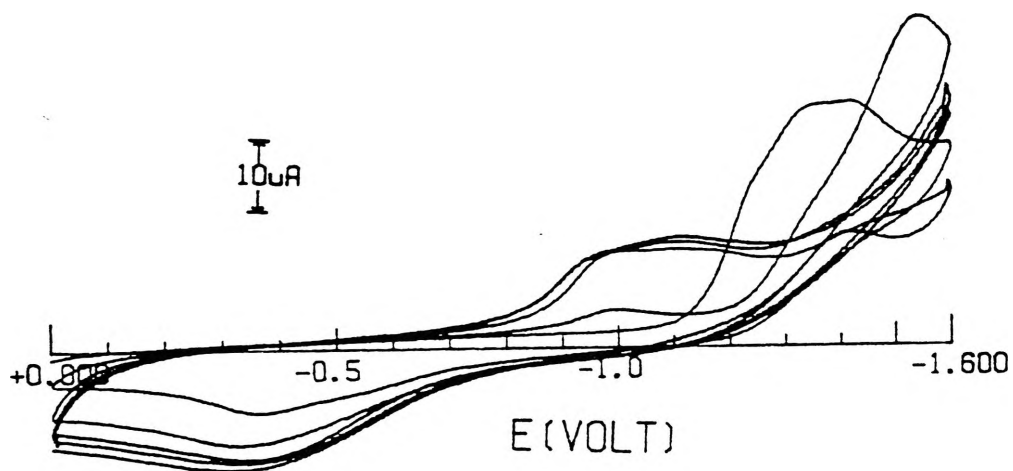
Multiple scans of  $\text{Cu}_2(\text{SAL-DPL})\text{PyO} \cdot 0.5\text{H}_2\text{O}$  (Table 8.10, Fig 8.33b) give the same result as for  $\text{Cu}_2(\text{SAL-DPL})\text{OH} \cdot 3\text{H}_2\text{O}$ , i.e. the redox process is irreversible.

		Peak 1	Peak 2		Peak Ratio		
DC Polarography		-1245mV	—		—		
DPV	GC	-1250mV	-1330mV		—		
	DME	-1100mV	-1230mV		—		
		Reduction	μA	Oxidation	μA	$I_R^P/I_F^P$	$E_A^P-E_C^P$
CV	Scan 1	-1350mV	15.2	-390mV	5.8	0.4	960mV
		-1430mV	15.2				
	Scan 5	-1000mV	—	—	—	—	—

Table 8.10: Electrochemical Data for  $\text{Cu}_2(\text{SAL-DPL})\text{PyO} \cdot 0.5\text{H}_2\text{O}$



a) Initial Scan



b) Multiple Scan

Fig 8.33: Cyclic Voltammogram of  $\text{Cu}_2(\text{SAL-DPL})\text{PyO} \cdot 0.5\text{H}_2\text{O}$

8.15  $\text{Cu}_2(\text{SAL-DPL})_4\text{-OHBzCOO}$ 

## a) DC Polarography

The DC Polarographic investigation of  $\text{Cu}_2(\text{SAL-DPL})_4\text{-OHBzCOO}$ , in the potential range 0 to -2000mV reveals one reduction process which occurs at  $E_{1/2} = -1000\text{mV}$  (Table 8.11, Fig 8.34). This result implies that the complex undergoes a single reduction consisting of four electrons

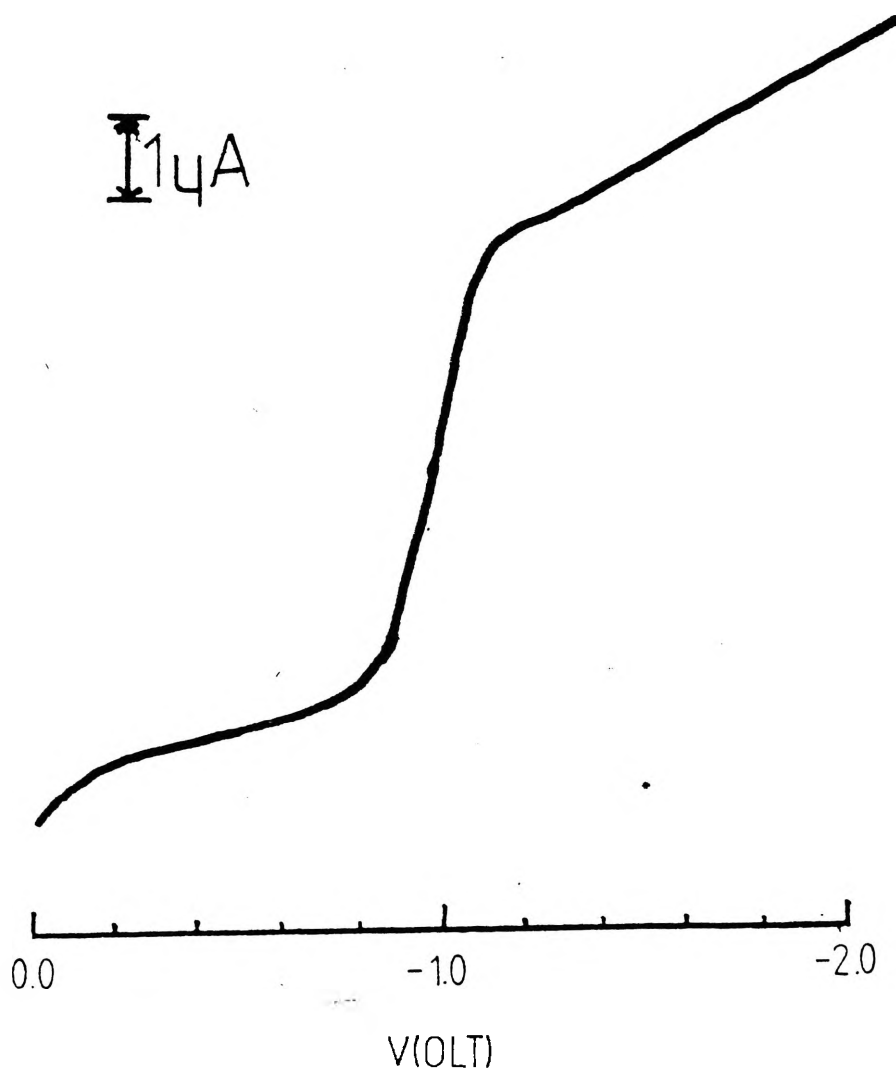


Fig 8.34: DC Polarogram of  $\text{Cu}_2(\text{SAL-DPL})_4\text{OHBzCOO}$



### b) Differential Pulse Voltammetry

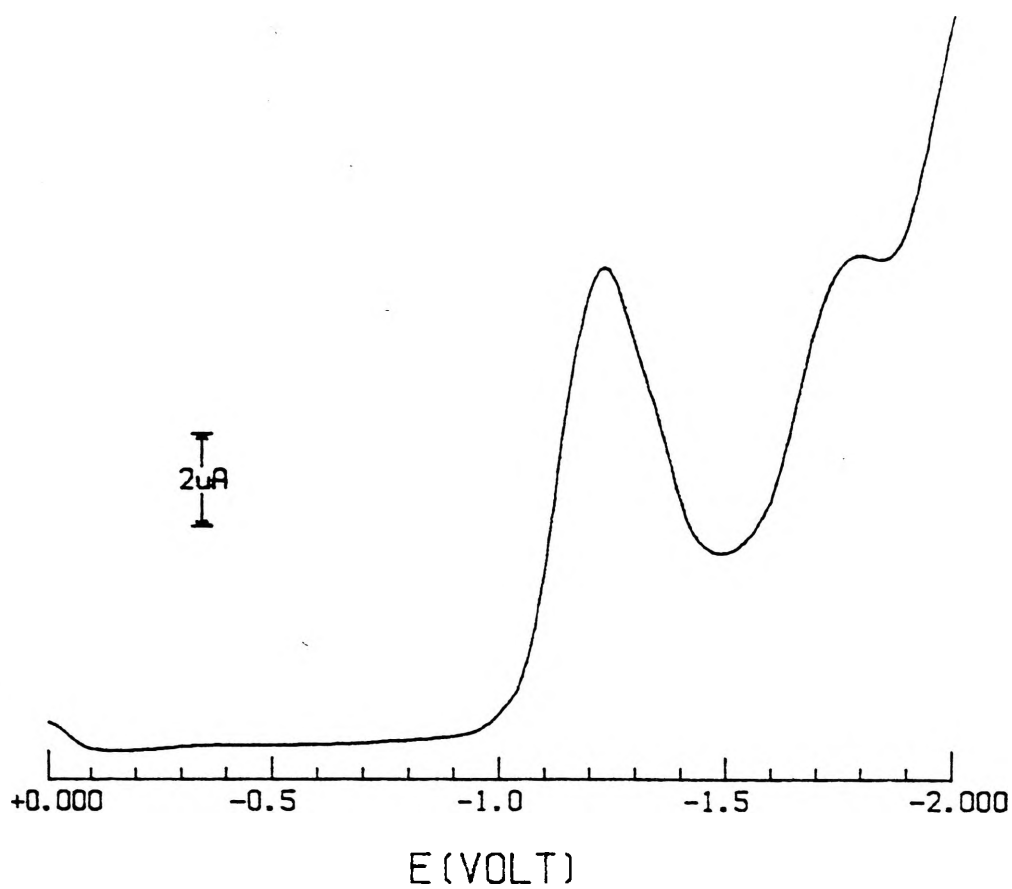
The differential pulse voltammetric measurements for  $\text{Cu}_2(\text{SAL-DPL})_4\text{-OHBzCOO}$  using a glassy carbon electrode indicates a single reduction process at  $E_{1/2} = -1230\text{mV}$  (Table 8.11, Fig 8.35a). This result agrees with the polarography result. The dropping mercury result also agrees with the polarography exhibiting one reduction process at  $E_{1/2} = -1030\text{mV}$  (Table 8.11, Fig 8.35b). These results support the proposition of  $\text{Cu}_2(\text{SAL-DPL})_4\text{-OHBzCOO}$  undergoing a single four electron reduction or two two electron reductions very close together. The shift in potential between the glassy carbon and the dropping mercury indicates that  $\text{Cu}_2(\text{SAL-DPL})_4\text{-OHBzCOO}$  is easier to reduce on mercury than on glassy carbon.

### c) Cyclic Voltammetry

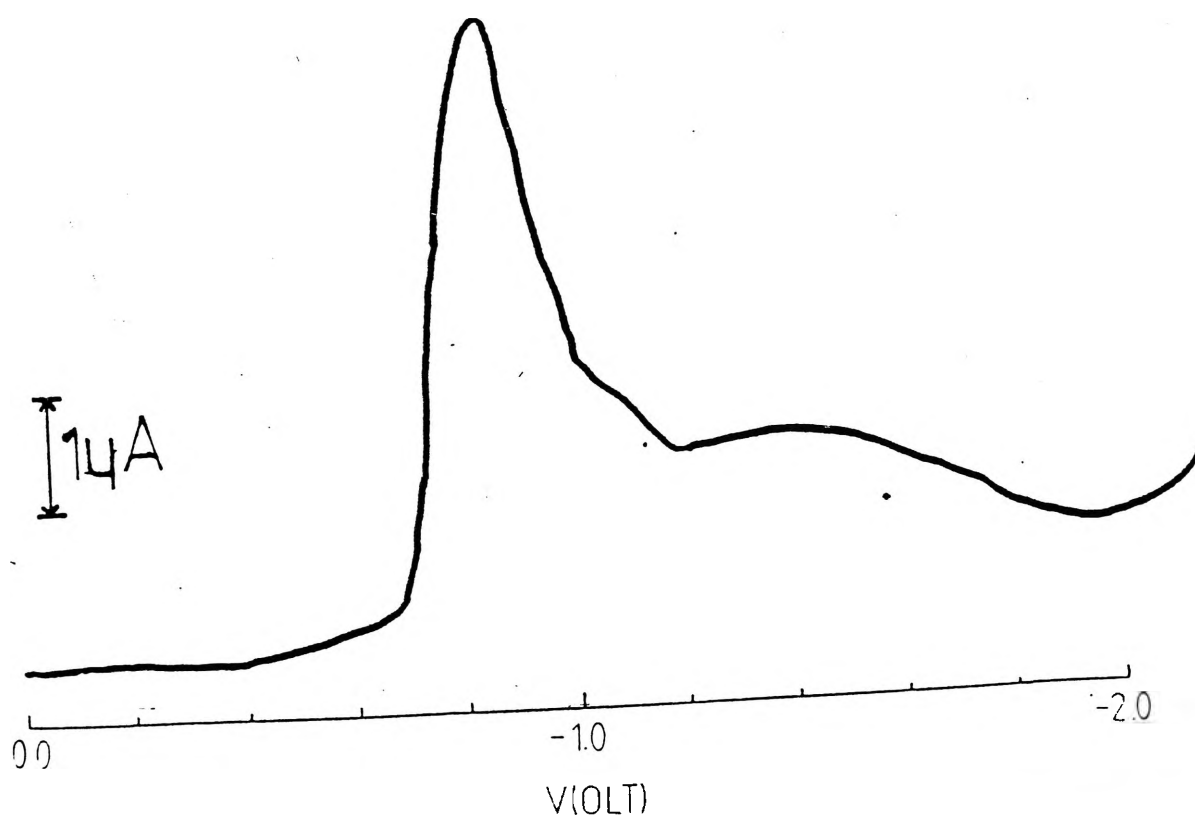
The glassy carbon cyclic voltammetric measurements for  $\text{Cu}_2(\text{SAL-DPL})_4\text{-OHBzCOO}$  indicates two reduction processes at  $E_{1/2} = -1200\text{mV}$  and  $E_{1/2} = -1300\text{mV}$ . There is also seen on the oxidative scan one process at  $E_{1/2} = -445\text{mV}$  which is believed to be that of free copper (Table 8.11, Fig 8.36a).

Multiple scans of  $\text{Cu}_2(\text{SAL-DPL})_4\text{-OHBzCOO}$  (Table 8.11, Fig 8.36b) show the same result as for  $\text{Cu}_2(\text{SAL-DPL})\text{OH}\cdot 3\text{H}_2\text{O}$ , i.e. the redox process is irreversible.

In conclusion it appears that  $\text{Cu}_2(\text{SAL-DPL})_4\text{-OHBzCOO}$  undergoes one four electron reduction step, although based on the earlier results it may be that the reduction occurs in two steps with, for this complex, the two steps being even closer together than previously observed.



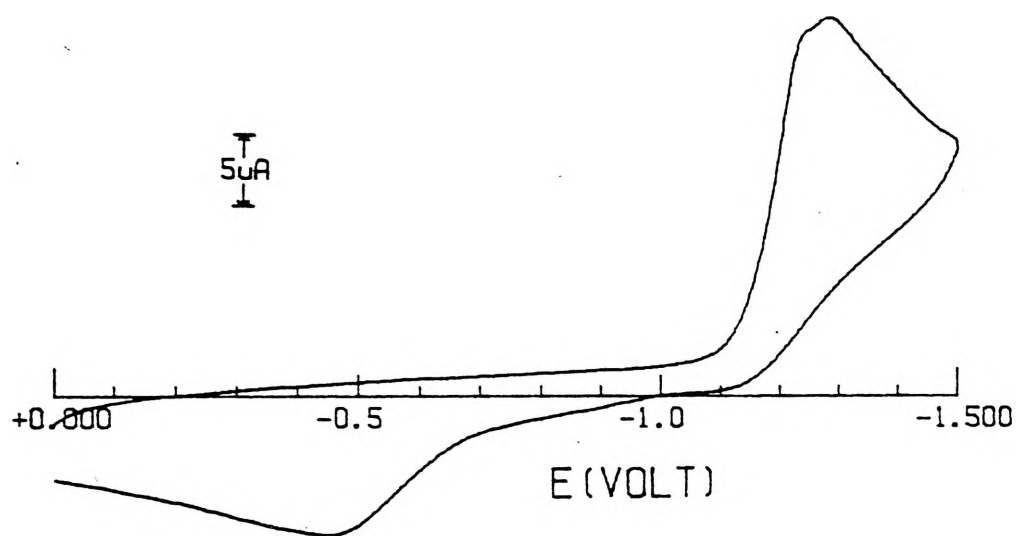
a) Glassy Carbon



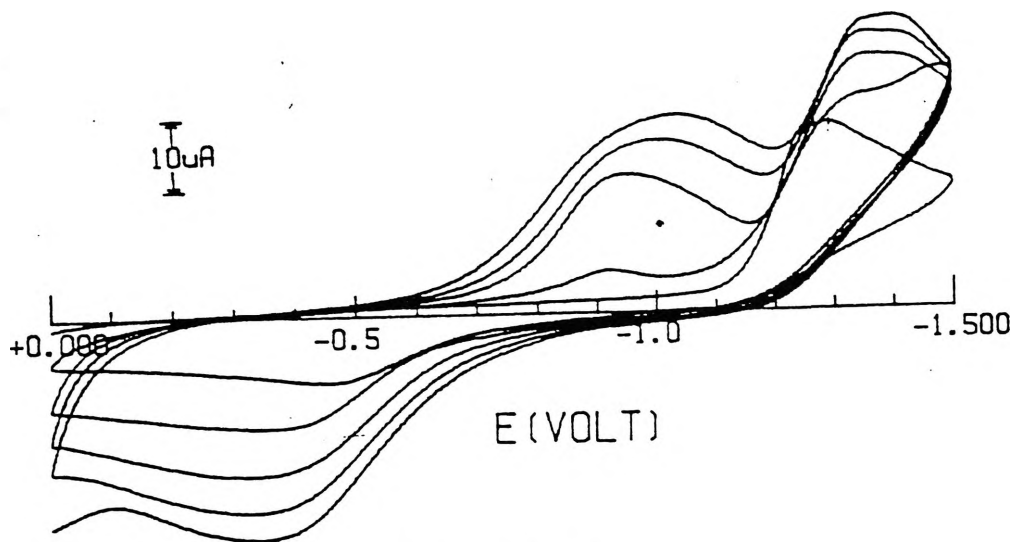
b) Dropping Mercury

Fig 8.35: Differential Pulse Voltammogram of  $\text{Cu}_2(\text{SAL-DPL})\text{OHBzCOO}$

DC Polarography		Peak 1	-1000mV				
DPV	GC		-1230mV				
	DME		-1030mV				
CV	RT	Reduction	$\mu\text{A}$	Oxidation	$\mu\text{A}$	$I_R^P/I_F^P$	$E_A^P-E_C^P$
		-1200mV	22.0	-445mV	4.7	0.21	755mV
		-1300mV	22.0	—	—	—	—
	Scan 5	-1000mV	10.0	—	—	—	—
		-1400mV	18.0	—	—	—	—
				—	—	—	—

Table 8.11: Electrochemical Data for  $\text{Cu}_2(\text{SAL-DPL})\text{OHBzCOO}$ 

a) Initial Scan



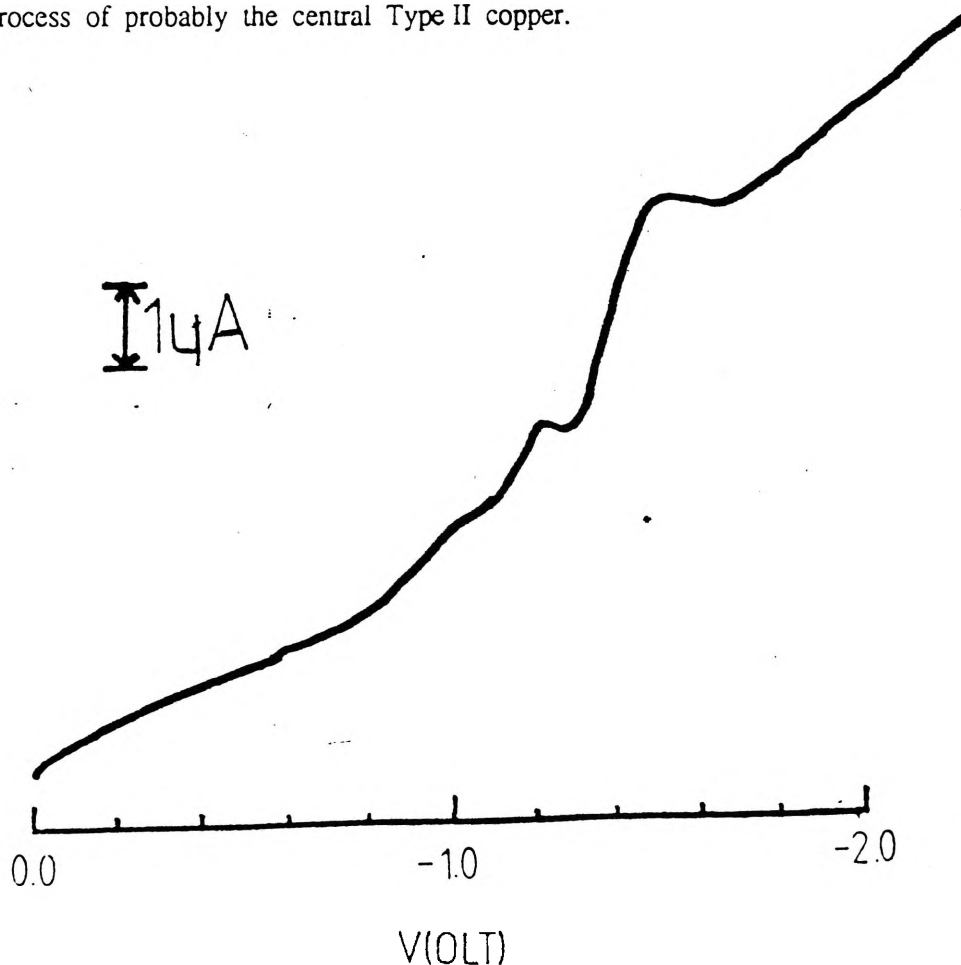
b) Multiple Scan

Fig 8.36: Cyclic Voltammogram of  $\text{Cu}_2(\text{SAL-DPL})\text{OHBzCOO}$

8.16  $\text{Cu}_5(\text{SAL-DPL.PAB.SAL})_2 \cdot 3\text{H}_2\text{O}$ 

## a) DC Polarography

The DC Polarographic scan of  $\text{Cu}_5(\text{SAL-DPL.PAB.SAL})_2 \cdot 3\text{H}_2\text{O}$  in the potential range 0 to -2000mV gives a result of two reduction processes at  $E_{1/2} = -1000\text{mV}$  and  $E_{1/2} = -1470\text{mV}$  with a peak height ratio of  $\sim 1:3$  (Table 8.12, Fig 8.37). This result does not seem to make sense as a ratio of 1:4 would be more reasonable. Examination of the polarogram reveals another process at  $E_{1/2} = -1220\text{mV}$  however this appears to be a polarographic maxima and is therefore not a valid peak given its appearance and size. The process at  $E_{1/2} = -1470\text{mV}$  is also associated with a polarographic maxima and therefore the peak height ratio is not accurate in regards to determining the number of electrons involved in each process. The appearance of the first reduction is a gradual slope rather than a sharp process implying it is a slow breakdown process of probably the central Type II copper.

Fig 8.37: Dc Polarogram of  $\text{Cu}_5(\text{SAL-DPL.PAB.SAL})_2 \cdot 3\text{H}_2\text{O}$

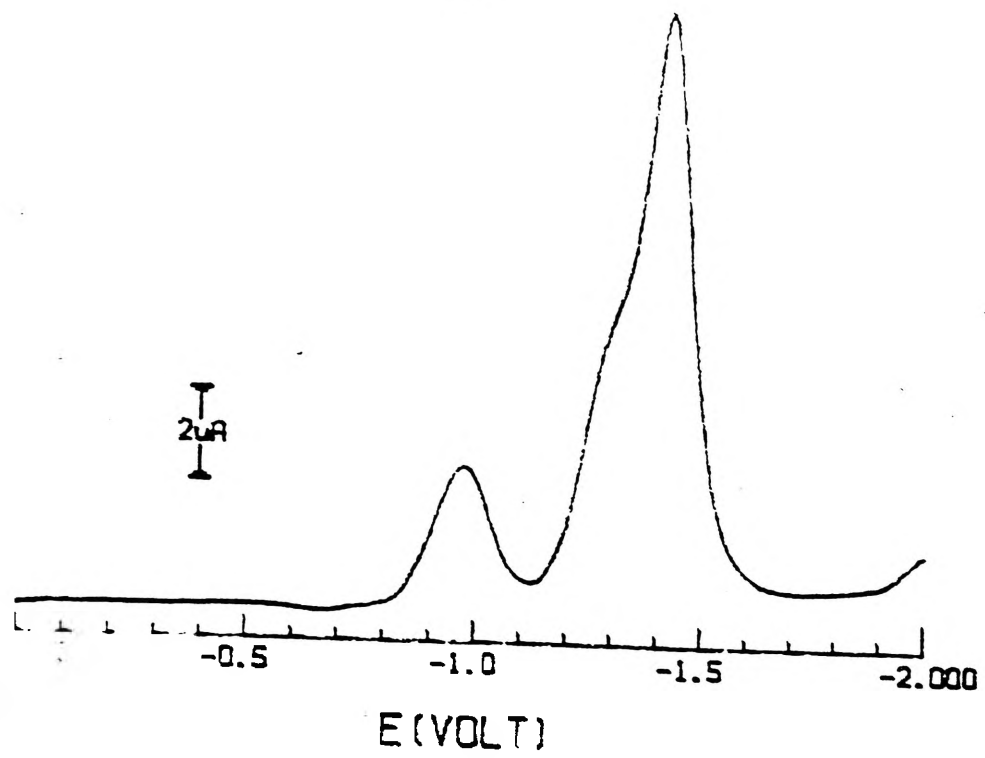
### b) Differential Pulse Voltammetry

Differential pulse voltammetry studies of  $\text{Cu}_5(\text{SAL-DPL.PAB.SAL})_2 \cdot 3\text{H}_2\text{O}$  using a glassy carbon electrode gives a result of two reduction processes at  $E_{1/2} = -970\text{mV}$  and  $E_{1/2} = -1410\text{mV}$ , with a peak area ratio of 1:5 (Table 8.12, Fig 8.38a). As with DC Polarography this result suggests that the copper atoms are reduced in two steps although a result of 1:4 would be more likely given the number of electrons available for reduction.

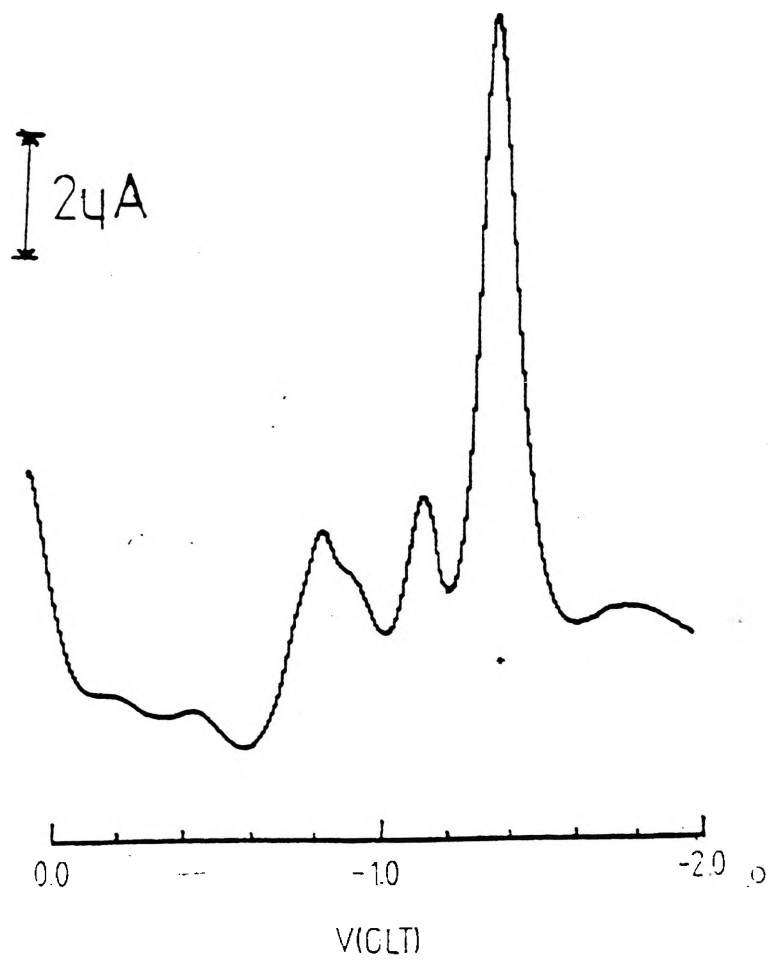
It should be noted that the second reduction peak is asymmetric in character with there being a shoulder on the higher potential side of the reduction peak. It is possible that there are two reduction processes very close together in potential as has been observed for a number of the binuclear complexes.

Using a dropping mercury electrode gives a result of three reduction processes at  $E_{1/2} = -880\text{mV}$ ,  $E_{1/2} = -1210\text{mV}$  and  $E_{1/2} = -1480\text{mV}$  (Table 8.12, Fig 8.38b). The three reduction peaks observed for the dropping mercury differential pulse voltammetry are reproducible as the three reduction processes appear when a second scan of  $\text{Cu}_5(\text{SAL-DPL.PAB.SAL})_2 \cdot 3\text{H}_2\text{O}$  using a fresh solution was conducted on a different day. The three reduction peaks for the fresh sample of  $\text{Cu}_5(\text{SAL-DPL.PAB.SAL})_2 \cdot 3\text{H}_2\text{O}$  occur at  $E_{1/2} = -980\text{mV}$ ,  $E_{1/2} = -1180\text{mV}$  and  $E_{1/2} = -1410\text{mV}$ . These results combined with the coulometry results mentioned earlier (see section 8.6) suggest that the copper atoms are reduced in a single two electron reduction above  $-1100\text{mV}$  (as already shown by coulometry) and two reduction processes below  $-1100\text{mV}$  with the number of electrons involved in each of these two processes being uncertain. The most logical reduction is two four electron reductions.

In an effort to determine if any of the reduction peaks were due to a polarographic maxima a solution of Triton X-100 was added to the  $\text{Cu}_5(\text{SAL-DPL.PAB.SAL})_2 \cdot 3\text{H}_2\text{O}$  solution in 50  $\mu\text{L}$  aliquots up to a total of 500  $\mu\text{L}$ . Triton X-100 is a known suppressant of polarographic maxima in aqueous solutions and it was hoped it would be successful for this solution. The result was that there was no substantial reduction in the current of any of the three reduction peaks nor was there any substantial shift in their potentials.



a) Glassy Carbon Electrode



b) Dropping Mercury Electrode

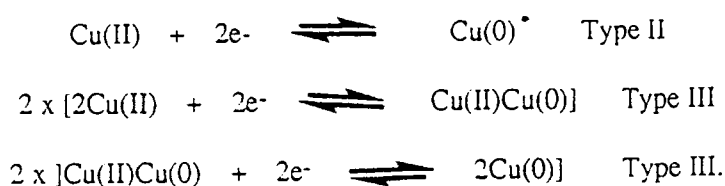
Fig 8.38: Differential Pulse Voltammogram of  $\text{Cu}_5(\text{SAL-DPL-PAB-SAL})_2 \cdot 3\text{H}_2\text{O}$

## c) Cyclic Voltammetry

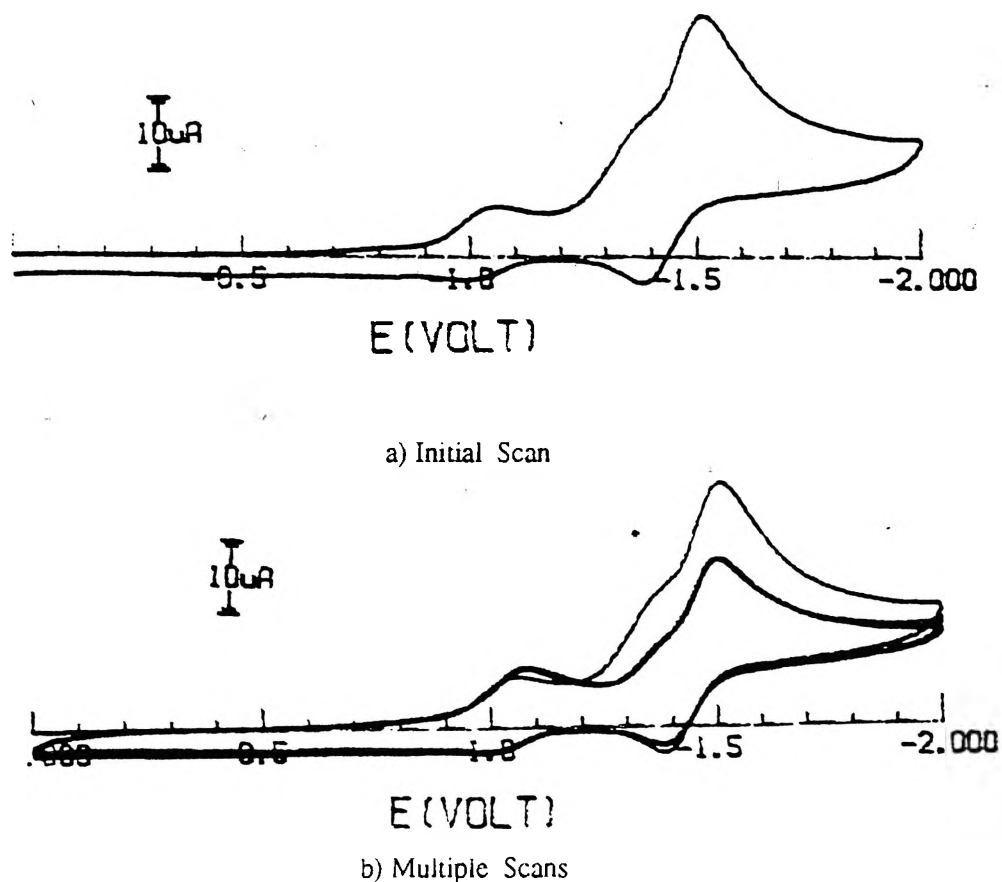
Cyclic voltammetric studies of  $\text{Cu}_5(\text{SAL-DPL.PAB.SAL})_2 \cdot 3\text{H}_2\text{O}$  using a glassy carbon electrode gives a result of two reduction processes at  $E_{1/2} = -1065\text{mV}$  and  $E_{1/2} = -1510\text{mV}$  and associated with these two reductions are two reoxidation processes at  $E_{1/2} = -965\text{mV}$  ( $I_{\text{P}_R}/I_{\text{P}_F} = 0.4$ ,  $E_{\text{P}_A} - E_{\text{P}_C} = 100\text{mV}$ ) and  $E_{1/2} = -1380\text{mV}$  ( $I_{\text{P}_R}/I_{\text{P}_F} = 0.6$ ,  $E_{\text{P}_A} - E_{\text{P}_C} = 130\text{mV}$ ) indicating that these reductions are quasi-reversible (Table 8.12, Fig 8.39a). The second reduction process shows a shoulder on the higher potential side as seen for the glassy carbon differential pulse voltammetry scan. It is possible that this shoulder is the second peak observed for mercury but with glassy carbon this peak has shifted very close to the lower potential peak.

Multiple scans of  $\text{Cu}_5(\text{SAL-DPL.PAB.SAL})_2 \cdot 3\text{H}_2\text{O}$  show the same result as was observed for  $\text{Cu}_2(\text{SAL-DPL})(\text{CAT})_{0.5}(\text{H}_2\text{O})_{0.5}$  (Table 8.12, Fig 8.39b), i.e. the redox process is quasi-reversible.

It appears that  $\text{Cu}_5(\text{SAL-DPL.PAB.SAL})_2 \cdot 3\text{H}_2\text{O}$  may undergo three reduction processes the first reduction occurring at  $E_{1/2} = -1000\text{mV}$  as described earlier in the coulometry (section 8.6). This reduction involves two electrons. There also appears to be two reduction processes in the  $-1450\text{mV}$  to  $-1500\text{mV}$  region with these two processes being very close together in potential with both involving four electrons. That is three reduction processes of two electrons, four electrons and four electrons. The first reduction would most likely be the central Type II copper atom and the two four electron reductions the two Type III copper centres with each Type III copper centre undergoing two two electron reductions, i.e.



		Peak 1	Peak 2	Peak 3	Peak Ratio
DC Polarography		-1000mV	-1470mV	—	1:3
DPV	GC	-970mV	-1410mV	—	1:5
	DME	-880mV	-1210mV	-1480mV	3:1:5(1:4)
	New Solution	-980mV	-1180mV	-1410mV	1:1:3
		Red $\mu\text{A}$	Oxid $\mu\text{A}$	$I^{\text{P}}_{\text{R}}/I^{\text{P}}_{\text{F}}$	$E^{\text{P}}_{\text{A}}-E^{\text{P}}_{\text{C}}$
CV	RT	-1065mV 4.7	-965mV 2.0	0.4	100mV
		-1510mV 12.7	-1380mV 8.1	0.6	130mV
	Scan 5	-1080mV 4.4	-945mV 2.1	0.5	135mV
		-1505mV 13.0	-1375mV 8.7	0.7	130mV

Table 8.12: Electrochemical Data for  $\text{Cu}_5(\text{SAL-DPL.PAB.SAL})_2 \cdot 3\text{H}_2\text{O}$ Fig 8.39: Cyclic Voltammetry of  $\text{Cu}_5(\text{SAL-DPL.PAB.SAL})_2 \cdot 3\text{H}_2\text{O}$



8.17  $\text{Cu}_5(\text{SAL-DPL.4ABA.SAL})_2 \cdot 2\text{H}_2\text{O}$ 

## a) DC Polarography

DC Polarographic measurements of  $\text{Cu}_5(\text{SAL-DPL.4ABA.SAL})_2 \cdot 2\text{H}_2\text{O}$  in the potential range 0 to -2000mV gives a result of two reduction processes at  $E_{1/2} = -610\text{mV}$  and  $E_{1/2} = -975\text{mV}$  (Table 8.13, Fig 8.40). This result indicates that the complex may undergo two five electron reductions

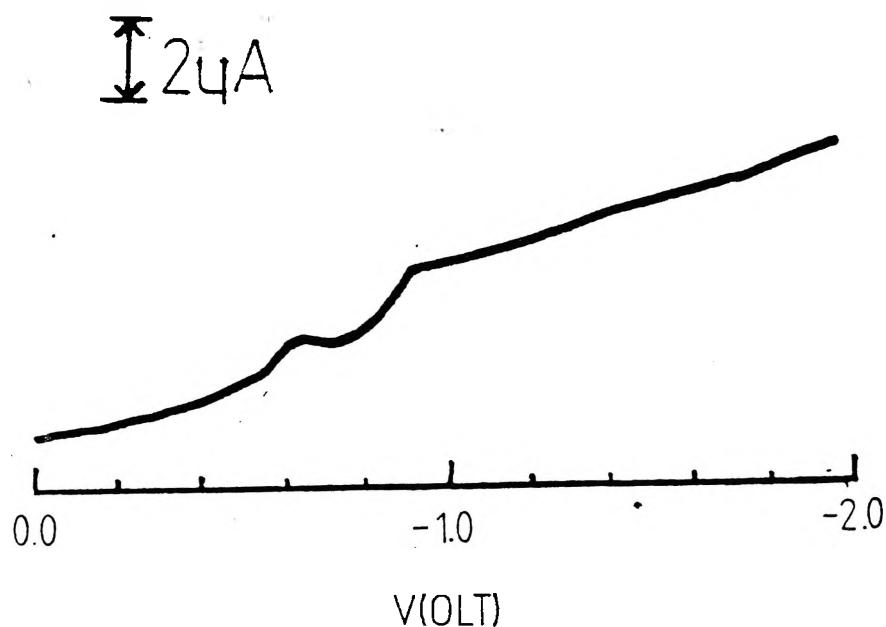
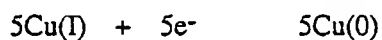
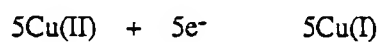


Fig 8.40: DC Polarogram of  $\text{Cu}_5(\text{SAL-DPL.4ABA.SAL})_2 \cdot 2\text{H}_2\text{O}$

### b) Differential Pulse Voltammetry

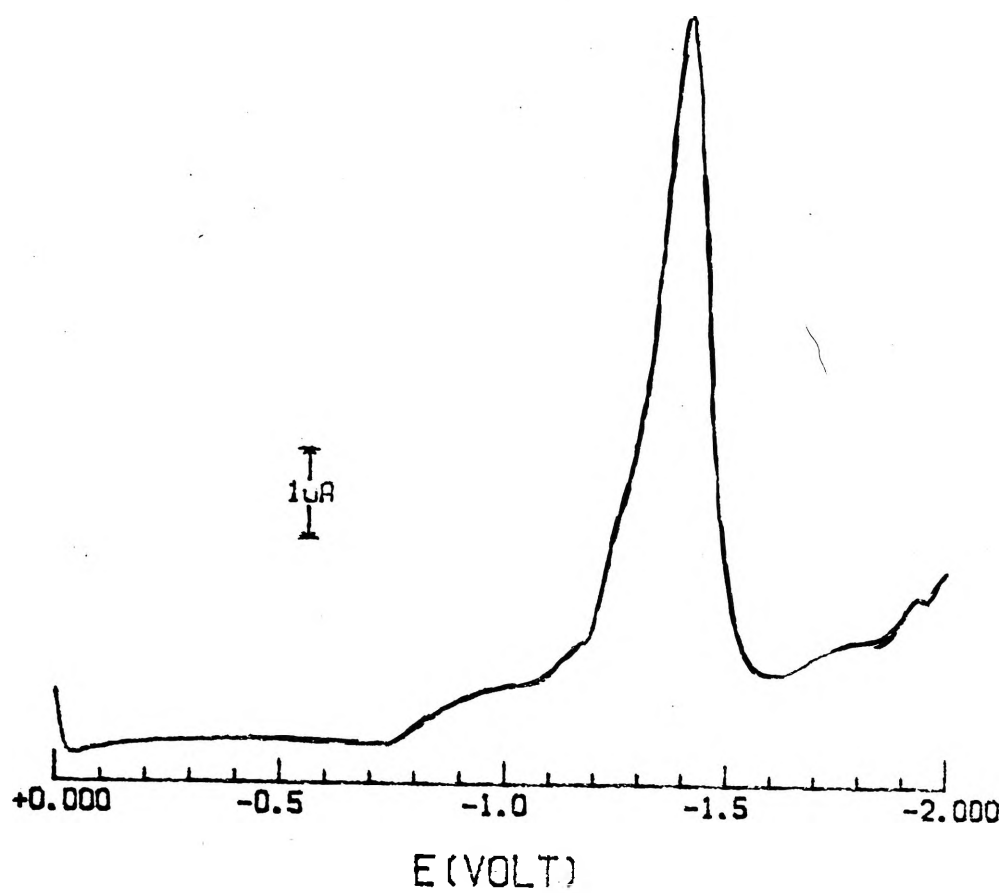
The differential pulse voltammetry of  $\text{Cu}_5(\text{SAL-DPL.4ABA.SAL})_2 \cdot 2\text{H}_2\text{O}$  using a glassy carbon electrode in the potential range 0 to -1600mV shows a result of one reduction peak at  $E_{1/2} = -1405\text{mV}$  (Table 8.13, Fig 8.41a). There also appears to be a small shoulder at  $\sim -1000\text{mV}$  which may correspond to the two electron reduction observed for  $\text{Cu}_5(\text{SAL-DPL.PAB.SAL})_2 \cdot 3\text{H}_2\text{O}$

Using a dropping mercury electrode gives a result of two reduction processes at  $E_{1/2} = -670\text{mV}$  and  $E_{1/2} = -1035\text{mV}$  with a peak area ratio of  $\sim 1:5$  (Table 8.13, Fig 8.41b). The potential of these two processes agrees with the DC Polarography. These two processes could reflect a situation where the Type II copper atom is reduced followed at a lower potential by the four Type III copper atoms with these two processes having merged into one process for glassy carbon as the glassy carbon differential pulse voltammetry peak is asymmetric with a shoulder appearing on the higher potential side with this shoulder representing the Type II copper atom. This result would agree with the  $\text{Cu}_5(\text{SAL-DPL.PAB.SAL})_2 \cdot 3\text{H}_2\text{O}$  result.

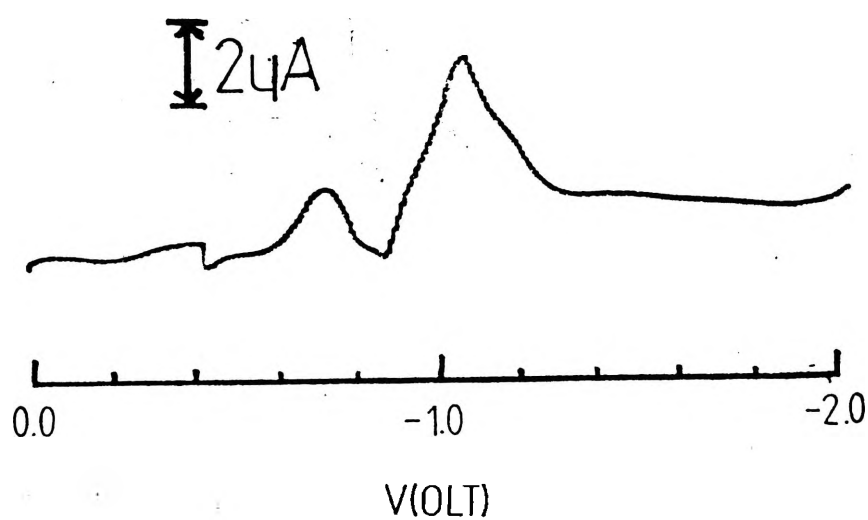
### c) Cyclic Voltammetry

The cyclic voltammetry of  $\text{Cu}_5(\text{SAL-DPL.4ABA.SAL})_2 \cdot 2\text{H}_2\text{O}$  exhibits a reduction process at  $E_{1/2} = -1450\text{mV}$  ( $I^P_R/I^P_F = 0.32$ ,  $E^P_A - E^P_C = 440\text{mV}$ ) (Table 8.13, Fig 8.42a). There also appears to be a shoulder at  $E_{1/2} = \sim -1000\text{mV}$  as was the case for glassy carbon differential pulse voltammetry. This shoulder possibly reflects a second reduction of the central Type II copper atom as was found for the  $\text{Cu}_5(\text{SAL-DPL.PAB.SAL})_2 \cdot 3\text{H}_2\text{O}$ .

Multiple scans of  $\text{Cu}_5(\text{SAL-DPL.4ABA.SAL})_2 \cdot 2\text{H}_2\text{O}$  show the same result as for  $\text{Cu}_2(\text{SAL-DPL})(\text{CAT})_{0.5}(\text{H}_2\text{O})_{0.5}$  (Table 8.13, Fig 8.42b), i.e. the redox process appears to be quasi-reversible.



a) Glassy Carbon



b) Dropping Mercury

Fig 8.41: Differential Pulse Voltammogram of  $\text{Cu}_5(\text{SAL-DPL.4ABA.SAL})_2 \cdot 2\text{H}_2\text{O}$

The complex appears to be easier to reduce on mercury than on glassy carbon as indicated by higher potential of the DC polarography and dropping mercury differential pulse results in comparison with the glassy carbon differential pulse and cyclic voltammetry results.

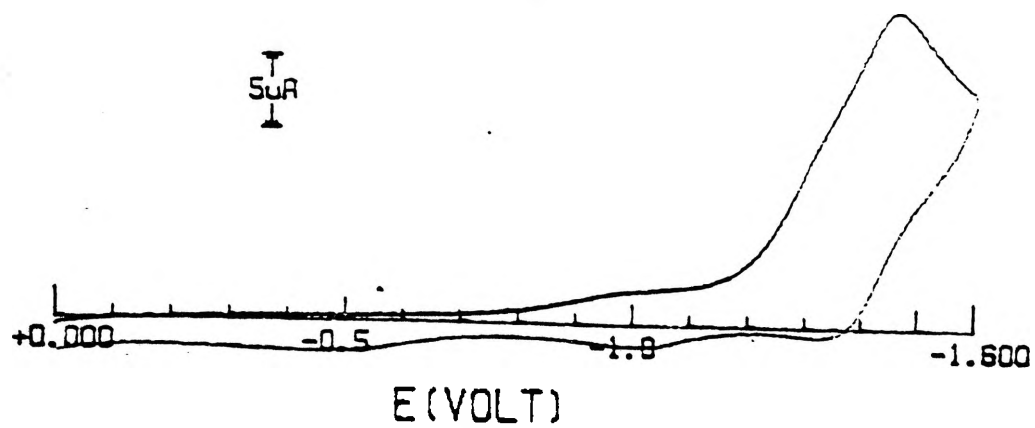
In conclusion  $\text{Cu}_5(\text{SAL-DPL.4ABA.SAL})_2 \cdot 2\text{H}_2\text{O}$  appears to undergo two reduction processes

1) the first being that of the single Type II copper atom, and

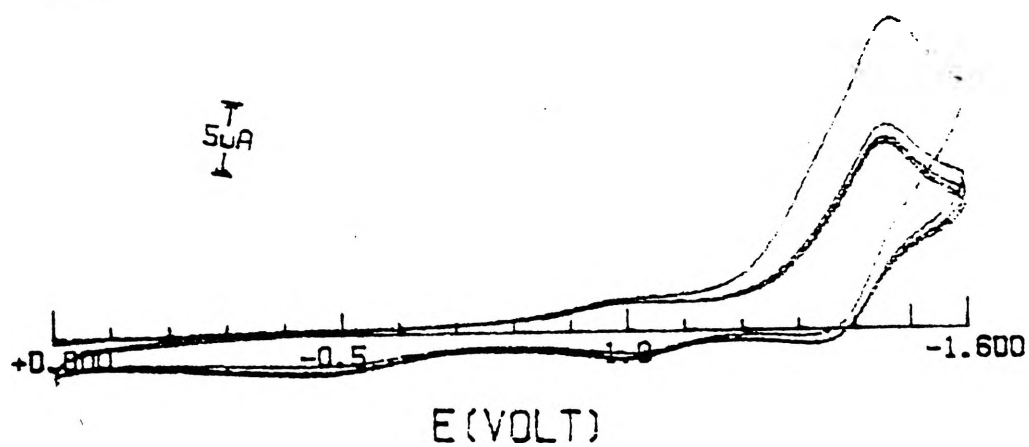
2) at lower potential the Type III binuclear copper centres are reduced with the reductions occurring as two very close together reductions in terms of their potentials.

		Peak 1	Peak 2		Peak Ratio		
DC Polarography		-610mV	-975mV		1:1		
DPV	GC	-1405mV	—		—		
	DME	-1035mV	—		—		
		Red	$\mu\text{A}$	Oxid	$\mu\text{A}$	$I^{\text{P}}_{\text{R}}/I^{\text{P}}_{\text{F}}$	$E^{\text{P}}_{\text{A}}-E^{\text{P}}_{\text{C}}$
CV	Scan 1	-1010mV	0.59	-990mV	1.2	2.03	20mV
		-1450mV	3.4	-1010mV	1.1	0.32	440mV
	Scan 5	-1010mV	0.59	-990mV	1.2	2.03	20mV
		-1450mV	6.4	-1320mV	2.2	0.34	130mV

Table 8.13: Electrochemical Data for  $\text{Cu}_5(\text{SAL-DPL.4ABA.SAL})_2 \cdot 2\text{H}_2\text{O}$



a) Initial Scan



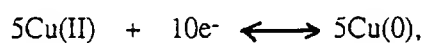
b) Multiple Scan

Fig 8.42: Cyclic Voltammogram of  $\text{Cu}_5(\text{SAL-DPL.4ABA.SAL})_2 \cdot 2\text{H}_2\text{O}$

8.18  $\text{Cu}_5(\text{ESAL-DPL.6Al.ESAL})_2 \cdot 2\text{H}_2\text{O}$ 

## a) DC Polarography

DC Polarographic investigation of  $\text{Cu}_5(\text{ESAL-DPL.6Al.ESAL})_2 \cdot 2\text{H}_2\text{O}$  in the potential range 0 to -2000mV results in a single reduction process at  $E_{1/2} = -1030\text{mV}$  (Table 8.14, Fig 8.43). This result indicates that the complex may undergo a single ten electron reduction



or that the reduction is very slow due to the Pi electron cloud distribution and more than one process blends into only one observed reduction process.

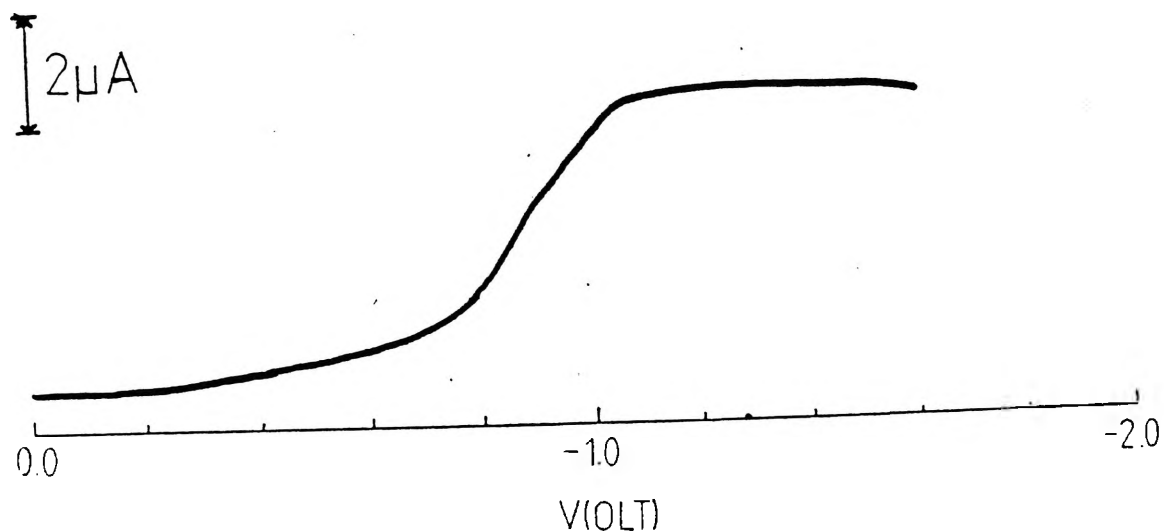
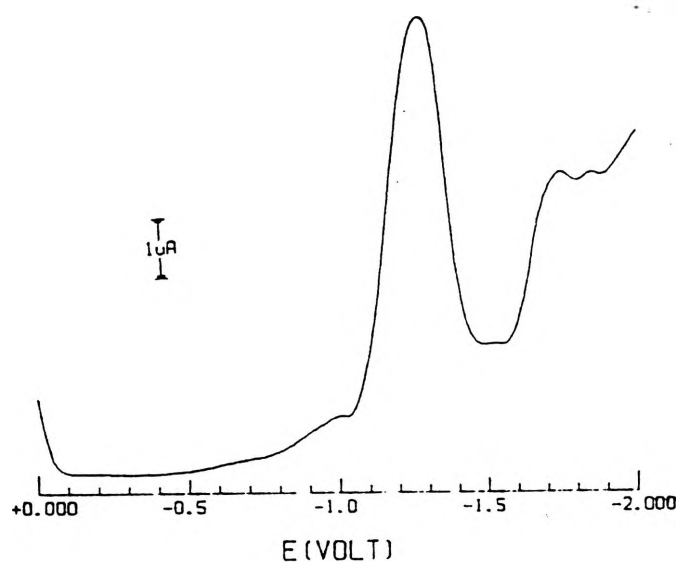


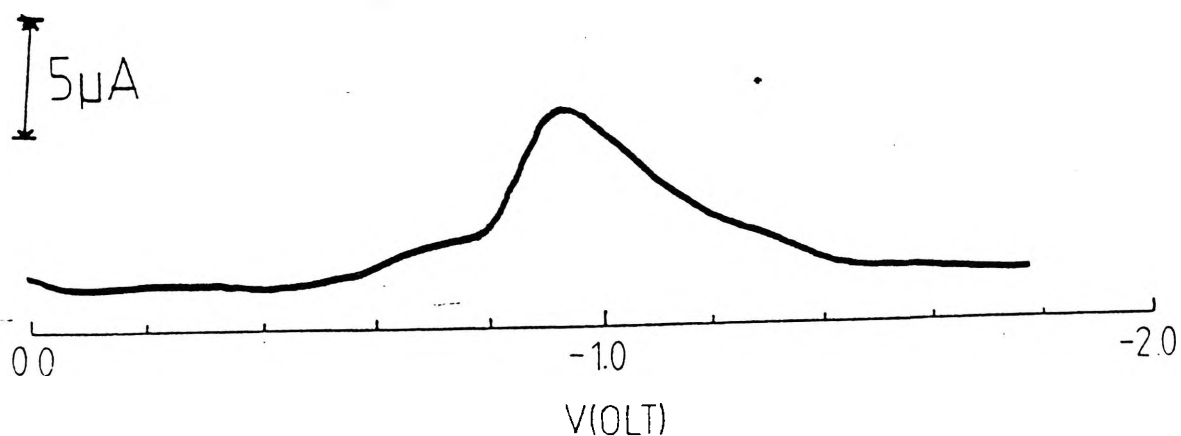
Fig 8.43: DC Polarogram of  $\text{Cu}_5(\text{ESAL-DPL.6Al.ESAL})_2 \cdot 2\text{H}_2\text{O}$

## b) Differential Pulse Voltammetry

The differential pulse voltammetric investigation of  $\text{Cu}_5(\text{ESAL-DPL.ESAL.6Al})_2 \cdot 2\text{H}_2\text{O}$  using a glassy carbon electrode gives a result of a single reduction peak at  $E_{1/2} = -1265\text{mV}$  (Table 8.14, Fig 8.44a) which given the differences in electrode material supports the DC Polarography result. Using a dropping mercury electrode, the voltammogram shows a result of a single reduction process at  $E_{1/2} = -935\text{mV}$  again supporting the DC Polarography result (Table 8.14, Fig 8.44b). There is also a small shoulder on the higher potential side of the peak at  $E_{1/2} = -1000\text{mV}$  on glassy carbon and  $E_{1/2} = -830\text{mV}$  on dropping mercury. it may be possible that this peak is that of the central Type II copper atom but this is not certain.



a) Glassy Carbon



b) Dropping Mercury

Fig 8.44: Differential Pulse Voltammogram of  $\text{Cu}_5(\text{ESAL-DPL.6Al.ESAL})_2 \cdot 2\text{H}_2\text{O}$

## c) Cyclic Voltammetry

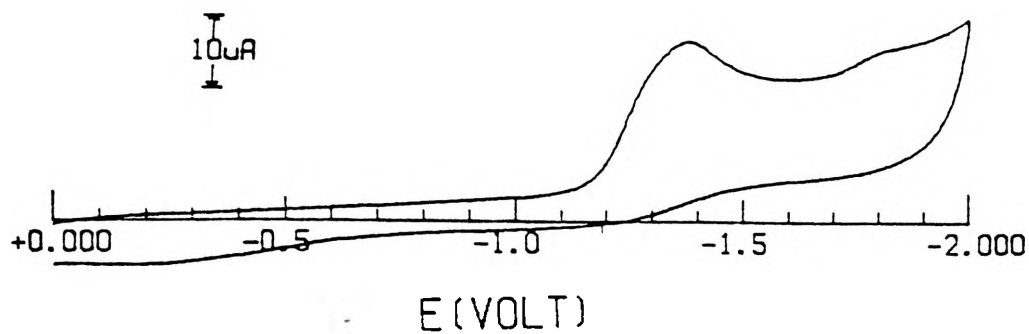
The cyclic voltammetry of  $\text{Cu}_5(\text{ESAL-DPL.6Al.ESAL})_2 \cdot 2\text{H}_2\text{O}$  in the potential range 0 to -2000mV gives a result of a single reduction peak at  $E_{1/2} = -1380\text{mV}$  with no identifiable reoxidation process in the potential range studied (Table 8.14, Fig 8.45a). This result agrees with the earlier results indicating that  $\text{Cu}_5(\text{ESAL-DPL.6Al.ESAL})_2 \cdot 2\text{H}_2\text{O}$  undergoes a single ten electron reduction to the copper metal state with the potential varying depending on electrode material and experimental technique with the mercury being approximately 300mV higher indicating that  $\text{Cu}_5(\text{ESAL-DPL.6Al.ESAL})_2 \cdot 2\text{H}_2\text{O}$  like a number of other complexes is easier to reduce with a mercury electrode than with a glassy carbon electrode.

Multiple scans of  $\text{Cu}_5(\text{ESAL-DPL.6Al.ESAL})_2 \cdot 2\text{H}_2\text{O}$  indicates that the complex is reasonably stable although the reduction at  $E_{1/2} = -1380\text{mV}$  is stable following the initial decrease in current. However a peak at  $E_{1/2} = \sim -900\text{mV}$  begins to appear with repeated scans (Table 8.14, Fig 8.45b). It seems possible that the  $\text{Cu}_2(\text{ESAL-DPL})_6\text{Al}$  Type III site is stable and this continues to appear at  $E_{1/2} = -1380\text{mV}$  while the type II site breaks down after the initial reduction and does not reform and this lone copper atom is what begins to appear with the  $E_{1/2} = \sim -900\text{mV}$  peak. In summary the Type III centres appear to exhibit a quasi-reversible redox process while the central Type II copper undergoes an irreversible redox process.

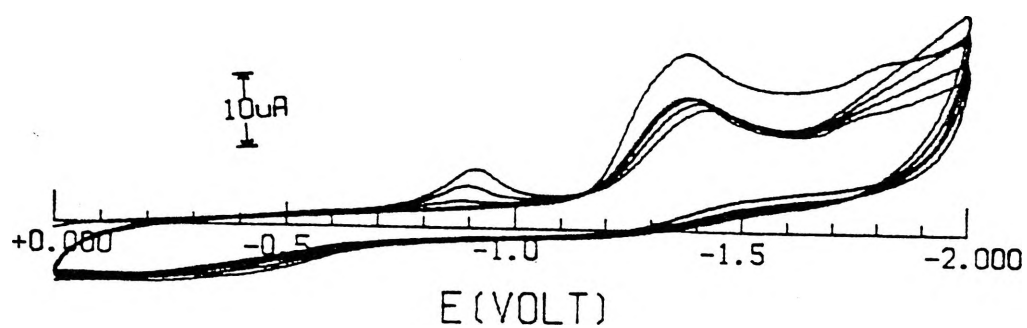
		Peak 1	Peak 2				
DC Polarography		-1030mV					
DPV	GC	-1000mV	-1265mV				
	DME	-830mV	-935mV				
CV	Scan 1	Reduction	$\mu\text{A}$	Oxidation	$\mu\text{A}$	$I^{\text{P}}_{\text{R}}/I^{\text{P}}_{\text{F}}$	$E^{\text{P}}_{\text{A}}-E^{\text{P}}_{\text{C}}$
		-1380mV	12.3	—	—	—	—
	Scan 5	-875mV	3.6	—	—	—	—
		-1385mV	8.8	—	—	—	—

Table 8.14: Electrochemical Data for  $\text{Cu}_5(\text{ESAL-DPL.6Al.ESAL})_2 \cdot 2\text{H}_2\text{O}$





a) Initial Scan



b) Multiple Scans

Fig 8.45: Cyclic Voltammogram of  $\text{Cu}_5(\text{ESAL-DPL.6Al.ESAL})_2 \cdot 2\text{H}_2\text{O}$

**9:**  
**Discussion**

## 9. Discussion

### 9.1 Models of Tyrosinase

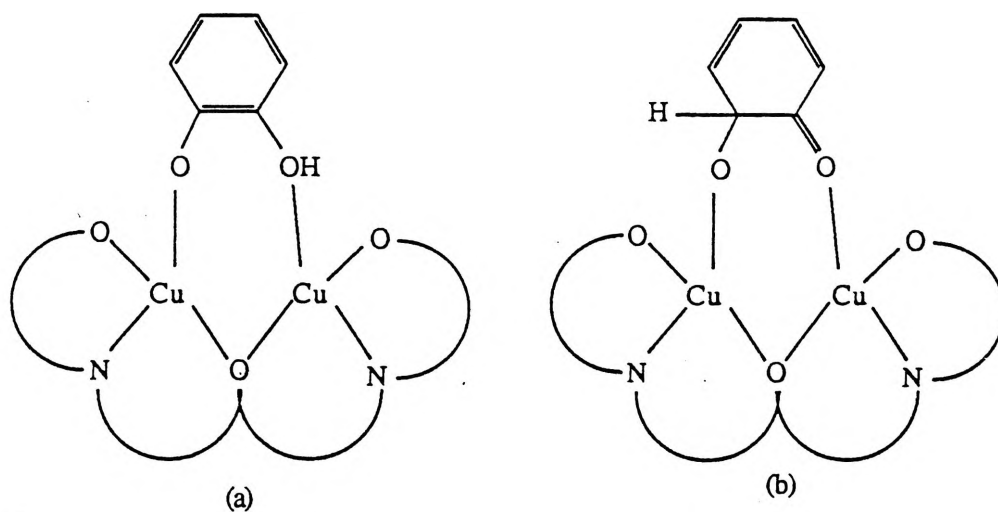
There are a number of features required by copper complexes to be considered as suitable models of Tyrosinase. The first and most obvious feature is that there should be two copper atoms per molecule of catechol or phenol.

The catecholate adduct should:-

- be stable at room temperature.
- have two to three heterocyclic nitrogen ligands per copper atom preferably histidine or imidazole.
- have square planar or square pyramidal environments around the copper atoms.
- possess an endogenous oxygen bridge.
- have  $\mu$ -1,2-catechol bridging.
- have UV-Vis spectra similar to that of Tyrosinase, i.e. a charge transfer band at  $\sim 345\text{nm}$  (16500) and a d-d transition band at  $\sim 600\text{nm}$  (1000).
- be diamagnetic at room temperature.
- give crystals suitable for X-ray crystallography.
- have a copper copper separation of  $\sim 3.6\text{\AA}$ .
- have the ability to oxidise catechol and/or hydroxylate phenols.
- have a fully reversible Cu (II)/Cu (I) pair.
- have reduction/oxidation at +360mV.

9.1.1 Cu<sub>2</sub>(XSAL-DPE)XCATH

The complexes with the pentanol backbone appear to be better models of Tyrosinase than the complexes with the propanol backbone because the empirical formulae of these complexes show that the complexes possess a ratio of two copper atoms per catechol molecule the same as predicted for Tyrosinase.<sup>46</sup> This ratio leads to questions about the method of the catechol bridging. There are two methods in which the catechol can bridge: (I)  $\mu$ -1,2 bridging as has been proposed for Tyrosinase<sup>46</sup> (Fig 9.1) with the second catechol oxygen either (a) being protonated or (b) the catechol could have been partially oxidised. If one oxygen is in the carbonyl form then the group should give a  $\nu_{C=O}$  stretch at  $\sim 1640\text{cm}^{-1}$ .

Fig 9.1:  $\mu$ -1,2-Catechol Bridge

(II)  $\mu$ -1,1-bridging (Fig 9.2) with the unbound oxygen being protonated.

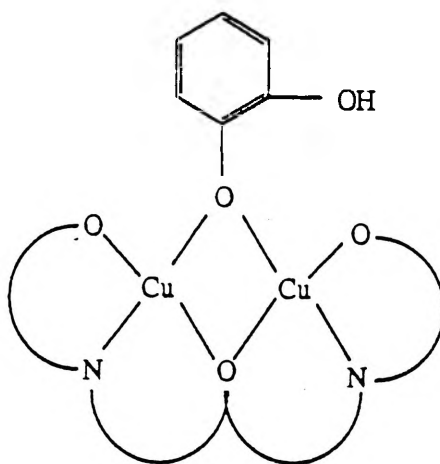


Fig 9.2:  $\mu$ -1,1-Catechol Bridge

These complexes are stable at room temperature. X-ray crystallography studies have been unable to be conducted as attempts to grow suitable crystals have been unsuccessful due to the formation of brown powders in solution upon standing which suggests that the catechol groups have been oxidised to some form of quinone. As a result of this the precise copper-copper separation is unknown however it is likely to be  $\sim 3.4\text{-}3.5\text{\AA}$  based upon similarities between these complexes and the complexes synthesised by Erickson<sup>120</sup> using the similar ligands with different exogenous bridges and those structures reported in this study whose crystal structures were solved and which have Cu-Cu distances of  $3.4\text{-}3.5\text{\AA}$ .

The IR spectra of these complexes exhibit a band at  $1615\text{cm}^{-1}$  to  $1625\text{cm}^{-1}$  which is assigned to the  $\nu_{\text{C=N}}$  stretch and due to the presence of this band it is difficult to determine if a  $\nu_{\text{C=O}}$  stretch, which usually occurs in the same region, is also present in these complexes. Some of the IR spectra give a hint of a second peak at  $\sim 1640\text{cm}^{-1}$  while others only give one sharp peak. The second peak maybe due to a carbonyl groups or it might be that the two imine groups have slightly different stretching frequencies resulting in two different signals occurring. In summary there is no clear indication that any carbonyl groups are present on the basis of Infra-red spectra.

These complexes possess no heterocyclic nitrogen ligand atoms but they do possess one imine nitrogen ligand atom per copper atom which is similar to the imidazole nitrogen atom for the purposes of model compounds.

The UV-Vis spectra of the  $\text{Cu}_2(\text{XSAL-DPE})\text{XCATH}$  complexes exhibit a single peak in both solid and solution spectra in the range 530-630nm which indicates that the copper atoms are in a square planar environment<sup>135</sup> with this band occurring in most of the complexes as a shoulder on a much more intense charge transfer band which occurs below 400nm. The position of these bands is very similar to the d-d band reported for Tyrosinase.

These complexes exhibit strong antiferromagnetic interaction at room temperature with magnetic moments well below the spin only value of 1.73B.M./Cu atom. The magnetic moments of these complexes approach diamagnetism at liquid nitrogen temperatures. Due to their low room temperature magnetism ( $\mu$  below 1.0B.M/Cu), they are considered to be essentially diamagnetic as is Tyrosinase.

The electrochemistry of these complexes will be discussed at later in this chapter when the electrochemistry of all the binuclear complexes will be reviewed in terms of their suitability as models of Type III copper proteins.

The ability of these complexes to oxidise catechols and hydroxylate phenols has not been examined in depth due to lack of time with the initial work being inconclusive. Binuclear complexes dissolved in DMF, with catechol also dissolved in the solution, were observed to change to a brown colour upon standing but no identifiable products were detectable by TLC (see Chapter 10 for more details of this work). Attempts to recrystallize the catecholate complexes were unsuccessful as, upon standing, a brown powder formed which is indicative of oxidised catechol.

Based on the empirical formulae of  $\text{Cu}_2(\text{SAL-DPE})\text{XCATH}$  a molecular model was constructed of the copper centres so as to examine in more detail the possible bonding of the catechol exogenous bridge. Both the  $\mu$ -1,2 and  $\mu$ -1,1 bridging methods shown in Figs 9.1 and 9.2 earlier were studied.

It was found from molecular model of  $\text{Cu}_2(\text{SAL-DPE})\text{XCATH}$ , that with square planar copper atoms, the catechol is able to bridge in a  $\mu$ -1,2 fashion with only a slight distortion of the ligand backbone. There was additional room available on the copper atoms to also possibly bridge a dioxygen molecule. A complex like this resembles the proposed method of bridging in Oxytyrosinase<sup>24</sup> (Fig 9.3).

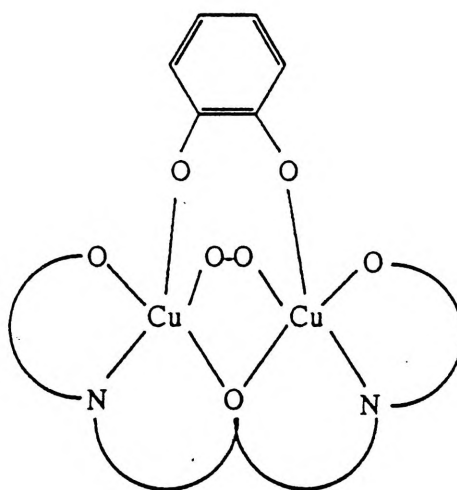


Fig 9.3: Possible Method of  $\mu$ -1,2-oxygen and  $\mu$ -1,2-catechol bridging in  $\text{Cu}_2(\text{SAL-DPE})\text{XCATH}$ <sup>24</sup>

Attempts to make a molecular model of the  $\mu$ -1,1-catechol bridged complex with square planar copper were unsuccessful so it appears likely that  $\mu$ -1,2-catechol bridging occurs for these complexes. The longer pentanol backbone reduces the possible problems of steric hindrance which occurs in the propanol complexes and the longer chain also allows the overall molecule greater flexibility.

### 9.1.2 $\text{Cu}_2(\text{SAL-DPL})(\text{XCAT})_{0.5}$

Based on the empirical formulae of the complexes, each of these complexes possess two copper atoms bridged to half a catechol molecule. The copper to catechol ratio is 4:1 which is double the ratio that these complexes should have to be good models of Tyrosinase. These complexes are stable at room temperature. As with the  $\text{Cu}_2(\text{SAL-DPE})\text{XCATH}$  complexes, these complexes provide only one imine nitrogen ligand per copper atom. The IR spectra of the  $\text{Cu}_2(\text{SAL-DPL})(\text{XCAT})_{0.5}$  complexes give a  $\nu_{\text{C=N}}$  stretch at  $\sim 1630\text{cm}^{-1}$  to  $1650\text{cm}^{-1}$ . The IR spectra are very similar to that of  $\text{Cu}_2(\text{SAL-DPE})\text{XCATH}$  in that some show one sharp peak and others a hint of two peaks.

Due to the lack of suitable crystals for X-ray crystallography we were unable to determine the copper-copper separation distance but it is believed, based on the crystal structures reported earlier and by Erickson,<sup>120</sup> that the Cu-Cu distance is 3.4-3.5 Å .

The UV-Vis spectra of the  $\text{Cu}_2(\text{SAL-DPL})(\text{XCAT})_{0.5}$  complexes show a single peak in the range 59-655nm. The position of this peak is not that far from that reported for Tyrosinase and, so in regards to Tyrosinase, the  $\text{Cu}_2(\text{SAL-DPL})(\text{XCAT})_{0.5}$  complexes would seem from spectral evidence to satisfy the requirement that the copper atoms be in a square planar/square pyramidal environment.

The magnetic moments of the  $\text{Cu}_2(\text{SAL-DPL})(\text{XCAT})_{0.5}$  complexes are above the spin only value of 1.73B.M/Cu which indicates that the complexes are considerably distorted from planarity causing disruption in the superexchange pathway. These complexes are not diamagnetic even at liquid nitrogen temperatures.



The electrochemistry of these complexes like that of the  $\text{Cu}_2(\text{SAL-DPE})\text{XCATH}$  complexes will be discussed later in this chapter.

The ability of these complexes to oxidise catechols or phenols was not investigated in detail and the work that was conducted in this area was inconclusive as was the case for the  $\text{Cu}_2(\text{SAL-DPE})\text{XCATH}$  complexes. Also, as with  $\text{Cu}_2(\text{SAL-DPE})\text{XCATH}$ , attempts to recrystallize these complexes resulted in the formation of a brown or purple powders indicating oxidation of the catechol.

The empirical formulae of these complexes suggested that the catechols bridge two binuclear copper (II) complexes (Fig 9.4), i.e. the complexes are dimers instead of monomers. This raised a number of questions. One is why would these complexes form dimers and what effect does this bridging have upon the copper atom environment and the complex overall. To attempt to answer these questions a molecular model of the  $\text{Cu}_2(\text{SAL-DPL})(\text{CAT})_{0.5}$  was constructed.

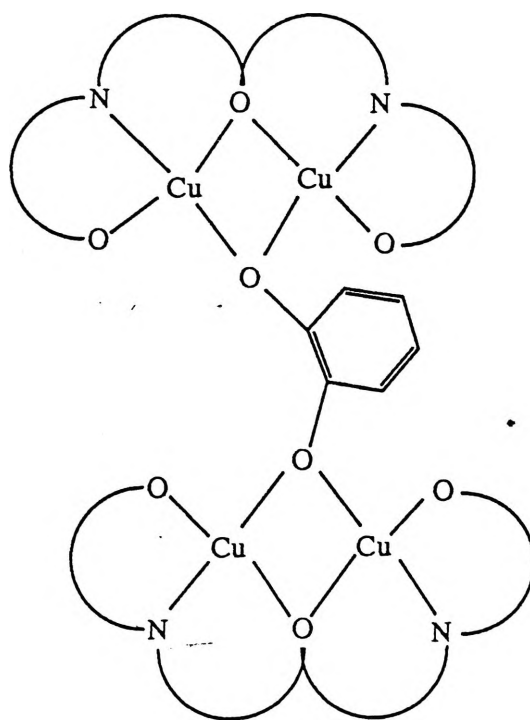


Fig 9.4: Model of  $\text{Cu}_2(\text{SAL-DPL})(\text{CAT})_{0.5}$  Dimer

Examination of this model indicates that, with square planar copper atoms, a m-1,2-catechol bridge can be formed (Fig 9.1) but the molecule is highly distorted due to the steric hindrance of the salicylaldimine rings. It is possible that this is the reason for formation of the dimer through single oxygen atom bridges instead. When a model of the m-1,1-bridging was constructed it was found that complex was still distorted, with distorted square planar copper atoms, although, this distortion was not as severe as in the m-1,2 case.

Therefore we can conclude from the models that the short propanol chain results in steric hindrance to the formation of m-1,2-catechol bridged  $\text{Cu}_2(\text{SAL-DPL})$  complexes. The formation of a m-1,1-catechol bridged dimer, as indicated by the empirical formulae, produces a less distorted structure.

Overall the  $\text{Cu}_2(\text{SAL-DPE})\text{XCATH}$  complexes are the best models of Tyrosinase as they are the first room temperature stable copper complexes with a m-1,2-catechol bridge that have been synthesised by reacting the catechol with copper (II), instead of by reducing quinone to catechol as done by Karlin et al.<sup>89</sup> They have similar spectra to Tyrosinase, are essentially diamagnetic and show some ability to oxidise catechols. The  $\text{Cu}_2(\text{SAL-DPL})(\text{XCATH})_{0.5}$  complexes are not as good a model of Tyrosinase as are the  $\text{Cu}_2(\text{SAL-DPE})\text{XCATH}$  complexes because they have the incorrect Cu:catechol ratio.

Table 9.1 gives an overall summary of the  $\text{Cu}_2(\text{SAL-DPL})(\text{XCAT})_{0.5}$  and  $\text{Cu}_2(\text{SAL-DPE})\text{CATH}$  complexes in regards to their satisfying the needs of models of Tyrosinase.

<u>Requirements</u>	<u><math>\text{Cu}_2(\text{SAL-DPE})\text{CATH}</math></u>	<u><math>\text{Cu}_2(\text{SAL-DPL})(\text{XCAT})_{0.5}(\text{H}_2\text{O})_{0.5}</math></u>
Cu/Catechol 2:1	Yes	No
Solid, stable at room temp	Yes	Yes
X-ray structure available	No	No
Cu-Cu $\sim 3.6\text{\AA}$	Yes*	Yes*
2-3 Heterocyclic Nitrogens/Cu atom	No	No
Endogenous Oxygen Bridge	Yes	Yes
cis- $\mu$ -1,2-Catechol Bridge	Yes	No
Reversible Cu(II)/Cu(I) at +360mV	No	No
UV-Vis Spectra Similar to Tyrosinase	Yes	Yes
Diamagnetic	Yes**	No
Oxidises Catechols/Phenols	Yes***	Yes***

\* as suggested by Cu-Cu distances in similar complexes, \*\* Very strong interaction ( $\sim 1.0\text{B.M}$  at room temperature), \*\*\* Inconclusive evidence but solutions do turn brown and give brown precipitates

## 9.2 Electrochemistry of Models of Tyrosinase and Multicopper Oxidases

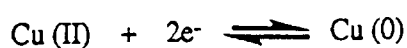
As mentioned in section 9.1, models of Tyrosinase (and Hemocyanin) need to exhibit fully reversible copper (II)/copper (I) cycles with the Type III copper centres undergoing a two electron reduction (one electron per copper atom) at a potential of approximately +360mV. Models of the multicopper oxidases also need to exhibit this type of behaviour although at different potentials (→+400 to +600mV) and in addition they need to undergo additional reductions of one electron for a Type II centre and one electron for a Type I centre with both of these oxidation/reductions being fully reversible and occurring at +300 to +500mV.

### 9.2.1 Cu(SAL-DPLH)

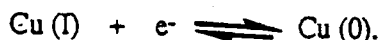
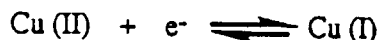
The simplest complex synthesised and studied electrochemically is the mononuclear complex Cu(SAL-DPLH). This complex is the simplest as it contains one copper (II) atom and therefore any electrochemical activity observed should relate to this copper atom. Polarography, differential pulse voltammetry and cyclic voltammetry data in Tables 9.2 to 9.5 show that Cu(SAL-DPLH) undergoes a single reduction/oxidation with the cyclic voltammetry data indicating that this process is quasi-reversible.

Coulometry measurements of Cu(SAL-DPLH) indicate that the complex undergoes a two electron transfer per mole of complex for both the reduction and oxidation processes.

A two electron transfer means that the copper atom is being reduced from copper (II) to copper metal and reoxidised back to copper (II). This reduction/oxidation can occur via two pathways. The first is a single two electron step



and the second pathway is via two one electron steps



The polarography, differential pulse voltammetry and cyclic voltammetry results all suggest that the copper atom is reduced by the first pathway above. It is possible that the second pathway is being followed but that the potentials of the two processes are so close together that they appear as one single process. There is no method readily available to determine which pathway is actually being followed. Based on the available evidence we can conclude that for the simplest system containing just one copper atom the complex appears to undergo a single two electron reduction at below -1000mV with this reduction being quasi-reversible.

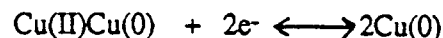
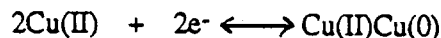
The more complicated binuclear complexes (models for Tyrosinase) can now be discussed.

### 9.2.2 Cu<sub>2</sub>(SAL-DPE)CATH

The Cu<sub>2</sub>(SAL-DPE)CATH is the best of four model complexes of Tyrosinase and so its electrochemistry is the most important of the binuclear complexes studied.

The polarographic, differential pulse voltammetry and cyclic voltammetry results (see Tables 9.2 to 9.5) all show two reduction processes with the reductions occurring at ~-1400mV and ~-1600mV. Both of these reductions are found to be quasi-reversible. Coulometry measurements give a result of four electrons oxidised/reduced per mole of complex. These results indicate that both copper atoms undergo two electron reduction/oxidation processes.

The reduction of the copper atoms can occur by two pathways the first consisting of one copper being fully reduced followed by the other



while the second pathway involves the two copper atoms both being reduced to copper (I) and then to copper metal



If Cu(SAL-DPLH) is reduced in one two electron step, then given the closeness of these two reduction processes the first pathway would seem to be the most likely.

Multiple cyclic voltammetry measurements of Cu<sub>2</sub>(SAL-DPE)CATH show a reduction in current after the first scan with the subsequent scans showing no further decrease in current. It would appear that a breakdown compound is fouling the electrode surface which causes the reduction in current.

In conclusion Cu<sub>2</sub>(SAL-DPE)CATH fails to satisfy all the requirements of a model of Tyrosinase in that

(I) the copper atoms are reduced to copper metal not copper (I),

(II) this reduction is not fully reversible and

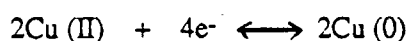
(III) the reductions occur at negative potentials instead of positive potentials.

This is not surprising due to the different environment of the copper atoms and the solvent systems involved compared to those in the protein.

### 9.2.3 $\text{Cu}_2(\text{XSAL-DPL})(\text{CAT})_{0.5}(\text{H}_2\text{O})_{0.5}$

This complex is the next best model of Tyrosinase studied electrochemically as it is the only other complex studied which possesses a catechol exogenous bridge. It was found using polarography, differential pulse voltammetry and cyclic voltammetry (see Tables 9.2 to 9.5) that this complex undergoes a single reduction at  $-1450$  to  $-1500\text{mV}$ . This reduction was found, like  $\text{Cu}_2(\text{SAL-DPE})\text{CATH}$ , to be quasi-reversible and involve a four electron transfer upon both reduction and reoxidation.

The single reduction process suggests that the complex undergoes a single four electron reduction



instead of the two two electron reduction observed for  $\text{Cu}_2(\text{SAL-DPE})\text{CATH}$ . This seems unusual as the two two electron reduction process seems to be the most reasonable process for the reduction of the copper atoms. However, if we refer back to the molecular model of this complex, it was found that this complex was very distorted. It could be that there is a sudden release of stereochemical strains in these molecules when the potential at which copper (II) reduces is reached. In simple terms, release the tension in these complexes and the complex disintegrates. This 'cascade effect' would result in only one reduction process being observed. The other possibility is that the reduction still occurs in two steps of two electrons but that the processes occur so close together in potential that they appear as just one process. This could be due to the first reduction being slightly more difficult due to the distortion and so it occurs at slightly lower potential and the second reduction is slightly easier due to the release of the stereochemical strain and so its potential is slightly higher.

Multiple cyclic voltammetric scans of  $\text{Cu}_2(\text{SAL-DPL})(\text{CAT})_{0.5}(\text{H}_2\text{O})_{0.5}$  show a similar result as was observed for  $\text{Cu}_2(\text{SAL-DPE})\text{CATH}$ , i.e. the redox process of the compound is quasi-reversible.

We can conclude that  $\text{Cu}_2(\text{SAL-DPL})(\text{CAT})_{0.5}(\text{H}_2\text{O})_{0.5}$  satisfies the requirement for a model of Tyrosinase in that there is only one reduction step, although this reduction may possibly be two steps which are very close together in their potentials. The reduction involves four electrons not two, is not fully reversible and occurs at negative potentials instead of at positive potentials as occurs in Tyrosinase.

#### 9.2.4 Binuclear Complexes

The other binuclear complexes can be considered together as a whole as none are particularly good models of Tyrosinase although their electrochemistry is interesting and useful for supporting the results found for the catechol bridged complexes.

Looking at Tables 9.2 to 9.5 it is apparent that like the catechol bridged complexes all the binuclear complexes undergo reduction/oxidation at negative potentials in the same general region, i.e.  $\sim -1200$  to  $\sim -1600$  mV. As with the catecholate complexes some of these complexes undergo reductions in two clear steps while others appear to undergo a single reduction. All the binuclear complexes were found to undergo four electron transfers per mole of complex.

We studied binuclear complexes with other types of exogenous bridges to see if the nature of the exogenous bridge affected the electrochemical behaviour. The type of exogenous bridge used were

- (I) hydroxides
- (II) pyrazolates, and
- (III) 4-OHBzCOO<sup>-</sup>.

These were selected as there was data available on the structure and properties of complexes of these types and so any correlation between structure and differences in electrochemistry would be able to be observed. No obvious correlation between the redox potential and the type of exogenous bridge was observed.



An important feature of these studies was that some of the complexes which at first appeared to undergo a one step reduction were found on closer examination and in different techniques to actually undergo two reduction steps. This supports the belief that all the binuclear complexes undergo two two electron reductions with the reductions occurring very close together in potential (within two hundred millivolts or less in most cases).

Multiple cyclic voltammetry scans of some of these binuclear complexes showed breakdown products through the appearance of a new reduction peak at  $\sim -1000\text{mV}$  coupled with the disappearance of the initial reduction peak. It is proposed that the  $\sim -1000\text{mV}$  reduction is that of a simple copper salt e.g.  $\text{Cu}(\text{DMF})_4^{2+}$ . When the  $\sim -1000\text{mV}$  reduction peak was observed on multiple scans it was found that, on the initial and subsequent oxidation scans, there was only one oxidation process observed at  $\sim -400\text{mV}$ . Where the  $\sim -1000\text{mV}$  reduction was not observed, there was observed on the oxidation scan a process below  $\sim -1000\text{mV}$ , sometimes with the  $\sim -400\text{mV}$  oxidation, sometimes on its own. In summary the presence of a single oxidation process at  $\sim -400\text{mV}$  indicates the breakdown of the complex. This is confirmed by the growth of a reduction process at  $\sim -1000\text{mV}$  due to the presence of a simple copper (II) salt and the single oxidation process at  $\sim -400\text{mV}$  due to free copper, e.g. see the electrochemistry of copper acetate in the electrochemistry chapter.

The second feature to note is that the more stable complexes appear to be those possessing an exogenous bridge containing a heterocyclic or aromatic ring. The exception to this trend is the pyridine-N-oxide (PyO) complex. It may be that the ring group has a stabilizing effect upon the complexes but there is no obvious reason for this trend.

The most surprising result of these electrochemical studies was finding that the copper (II) was reduced to copper metal. When we first began the studies it was assumed that the redox processes being observed involved the reduction of copper (II) to copper (I). This assumption was based on previous work and logic which said that the reduction of copper (II) to copper (I) is much easier than the reduction of copper (II) to copper metal. It was not until coulometry measurements were conducted that we found that the complexes were reduced to copper metal.

When we found that the copper metal was being produced it was realised that the solid surfaces of the electrodes would suffer from fouling by breakdown products and so other electrodes would be needed. It was also felt that the use of a number of techniques would overcome the limitations associated with any one technique.

It was not until we observed consistent results over a number of techniques, for a complex, that we believed we had an accurate picture of its electrochemistry. This was because we had learnt to distrust any one result following the problem of oxygen in the cell of Cu(SAL-DPLH).

Overall, if an accurate picture is to be obtained about the electrochemistry of copper (II) complexes, then a range of techniques and electrodes are required.

We can conclude by saying that binuclear copper (II) complexes appear to undergo two two electron reductions with these reductions occurring at negative potentials. These two reduction steps are close together in potential and they are not fully reversible. There is no obvious relationship between the nature of the exogenous bridge and the redox potential in the complexes studied.

### 9.2.5 Multicopper Oxidases Model Compounds

The pentanuclear complexes first synthesised by Werakso<sup>123</sup> allow the study of models of the multicopper oxidases. To be good models electrochemically they should possess a two electron reduction of a Type III centre, a one electron reduction of a Type II centre and a one electron reduction of a Type I centre. The complexes of Werakso's only possess a Type II centre and two Type III centres and so should undergo a one electron reduction for the Type II centre distinct from the four electron reduction for the two Type III centres. All the reductions should be fully reversible and occur at positive potentials.

Three pentanuclear complexes were studied which for the sake of convenience we will call Cu<sub>5</sub>PAB (Cu<sub>5</sub>(SAL-DPL.PAB.SAL)<sub>2</sub>.3H<sub>2</sub>O), Cu<sub>5</sub>4ABA (Cu<sub>5</sub>(SAL-DPL.4ABA.SAL)<sub>2</sub>.2H<sub>2</sub>O) and Cu<sub>5</sub>6AI (Cu<sub>5</sub>(ESAL-DPL.6AI.ESAL)<sub>2</sub>.2H<sub>2</sub>O).

All three complexes were found to undergo reduction at negative potentials with there being a total of ten electrons transferred per mole of complex for these reductions (see Tables 9.2 to 9.5). It was found overall that Cu<sub>5</sub>PAB and Cu<sub>5</sub>4ABA undergo two reduction steps at ~-1000mV and ~-1400mV while Cu<sub>5</sub>6AI undergoes a single reduction step at ~-1300mV.

Cu<sub>5</sub>PAB was found to undergo a two electron transfer during the first reduction step which implies that the central Type II copper centre is being reduced separately to the Type III centres in both Cu<sub>5</sub>PAB and Cu<sub>5</sub>4ABA complexes. In this regard these complexes are good models of the multicopper oxidases.

The reason the Cu<sub>5</sub>6AI complex does not show a separate reduction for the Type II centre is possibly due to the delocalization of the Pi electron cloud of the indazole and aromatic groups over the entire complex resulting in all the copper atoms appearing electrochemically alike and therefore reducing at the same potential.

While the reduction of the Type III centres all appear to be single reductions however, as in the binuclear case, on which these ligands are based, it seems likely that each Type III centre is undergoing two two electron reductions with the potentials of these reductions being very close together.

In conclusion the Cu<sub>5</sub>PAB and Cu<sub>5</sub>4ABA complexes are better models than the Cu<sub>5</sub>6AI complex for multicopper oxidases in that the Type II centre is reduced separately to the Type III centres, although all are reduced at negative potentials, the reductions are not fully reversible and there are ten electrons transferred instead of five.

<u>Compound</u>	<u>Peak 1</u>	<u>Peak 2</u>
Cu(SAL-DPLH)	-970mV	
Cu <sub>2</sub> (SAL-DPL)OH.3H <sub>2</sub> O	-1430mV	
Cu <sub>2</sub> (SAL-DPE)OH	-1110mV	
Cu <sub>2</sub> (SAL-DPL)(CAT) <sub>0.5</sub> .(H <sub>2</sub> O) <sub>0.5</sub>	-1440mV	
Cu <sub>2</sub> (SAL-DPE)CATH	-1390mV	-1570mV
Cu <sub>2</sub> (SAL-DPL)Pz	-1450mV	
Cu <sub>2</sub> (SAL-DPE)Pz	-1430mV	
Cu <sub>2</sub> (SAL-DPL)PyO.(H <sub>2</sub> O) <sub>0.5</sub>	-1245mV	
Cu <sub>2</sub> (SAL-DPL)4-OHBzCOO	-1000mV	
Cu <sub>5</sub> (SAL-DPL.PAB.SAL) <sub>2</sub> .3H <sub>2</sub> O	-1000mV	-1470mV
Cu <sub>5</sub> (SAL-DPL.4ABA.SAL) <sub>2</sub> .2H <sub>2</sub> O	-610mV	-975mV
Cu <sub>5</sub> (ESAL-DPL.6AI.ESAL) <sub>2</sub> .2H <sub>2</sub> O	-1030mV	

Table 9.2: Compiled DC Polarography Reduction Potentials

<u>Compound</u>	<u>Peak 1</u>	<u>Peak 2</u>	<u>Peak 3</u>
Cu(SAL-DPLH)	-935mV		
Cu <sub>2</sub> (SAL-DPL)OH.3H <sub>2</sub> O	-1490mV		
Cu <sub>2</sub> (SAL-DPE)OH	-1045mV		
Cu <sub>2</sub> (SAL-DPL)(CAT) <sub>0.5</sub> .(H <sub>2</sub> O) <sub>0.5</sub>	-1420mV		
Cu <sub>2</sub> (SAL-DPE)CATH	-1430mV	-1530mV	
Cu <sub>2</sub> (SAL-DPL)Pz	-1420mV		
Cu <sub>2</sub> (SAL-DPE)Pz	-1380mV	-1580mV	
Cu <sub>2</sub> (SAL-DPL)PyO.(H <sub>2</sub> O) <sub>0.5</sub>	-1100mV	-1230mV	
Cu <sub>2</sub> (SAL-DPL)4-OHBzCOO	-1030mV		
Cu <sub>5</sub> (SAL-DPL.PAB.SAL) <sub>2</sub> .3H <sub>2</sub> O	-980mV	-1180mV	-1410mV
Cu <sub>5</sub> (SAL-DPL.4ABA.SAL) <sub>2</sub> .2H <sub>2</sub> O	-1035mV		
Cu <sub>5</sub> (ESAL-DPL.6AIESAL) <sub>2</sub> .2H <sub>2</sub> O	-830mV	-935mV	

**Table 9.3:** Compiled Dropping Mercury Differential Pulse Voltammetry Reduction Potentials

<u>Compound</u>	<u>Peak 1</u>	<u>Peak 2</u>
Cu(SAL-DPLH)	-1420mV	
Cu <sub>2</sub> (SAL-DPL)OH.3H <sub>2</sub> O	-1260mV	
Cu <sub>2</sub> (SAL-DPE)OH	-1135mV	
Cu <sub>2</sub> (SAL-DPL)(CAT) <sub>0.5</sub> .(H <sub>2</sub> O) <sub>0.5</sub>	-1430mV	
Cu <sub>2</sub> (SAL-DPE)CATH	-1310mV(sh)	-1500mV
Cu <sub>2</sub> (SAL-DPL)Pz	-1400mV	
Cu <sub>2</sub> (SAL-DPE)Pz	-1300mV	-1520mV
Cu <sub>2</sub> (SAL-DPL)PyO.(H <sub>2</sub> O) <sub>0.5</sub>	-1250mV	-1330mV
Cu <sub>2</sub> (SAL-DPL)4-OHBzCOO	-1230mV	
Cu <sub>5</sub> (SAL-DPL.PAB.SAL) <sub>2</sub> .3H <sub>2</sub> O	-970mV	-1410mV
Cu <sub>5</sub> (SAL-DPL.4ABA.SAL) <sub>2</sub> .2H <sub>2</sub> O	-1405mV	
Cu <sub>5</sub> (ESAL-DPL.6AIESAL) <sub>2</sub> .2H <sub>2</sub> O	-1000mV	-1265mV

**Table 9.4:** Compiled Glassy Carbon Differential Pulse Voltammetry Reduction Potentials

<u>Compound</u>	<u>Scan 1 Reduction</u>	<u>Scan 5 Reduction</u>
Cu(SAL-DPLH)	-1490mV	-1490mV
Cu <sub>2</sub> (SAL-DPL)OH.3H <sub>2</sub> O	-1340mV	-1075mV
	-1430mV	—
Cu <sub>2</sub> (SAL-DPE)OH	-1230mV	—
Cu <sub>2</sub> (SAL-DPL)(CAT) <sub>0.5</sub> .(H <sub>2</sub> O) <sub>0.5</sub>	-1530mV	-1550mV
Cu <sub>2</sub> (SAL-DPE)CATH	-1600mV	-1600mV
	-1670mV	-1665mV
Cu <sub>2</sub> (SAL-DPL)Pz	-1475mV	-1480mV
Cu <sub>2</sub> (SAL-DPE)Pz	-1355mV	-1365mV
	-1600mV	-1600mV
Cu <sub>2</sub> (SAL-DPL)PyO.(H <sub>2</sub> O) <sub>0.5</sub>	-1350mV	-1000mV
	-1430mV	—
Cu <sub>2</sub> (SAL-DPL)4-OHBzCOO	-1230mV	-1000mV
	-1300mV	-1400mV
Cu <sub>5</sub> (SAL-DPL.PAB.SAL) <sub>2</sub> .3H <sub>2</sub> O	-1065mV	-1080mV
	-1510mV	-1505mV
Cu <sub>5</sub> (SAL-DPL.4ABA.SAL) <sub>2</sub> .2H <sub>2</sub> O	-1010mV	-1010mV
	-1450mV	-1450mV
Cu <sub>5</sub> (ESAL-DPL.6AIESAL) <sub>2</sub> .2H <sub>2</sub> O	-1380mV	-875mV
	—	-1385mV

Table 9.5: Compiled Glassy Carbon Cyclic Voltammetry Reduction Potentials

**10:**  
**Other Work**



## 10: Other Work

Attempts were made to synthesise dioxygen bridged copper complexes using electrochemical methods. This involved passing an electric charge through an inert solvent (preferably DMF) using a copper plate (99.9%) electrode and a platinum electrode. The solution contained the Schiff base ligand (SAL-DPLH<sub>3</sub>). A green compound was isolated that exhibited in the reaction solution (before precipitation) a copper d-d transition in the 500-700nm region (Figs 10.1 and 10.2 and Tables 10.2 and 10.3). Figure 10.1 displays how absorbance increases with time in the 600 to 700nm region while Table 10.2 gives the specific absorbance and the peak position with time. Figure 10.2 displays the formation of the copper d-d transition for selected compounds and Table 10.3 gives the relevant data. Two copper atoms were reduced per mole of Schiff base. This was determined by measuring the weight loss of the copper electrode compared to the weight gain of the platinum electrode. Microanalyses on the solid product were unsatisfactory (Table 10.1) and did not indicate formation of complexes of the formula Cu<sub>2</sub>(SAL-DPL)O<sub>2</sub>. The exact nature of the complexes formed have not yet been determined.

An attempt was made to investigate any catalytic activity of the copper complexes on the oxidation of catechols, this activity being distinctive of Tyrosinase. This was done by dissolving a binuclear copper complex in DMF and adding catechol plus aniline. The aniline was added to prevent polymerization of any quinone formed. This occurs by the aniline binding to the quinone (Fig 10.3). Although the solution changed colour with time TLC's comparing the product with a reference compound showed no formation of the relevant oxidised quinone.

Lack of time prevented further studies in these two areas of work.

$\text{Cu}_2(\text{SAL-DPL})\text{O}_2$	%C	%H	%N
C	44.94	3.33	6.16
F	43.14	4.76	5.14
$\text{Cu}_2(5\text{-MeSAL-DPL})\text{O}_2$			
C	47.30	3.97	5.81
F	44.76	4.68	4.89
$\text{Cu}_2(\text{SAL-DL})\text{SAL}$			
C	53.04	3.71	5.15
F	48.51	6.66	4.96

Table 10.1: Empirical Data of Electrically Synthesised Complexes

	Time	Abs	nm
$\text{Cu}_2(\text{SAL-DPL})\text{O}_2$	30	0.06	612
	60	0.12	612
	120	0.32	614
	300	0.46	614
$\text{Cu}_2(5\text{-MeSAL-DPL})\text{O}_2$	30	0.16	612
	60	0.22	624
	120	0.35	628
	240	0.58	628
$\text{Cu}_2(\text{SAL-DPL})\text{SAL}$	30	0.11	622
	60	0.12	627
	120	0.15	640
	240	0.16	650

Table 10.2: Time, Absorbance and Wavelength Data

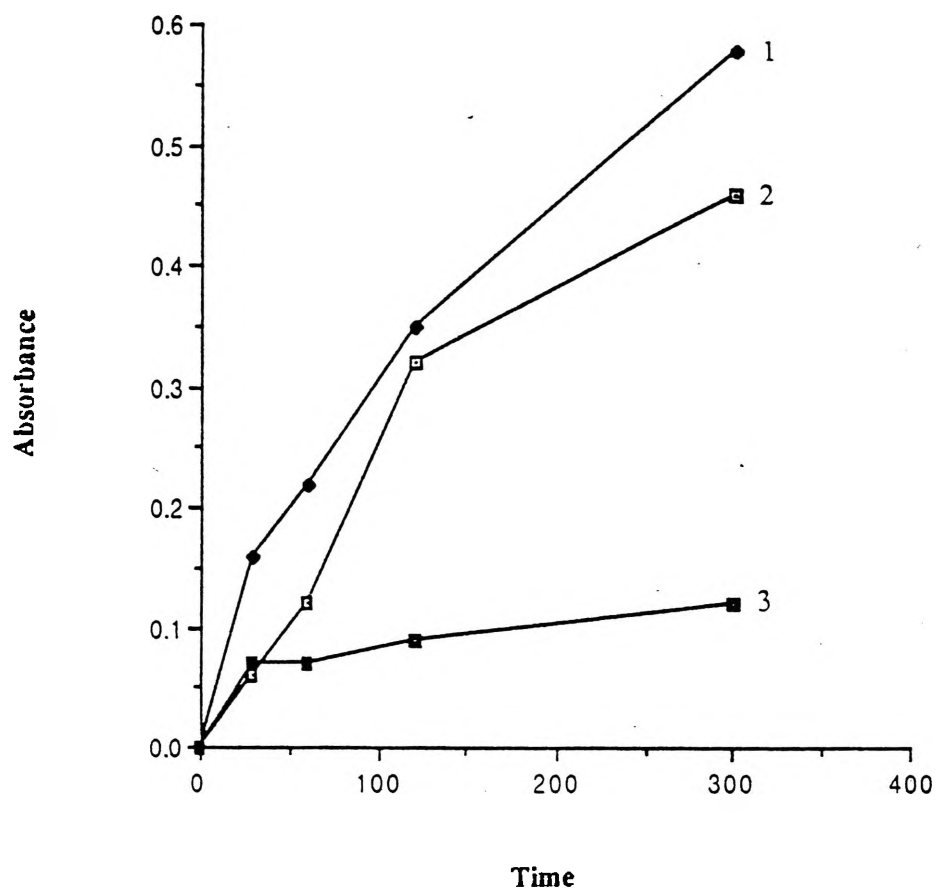


Fig 10.1: Time vs Absorbance in the 600-700nm Region

1 =  $\text{Cu}_2(\text{SAL-DPL})\text{O}_2$

2 =  $\text{Cu}_2(5\text{-MeSAL-DPL})\text{O}_2$

3 =  $\text{Cu}_2(\text{SAL-DPL})\text{SAL}$

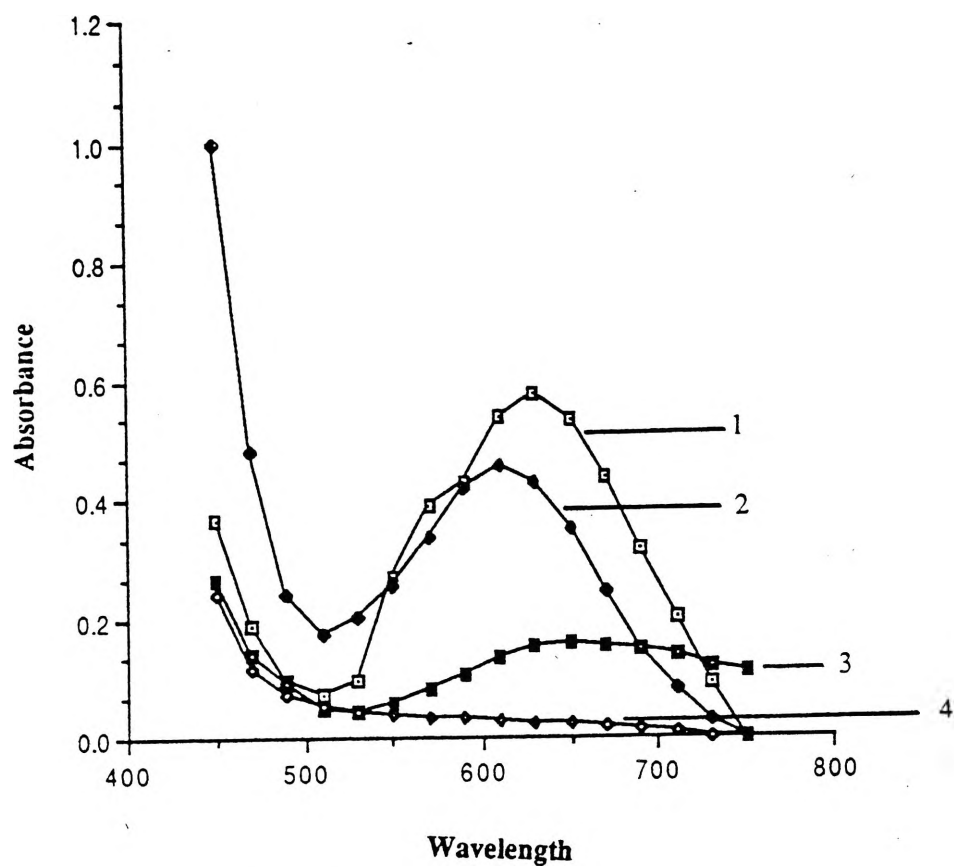


Fig 10.2: Change in Absorbance from Initial to Final Spectra for Selected Complexes

1 =  $\text{Cu}_2(\text{SAL-DPL})\text{O}_2$

2 =  $\text{Cu}_2(5\text{-MeSAL-DPL})\text{O}_2$

3 =  $\text{Cu}_2(\text{SAL-DPL})\text{SAL}$

4 =  $\text{SAL-DPLH}_3$

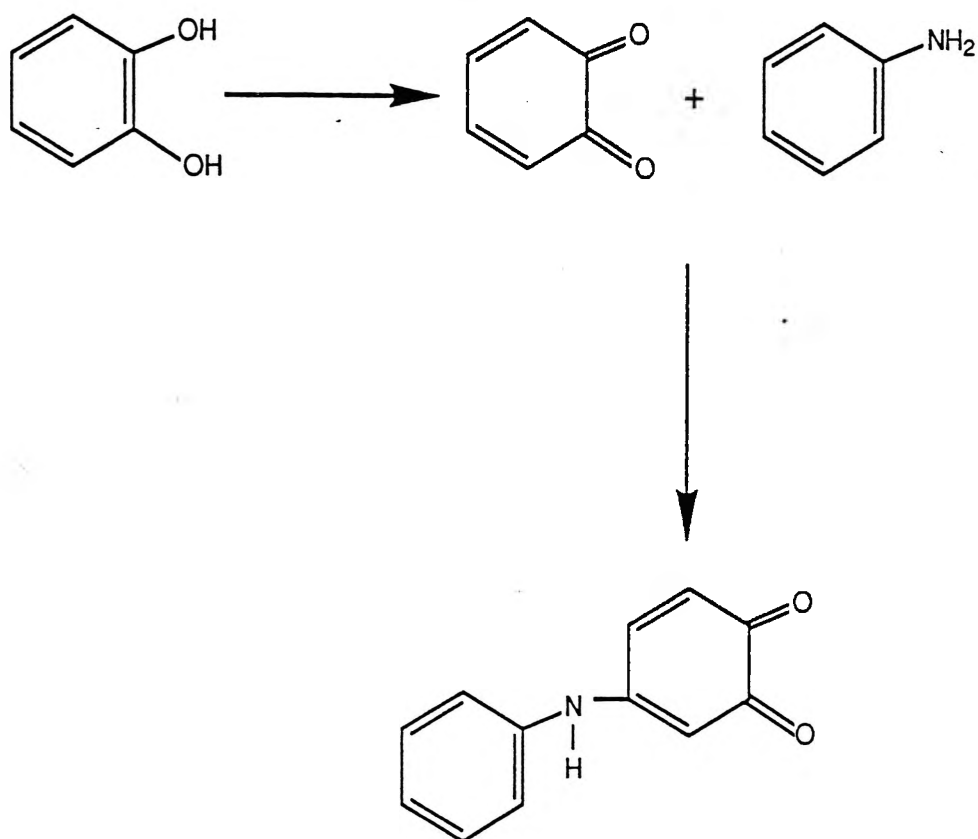


**Fig 10.3:** Catechol to Quinone Reaction with Aniline to Stop Polymerization

$\lambda$ (nm)	$\text{Cu}_2(\text{SAL-DPL})\text{O}_2$	$\text{Cu}_2(5\text{-MeSAL-DPL})\text{O}_2$	$\text{Cu}_2(\text{SAL-DPL})\text{SAL}$	$\text{SAL-DPLH}_3$
750	0	0	0.11	0
730	0.09	0.03	0.12	0
710	0.2	0.08	0.14	0.01
690	0.32	0.15	0.15	0.015
670	0.44	0.245	0.155	0.02
650	0.535	0.35	0.16	0.022
630	0.577	0.43	0.155	0.025
610	0.54	0.46	0.135	0.03
590	0.43	0.42	0.105	0.032
570	0.39	0.335	0.08	0.035
550	0.27	0.255	0.06	0.041
510	0.07	0.175	0.05	0.055
490	0.095	0.24	0.09	0.07
470	0.19	0.48	0.14	0.115
450	0.365	1.00	0.265	0.242

Table 10.3: Initial And Final Data of Wavelength vs Absorbance

**11:**  
**Conclusion**

## 11: Conclusion

The first aim of the project was to synthesise and study catechol bridged binuclear copper complexes. To this end a number of such compounds were synthesised using SAL-DPLH<sub>3</sub> and SAL-DPEH<sub>3</sub> schiff base ligands. These complexes were exogenously bridged by either catechol or substituted catechols. It was found that the SAL-DPLH<sub>3</sub> complexes bridged only half a catechol group each, i.e. one catechol group per four copper atoms. The SAL-DPEH<sub>3</sub> ligand complexes were found to bridge one catechol group each, i.e. one catechol group per two copper atoms. These SAL-DPEH<sub>3</sub> complexes are better models of Tyrosinase as they have the same ratio of copper atoms to catechols as proposed for the protein.

It is proposed, based on molecular models of these complexes, that the catechol in the SAL-DPLH<sub>3</sub> complexes is bridged in a -1,1- fashion while in SAL-DPEH<sub>3</sub> it is bridged in a -1,2-fashion. This method of bridging is supported by the magnetic studies with the SAL-DPEH<sub>3</sub> complexes being basically diamagnetic at room temperature, as found for Tyrosinase, while the SAL-DPLH<sub>3</sub> complexes have much weaker magnetic interaction.

Suitable crystals for X-ray crystallography were not able to be grown due to the complexes oxidising the catechol when recrystallization was attempted. Similar binuclear complexes, which did give suitable crystals were found to have a copper-copper separation of  $\sim 3.3$  to  $3.5\text{\AA}$  and it is proposed that the catechol bridged complexes have a similar copper-copper separation. It may be possible to grow crystals in an inert atmosphere but there was insufficient time to attempt this.



Overall the SAL-DPEH<sub>3</sub> ligand complexes are better models of Tyrosinase due to the copper to catechol ratio of 2:1 and being diamagnetic at room temperature. All the complexes are interesting as they are the first stable catechol bridged binuclear copper (II) complexes synthesised by reacting catechol with the binuclear copper (II) complex.

The electrochemistry investigation gave an unexpected result when it was found that, in all cases, the copper was reduced to copper metal instead of to the expected copper (I). All the complexes are found to undergo redox processes at negative potentials. Cu(SAL-DPLH) was found to undergo a one step reduction. All the binuclear complexes undergo a two step reduction and the pentanuclear complexes were found to be reduced in either two or three steps. All the complexes were found to be reduced either quasi-reversibly or irreversibly.

Therefore the complexes do not accurately mimic the eletrochemistry of Tyrosinase or the multi-copper oxidases, although they do provide some important insights into previous studies of model compounds. The most important being that all available electrochemical techniques should be used in these studies instead of just running cyclic voltammetry, as most previous workers have done. This is not adequate as the technique fails to tell you exactly how many electrons are transferred and in how many steps. It was only after conducting coulometry measurements that we found that the copper was reduced to the copper metal and not to copper (I) as we and others had previously believed.

Also, the total exclusion of oxygen is very important otherwise peaks due to the presence of oxygen can be mistaken for a copper reduction process.

In summary, a series of binuclear copper complexes were synthesised and studied and provided an additional insight into the structure and function of the copper site of Tyrosinase.

**12:**  
**Experimental**

## 12: Experimental

### 12.1 Synthesis of 1,5-Diamino-3-Pentanol (DPE)

The synthesis consists of three steps:

#### 1) Synthesis of 1,5-dichloro-3-pentanone:<sup>183</sup>

3-Chloropropionyl chloride (250g, 1.97 mol) was added slowly over 1 hour to a stirred suspension of aluminium chloride (367.5g, 2.76 mol) in dichloromethane (300 mL) in a three necked flask (1L) in an ice water bath. Ethylene gas (dried over KOH and CaSO<sub>4</sub>) was bubbled through the reaction mixture, which was allowed to warm to and was held at 20°C, for four hours. The resulting mixture was then added slowly with stirring to dichloromethane (500mL), 2Kg of ice and enough 10M HCl to give a 1M solution of HCl. The temperature was not allowed to rise above 20°C. The organic layer was separated and was washed with water (3 x 2L) and dried with MgSO<sub>4</sub> (anhydrous). The solvent was removed on a rotary evaporator to give 274g of 1,5-dichloro-3-pentanone (90% yield) as a brown oil (Fig 12.1).

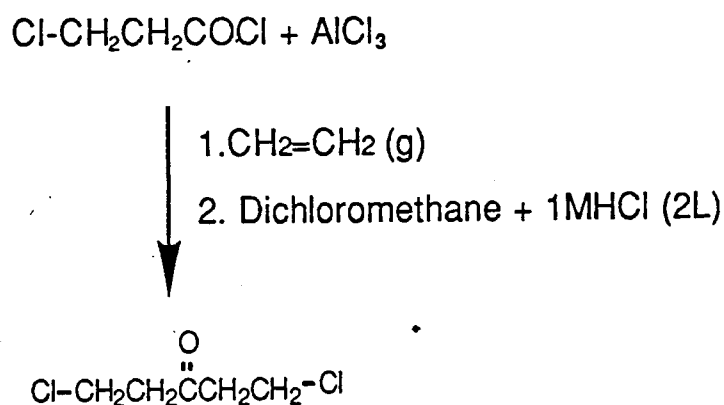


**Fig 12.1:** Dichloropentanone Pathway

2) Synthesis of 1,5-diamino-3-pentanone.dihydrochloride:184

Potassium phthalimide (422.4g, 2.28 mol) was suspended in 1.5L of dry DMF. Crude 1,5-dichloro-3-pentanone (274g) was added slowly over 1 hour with stirring. The mixture was then heated at 80-85°C for 6 hours and allowed to stand overnight at room temperature. The white powder was collected by filtration and washed successively with chloroform, water and acetone. The yield was 336g (75%) (Fig 12.2).

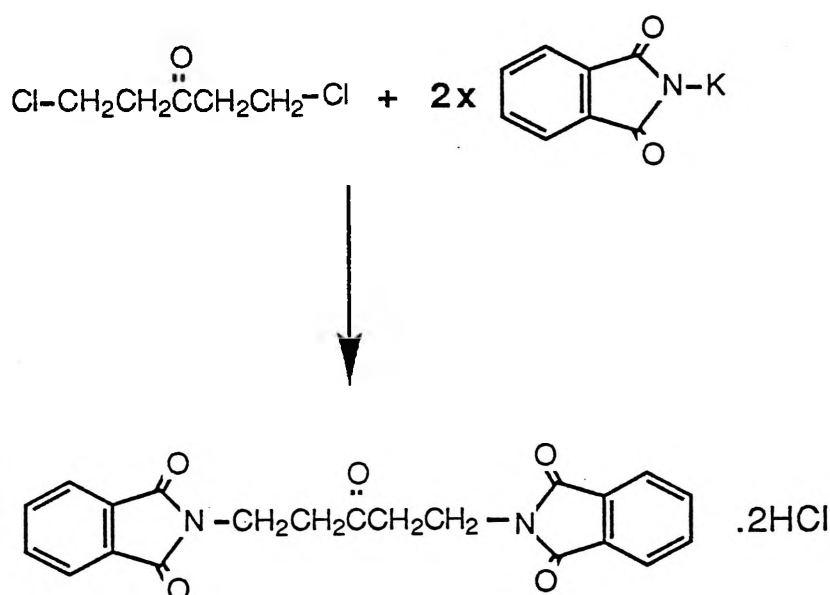


Fig 12.2: Diphthalimidopentanone Pathway

The crude 1,5-diphthalimido-3-pentanone.dihydrochloride was refluxed with 460mL of glacial acetic acid and 300mL 10M HCl for seven days. Every 10 hours a further 33mL of 10M HCl was added up to a total of 165mL. On cooling phthalic acid precipitated and was removed by filtration. The solvent was removed by rotary evaporation and the residue washed with water. The water was removed by rotary evaporation and approximately 2 litres of ethanol was added. The product precipitated on standing. The yield was 146g (95%) as a cream solid of MP 190-192°C (Fig 12.3).

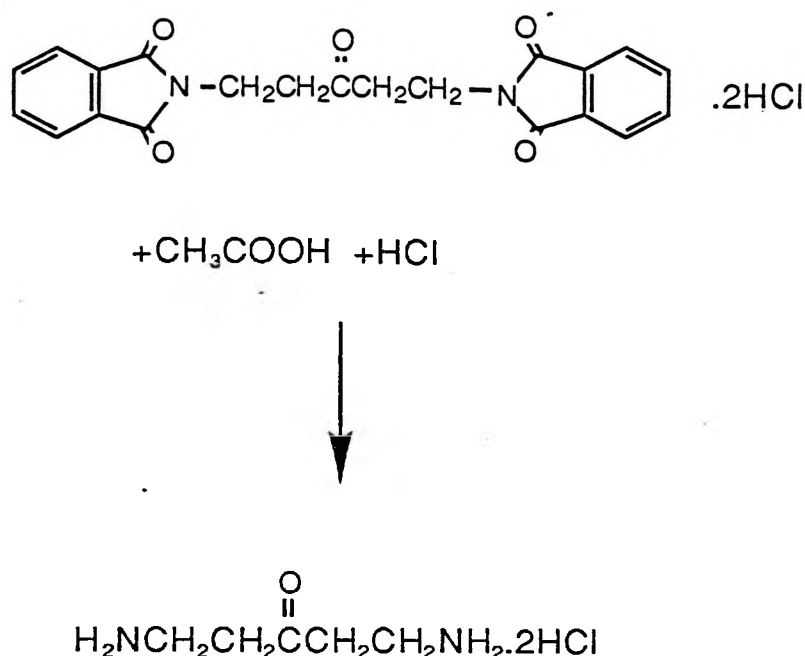


Fig 12.3: Diaminopentanone Pathway

### 3) Synthesis of 1,5-diamino-3-pentanone.dihydrochloride:<sup>184</sup>

Crude 1,5-diamino-3-pentanone.dihydrochloride (40g, 0.21 mol) was added in portions, keeping the temperature below 20°C, to a solution of 17g (0.4 mol) sodium hydroxide and 8g (0.2 mol) sodium borohydride in 300mL water. The solution was stirred at room temperature for 48 hours and then dilute HCl was added carefully to the cooled solution until a pH of 1 was achieved. The solution was rotary evaporated and washed with 200mL methanol which was then rotary evaporated off. This was repeated several times to remove boric acid. The final residue was boiled in 500mL of methanol and filtered to remove sodium chloride and the filtrate concentrated to a small volume. A large amount of ether was added (approximately 400mL) and the solution was kept in a freezer overnight. The product was filtered off, washed with ether and stored in a dessicator. The yield was 22g (80%) with a MP of 154-156°C (crude) (Fig 12.4).

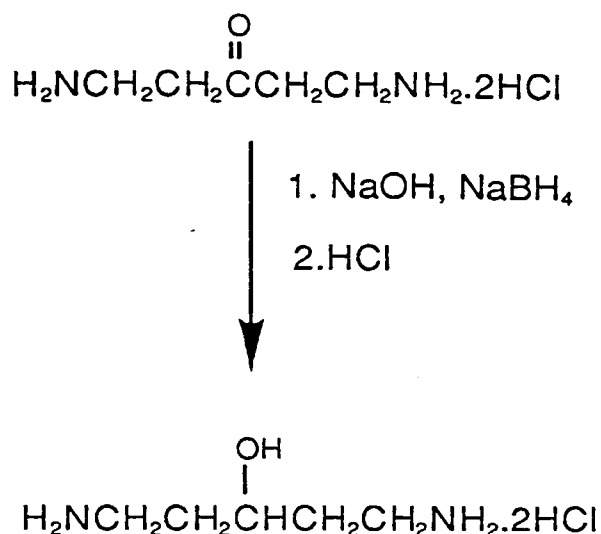


Fig 12.4: Diaminopentanol Pathway

### 12.2 Synthesis of 4,5'-dimethyl-2-hydroxybenzophenone (M<sup>2</sup>BP)

A mixture of 42g (0.31 mol) aluminium chloride, 48.5g (0.31 mol) of p-toluychloride and 35g (0.32 mol) p-cresol was heated at 160-180°C for 40 minutes. This mixture was cooled to room temperature and 400mL of 5% HCl added. The solution was decanted and the product washed with water (2 x 200mL). The product was then dissolved in 1L of hot methanol and filtered. The solution was reduced to 400mL and cooled. The yellow product crystallised out upon standing. The crystals were recrystallized from hot methanol and charcoal. The yellow crystals were filtered off and washed with 40-60°C b.p. petroleum spirits. The yield was 37.3g (55%) (Fig 12.5).

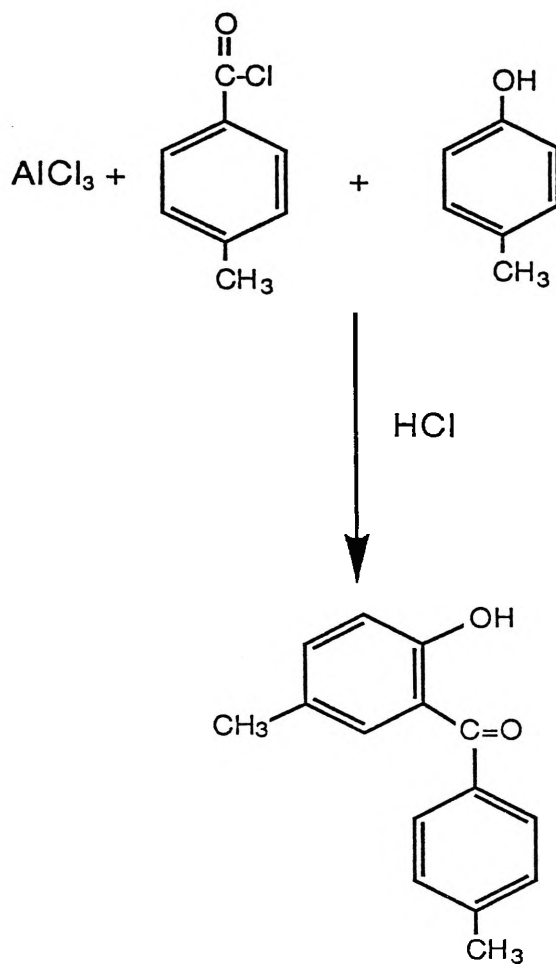
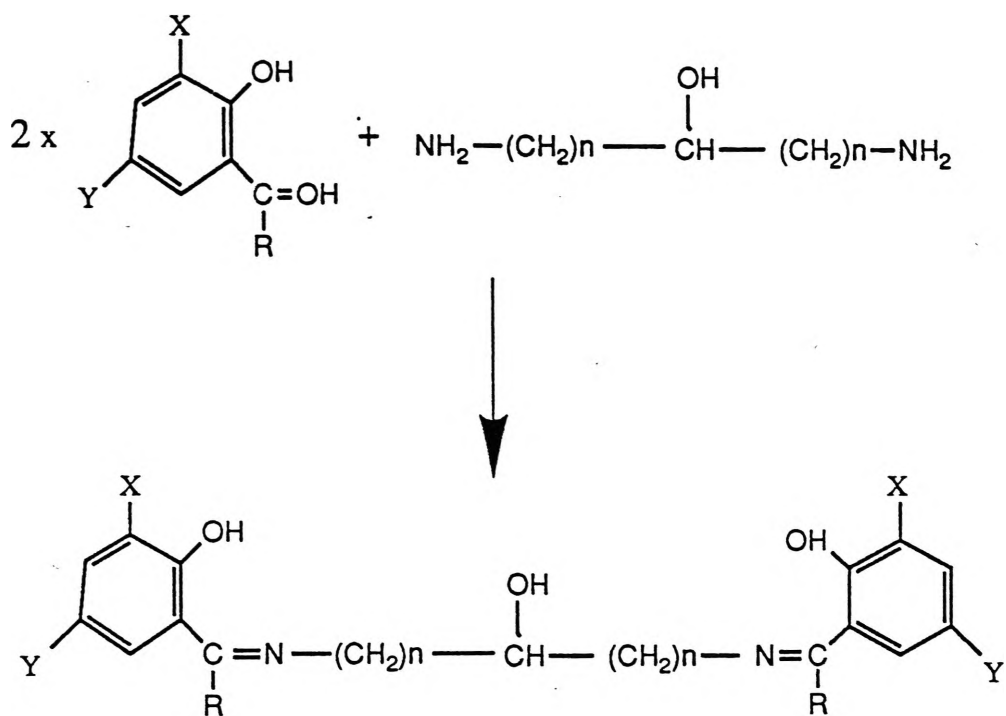


Fig 12.5: 4,5'-Dimethyl-2-hydroxybenzophenone Pathway

### 11.3 Synthesis of the Schiff Base Ligand

The ligand was prepared by dissolving 2 molar equivalents of the appropriate salicylaldehyde or 4,5'-dimethyl-2-hydroxybenzophenone in methanol (500mL) with either 1,3-diamino-2-propanol (DPL) or 1,5-diamino-3-pentanone (DPE).dihydrochloride. The solution was refluxed for 30 minutes and then cooled to room temperature. The ligand precipitated on standing, was filtered off and recrystallized from hot methanol and charcoal (Fig 12.6).



X= H, Y= H, R= H, n= 1	SAL-DPL
X= H, Y= H, R= H, n= 2	SAL-DPE
X= 3-OC <sub>2</sub> H <sub>5</sub> , Y= H, R= H, n= 1	ESAL-DPL
X= 3-OC <sub>2</sub> H <sub>5</sub> , Y= H, R= H, n= 2	ESAL-DPE
X= H, Y= CH <sub>3</sub> , R= p-CH <sub>3</sub> -C <sub>6</sub> H <sub>4</sub> , n= 1	M <sup>2</sup> BP-DPL
X= H, Y= CH <sub>3</sub> , R= p-CH <sub>3</sub> -C <sub>6</sub> H <sub>4</sub> , n= 2	M <sup>2</sup> BP-DPE

Fig 12.6: Schiff Base Ligand Synthesis



#### 12.4 Synthesis of Cu(XSAL)<sub>2</sub>

One molar equivalent of copper(II) acetate.hydrate was dissolved in hot water and filtered. To this solution was added two molar equivalents of XSALH in hot methanol. The brown product precipitated immediately, was filtered off and washed with 40-60°C B.P. petroleum spirits and then dried (Fig 12.7).

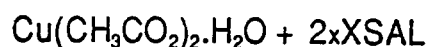


Fig 12.7: Copper Salicylaldehyde Synthesis

##### 12.5.1 Synthesis of Binuclear Copper(II) Complexes of the DPL Schiff Base Ligand

The complexes were formed by refluxing 1 molar equivalent of ligand, 2 molar equivalent of either copper(II)acetate.hydrate (CuAc.H<sub>2</sub>O) or Cu(XSAL)<sub>2</sub> and the exogenous bridging group (1 molar equivalent) in methanol with 1-2ml of piperidine for 30 minutes. The solution was cooled to room temperature and the crude product filtered off. The complex was then recrystallised from acetonitrile, dichloromethane or DMF (Fig 12.8).

##### 12.5.2 Synthesis of Binuclear Copper Complexes of the DPE Schiff Base Ligand

The procedure was the same as for DPL except that the solvent methanol was replaced by acetonitrile (Fig 12.8). If methanol was used as solvent, the hydroxy bridged binuclear complex was always obtained despite the presence of the bridging group in solution.

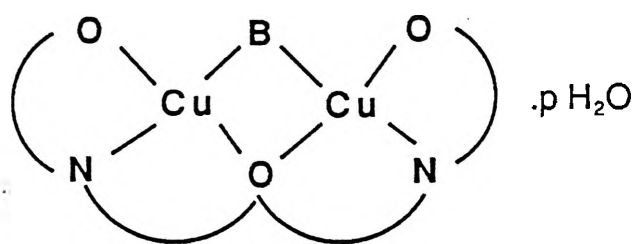
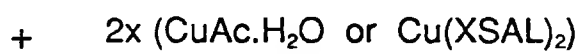
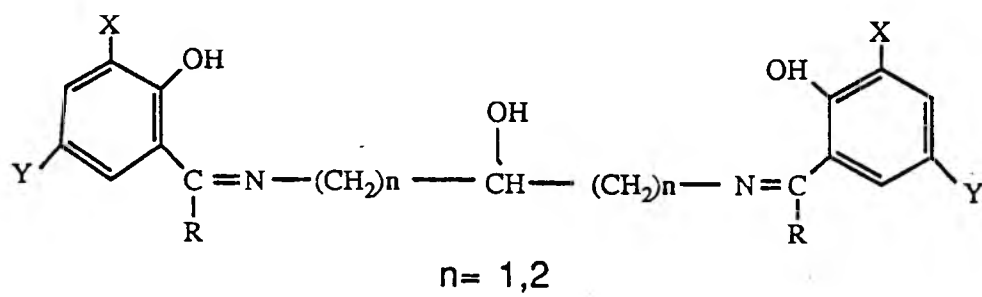


Fig 12.8: Binuclear Copper (II) Complex Synthesis

## 12.6 Synthesis of the Pentanuclear Copper Complexes

### 12.6.1 Pentanuclear Complexes not containing the 6-aminoindazole bridge:

Five molar equivalents of  $\text{Cu}(\text{XSAL})_2$  were refluxed with 2.1 molar equivalents of the ligand and 2.1 molar equivalents of the bridging group (B) in methanol with piperidine (1-2ml) for 2 hours. The hot solution was filtered and the product precipitated on standing. The products were recrystallised from DMF (Fig 12.9).

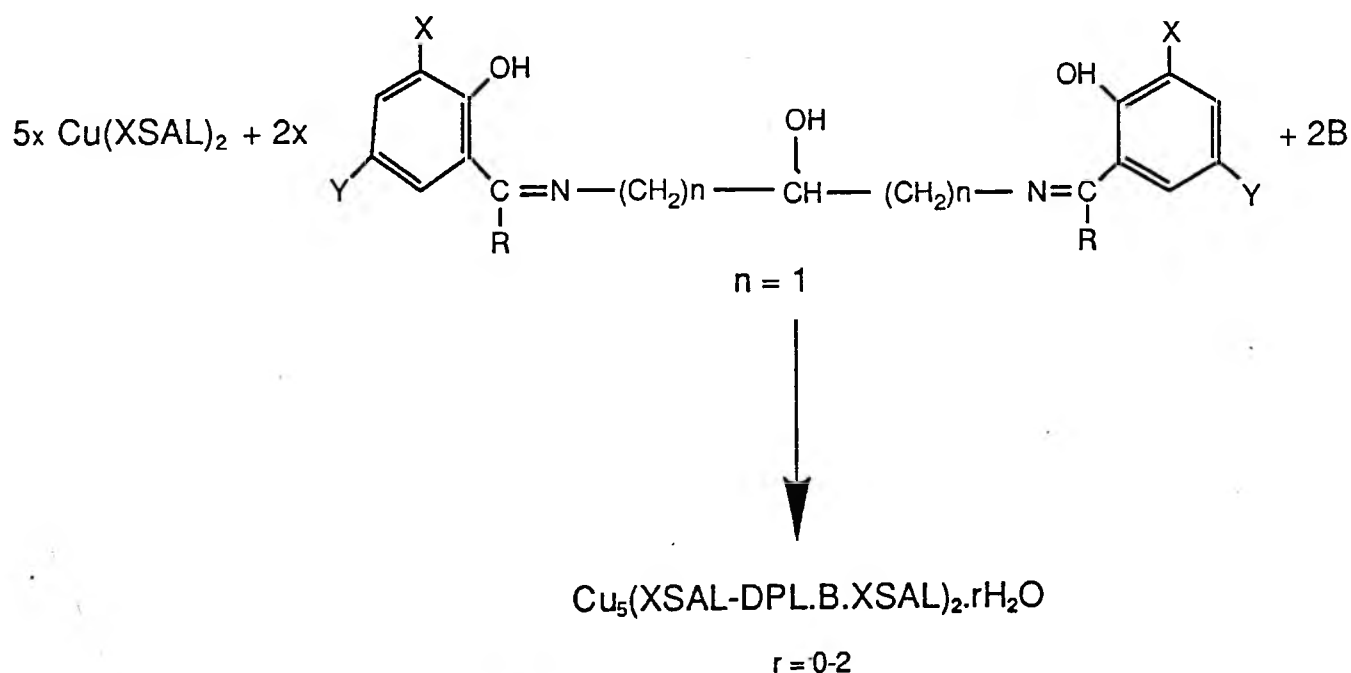


Fig 12.9: Pentanuclear Copper (II) Complex Synthesis (no 6-aminoindazole)

### 12.6.2 Pentanuclear Complexes Containing 6-aminoindazole:

XSAL-DPLH<sub>3</sub> (1 molar equivalent) was dissolved in hot methanol (25mL) and piperidine (1-2mL). To this was added 6-aminoindazole (1 molar equivalent) dissolved in hot methanol (25mL). When the combined solution was added to Cu(BF<sub>4</sub>)<sub>2</sub>.6H<sub>2</sub>O (2 molar equivalents) dissolved in hot methanol (50mL) initially a green powder precipitated which changed to a purple powder on standing and analysed as Cu<sub>2</sub>(XSAL-DPL)6AI.

Cu<sub>2</sub>(XSAL-DPL)6AI (2 molar equivalents) was then refluxed with Cu(XSAL)<sub>2</sub> (1 molar equivalent) in DMF (100mL) plus piperidine (1-2mL) for one hour. The solution was filtered and Cu<sub>5</sub>(XSAL-DPL.6AI.XSAL)<sub>2</sub> precipitated on cooling to room temperature and was recrystallized from DMF (Fig 12.10).

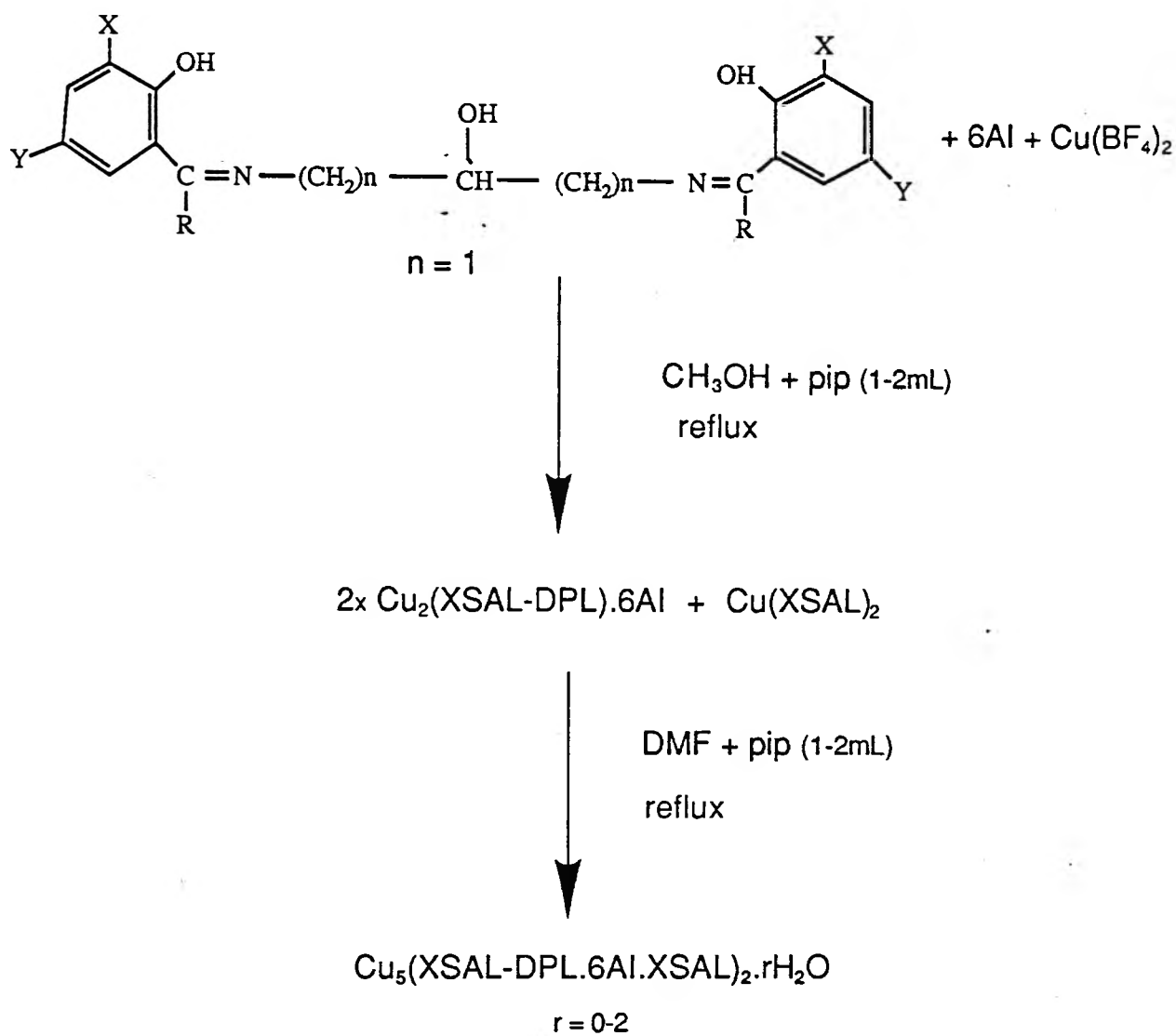


Fig 12.10: 6-aminoindazole Pentanuclear Copper (II) Complex Synthesis

### 11.7 Microanalyses

Carbon, hydrogen and nitrogen analyses were measured at the Microanalytical Laboratory, the Research School of Chemistry, Australian National University and Chemical and Microanalytical Services (CMAS), North Essendon, Victoria.

### 12.8 Infra-red Spectroscopy

Infra-red spectra were recorded as Nujol mulls on sodium chloride cells on a Perkins Elmer 283B recording spectrophotometer.

FTIR spectra were recorded as Potassium bromide disks on a BIO-RAD FTS 60 in the Environmental Science Section, ANSTO, Lucas Heights.

### 12.9 UV-Visible Spectroscopy

Solid state spectra were run on either a Cary 17 UV-Visible-Near IR recording spectrophotometer or a Shimadzu UV-265 recording spectrophotometer as Nujol mulls on filter paper.

Solution spectra were run on Cary 17 UV-Visible-Near IR recording spectrophotometer or a Shimadzu UV-265 recording spectrophotometer as  $1 \times 10^{-3}$ - $1 \times 10^{-4}$ M solutions in DMF and dichloromethane.

### 12.10 Magnetism

Room temperature magnetic moments were carried out using the Gouy method with copper sulphate pentahydrate as calibrant. Variable temperature magnetic moments between 80-300K were measured with an apparatus similar to that described by Figgis and Nyholm.<sup>185</sup>

### 12.11 Mass Spectroscopy

F.A.B. mass spectra were run on a VG Analytical MM12-12 mass spectrometer.

### 12.12 Thermogravimetry

Thermogravimetry measurements were carried out on a Rigaku Thermogravimetric Balance, referenced to aluminium oxide in aluminium crucibles.

### 12.13 Crystal Structure

Crystal structures were solved at Howard University, Washington, D.C., U.S.A. by Dr Ray Butcher and at the University of Virginia, Charlottesville, Virginia, U.S.A. by Dr Ekk Sinn.

### 12.14 Electrochemistry

Cyclic voltammetry and differential pulse voltammetry studies were conducted at room temperature or low temperature in freshly distilled and dried DMF. The DMF was distilled under dry nitrogen and was collected and stored over molecular sieve 3A, in the dark and used within 24 hours. The concentration was  $1 \times 10^{-3} \text{M}$  (with 0.1M tetraethylammonium perchlorate or 0.1M tetrabutylammonium perchlorate as supporting electrolyte) under  $\text{O}_2$ -free conditions using a BAS 100A Electrochemical Analyzer. A three electrode system was used with a working electrode of glassy carbon, a counter electrode of platinum gauze and  $\text{Ag}/\text{Ag}^+$  reference electrode. The scan rate was 100 mV/sec for CV and 10 mV/sec for DPV measurements over a range of -3.0V to 0.0V. The same system was used for platinum electrode experiments with varying scan rates. The hanging mercury electrode drop cyclic voltammogram experiments were conducted using an EG&G Model 303 SMDE connected to a Par Model 174 Polarographic Analyser with a Bas X-Y or Omni X-Y chart recorder using either platinum gauze or platinum wire.

Coulometry experiments were conducted on a CV27 voltammograph connected to an ICI Instruments DP-600 chart recorder, using freshly distilled, dried DMF ( $1 \times 10^{-4} \text{M}$ ) with same supporting electrolyte as for CV-DPV measurements (0.1M) plus hydrazine. Hydrazine is used as an anionic depolarizer to prevent unwanted secondary reactions around the platinum gauze electrode giving a sharp end point.

A two cell system was used consisting of a mercury pool working electrode, platinum gauze counter electrode in the second cell connected by a glass bridge with sintered glass membranes at each end, and a  $\text{Ag}/\text{Ag}^+$  reference electrode (Fig 12.11). The copper solution was stirred continuously.

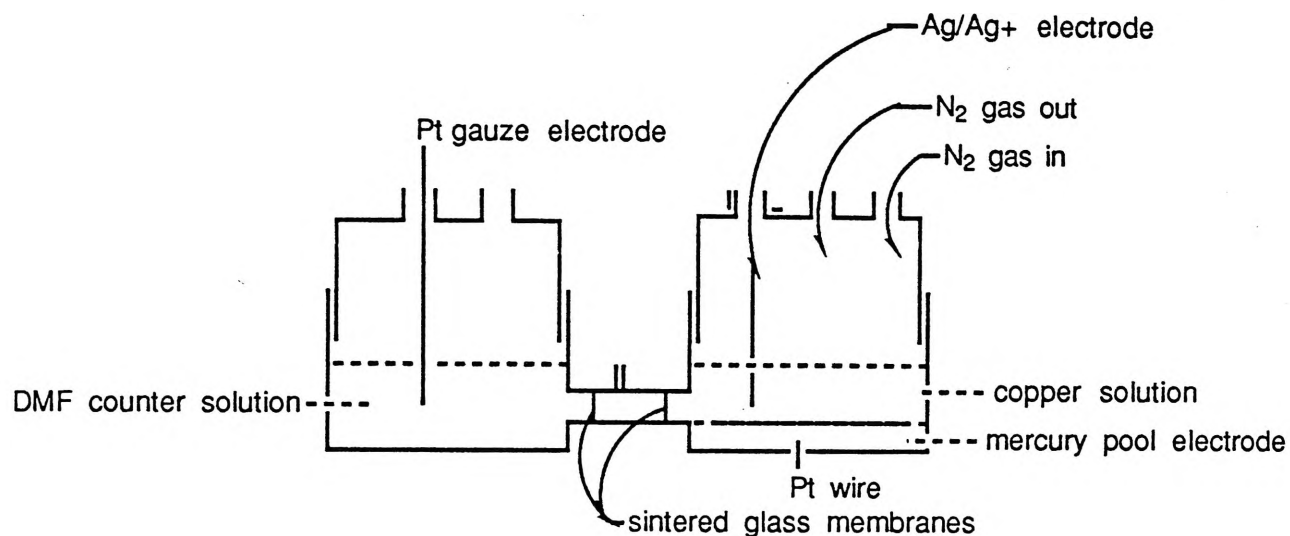
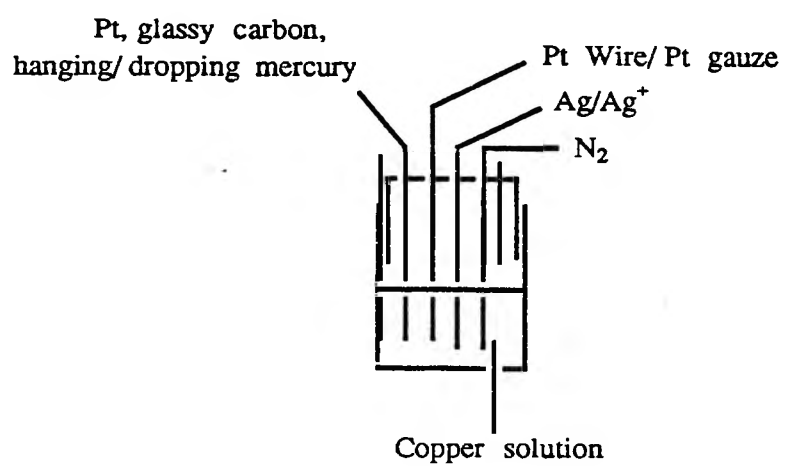


Fig 12.11: Coulometry Cell Set-up

Polarographic measurements were conducted on either a PAR Model 174 Polarographic Analyser connected to an Omnigraphic 2000 X-Y recorder or a BAS X-Y chart recorder. The cell consisted of a single cell with tight fitting lid, with a three electrode system (Fig 12.12) consisting of a dropping mercury electrode,  $\text{Ag}-\text{Ag}^+$  reference electrode and platinum gauze. The scan rate was  $10\text{mV/s}$  and drop time of 1 drop/s with the other conditions as usual.





**Fig 12.12:** Polarography, Differential Pulse Voltammetry and Cyclic Voltammetry Cell Set-up

**13:**  
**Appendix**

13.1: "Cu<sub>2</sub>(SAL-DPL)NH<sub>2</sub>O.H<sub>2</sub>O"

Space Group P21/C

Unit Cell Dimensions  $a = 15.468(6)\text{\AA}$ ,  $b = 16.573(6)\text{\AA}$ ,  $c = 6.905(3)$ Vol =  $1768\text{\AA}^3$ 

Empirical Formula	Cu	O	N	C	H
	26.90	16.93	8.89	43.22	4.05

Formula Weight 472

 $Z = 4$ ,  $D_{\text{calc}} = 1.774$ , Abs Coeff = 24.457

## 13.1.1: Table of General Temperature Expressions- U's

Name	U(1,1)	U(2,2)	U(3,3)	U(1,2)	U(1,3)	U(2,3)
Cu1	0.0342(4)	0.0329(3)	0.0340(4)	0.0024(3)	0.0012(3)	0.0037(4)
Cu2	0.0327(4)	0.0347(3)	0.0337(4)	0.0024(3)	0.0019(3)	0.0013(4)
O(W)	0.064(3)	0.046(2)	0.036(3)	0.006(2)	0.004(2)	-0.008(2)
O11	0.031(2)	0.037(2)	0.060(3)	0.001(2)	0.001(2)	0.004(2)
O12	0.038(3)	0.034(2)	0.071(3)	0.003(2)	0.017(2)	0.009(2)
O21	0.033(2)	0.040(2)	0.040(3)	0.005(2)	0.004(2)	0.006(2)
O22	0.034(2)	0.033(2)	0.046(3)	0.003(2)	0.004(2)	0.002(2)
N11	0.034(3)	0.042(3)	0.038(3)	0.003(2)	-0.003(3)	0.002(2)
N12	0.049(3)	0.036(2)	0.054(4)	0.003(3)	0.007(3)	0.003(3)
N21	0.034(3)	0.031(2)	0.037(3)	0.003(2)	0.001(2)	-0.003(2)
C11	0.029(3)	0.050(3)	0.040(4)	0.001(3)	0.001(2)	-0.002(3)
C12	0.032(3)	0.040(3)	0.042(4)	0.005(3)	0.004(3)	0.002(3)
C13	0.034(4)	0.049(3)	0.069(5)	0.002(3)	0.004(3)	-0.005(4)
C14	0.050(4)	0.051(4)	0.096(6)	0.017(4)	0.007(5)	0.004(4)
C15	0.039(4)	0.067(4)	0.079(6)	0.014(4)	0.003(4)	0.006(4)
C16	0.033(4)	0.055(4)	0.068(5)	-0.001(3)	0.004(4)	0.006(4)
C17	0.033(3)	0.055(3)	0.37(4)	-0.010(3)	-0.002(3)	0.004(3)
C18	0.045(4)	0.040(3)	0.048(4)	-0.004(3)	-0.000(4)	-0.005(2)
C19	0.044(4)	0.046(3)	0.115(7)	-0.001(3)	0.014(5)	0.022(4)
C21	0.032(3)	0.043(3)	0.017(3)	-0.003(3)	-0.000(3)	-0.003(3)
C22	0.038(4)	0.039(3)	0.029(3)	0.003(3)	0.004(3)	0.001(3)
C23	0.043(4)	0.044(3)	0.052(4)	0.012(3)	0.004(4)	0.006(3)
C24	0.038(4)	0.068(4)	0.040(4)	0.006(4)	0.002(3)	-0.001(4)
C25	0.037(4)	0.070(4)	0.049(4)	-0.005(4)	0.008(3)	0.009(4)
C26	0.042(4)	0.049(3)	0.030(4)	-0.000(3)	-0.002(3)	0.0013(3)
C27	0.042(4)	0.035(3)	0.028(3)	0.002(3)	-0.002(3)	0.007(3)
C110	0.043(4)	0.035(3)	0.059(5)	-0.005(3)	-0.000(4)	0.004(3)

The form of the anisotropic thermal parameter is:

$$\exp[-\pi^2(h^2a^2U(1,1) + k^2b^2U(2,2) + l^2c^2U(3,3) + 2hkaU(1,2) + 2hlcU(1,3) + 2klcU(2,3))]$$

where a, b, and c are reciprocal lattice constants.

13.1.2: Table of Root-Mean-Square Amplitudes of Thermal Vibration in Angstroms

Atom	Min	Int'med	Max
Cu1	0.17	0.185	0.194
Cu2	0.176	0.182	0.192
O(W)	0.175	0.222	0.256
O11	0.176	0.191	0.245
O12	0.179	0.179	0.278
O21	0.174	0.187	0.219
O22	0.175	0.189	0.216
N11	0.173	0.202	0.208
N12	0.187	0.215	0.239
N21	0.169	0.187	0.197
C11	0.17	0.199	0.224
C12	0.171	0.198	0.211
C13	0.183	0.219	0.265
C14	0.184	0.257	0.311
C15	0.184	0.263	0.287
C16	0.184	0.229	0.265
C17	0.17	0.191	0.245
C18	0.187	0.218	0.224
C19	0.189	0.218	0.35
C21	0.18	0.179	0.21
C22	0.168	0.188	0.205
C23	0.176	0.218	0.244
C24	0.192	0.199	0.262
C25	0.178	0.223	0.271
C26	0.153	0.206	0.297
C27	0.151	0.198	0.203
C110	0.18	0.212	0.246

## 13.1.3: Table of Positional Parameters and their Estimated Standard Deviations

Atom	x	y	z	B(A <sup>2</sup> )
Cu1	0.44007(5)	0.10203(4)	0.2416(1)	2.66(1)
Cu2	0.27518(5)	0.22921(4)	0.2469(1)	2.66(1)
O(W)	0.4408(3)	0.0823(3)	-0.1148(7)	3.8(1)
O11	0.2217(3)	0.3323(2)	0.2553(7)	3.4(1)
O12	0.3217(3)	0.1254(3)	0.2535(7)	3.7(1)
O21	0.5595(3)	0.0766(2)	0.2738(6)	2.97(9)
O22	0.3882(3)	0.2737(2)	0.2004(7)	2.97(9)
N11	0.1671(3)	0.1709(3)	0.2771(8)	3.0(1)
N12	0.4006(4)	-0.0131(3)	0.3036(8)	3.6(1)
N21	0.4561(3)	0.2197(3)	0.2031(8)	2.7(1)
C11	0.0743(4)	0.2878(4)	0.286(1)	3.1(1)
C12	0.1393(4)	0.3469(4)	0.266(1)	3.0(1)
C13	0.1112(5)	0.4278(4)	0.257(1)	4.0(2)
C14	0.0258(5)	0.4479(4)	0.271(1)	5.2(2)
C15	-0.0372(5)	0.3893(5)	0.290(1)	4.9(2)
C16	-0.0120(5)	0.3113(4)	0.298(1)	4.1(2)
C17	0.0925(4)	0.2031(4)	0.293(1)	3.8(1)
C18	0.1781(5)	0.0835(4)	0.278(1)	3.5(2)
C19	0.2697(5)	0.0654(4)	0.332(1)	5.4(2)
C21	0.6112(4)	0.2065(4)	0.1622(8)	2.5(1)
C22	0.6227(4)	0.1253(4)	0.2181(9)	2.8(1)
C23	0.7075(5)	0.0933(4)	0.215(1)	3.6(2)
C24	0.7783(5)	0.1392(5)	0.168(1)	3.8(2)
C25	0.7656(5)	0.2191(5)	0.112(1)	4.1(2)
C26	0.6842(5)	0.2514(4)	0.113(1)	3.2(1)
C27	0.5295(4)	0.2499(4)	0.1633(9)	2.8(1)
C110	0.3057(5)	-0.0149(4)	0.280(1)	3.6(2)
H13	0.147(4)	0.468(4)	0.525(8)	3(1)*
H14	0.013(5)	0.490(5)	0.26(1)	7(2)*
H15	-0.083(5)	0.405(4)	0.34(1)	4(2)*
H16	-0.049(4)	0.276(4)	0.314(9)	4(2)*
H17	0.058(4)	0.175(4)	0.309(9)	4(2)*
H19	0.293(6)	0.050(6)	0.50(1)	11(3)*
H23	0.722(4)	0.043(3)	0.262(8)	3(1)*
H24	0.847(4)	0.107(4)	0.174(9)	4(1)*
H25	0.810(4)	0.254(4)	0.07(1)	5(2)*
H26	0.677(4)	0.305(3)	0.079(8)	3(1)*
H27	0.520(4)	0.306(4)	0.121(9)	5(2)*
HN121	0.416(5)	-0.044(4)	0.20(1)	6(2)*
HN122	0.421(6)	-0.016(6)	0.43(1)	11(3)*
H181	0.134(4)	0.065(3)	0.313(8)	3(1)*
H182	0.172(3)	0.069(3)	0.162(7)	1(1)*
H1101	0.287(6)	0.002(5)	0.14(1)	10(3)*
H1102	0.284(4)	-0.055(3)	0.324(9)	3(1)*

Starred atoms are refined isotropically.

Anisotropically refined atoms are given in the form of the isotropic equivalent thermal parameter

defined:

$$(4/3) * [a^2 * B(1,1) + b^2 * B(2,2) + c^2 * B(3,3) + ab(\cos \gamma) * B(1,2) + ac(\cos \beta) * B(1,3) + bc(\cos \alpha) * B(2,3)]$$

13.1.4: Table of Bond Distances in Å

Atom 1	Atom 2	Distance	Atom 1	Atom 2	Distance
Cu1	O(W)	2.483(4)	N12	HN122	0.92(9)
Cu1	O12	1.877(4)	N21	C27	1.282(6)
Cu1	O21	1.899(3)	C11	C12	1.416(7)
Cu1	N12	2.055(5)	C11	C16	1.396(7)
Cu1	N21	1.984(4)	C11	C17	1.433(8)
Cu2	O11	1.900(3)	C12	C13	1.409(7)
Cu2	O12	1.865(3)	C13	C14	1.371(9)
Cu2	O22	1.936(3)	C13	H13	0.86(5)
Cu2	N11	1.951(4)	C14	C15	1.385(10)
O11	C12	1.302(6)	C14	H14	0.73(7)
O12	C19	1.403(7)	C15	C16	1.351(9)
O21	C22	1.336(6)	C15	H15	0.84(6)
O22	N21	1.380(5)	C16	H16	0.83(6)
N11	C17	1.280(7)	C17	H17	0.72(5)
N11	C18	1.458(7)	C18	C19	1.480(9)
N12	C110	1.470(8)	C18	H181	0.79(5)
N12	HN121	0.91(7)	C18	H182	0.84(4)

Atom 1	Atom 2	Distance
C19	C110	1.492(8)
C19	H19	1.20(9)
C21	C22	1.410(7)
C21	C26	1.405(7)
C21	C27	1.454(7)
C22	C23	1.416(7)
C23	C24	1.385(8)
C23	H23	0.91(5)
C24	C25	1.391(8)
C24	H24	1.19(5)
C25	C26	1.368(8)
C25	H25	0.96(6)
C26	H26	0.92(5)
C27	H27	0.99(6)
C110	H1101	1.03(8)
C110	H1102	0.81(5)

Numbers in parentheses are estimated standard deviations in the least significant digits.

13.1.5: Table of Bond Angles in Degrees

Atom 1	Atom 2	Atom 3	Angle	Atom 1	Atom 2	Atom 3	Angle
O(W)	Cu1	O12	96.7(2)	Cu1	N21	C27	122.0(3)
O(W)	Cu1	O21	92.4(1)	O22	N21	C27	115.1(4)
O(W)	Cu1	N12	95.7(2)	C12	C11	C16	119.9(5)
O(W)	Cu1	N21	89.5(2)	C12	C11	C17	122.8(5)
O12	Cu1	O21	170.7(2)	C16	C11	C17	117.3(5)
O12	Cu1	N12	83.3(2)	O11	C12	C11	125.3(5)
O12	Cu1	N21	86.1(2)	O11	C12	C13	118.4(5)
O21	Cu1	N12	93.8(2)	C11	C12	C13	116.3(5)
O21	Cu1	N21	96.1(2)	C12	C13	C14	121.6(6)
N12	Cu1	N21	168.6(2)	C12	C13	H13	122.(4)
O11	Cu2	O12	175.5(2)	C14	C13	H13	116.(4)
O11	Cu2	O22	93.4(1)	C13	C14	C15	121.3(6)
O11	Cu2	N11	93.8(2)	C13	C14	H14	119.(6)
O12	Cu2	O22	90.3(2)	C15	C14	H14	119.(6)
O12	Cu2	N11	82.6(2)	C14	C15	C16	118.2(6)
O22	Cu2	N11	172.1(2)	C14	C15	H15	116.(5)
Cu2	O11	C12	126.6(3)	C16	C15	H15	121.(5)
Cu1	O12	Cu2	124.4(2)	C11	C16	C15	122.6(6)
Cu1	O12	C19	116.6(3)	C11	C16	H16	118.(4)
Cu2	O12	C19	115.9(4)	C15	C16	H16	119.(4)
Cu1	O21	C22	123.5(3)	N11	C17	C11	125.6(5)
Cu2	O22	N21	116.3(3)	N11	C17	H17	115.(5)
Cu2	N11	C17	125.6(4)	C11	C17	H17	120.(5)
Cu2	N11	C18	113.1(4)	N11	C18	C19	108.3(5)
C17	N11	C18	121.3(5)	N11	C18	H181	106.(4)
Cu1	N12	C110	107.4(4)	N11	C18	H182	106.(3)
Cu1	N12	HN121	106.(4)	C19	C18	H181	132.(4)
Cu1	N12	HN122	98.(6)	C19	C18	H182	105.(3)
C110	N12	HN121	101.(4)	H181	C18	H182	97.(5)
C110	N12	HN122	114.(5)	O12	C19	C18	108.5(5)
HN121	N12	HN122	128.(7)	O12	C19	C110	108.2(5)
Cu1	N21	O22	122.6(3)	O12	C19	H19	111.(4)



13.1.5: Table of Bond Angles in Degrees (continued)

Atom 1	Atom 2	Atom 3	Angle
C18	C19	C110	118.8(6)
C18	C19	H19	121.(4)
C110	C19	H19	87.(4)
C22	C21	C26	118.5(5)
C22	C21	C27	124.8(5)
C26	C21	C27	116.5(4)
O21	C22	C21	124.8(5)
O21	C22	C23	117.8(5)
C21	C22	C23	117.4(5)
C22	C23	C24	122.7(5)
C22	C23	H23	123.(3)
C24	C23	H23	114.(3)
C23	C24	C25	119.0(6)
C23	C24	H24	117.(3)
C25	C24	H24	124.(3)
C24	C25	C26	119.4(6)
C24	C25	H25	124.(4)
C26	C25	H25	117.(4)
C21	C26	C25	122.9(5)
C21	C26	H26	119.(3)
C25	C26	H26	118.(3)
N21	C27	C21	125.8(4)
N21	C27	H27	108.(3)
C21	C27	H27	126.(3)
N12	C110	C19	109.7(5)
N12	C110	H1101	110.(5)
N12	C110	H1102	114.(4)
C19	C110	H1101	83.(4)
C19	C110	H1102	118.(4)
H1101	C110	H1102	124.(3)

Numbers in parentheses are estimated standard deviations in the least significant digits.

13.2: Cu<sub>2</sub>(SAL-DPL)6AlSpace Group P2<sub>1</sub>/C

Unit Cell Dimensions a = 16.300(6)Å, b = 8.612(6)Å, c = 19.477(3)

Vol = 2648Å<sup>3</sup>

Empirical Formula	Cu	O	N	C	H
	20.25	10.20	13.39	51.67	4.50

Formula Weight 627

Z = 4, D<sub>calc</sub> = 1.574, Abs Coeff = 16.541

13.2.1: Table of General Temperature Expressions- U's

<u>Name</u>	<u>U(1,1)</u>	<u>U(2,2)</u>	<u>U(3,3)</u>	<u>U(1,2)</u>	<u>U(1,3)</u>	<u>U(2,3)</u>
CU1	0.0479(4)	0.0453(4)	0.0483(4)	0.0033(4)	0.0129(3)	0.0046(4)
CU2	0.0492(4)	0.0573(5)	0.0499(4)	0.0054(4)	0.0114(3)	0.0042(4)
O	0.046(2)	0.071(3)	0.055(2)	0.004(2)	0.009(2)	0.019(2)
O(D)	0.134(5)	0.143(6)	0.142(5)	0.012(5)	0.025(4)	0.007(5)
O11	0.048(2)	0.073(3)	0.057(2)	0.003(2)	0.010(2)	0.017(2)
O21	0.055(2)	0.084(3)	0.057(2)	0.001(3)	0.017(2)	0.003(3)
N(D)	0.094(5)	0.096(5)	0.113(5)	0.010(4)	0.015(4)	-0.018(5)
N1	0.045(2)	0.047(3)	0.041(2)	-0.003(3)	0.011(2)	0.004(3)
N2	0.051(3)	0.048(3)	0.050(3)	0.004(3)	0.014(2)	-0.002(3)
N3	0.064(3)	0.068(4)	0.068(3)	0.001(3)	0.007(3)	0.020(3)
N11	0.053(3)	0.045(3)	0.052(3)	0.000(3)	0.014(2)	-0.001(3)
N21	0.052(3)	0.051(3)	0.057(3)	0.009(3)	0.006(2)	0.011(3)
C(D1)	0.158(9)	0.138(9)	0.146(9)	0.035(8)	0.035(7)	-0.022(8)
C(D2)	0.20(1)	0.15(1)	0.125(8)	0.049(9)	0.008(8)	0.047(8)
C(D3)	0.233(9)	0.126(9)	0.27(1)	-0.064(7)	0.140(7)	0.041(8)
C3	0.056(3)	0.057(4)	0.053(3)	-0.009(4)	0.021(3)	-0.005(3)
C4	0.072(4)	0.052(5)	0.058(4)	0.001(4)	0.016(3)	0.003(4)
C5	0.081(4)	0.052(4)	0.058(3)	0.001(4)	0.030(3)	0.018(4)
C6	0.068(4)	0.042(4)	0.053(4)	0.003(4)	0.013(3)	-0.001(3)
C7	0.061(3)	0.037(4)	0.049(3)	0.001(3)	0.020(3)	-0.001(3)

13.2.1: Table of General Temperature Expressions- U's (continued)

Name	U(1,1)	U(2,2)	U(3,3)	U(1,2)	U(1,3)	U(2,3)
C8	0.055(3)	0.032(4)	0.042(3)	0.003(3)	0.015(2)	-0.006(3)
C9	0.056(3)	0.050(4)	0.047(3)	0.001(3)	0.017(3)	-0.007(3)
C11	0.044(3)	0.045(4)	0.068(4)	-0.008(3)	0.016(3)	-0.012(4)
C12	0.044(3)	0.044(4)	0.063(3)	-0.001(3)	0.018(3)	-0.009(3)
C13	0.049(3)	0.044(4)	0.064(4)	0.003(3)	0.011(3)	-0.005(4)
C14	0.060(4)	0.059(5)	0.073(4)	0.004(4)	0.008(3)	-0.012(4)
C15	0.050(4)	0.083(6)	0.112(6)	-0.019(4)	0.015(4)	-0.006(5)
C16	0.063(4)	0.072(5)	0.082(4)	-0.014(4)	0.027(3)	0.010(4)
C17	0.066(3)	0.047(4)	0.053(3)	-0.005(3)	0.024(3)	0.002(3)
C18	0.063(4)	0.047(4)	0.055(3)	0.006(3)	0.017(3)	0.014(3)
C19	0.061(4)	0.067(5)	0.059(4)	-0.003(4)	0.012(3)	0.016(4)
C21	0.055(3)	0.049(4)	0.062(4)	0.007(4)	0.008(3)	-0.004(4)
C22	0.059(4)	0.054(4)	0.059(4)	0.009(4)	0.012(3)	-0.006(4)
C23	0.062(4)	0.076(5)	0.066(4)	-0.005(4)	0.023(3)	-0.007(4)
C24	0.062(4)	0.081(5)	0.073(4)	-0.010(4)	0.021(3)	-0.017(4)
C25	0.050(4)	0.072(5)	0.084(5)	-0.004(4)	-0.001(4)	-0.011(4)
C26	0.067(4)	0.057(5)	0.067(4)	0.005(4)	0.000(4)	0.009(4)
C27	0.074(4)	0.048(4)	0.054(4)	0.004(4)	0.005(3)	0.015(3)
C28	0.068(4)	0.077(6)	0.059(4)	0.004(4)	0.007(3)	0.019(4)

-----  
The form of the anisotropic thermal parameter is:

$\exp[-2\pi^2(h^2a^2U(1,1) + k^2b^2U(2,2) + l^2c^2U(3,3) + 2hkaU(1,2) + 2hlcU(1,3) + 2klbU(2,3))]$  where a, b, and c are reciprocal lattice constants.

13.2.2: Table of Root-Mean-Square Amplitudes of Thermal Vibration in Angstroms

Atom	Min.	Int 'med.	Max.
-----	-----	-----	-----
CU1	0.204	0.216	0.229
CU2	0.213	0.226	0.246
O	0.202	0.224	0.289
O(D)	0.350	0.388	0.388
O11	0.212	0.226	0.289
O21	0.228	0.240	0.291
N(D)	0.286	0.303	0.368
N1	0.194	0.211	0.227
N2	0.208	0.226	0.231
N3	0.218	0.256	0.305
N11	0.211	0.226	0.231
N21	0.193	0.246	0.257
C(D1)	0.315	0.385	0.443
C(D2)	0.278	0.428	0.487
C(D3)	0.223	0.473	0.562
C3	0.210	0.224	0.261
C4	0.224	0.243	0.269
C5	0.179	0.258	0.293
C6	0.204	0.231	0.264
C7	0.191	0.211	0.250

Atom	Min.	Int 'med.	Max.
-----	-----	-----	-----
C8	0.165	0.211	0.235
C9	0.197	0.235	0.239
C11	0.189	0.215	0.270
C12	0.197	0.208	0.259
C13	0.205	0.223	0.260
C14	0.228	0.240	0.295
C15	0.205	0.303	0.339
C16	0.209	0.282	0.299
C17	0.202	0.227	0.264
C18	0.191	0.243	0.261
C19	0.215	0.245	0.286
C21	0.210	0.232	0.267
C22	0.213	0.240	0.266
C23	0.234	0.253	0.285
C24	0.239	0.247	0.309
C25	0.210	0.267	0.317
C26	0.216	0.252	0.298
C27	0.188	0.253	0.288
C28	0.214	0.270	0.301

13.2.3: Table of Positional Parameters and their Estimated Standard Deviations

Atom ----	x --	y --	z --	B (A <sup>2</sup> ) -----
CU1	0.04375 (4)	0.31287 (9)	0.98822 (4)	3.71 (2)
CU2	0.25360 (5)	0.3408 (1)	1.05470 (4)	4.13 (2)
O	0.1463 (2)	0.2588 (5)	1.0548 (2)	4.6 (1)
O (D)	0.2410 (4)	0.4406 (9)	0.2923 (4)	11.2 (2)
O11	-0.0632 (2)	0.3618 (5)	0.9266 (2)	4.7 (1)
O21	0.3663 (3)	0.4048 (6)	1.0558 (2)	5.1 (1)
N (D)	0.3572 (4)	0.4433 (9)	0.3838 (4)	8.1 (2)
N1	0.1142 (3)	0.4154 (6)	0.9323 (2)	3.5 (1)
N2	0.2005 (3)	0.4289 (6)	0.9618 (2)	3.9 (1)
N3	-0.0531 (3)	0.6240 (7)	0.7066 (3)	5.4 (2)
N11	-0.0055 (3)	0.1886 (6)	1.0512 (2)	3.9 (1)
N21	0.2860 (3)	0.2418 (6)	1.1470 (3)	4.3 (1)
C (D1)	0.2787 (7)	0.383 (1)	0.3519 (6)	11.7 (4)
C (D2)	0.3955 (8)	0.364 (1)	0.4490 (6)	13.1 (4)
C (D3)	0.3974 (7)	0.570 (1)	0.3614 (7)	15.5 (4)
C3	0.2355 (4)	0.5152 (8)	0.9197 (3)	4.3 (2)
C4	0.1737 (4)	0.6485 (8)	0.7986 (3)	4.8 (2)
C5	0.0980 (4)	0.6673 (8)	0.7503 (3)	4.9 (2)
C6	0.0219 (4)	0.6033 (8)	0.7605 (3)	4.3 (2)
C7	0.0209 (4)	0.5187 (7)	0.8201 (3)	3.8 (1)

13.2.3: Table of Positional Parameters and their Estimated Standard Deviations (continued)

Atom ----	x --	y --	z --	B (A <sup>2</sup> ) -----
C8	0.0987 (3)	0.4972 (7)	0.8708 (3)	3.3 (1)
C9	0.1747 (4)	0.5601 (8)	0.8604 (3)	4.0 (2)
C11	-0.1517 (3)	0.2120 (7)	0.9844 (3)	4.1 (2)
C12	-0.1368 (3)	0.3081 (8)	0.9305 (3)	3.9 (1)
C13	-0.2083 (4)	0.3515 (8)	0.8762 (3)	4.2 (2)
C14	-0.2876 (4)	0.3005 (9)	0.8764 (4)	5.2 (2)
C15	-0.3014 (4)	0.209 (1)	0.9290 (4)	6.5 (2)
C16	-0.2333 (4)	0.1628 (9)	0.9825 (4)	5.6 (2)
C17	-0.0838 (4)	0.1589 (8)	1.0436 (3)	4.3 (2)
C18	0.0575 (4)	0.1249 (8)	1.1129 (3)	4.3 (2)
C19	0.1356 (4)	0.2212 (9)	1.1228 (3)	4.9 (2)
C21	0.4302 (4)	0.3388 (8)	1.1782 (3)	4.4 (2)
C22	0.4308 (4)	0.4042 (8)	1.1118 (3)	4.6 (2)
C23	0.5068 (4)	0.4782 (9)	1.1064 (3)	5.3 (2)
C24	0.5771 (4)	0.4826 (9)	1.1615 (4)	5.6 (2)
C25	0.5770 (4)	0.4141 (9)	1.2245 (4)	5.7 (2)
C26	0.5058 (4)	0.3426 (8)	1.2332 (4)	5.2 (2)
C27	0.3582 (4)	0.2583 (8)	1.1913 (3)	4.8 (2)
C28	0.2173 (4)	0.1532 (9)	1.1633 (4)	5.5 (2)
H3	0.297 (3)	0.551 (7)	0.930 (3)	6 (2) *

13.2.3: Table of Positional Parameters and their Estimated Standard Deviations (continued)

Atom ----	x --	y --	z --	B(A2) -----
H4	0.232(4)	0.722(8)	0.802(3)	8(2)*
H5	0.094(3)	0.726(7)	0.706(3)	6(2)*
H7	-0.027(3)	0.479(7)	0.836(3)	6(1)*
H13	-0.208(3)	0.420(7)	0.839(3)	5(1)*
H14	-0.327(3)	0.342(7)	0.839(3)	5(1)*
H15	-0.343(3)	0.171(6)	0.929(2)	4(1)*
H16	-0.242(2)	0.105(5)	1.018(2)	2(1)*
H17	-0.101(3)	0.102(5)	1.082(2)	2(1)*
H19	0.126(4)	0.329(8)	1.146(3)	7(2)*
H23	0.505(3)	0.530(6)	1.065(2)	4(1)*
H24	0.626(3)	0.527(7)	1.150(3)	6(2)*
H25	0.627(3)	0.420(6)	1.262(2)	4(1)*
H26	0.499(3)	0.294(6)	1.273(2)	4(1)*
H27	0.360(3)	0.220(6)	1.236(3)	5(1)*
HN31	0.103(2)	0.398(5)	0.284(2)	2(1)*
HN32	0.950(3)	0.786(8)	0.177(3)	7(2)*
H181	0.038(3)	0.115(7)	1.154(3)	5(1)*
H182	0.070(3)	0.025(6)	1.098(2)	3(1)*
H281	0.217(4)	0.053(9)	1.145(3)	9(2)*
H282	0.221(3)	0.148(6)	1.208(2)	4(1)*

-----

Starred atoms were refined isotropically.

Anisotropically refined atoms are given in the form of the isotropic equivalent thermal parameter defined as:

$$(4/3) * [a^2*B(1,1) + b^2*B(2,2) + c^2*B(3,3) + ab(\cos \gamma)*B(1,2) + ac(\cos \beta)*B(1,3) + bc(\cos \alpha)*B(2,3)]$$



## 13.2.4: Table of Bond Distances in Å

Atom1 -----	Atom2 -----	Distance -----	Atom1 -----	Atom2 -----	Distance -----	Atom1 -----	Atom2 -----	Distance -----
CU1	O	1.901(4)	N21	C28	1.455(9)	C16	H16	0.89(5)
CU1	O11	1.902(4)	C3	C9	1.376(8)	C17	H17	0.98(5)
CU1	N1	1.976(5)	C3	H3	1.02(6)	C18	C19	1.490(10)
CU1	N11	1.945(5)	C4	C5	1.362(9)	C18	H181	0.93(6)
CU2	O	1.887(4)	C4	C9	1.422(9)	C18	H182	0.95(6)
CU2	O21	1.913(4)	C4	H4	1.13(7)	C19	C28	1.488(10)
CU2	N2	1.954(5)	C5	C6	1.417(9)	C19	H19	1.06(7)
CU2	N21	1.941(5)	C5	H5	0.98(6)	C21	C22	1.412(9)
O	C19	1.416(8)	C6	C7	1.374(8)	C21	C26	1.418(8)
O(D)	C(D1)	1.270(13)	C7	C8	1.412(8)	C21	C27	1.440(9)
O11	C12	1.305(7)	C7	H7	0.96(6)	C22	C23	1.421(9)
O21	C22	1.313(7)	C8	C9	1.413(8)	C23	C24	1.362(10)
N(D)	C(D1)	1.377(14)	C11	C12	1.405(9)	C23	H23	0.92(5)
N(D)	C(D2)	1.443(12)	C11	C16	1.388(9)	C24	C25	1.361(10)
N(D)	C(D3)	1.400(12)	C11	C17	1.460(9)	C24	H24	0.96(7)
N1	N2	1.385(6)	C12	C13	1.415(8)	C25	C26	1.361(10)
N1	C8	1.358(7)	C13	C14	1.366(9)	C25	H25	0.95(5)
N2	C3	1.336(8)	C13	H13	0.94(6)	C26	H26	0.92(6)
N3	C6	1.411(8)	C14	C15	1.355(11)	C27	H27	0.93(6)
N11	C17	1.273(7)	C14	H14	0.91(6)	C28	H281	0.94(8)
N11	C18	1.477(8)	C15	C16	1.379(11)	C28	H282	0.87(6)
N21	C27	1.282(8)	C15	H15	0.75(6)			

-----  
Numbers in parentheses are estimated standard deviations in the least significant digits.

## 13.2.5: Table of Bond Angles in Degrees

Atom1 .....	Atom2 .....	Atom3 .....	Angle .....	Atom1 .....	Atom2 .....	Atom3 .....	Angle .....	Atom1 .....	Atom2 .....	Atom3 .....	Angle .....
O	CU1	O11	175.7(2)	C9	C4	H4	115.(3)	N11	C18	H181	115.(4)
O	CU1	N1	87.3(2)	C4	C5	C6	122.1(7)	N11	C18	H182	105.(3)
O	CU1	N11	82.3(2)	C4	C5	H5	121.(4)	C19	C18	H181	113.(4)
O11	CU1	N1	96.9(2)	C6	C5	H5	117.(4)	C19	C18	H182	108.(3)
O11	CU1	N11	93.6(2)	N3	C6	C5	118.2(7)	H181	C18	H182	109.(5)
N1	CU1	N11	168.7(2)	N3	C6	C7	120.4(7)	O	C19	C18	107.8(6)
O	CU2	O21	174.7(2)	C5	C6	C7	121.3(6)	O	C19	C28	106.5(6)
O	CU2	N2	87.1(2)	C6	C7	C8	117.6(6)	O	C19	H19	105.(4)
O	CU2	N21	82.7(2)	C6	C7	H7	130.(4)	C18	C19	C28	118.2(7)
O21	CU2	N2	95.8(2)	C8	C7	H7	113.(4)	C18	C19	H19	110.(4)
O21	CU2	N21	94.4(2)	N1	C8	C7	128.5(6)	C28	C19	H19	109.(4)
N2	CU2	N21	169.8(2)	N1	C8	C9	110.4(5)	C22	C21	C26	118.6(7)
CU1	O	CU2	124.4(2)	C7	C8	C9	121.1(6)	C22	C21	C27	123.2(6)
CU1	O	C19	113.7(4)	C3	C9	C4	135.6(7)	C26	C21	C27	118.1(7)
CU2	O	C19	114.6(4)	C3	C9	C8	104.3(6)	O21	C22	C21	125.1(6)
CU1	O11	C12	126.6(4)	C4	C9	C8	120.1(6)	O21	C22	C23	118.0(7)
CU2	O21	C22	125.2(4)	C12	C11	C16	120.3(7)	C21	C22	C23	116.9(7)
C(D1)	N(D)	C(D2)	112.(1)	C12	C11	C17	122.5(6)	C22	C23	C24	122.2(8)
C(D1)	N(D)	C(D3)	128.(1)	C16	C11	C17	117.2(7)	C22	C23	H23	116.(4)
C(D2)	N(D)	C(D3)	121.(1)	O11	C12	C11	125.8(6)	C24	C23	H23	122.(4)
CU1	N1	N2	118.6(4)	O11	C12	C13	117.5(6)	C23	C24	C25	120.5(8)
CU1	N1	C8	135.4(4)	C11	C12	C13	116.7(6)	C23	C24	H24	114.(4)
N2	N1	C8	105.6(5)	C12	C13	C14	121.2(8)	C25	C24	H24	125.(4)
CU2	N2	N1	121.4(4)	C12	C13	H13	126.(4)	C24	C25	C26	120.1(8)
CU2	N2	C3	128.8(4)	C14	C13	H13	113.(4)	C24	C25	H25	118.(4)
N1	N2	C3	109.8(5)	C13	C14	C15	121.6(8)	C26	C25	H25	122.(4)
CU1	N11	C17	126.6(5)	C13	C14	H14	110.(4)	C21	C26	C25	121.6(8)
CU1	N11	C18	113.8(4)	C15	C14	H14	128.(4)	C21	C26	H26	111.(4)
C17	N11	C18	119.6(6)	C14	C15	C16	119.0(8)	C25	C26	H26	127.(4)
CU2	N21	C27	124.6(5)	C14	C15	H15	125.(5)	N21	C27	C21	125.8(7)
CU2	N21	C28	112.7(4)	C16	C15	H15	115.(5)	N21	C27	H27	114.(4)
C27	N21	C28	122.6(6)	C11	C16	C15	121.1(8)	C21	C27	H27	120.(4)
O(D)	C(D1)	N(D)	117.(1)	C11	C16	H16	120.(3)	N21	C28	C19	108.3(6)
N2	C3	C9	110.0(6)	C15	C16	H16	119.(3)	N21	C28	H281	109.(5)
N2	C3	H3	127.(4)	N11	C17	C11	124.7(6)	N21	C28	H282	113.(4)
C9	C3	H3	123.(4)	N11	C17	H17	118.(3)	C19	C28	H281	104.(5)
C5	C4	C9	117.8(7)	C11	C17	H17	117.(3)	C19	C28	H282	112.(4)
C5	C4	H4	125.(3)	N11	C18	C19	107.3(6)	H281	C28	H282	109.(7)

Numbers in parentheses are estimated standard deviations in the least significant digits.

13.3: Cu<sub>2</sub>(M<sup>2</sup>BP-DPL)M<sup>2</sup>Pz

Space Group P-1

Unit Cell Dimensions  $a = 14.416(6)\text{\AA}$ ,  $b = 14.5760(6)\text{\AA}$ ,  $c = 9.700(3)$ Vol =  $1786\text{\AA}^3$ 

Empirical Formula	Cu	O	N	C	H
	17.08	8.60	7.53	61.36	5.42

Formula Weight 743

 $Z = 2$ ,  $D_{\text{calc}} = 1.383$ , Abs Coeff = 12.359

13.3.1: Table of General Temperature Expressions- U's

<u>Name</u>	<u>U(1,1)</u>	<u>U(2,2)</u>	<u>U(3,3)</u>	<u>U(1,2)</u>	<u>U(1,3)</u>	<u>U(2,3)</u>
CU1	0.0267(1)	0.0455(1)	0.0340(2)	0.0139(1)	0.0011(1)	0.0154(1)
CU2	0.0266(1)	0.0488(2)	0.0470(2)	0.0085(1)	-0.0003(1)	0.0212(1)
O	0.0281(8)	0.064(1)	0.043(1)	0.0062(7)	-0.0032(8)	0.0274(8)
O1	0.0347(8)	0.064(1)	0.0330(9)	0.0196(7)	0.0046(8)	0.0195(8)
O2	0.0313(9)	0.087(1)	0.079(1)	0.0101(9)	0.0045(9)	0.050(1)
N1	0.0290(9)	0.044(1)	0.032(1)	0.0139(7)	0.0037(9)	0.0136(9)
N2	0.0284(9)	0.047(1)	0.045(1)	0.0114(8)	0.0055(9)	0.0210(9)
N3	0.0322(9)	0.043(1)	0.039(1)	0.0155(8)	-0.0018(9)	0.009(1)
N4	0.033(1)	0.047(1)	0.044(1)	0.0111(9)	-0.000(1)	0.012(1)
C1	0.038(1)	0.047(1)	0.035(1)	0.0228(9)	0.012(1)	0.013(1)
C1'	0.041(1)	0.035(1)	0.041(2)	0.013(1)	0.013(1)	0.010(1)
C2'	0.034(1)	0.046(1)	0.055(2)	0.011(1)	0.007(1)	0.014(1)
C2	0.039(1)	0.051(1)	0.032(1)	0.0242(9)	0.011(1)	0.013(1)
C3'	0.037(1)	0.069(2)	0.072(2)	0.011(1)	0.010(2)	0.023(2)
C3	0.052(1)	0.077(2)	0.036(1)	0.033(1)	0.012(1)	0.021(1)
C4	0.070(2)	0.096(2)	0.045(2)	0.044(1)	0.027(1)	0.039(1)
C4'	0.048(2)	0.064(2)	0.076(2)	0.005(2)	0.024(2)	0.025(2)
C5	0.056(1)	0.078(2)	0.067(2)	0.037(1)	0.035(1)	0.043(1)
C5'	0.061(2)	0.057(2)	0.057(2)	0.015(1)	0.024(1)	0.023(1)
C6	0.040(1)	0.067(2)	0.058(2)	0.027(1)	0.019(1)	0.030(1)
C6'	0.050(1)	0.049(1)	0.046(2)	0.017(1)	0.016(1)	0.017(1)
C7	0.030(1)	0.044(1)	0.038(1)	0.0182(8)	0.006(1)	0.012(1)
C7'	0.038(1)	0.036(1)	0.038(1)	0.0166(9)	0.009(1)	0.009(1)

13.3.1: Table of General Temperature Expressions- U's (continued)

<u>Name</u>	<u>U(1,1)</u>	<u>U(2,2)</u>	<u>U(3,3)</u>	<u>U(1,2)</u>	<u>U(1,3)</u>	<u>U(2,3)</u>
C8'	0.089(3)	0.117(3)	0.101(2)	0.008(2)	0.031(2)	0.074(2)
C8	0.069(2)	0.126(3)	0.110(2)	0.043(2)	0.052(2)	0.078(2)
C9'	0.031(1)	0.065(2)	0.046(1)	0.011(1)	0.000(1)	0.028(1)
C9	0.026(1)	0.063(1)	0.043(1)	0.010(1)	-0.001(1)	0.027(1)
C10	0.030(1)	0.099(2)	0.064(2)	0.007(1)	-0.003(1)	0.049(1)
C11	0.026(1)	0.045(1)	0.041(1)	0.0149(8)	0.007(1)	0.017(1)
C11'	0.040(1)	0.035(1)	0.034(1)	0.0164(9)	0.007(1)	0.012(1)
C12'	0.065(1)	0.069(2)	0.051(2)	0.045(1)	0.004(2)	0.001(2)
C12	0.040(1)	0.062(2)	0.077(3)	0.024(1)	-0.003(2)	0.001(2)
C13'	0.080(2)	0.079(2)	0.040(2)	0.046(1)	-0.007(2)	-0.008(2)
C13	0.047(2)	0.072(2)	0.083(3)	0.016(1)	-0.018(2)	-0.003(2)
C14	0.032(1)	0.080(2)	0.082(2)	0.020(1)	0.002(1)	0.036(2)
C14'	0.064(2)	0.054(1)	0.050(2)	0.031(1)	-0.005(1)	0.012(1)
C15'	0.060(1)	0.057(1)	0.060(2)	0.037(1)	0.004(1)	0.010(1)
C15	0.046(1)	0.085(2)	0.109(3)	0.041(1)	0.008(2)	0.025(2)
C16	0.044(1)	0.072(2)	0.073(3)	0.031(1)	0.002(2)	0.003(2)
C16'	0.055(1)	0.049(1)	0.036(2)	0.026(1)	0.004(1)	0.002(1)
C17'	0.111(2)	0.117(2)	0.074(3)	0.076(1)	-0.028(2)	0.007(2)
C17	0.049(2)	0.132(3)	0.143(4)	0.029(2)	-0.022(2)	0.054(3)
C18	0.038(1)	0.059(2)	0.063(2)	0.005(1)	-0.006(1)	0.013(2)
C19	0.043(1)	0.060(2)	0.055(2)	0.011(1)	-0.017(1)	0.002(2)
C20	0.044(1)	0.050(1)	0.038(2)	0.0245(9)	-0.002(1)	0.004(1)
C21	0.050(2)	0.098(3)	0.086(3)	-0.019(2)	-0.008(2)	0.027(2)
C22	0.057(1)	0.066(2)	0.038(2)	0.031(1)	-0.001(1)	0.013(1)

-----  
The form of the anisotropic thermal parameter is:  
 $\exp[-2\pi i^2(h^2a^2U(1,1) + k^2b^2U(2,2) + l^2c^2U(3,3) + 2hkabU(1,2) + 2hlacU(1,3) + 2klbcU(2,3))]$  where a, b, and c are reciprocal lattice constants.

13.3.2: Table of Root-Mean-Square Amplitudes of Thermal Vibration in Angstroms

Atom	Min.	Int.'med.	Max.
CU1	0.146	0.181	0.235
CU2	0.157	0.182	0.273
O	0.150	0.180	0.311
O1	0.158	0.193	0.267
O2	0.176	0.201	0.373
N1	0.158	0.178	0.226
N2	0.168	0.177	0.257
N3	0.159	0.205	0.230
N4	0.171	0.205	0.252
C1	0.176	0.182	0.220
C1'	0.178	0.203	0.217
C2'	0.182	0.217	0.252
C2	0.171	0.187	0.227
C3'	0.190	0.247	0.306
C3	0.176	0.222	0.280
C4	0.165	0.250	0.320
C4'	0.175	0.276	0.311
C5	0.177	0.223	0.313
C5'	0.186	0.256	0.283
C6	0.186	0.200	0.282
C6'	0.188	0.228	0.245
C7	0.164	0.191	0.216
C7'	0.184	0.194	0.200
C8'	0.180	0.317	0.449

Atom	Min.	Int.'med.	Max.
C8	0.185	0.281	0.411
C9'	0.161	0.188	0.304
C9	0.146	0.181	0.298
C10	0.162	0.194	0.389
C11	0.159	0.178	0.234
C11'	0.164	0.195	0.210
C12'	0.200	0.219	0.295
C12	0.187	0.246	0.303
C13'	0.186	0.246	0.326
C13	0.182	0.290	0.336
C14	0.171	0.236	0.339
C14'	0.181	0.234	0.289
C15'	0.190	0.241	0.274
C15	0.175	0.289	0.340
C16	0.193	0.257	0.297
C16'	0.187	0.215	0.246
C17'	0.184	0.311	0.410
C17	0.179	0.325	0.459
C18	0.175	0.243	0.308
C19	0.159	0.260	0.303
C20	0.172	0.214	0.240
C21	0.179	0.279	0.434
C22	0.174	0.256	0.259

13.3.3: Table of Positional Parameters and their Estimated Standard Deviations

Atom ----	x --	y --	z --	B (Å <sup>2</sup> ) -----
CU1	0.51401(2)	0.39308(2)	0.52430(4)	2.879(7)
CU2	0.37585(2)	0.22878(3)	0.71895(4)	3.488(8)
O	0.5018(1)	0.3238(2)	0.6805(2)	3.99(5)
OW1	0.500	0.000	0.500	15.0(8) #
O1	0.5396(1)	0.4678(2)	0.3738(2)	3.52(5)
O2	0.2565(2)	0.1452(2)	0.7795(2)	5.55(6)
OW2	0.465(1)	0.934(1)	0.366(2)	17.9(7) #
OW3	0.566(2)	0.937(2)	0.468(3)	18(1) #
OW4	0.462(3)	0.037(3)	0.527(4)	22(1) #
N1	0.6666(2)	0.4610(2)	0.6198(2)	2.83(5)
N2	0.4707(2)	0.2329(2)	0.8959(3)	3.31(6)
N3	0.3649(2)	0.2895(2)	0.4372(3)	3.16(6)
N4	0.3081(2)	0.2229(2)	0.5199(3)	3.56(6)
C1	0.7310(2)	0.5526(2)	0.4357(3)	2.96(6)
C1'	0.3394(2)	0.1044(2)	0.9884(3)	3.15(7)
C2'	0.2509(2)	0.0937(2)	0.8841(4)	3.78(8)
C2	0.6305(2)	0.5202(2)	0.3428(3)	3.04(6)
C3'	0.1501(2)	0.0227(3)	0.8941(4)	5.01(9)
C3	0.6288(2)	0.5466(3)	0.2061(3)	4.17(8)
C4	0.7195(3)	0.6094(3)	0.1689(3)	5.05(9)
C4'	0.1360(3)	-0.0354(3)	0.9973(4)	5.4(1)
C5	0.8176(2)	0.6475(3)	0.2613(4)	4.71(8)
C5'	0.2204(3)	-0.0276(3)	1.0995(4)	4.73(9)

13.3.3: Table of Positional Parameters and their Estimated Standard Deviations (continued)

Atom ----	x --	y --	z --	B (Å <sup>2</sup> ) -----
C6	0.8215 (2)	0.6180 (2)	0.3915 (3)	4.06 (7)
C6'	0.3194 (2)	0.0417 (2)	1.0929 (3)	3.89 (8)
C7	0.7452 (2)	0.5199 (2)	0.5721 (3)	2.89 (6)
C7'	0.4478 (2)	0.1752 (2)	0.9906 (3)	2.94 (6)
C8'	0.2052 (4)	-0.0932 (4)	1.2145 (5)	8.8 (1)
C8	0.9158 (3)	0.7206 (3)	0.2202 (4)	7.4 (1)
C9'	0.5813 (2)	0.3036 (2)	0.9025 (3)	4.04 (7)
C9	0.6865 (2)	0.4257 (2)	0.7555 (3)	3.76 (7)
C10	0.5849 (2)	0.3758 (3)	0.7996 (4)	5.68 (9)
C11	0.8552 (2)	0.5492 (2)	0.6538 (3)	2.94 (6)
C11'	0.5355 (2)	0.1807 (2)	1.1064 (3)	2.87 (6)
C12'	0.5608 (2)	0.2354 (2)	1.2414 (4)	4.60 (9)
C12	0.9099 (2)	0.6329 (3)	0.7602 (4)	4.93 (9)
C13'	0.6431 (3)	0.2399 (3)	1.3451 (4)	5.3 (1)
C13	1.0079 (3)	0.6518 (3)	0.8420 (5)	6.1 (1)
C14	1.0522 (2)	0.5875 (3)	0.8177 (4)	5.26 (9)
C14'	0.7026 (2)	0.1910 (2)	1.3149 (4)	4.49 (8)
C15'	0.6765 (2)	0.1362 (2)	1.1809 (4)	4.46 (8)
C15	0.9982 (2)	0.5051 (3)	0.7094 (5)	6.0 (1)
C16	0.9011 (2)	0.4872 (3)	0.6277 (4)	5.0 (1)
C16'	0.5940 (2)	0.1309 (2)	1.0770 (3)	3.72 (8)
C17'	0.7943 (3)	0.1974 (3)	1.4265 (5)	7.9 (1)
C17	1.1571 (3)	0.6050 (4)	0.9088 (6)	9.2 (1)



## 13.3.3: Table of Positional Parameters and their Estimated Standard Deviations (continued)

Atom	x	y	z	B(A <sup>2</sup> )
C18	0.2121(2)	0.1596(3)	0.4359(4)	4.86(9)
C19	0.2061(2)	0.1834(3)	0.3031(4)	4.86(9)
C20	0.3016(2)	0.2642(2)	0.3062(3)	3.51(7)
C21	0.1268(3)	0.0771(4)	0.4879(5)	7.8(1)
C22	0.3320(2)	0.3177(2)	0.1853(3)	4.28(8)
H3	0.560(2)	0.523(2)	0.146(3)	5.3(8)*
H3'	0.092(2)	0.015(2)	0.819(3)	6.3(9)*
H4'	0.073(2)	-0.080(2)	0.998(3)	4.5(7)*
H4	0.713(2)	0.617(2)	0.079(3)	5.7(9)*
H6'	0.376(2)	0.054(2)	1.162(3)	4.3(7)*
H6	0.887(2)	0.642(2)	0.455(3)	4.7(8)*
H10	0.593(2)	0.310(2)	0.749(3)	2.9(6)*
H12	0.883(2)	0.671(2)	0.778(3)	5.4(8)*
H12'	0.527(2)	0.269(2)	1.270(3)	3.9(7)*
H13'	0.654(2)	0.279(2)	1.437(3)	5.9(9)*
H13	1.032(2)	0.704(2)	0.898(3)	5.3(8)*
H15'	0.713(2)	0.107(2)	1.151(3)	6.0(9)*
H15	1.027(3)	0.460(3)	0.681(4)	10(1)*
H16	0.875(2)	0.441(2)	0.555(3)	4.5(7)*
H16'	0.580(2)	0.099(2)	0.995(3)	2.7(6)*
H19	0.150(2)	0.152(2)	0.227(3)	5.4(8)*
H81'	0.257(4)	-0.055(4)	1.302(6)	16(2)*
H81	0.915(3)	0.784(4)	0.210(5)	12(2)*
H82'	0.170(4)	-0.082(4)	1.249(6)	16(2)*
H82	0.922(4)	0.679(4)	0.141(5)	12(2)*
H83'	0.162(3)	-0.155(3)	1.177(5)	12(2)*
H83	0.973(3)	0.732(3)	0.266(4)	9(1)*
H91	0.743(2)	0.478(2)	0.821(3)	4.6(8)*
H91'	0.614(2)	0.342(2)	0.997(3)	4.8(8)*
H92'	0.612(3)	0.259(3)	0.879(4)	9(1)*
H92	0.717(1)	0.381(3)	0.735(4)	10(1)*
H171	1.142(3)	0.554(4)	0.964(5)	13(2)*
H171'	0.864(4)	0.246(4)	1.411(6)	16(1)*
H172'	0.800(3)	0.137(3)	1.421(5)	10(1)*
H172	1.181(3)	0.663(4)	0.961(5)	14(2)*
H173	1.185(4)	0.603(4)	0.849(6)	13(2)*
H173'	0.789(3)	0.215(3)	1.509(4)	8(1)*
H211	0.145(3)	0.026(3)	0.523(4)	10(1)*
H212	0.068(3)	0.034(4)	0.402(5)	12(1)*
H213	0.092(3)	0.105(4)	0.552(5)	12(2)*
H221	0.340(2)	0.390(3)	0.189(4)	8(1)*
H222	0.395(2)	0.327(2)	0.161(4)	7(1)*
H223	0.280(2)	0.288(3)	0.108(4)	7(1)*

Starred atoms are refined isotropically.

Anisotropically refined atoms are given in the form of the isotropic equivalent thermal parameter defined:

$$(4/3) * [a^2 * B(1,1) + b^2 * B(2,2) + c^2 * B(3,3) + ab(\cos \gamma) * B(1,2) + ac(\cos \beta) * B(1,3) + bc(\cos \alpha) * B(2,3)]$$

## 13.3.4: Table of Bond Distances in Å

Atom 1	Atom 2	Distance	Atom 1	Atom 2	Distance	Atom 1	Atom 2	Distance
Cu 1	O	1.890(2)	C4	C5	1.384(5)	C12	H12	0.82(3)
Cu 1	O1	1.897(2)	C4	H4	0.89(3)	C13'	C14'	1.377(5)
Cu 1	N1	1.988(2)	C4'	C5'	1.386(5)	C13'	H13'	0.96(4)
Cu 1	N3	1.999(2)	C4'	H4'	0.87(3)	C13	C14	1.364(6)
Cu 2	O	1.885(2)	C5	C6	1.372(4)	C13	H13	0.79(4)
Cu 2	O2	1.870(2)	C5	C8	1.514(5)	C14	C15	1.356(6)
Cu 2	N2	1.979(2)	C5'	C6'	1.372(4)	C14	C17	1.516(5)
Cu 2	N4	1.984(2)	C5'	C8'	1.521(6)	C14'	C15'	1.360(5)
O	C10	1.390(4)	C6	H6	0.94(3)	C14'	C17'	1.520(5)
OW1	OW4	0.97(7)	C6'	H6'	0.89(3)	C15'	C16'	1.389(4)
O1	C2	1.313(3)	C7	C11	1.501(3)	C15'	H15'	0.87(4)
O2	C2'	1.311(3)	C7'	C11'	1.507(4)	C15'	C16	1.386(5)
OW2	OW3	1.59(5)	C8'	H81'	0.96(7)	C15'	H15	0.97(5)
N1	C7	1.291(3)	C8'	H82'	0.72(7)	C16	H16	0.84(3)
N1	C9	1.484(3)	C8'	H83'	0.84(6)	C16'	H16'	0.83(3)
N2	C7'	1.294(3)	C8	H81	0.95(6)	C17'	H171'	1.00(6+)
N2	C9'	1.473(3)	C8	H82	0.97(6)	C17'	H172'	0.91(5)
N3	N4	1.398(3)	C8	H83	0.80(5)	C17'	H173'	0.84(5)
N3	C20	1.345(3)	C9'	C10	1.507(4)	C17	H171	0.93(6)
N4	C18	1.347(4)	C9'	H91'	0.95(3)	C17	H172	0.83(6)
C1	C2	1.422(4)	C9'	H92'	0.96(4)	C17	H173	0.76(7)
C1	C6	1.418(4)	C9	C10	1.493(4)	C18	C19	1.363(5)
C1	C7	1.458(3)	C9	H91	0.92(3)	C18	C21	1.512(5)
C1'	C2'	1.425(4)	C9	H92	0.95(5)	C19	C20	1.374(4)
C1'	C6'	1.414(4)	C10	H10	1.10(3)	C19	H19	0.91(3)
C1'	C7'	1.457(4)	C11	C12	1.357(5)	C20	C22	1.495(4)
C2'	C3'	1.409(4)	C11	C16	1.357(5)	C21	H211	0.96(5)
C2	C3	1.415(4)	C11'	C12'	1.370(5)	C21	H212	1.01(5)
C3'	C4'	1.358(5)	C11'	C16'	1.372(4)	C21	H213	1.02(6)
C3'	H3'	0.97(4)	C12'	C13'	1.390(5)	C22	H221	1.01(4)
C3	C4	1.374(4)	C12'	H12'	0.88(3)	C22	H222	0.945(4)
C3	H3	0.95(3)	C12	C13	1.394(5)	C22	H223	0.88(4)

Numbers in parentheses are estimated standard deviations in the least significant digits.

13.3.5: Table of Bond Angles in Degrees

Atom 1	Atom 2	Atom 3	Angle	Atom 1	Atom 2	Atom 3	Angle
O	Cu1	O1	174.85(7)	C4'	C5'	C8'	121.9(4)
O	Cu1	N1	83.42(8)	C6'	C5'	C8'	120.8(4)
O	Cu1	N3	86.03(8)	C1	C6	C5	123.6(3)
O1	Cu1	N1	91.46(8)	C1	C6	H6	118.(2)
O1	Cu1	N3	98.86(8)	C5	C6	H6	119.(2)
N1	Cu1	N3	164.03(9)	C1'	C6'	C5'	123.8(3)
O	Cu2	O2	172.8(1)	C1'	C6'	H6'	115.(2)
O	Cu2	N2	83.77(8)	C5'	C6'	H6'	121.(2)
O	Cu2	N4	86.04(8)	N1	C7	C1	122.3(2)
O2	Cu2	N2	91.61(9)	N1	C7	C11	119.0(2)
O2	Cu2	N4	99.40(9)	C1	C7	C11	118.5(2)
N2	Cu2	N4	166.0(1)	N2	C7'	C1'	121.9(2)
Cu1	O	CU2	126.54(9)	N2	C7'	C11'	119.3(2)
Cu1	O	C10	114.0(2)	C1'	C7'	C11'	118.9(2)
Cu2	O	C10	114.8(2)	C5'	C8'	H81'	110.(4)
Cu1	O1	C2	127.4(2)	C5'	C8'	H82'	103.(7)
Cu2	O2	C2'	128.5(2)	C5'	C8'	H83'	109.(4)
Cu1	N1	C7	128.6(2)	H81'	C8'	H82'	86.(7)
Cu1	N1	C9	111.4(2)	H81'	C8'	H83'	139.(6)
C7	N1	C9	119.6(2)	H82'	C8'	H83'	96.(6)
Cu2	N2	C7'	128.1(2)	C5	C8	H81	112.(4)
Cu2	N2	C9'	111.3(2)	C5	C8	H82	104.(4)
C7'	N2	C9'	120.1(2)	C5	C8	H83	120.(3)
Cu1	N3	N4	119.0(2)	H81	C8	H82	120.(5)
Cu1	N3	C20	133.7(2)	H81	C8	H83	109.(5)
N4	N3	C20	107.3(2)	H82	C8	H83	92.(5)
Cu2	N4	N3	120.4(2)	N2	C9'	C10	109.3(2)
Cu2	N4	C18	132.2(2)	N2	C9'	H91'	109.(2)
C12'	C13'	H13'	115.(2)	C14	C15	C16	120.8(4)
C14'	C13'	H13'	124.(2)	C14	C15	H15	122.(3)
C12	C13	C14	121.3(4)	C16	C15	H15	117.(3)
C12	C13	H13	111.(3)	C11	C16	C15	122.0(4)
C14	C13	H13	128.(3)	C11	C16	H16	120.(2)
C13	C14	C15	117.6(3)	C15	C16	H16	117.(2)
C13	C14	C17	122.0(6)	C11'	C16'	C15'	121.0(4)
C15	C14	C17	120.4(6)	C11'	C16'	H16'	118.(2)
C13'	C14'	C15'	117.6(3)	C15'	C16'	H16'	121.(2)
C13'	C14'	C17'	121.6(4)	C14'	C17'	H171'	112.(4)
C15'	C14'	C17'	120.8(4)	C14'	C17'	H172'	113.(3)
C14'	C15'	C16'	121.5(4)	C14'	C17'	H173'	110.(4)
C14'	C15'	H15'	123.(3)	H171'	C17'	H172'	102.(5)
C16'	C15'	H15'	115.(3)	H171'	C17'	H173'	111.(5)

## 13.3.5: Table of Bond Angles in Degrees (continued)

Atom 1	Atom 2	Atom 3	Angle	Atom 1	Atom 2	Atom 3	Angle
N3	N4	C18	107.2(2)	N2	C9'	H92'	104.(3)
C2	C1	C6	118.1(3)	C10	C9'	H91'	110.(2)
C2	C1	C7	123.1(2)	C10	C9'	H92'	113.(3)
C6	C1	C7	118.8(2)	H91'	C9'	H92'	111.(3)
C2'	C1'	C6'	117.4(3)	N1	C9	C10	108.6(2)
C2'	C1'	C7'	123.3(2)	N1	C9	H91	111.(2)
C6'	C1'	C7'	119.3(3)	N1	C9	H92	104.(3)
O2	C2'	C1'	124.8(2)	C10	C9	H91	118.(2)
O2	C2'	C3'	117.6(3)	C10	C9	H92	115.(3)
C1'	C2'	C3'	117.7(3)	H91	C9	H92	100.(3)
O1	C2	C1	125.3(2)	O	C10	C9'	109.3(3)
O1	C2	C3	117.5(2)	O	C10	C9	110.3(3)
C1	C2	C3	117.2(3)	O	C10	H10	71.(2)
C2'	C3'	C4'	122.1(3)	C9'	C10	C9	115.4(3)
C2'	C3'	H3'	116.(2)	C9'	C10	H10	70.(2)
C4'	C3'	H3'	122.(2)	C9	C10	H10	77.(2)
C2	C3	C4	121.6(3)	C7	C11	C12	122.9(3)
C2	C3	H3	115.(2)	C7	C11	C16	119.6(3)
C4	C3	H3	123.(2)	C12	C11	C16	117.4(3)
C3	C4	C5	122.0(3)	C7'	C11'	C12'	122.4(3)
C3	C4	H4	116.(2)	C7'	C11'	C16'	119.7(3)
C5	C4	H4	121.(2)	C12'	C11'	C16'	117.9(3)
C3'	C4'	C5'	121.7(3)	C11'	C12'	C13'	120.8(4)
C3'	C4'	H4'	119.(2)	C11'	C12'	H12'	124.(2)
C5'	C4'	H4'	119.(2)	C13'	C12'	H12'	115.(2)
C4	C5	C6	117.2(3)	C11	C12	C13	120.9(4)
C4	C5	C8	120.9(4)	C11	C12	H12	119.(3)
C6	C5	C8	121.9(4)	C13	C12	H12	120.(3)
C4'	C5'	C6'	117.4(3)	C12'	C13'	C14'	121.2(4)
H172'	C17'	H173'	110.(5)	N3	C20	C22	124.4(3)
C14	C17	H171	107.(4)	C19	C20	C22	126.3(3)
C14	C17	H172	106.(5)	C18	C21	H211	115.(3)
C14	C17	H173	99.(6)	C18	C21	H212	108.(3)
H171	C17	H172	110.(6)	C18	C21	H213	114.(3)
H171	C17	H173	119.(8)	H211	C21	H212	101.(4)
H172	C17	H173	115.(8)	H211	C21	H213	114.(4)
N4	C18	C19	109.5(3)	H212	C21	H213	104.(4)
N4	C18	C21	123.1(3)	C20	C22	H221	119.(2)
C19	C18	C21	127.3(3)	C20	C22	H222	119.(2)
C18	C19	C20	106.7(3)	C20	C22	H223	110.(3)
C18	C19	H19	127.(2)	H221	C22	H222	99.(3)
C20	C19	H19	127.(2)	H221	C22	H223	98.(3)
N3	C20	C19	109.3(3)	H222	C22	H223	109.(4)

Numbers in parentheses are estimated standard deviations in the least significant digits.

**14:**

## **References**

1. Lerch,K; Huber,M; Schneider,H.J; Drexel,R; and Linzen,B; Inorg.Chem; 1986; 26; 213.
2. Ochiai,E.I; 'Bioinorganic Chemistry: An Introduction'; Allyn and Bacon; 1977; Boston.
3. Hughes,M.N; 'The Inorganic Chemistry of Biological Processes; 2nd edition; John Wiley and Sons; 1972; New York.
4. McAuliffe,C.A; 'Inorganic Biochemistry,' Vol 1; Hill,H.A.O. (ed); The Chemical Society; London; 1979.
5. Solomon,E.I; 'Metal Ions in Biology,' Vol 3; Spiro,T.G. (ed); Wiley Interscience; 1981; New York.
6. Lontie,R; and Witters,R; Met.Ions.Biol.Syst; 1981; 13; 229.
7. Solomon,E.I; 'Copper Coordination Chemistry: Biochemical and Inorganic Perspectives'; Karlin,K.D. and Zubieta,J. (eds); Adenine Press; 1983; New York.
8. Gultneh,Y; and Karlin,K.D; J.Chem.Ed; 1985; 62; 983.
9. Hanzlik, R.P; 'Inorganic Aspects of Biological and Organic Chemistry'; Academic Press; 1976; New York.
10. Vannegard,T; in Fee,J.A; in 'Structure and Bonding, Vol 23'; Junitz,J.D. (ed); Springer-Verlag; Berlin; 1979.
11. Coleman,P.J; Freeman,H.C; Guss,J.M; Murata,M; Norris,V; Ramshaw,A; and Venkatappa,M.P; Nature; 1978; 272; 319.

- 12a. Mockler,G.M; MSc Lecture Notes; University of Wollongong; 1992.
- b. Beinert,H; Nature; 1991; 350; 87-90.
13. Brunori,M; Giardina,B; and Bannister,J.V; 'Oxygen Transport Proteins' in 'Inorganic Biochemistry, Vol 1'; Hill,H.A.O. (ed); The Chemical Society; 1979; London.
14. Harless,E; Arch.Anat.Physiol; 1847; 148.
15. Fredericq,L; Compt.Rend.Acad.Sci.Paris; 1878; 87; 996.
16. Niederhoffer,E.C; Timmons,J.H; and Martell,A.E; Chem.Rev; 1984; 84; 137.
17. Lontie,R; and Witters,R; Inorganic Biochemistry, Vol 1'; Eichorn,G.L. (ed); Elsevier; 1973; Amsterdam.
18. Senozan,N.M; J.Chem.Ed; 1976; 53; 684.
19. Himmelwright,R.S., Eickman,N.C., LuBien,C.D., and Solomon,E.I.; J.Am.Chem.Soc., 1980, 102, 5378.
20. Bertrand,G; C.R.Acad.Sci.Paris; 1896; 122' 1215.
21. Robb,D.A; 'Tyrosinase' in 'Copper Proteins and Copper Enzymes, Vol II; Lontie,R. (ed); C.R.C.Press; 1984; Boca Raton.

22. Hackman,R.H; 'The Physiology of the Insecta,' Vol 6; 2nd edition; Rockstein,M. (ed); Academic Press; 1974; New York.
23. Crouch,R.K; Kersler,T.W; Oberley,L.W; and Sorenson,J.R.J; 'Biological and Inorganic Copper Chemistry,' Vol 1; Karlin,K.D., and Zubieta,J. (eds); Adenine Press; 1985; New York.
24. Loehr,T.M; and Sanders-Loehr,J; 'Structural Information on Copper Proteins from Resonance Raman Spectroscopy' in 'Copper Proteins and Copper Enzymes,' Vol 1; Ch 5, Lontie, R. (ed); C.R.C. Press; 1984; Boca Raton.
25. Himmelwright,R.S; Eickman,N.C; LuBien,C.D; Lerch,K; and Solomon,E.I; J.Am.Chem.Soc; 1980; 102; 7339.
26. Hay,R.W; 'Bioinorganic Chemistry'; John Wiley and Sons; Chichester; 1984.
27. Morie-Bebel, M.M; Menzie,J.L; and McMillin,D.R; 'Biological and Inorganic Copper Chemistry, Vol 1'; Karlin,K.D. and Zubieta,J. (eds); Adenine Press; 1985; New York.
- 28a. Himmelwright,R.S; Eickman,N.C; and Solomon,E.I; Biochem.Biophys.Res.Comm; 1978; 81; 243.
- b. Himmelwright,R.S; Eickman,N.C; and Solomon,E.I; J.Am.Chem.Soc; 1979; 101; 1576.
- c. Eickman,N.C; Himmelwright,R.S; and Solomon,E.I; Proc.Natl.Acad.Sci,U.S.A; 1979; 76; 2094.



- 29a. Suzuki,S; Mori,W; Kino,J; and Nakahara,A; J.Biochem; 1980; 88; 207.
  - b. Suzuki,S; Kino,J; Kimura,M; Mori,W; and Nakahara,A; Inorg.Chimica.Acta; 1982; 66; 41.
  - c. Suzuki,S; Kino,J; and Nakahara,A; Bull.Chem.Soc.Jap; 1982; 55; 212.
  - d. Mori,W; Suzuki,S; Kimura,M; Yamauchi,O; and Nakahara,A; J.Inorg.Biochem; 1980; 12; 179.
- 
- 30a. DeLey,M; and Lontie,R; Biochim.Biophys.Acta; 1972; 278; 404.
  - b. Lontie,R; Blaton,V; Albert,M; and Peeters,B; Arch.Int.Physiol.Biochim; 1965; 73; 150.
  - c. Witters,R; Groeseneken,D; Jacobs,P; and Lontie,R; J.Inorg.Biochem; 1982; 16; 273.
- 
31. Salvato,B., Beltramini,M., Ruchelli,F., and Tallandini,L.; 'Invertebrate Oxygen Binding Proteins: Structure, Active Site, and Function', Lamy,J., and Lamy,J. (eds), Marcel Dekker, New York, 1981.
  32. Sorell,T.N., and Jameson,D.L.; J.Am.Chem.Soc., 1982, 104, 2053.
  33. Brunori,M., Zolla,L., Kuiper,H.A., and Finazzi-Agro,A.; J.Mol.Biol., 1981, 153, 1111.
  34. Bonnaventura,C., Sullivan,B., Bonnaventura,J., and Bourne,S.; Biochemistry, 1974, 13, 4784.
  35. Wood,E.J., Nature, 1979, 281, 341.
  36. Mori,W; Yamauchi,O; Nakao,Y; and Nakahra,A; Biochem.Biophys.Res.Communi; 1975; 66; 725.

37. Nickerson,K.W; and Van Holde,K.E; Comp.Biochem.Physiol; 1971; 39B; 855.
38. Schoot-Viterkamp,A.J.M; F.E.B.S.Lett; 1973; 20; 93.
39. Schoot-Viterkamp,A.J.M; and Mason,H.S; Proc.Natl.Acad.Sci.U.S.A; 1973; 70; 999.
40. Larrabee,J.A; and Spiro,T.G; J.Am.Chem.Soc; 1980; 102; 4217.
41. Kirchner,R.F; and Loew,G.H; J.Am.Chem.Soc; 1977; 99; 4639.
- 42a. Loehr,J.S; Freedman,T.B; and Loehr,Th.M; Biochem.Biophys.Res.Comm; 1974; 56; 510.
- b. Thamman,T.J; Loehr,J.S; and Loehr,Th.M; J.Am.Chem.Soc; 1974; 99; 4187.
- 43a. Solomon,E.I; Dooley,D.M; Wong,R.H; Gray,H.B; Cerdino,M; Mogno,F; and Romani,R.L; J.Am.Chem.Soc; 1976; 98; 1029.
- b. Dooley,D.M; Scott,R.A; Elkinghaus,R.S; Solomon,E.I; and Gray,H.B; Proc.Natl.Acad.Sci; U.S.A; 1978; 75; 3019.
- 44a. Van Schiack,E.J.M; Schutter,W.G; Gaykema,W.P.J; Schepman,A.M.H; and Hol,W.G.J; J.Mol.Biol; 1982; 158; 457.
- b. Gaykema,W.P.J; Hol,W.G.J; Verijken,J.M; Soeter,N.M; Bak,H.J; and Beintema,J.G; Nature; 1984; 309; 23.

- 45a. Magnus,K.A; and Love,W.E; Life.Chem.Reports; Supp 1; 1983; 61.
- b. Fearon,E.R; Love,W.E; Magnus,K.A; Lamy,J; and Lamy,J; Life.Chem.Reports; Supp 1; 1983; 65.
46. Brown,J.M; Powers,L; Kincaid,B; Larrabee,J.A; and Spiro,T.G; J.Am.Chem.Soc; 1980; 102; 4210.
- 47a. Co,M.S; Hodgson,K.O; Eccles,T.K; and Lontie,R; J.Am.Chem.Soc; 1981; 103; 984.
- b. Co,M.S; Scott,R.A; and Hodgson,K.O; J.Am.Chem.Soc; 1981; 103; 986.
- c. Co,M.S; and Hodgson,K.O; J.Am.Chem.Soc; 1981; 103; 3200.
- 48a. Wood,E.J; 'Structure and Functioning of Hemocyanin'; Bannister,J.V.(ed); Springer-Verlag; Berlin; 1977.
- b. Wood,E.J; and Mosby,L.J; Biochem.Soc.Trans; 1977; 5; 694.
49. Lerch,K; Huber,M; Schneider,H.J; Drexel,R; and Linzen,B; J.Inorg.Biochem; 1986; 26; 213.
50. Wibo,M; Masters Thesis; University of Lauvain; Belgium; 1966.
51. Van Bruggen,E.F.J; Schuiter,V; Wiebenga,E.H; and Gruber,M; J.Mol.Biol; 1963; 7; 249.
52. Van Breeman,J.F.L; Schuurhuis,G.J; and Van Bruggen,E.F.J; 'Structure and Functioning of Hemocyanin'; Bannister,J.V. (ed); Springer-Verlag; Berlin; 1977.
53. Mellema,J.E; and Klug,A; Nature; 1972; 239; 146.

54. Solomon,E.I; Penfield,K.W; and Wilcox,D.E; 'Structure and Bonding,' Vol 53; Clarke,M.J. (ed); Springer-Verlag; Berlin; 1983.
55. Messerschmidt,A; Rossi,A; Laderstein,R; Huber,R; Bolognesi,M; Gatti,G; Machesini,A; Petruzzelli,R; and Finazzi-Agro,A; J.Mol.Biol; 1989; 206; 513.
56. Cole,J.L; Ballou,D.P.; and Solomon,E.I; J.Am.Chem.Soc; 1991; 113; 8544.
57. Ibers,J.A; and Holm,R.H; Science; 1980; 209; 223.
- 58a. Karlin,K.D; Shi,J; Hayes,J.C; KcKown,J.W; Hutchinson,J.P; and Zubieta,J; Inorg.Chimica.Acta; 1984; 91; L3.
- b. Karlin,K.D; Haka,M.S; Cruse,R.W; and Gultneh,Y; J.Am.Chem.Soc; 1985; 107; 5828.
- 59a. Karlin,K.D; Haka,M.S; Cruse,R.W; Meyer,G.J; Farooq,A; Gultneh,Y; Hayes,J.C; and Zubieta,J; J.Am.Chem.Soc; 1988; 110; 1196.
- b. Blackburn,N.J; Strange,R.W; Farooq,A; Haka,M.S; and Karlin,K.D; J.Am.Chem.Soc; 1988; 110; 4263.
60. Tyeklar,Z; Paul,P.P; Jacobson,R.R; Farooq,A; Karlin,K.D; and Zubieta,J; J.Am.Chem.Soc; 1989; 111; 388.
61. Wilcox, D.E; Long, J.R; and Solomon, E.I; J.Am.Chem.Soc; 1984; 106; 2186.
62. Karlin,K.D; Hayes,J.C; Juen,S; Hutchinson,J.P; and Zubieta,J; Inorg.Chem; 1982; 21; 4106.

63. Zubieta,J; Karlin,K.D; and Hayes,J.C; 'Copper Coordination Chemistry: Biological and Inorganic Perspectives,' Ch5; Karlin,K.D. and Zubieta,J. (eds); Adenine Press; New York; 1983.
64. Karlin,K.D; Gultneh,Y; Hayes,J.C; and Zubieta,J; Inorg.Chem; 1984; 23; 519.
65. Jacobson,R.R; Tyeklar,Z; Farooq,A; Karlin,K.D; Liu,S; and Zubieta,J; J.Am.Chem.Soc; 1988; 110; 3690.
- 66a. Thompson, J. S; J.Am.Chem.Soc; 1984; 106; 4057.
- b. Thompson, J. S; J.Am.Chem.Soc; 1984; 106; 8308.
67. Kitajima,N; Koda,T; Hashimoto,S; Kitagawa,T; and Moro-oka,Y; J.Chem.Soc.Chem.Commun; 1988; 151.
68. Robson,R; Inorg.Nucl.Chem.Lett; 1970; 6; 125.
69. Robson,R; Aust.J.Chem; 1970; 23; 2217.
70. Hoskins, B.F; Robson,R; Schaap,H; Inorg.Nucl.Chem.Lett; 1972; 8; 21.
71. McFayden,W.D; Robson,R; and Schaap,H; Inorg.Chem; 1972; 11; 1777.
72. Dickson,I.E; and Robson,R; Inorg.Chem; 1974; 13; 1301.
73. McFayden,W.D; and Robson,R; J.Coord.Chem; 1976; 5; 49.

74. Robson,R; Williams,G.A; and Hoskins,B.F; *Inorg.Chimica.Acta*; 1976; 10; 121.
75. Sorrell,T.N; Malachowski,M.R; and Jameson,D.L; *Inorg.Chem*; 1982; 21; 3250.
76. Sorrell,T.N; Jameson,D.L; and O'Connor,C.J; *Inorg.Chem*; 1984; 23; 190.
77. Sorrell,T.N; and Borowik,A.S; *J.Chem.Soc.Chem.Commun*; 1984; 1489.
78. Sorrell,T.N; O'Connor,C.J; Anderson,O.P; and Reibenspies,J.H; *J.Am.Chem.Soc*; 1985; 107; 4199.
- 79a. Sorrell,T.N; Shen,C.C; and O'Connor,C.J; *Inorg.Chem*; 1987; 26; 1755.
- b. Sorrell,T.N; and Vankai,V.A; *Inorg Chem*; 1990; 29; 1687.
- c. Sorrell,T.N; Vankai,V.A; and Garrity,M.L; *Inorg Chem*; 1991; 30; 207.
- d. Sorrell,T.N; and Garrity,M.L; *Inorg Chem*; 1991; 30; 210.
80. Eduok,E.E; and O'Connor,C.J; *Inorg.Chimica.Acta*; 1984; 88; 229.
81. O'Connor,C.J; Firmin,D; Pant,A.K; Babu,B.R; and Stevens,E.D; *Inorg.Chem*; 1986; 25; 2300.
82. Karlin,K.D; Gultneh,Y; Hutchinson,J.P; and Zubieta,J; *J.Am.Chem.Soc*; 1982; 104; 5240.
83. Karlin,K.D; Hayes,J.C; and Zubieta,J; 'Copper Coordination Chemistry: Biochemical and Inorganic Perspectives,' Ch22; Karlin,K.D., and Zubieta,J. (eds); Adenine Press; New York; 1983.

84. Karlin,K.D; Hayes,J.C; Hutchinson,J.P; and Zubieta,J; J.Chem.Soc.Chem.Commun; 1983; 376.
85. Karlin,K.D; Hayes,J.C; Hutchinson,J.P; and Zubieta,J; Inorg.Chimica.Acta; 1983; 78; L45.
86. Karlin,K.D; Hayes,J.C; Gultneh,Y; Cruse,R.W; KcKown,J.W; Hutchinson,J.P; and Zubieta,J; J.Am.Chem.Soc; 1984; 106; 2121.
87. Karlin,K.D; Cruse,R.W; Gultneh,Y; Hayes,J.C; and Zubieta,J; J.Am.Chem.Soc; 1984; 106; 3372.
88. Pynz,J.W; Karlin,K.D; Sorrell,T.N; Vogel,J.C; and Que,L; Inorg.Chem; 1984; 23; 4581.
89. Karlin,K.D; Gultneh,Y; Nicholson,T; and Zubieta,J; Inorg.Chem; 1985; 24; 3725.
90. Karlin,K.D; Cruse,R.W; Haka,M.S; Gultneh,Y; and Cohen,B.I; Inorg.Chimica.Acta; 1986; 125; L43.
91. Karlin,K.D; Cohen,B.I; Hayes,J.C; Farooq,A; and Zubieta,J; Inorg.Chem; 1987; 26; 147.
92. Karlin,K.D; Farooq,A; Hayes,J.C; Cohen,B.I; Rowe,T.M; Sinn,E; and Zubieta,J; Inorg.Chem; 1987; 26; 1271.
93. Blackburn,N.J; Strange,R.W; Cruse,R.W; and Karlin,K.D; J.Am.Chem.Soc; 1987; 109; 1235.
94. Karlin,K.D; Cruse,R.W; Gultneh,Y; Fraooq,A; Hayes,J.C; and Zubieta,J; J.Am.Chem.Soc; 1987; 109; 2668.
95. Pate,J.E; Cruse,R.W; Karlin,K.D; and Soloman,E.I; J.Am.Chem.Soc; 1987; 109; 2624.

96. Cruse,R.W; Kaderli,S; Meyer,C.J; Zuberbuhler,A.D; and Karlin,K.D; J.Am.Chem.Soc; 1988; 110; 5020.
97. Karlin,K.D; Farooq,A; Gultneh,Y; Hayes,J.C; and Zubieta,J; Inorg.Chimica.Acta; 1988; 153; 73.
- 98a. Karlin,K.D; Ghosh,P; Cruse,R.W; Farooq,A; Gultneh,Y; Jacobson,R.R; Blackburn,N.J; Strange,R.W; and Zubieta,J; J.Am.Chem.Soc; 1988; 110; 6769.
- b. Nasir,M.S; Karlin,K.D; McGaurty,D; and Zubieta,J; J.Am.Chem.Soc; 1991; 113; 698.
99. Ghosh,P; Tyeklar,Z; Karlin,K.D; Jacobson,R.R; and Zubieta,J; J.Am.Chem.Soc; 1987; 109; 6889.
100. Karlin,K.D; Cruse,R.W; and Gultneh,Y; J.Chem.Soc.Chem.Comm; 1987; 599.
101. Casella,L; and Rigoni,L; J.Chem.Soc.Chem.Comm; 1985; 1668.
102. Casella,L; Gullotti,M; and Pallanza,G; Biochem.Soc.Trans; 1988; 16; 821.
103. Casella,L; Gullotti,M; Pallanza,G and Rigoni,L; J.Am.Chem.Soc; 1988; 110; 4221.
104. Casella,L; Gullotti,M; Bartosek,M; Pallanza,G; and Laurenti,E; J.Chem.Soc.Chem.Comm; 1991; 1235.
- 105a. Nishida,Y; Shimo,H; Machara,H; and Kida,S; J.Chem.Soc.Dalton.Trans; 1985; 1945.
- 105b. Suzuki,M; Kanatomi,H; Demura,Y; and Murase,I; J.Bull.Chem.Soc.Jpn; 1984; 57; 1003.
106. McKee,V; Dadigan,J.V; Bau,R; and Reed,C.A; J.Am.Chem.Soc; 1981; 103; 7000.



- 107a. McKee,V; Zvagulis,M; and Reed,C.A; Inorg.Chem; 1985; 24; 2914.
- b. Patch,M.G; Choi,H; Chapman,D.R; Bau,R; McKee,V; and Reed,C.A; Inorg.Chem; 1990; 29; 110.
108. Nishida,Y; Takeuchi,M; Takahashi,K; and Kida,S; Chem.Soc.Jpn.Chem.Lett; 1983; 1815.
109. Nishida,Y; Takeuchi,M; Takahashi,K; and Kida,S; Chem.Soc.Jpn.Chem.Lett; 1985; 631.
110. Nishida,Y; and Kida,S; J.Chem.Soc.Dalton.Trans; 1986; 2633.
111. Nishida,Y; and Kida,S; Inorg.Chem; 1988; 27; 447.
112. Mazurek,W; Berry,K.J; Murray,K.S; O'Connor,M.J; Snow,M.R; and Wedd,A.G; Inorg.Chem; 1982; 21; 3071.
113. Fallon,G.D; Murray,K.S; Mazurek,W; and O'Connor,M.J; Inorg.Chimica.Acta; 1985; 96; L53.
114. Mazurek,W; Kennedy,B.J; Murray,K.S; O'Connor,M.J; Rodgers,J.R; Snow,M.R; Wedd,A.G; and Zwack,P.R; Inorg.Chem; 1985; 24; 3258.
115. Boge,E.M; Freyberg,D.P; Kokot,E; Mockler,G.M; and Sinn,E; Inorg.Chem; 1977; 16; 1655.
116. Erickson,G.R; Honours Thesis; 1982; Wollongong University.
117. Diven,G.W; Honours Thesis; 1983; Wollongong University.
118. Butcher,R.J; Diven,G.W; Erickson,G.R; Mockler,G.M; and Sinn,E; Inorg.Chimica.Acta; 1986; 111; L55.

119. Butcher,R.J; Diven,G.W; Erickson,G.R; Mockler,G.M; and Sinn,E; *Inorg.Chimica.Acta.B*; 1986; 123; B15; L17.
120. Erickson,G.R; PhD Thesis; 1987; Wollongong University.
121. Adams,H; Bailey,N.A; Dwyer,M.J.S; Fenton,D.E; Hellier,P.C; and Hempstead,P.D; *J.Chem.Soc.Chem.Commun*; 1991; 1297.
- 122a. Karlin,K.D; Gan,Q; Farooq,A; Lui,S; and Zubieta,J; *Inorg.Chimica.Acta*; 1989; 165; 37.
- b. Karlin,K.D; Gan,Q; Farooq,A; Lui,S; and Zubieta,J; *Inorg.Chem*; 1990; 29; 2551.
123. Werakso,S; Honours Thesis; 1988; Wollongong University.
- 124a. Sharma,P; and Vigee,G.S; *Inorg.Chimica.Acta*; 1984; 88; 139.
- b. Bolus,D; and Vigee,G.S; *Inorg.Chimica.Acta*; 1982; 67; 19.
- c. Moore,K; and Vigee,G.S; *Inorg.Chimica.Acta*; 1982; 66; 125.
125. Davies,G; El-Sayed,M.A; and Henary,M; *Inorg.Chem*; 1987; 26; 3266.
126. Cabras,M.A; and Zorodda,M.A; *Inorg.Chimica.Acta*; 1987; 139; L19.
127. Thompson,J.S; and Calabrese,J.C; *J.Am.Chem.Soc*; 1986; 108; 1903.
128. Casella,L; Gullotti,M; Radaelli,R; and Di Gennaro,P; *J.Chem.Soc.Chem.Commun*; 1991; 1611.

129. Grzybowski,J.J; Merrell,P.H; and Urbach,F.L; Inorg.Chem; 1978; 17; 3078.
130. Gagne,R.R; Kreh,R.P; and Dodge,J.A; J.Am.Chem.Soc; 1979; 10; 6917.
131. Li,N.C; Tzou,J.R; Chen,S.W; Wang,S.M; Chou,Y.C; Liang,N.T; and Lin,H.J; Inorg.Chimica.Acta; 1987; 138; 121.
- 132a. Mazurek,W; Bond,A.M; Murray,K.S; O'Connor,M.J; and Wedd,A.G; Inorg.Chem; 1985; 24; 2484.
- b. Mazurek,W; Bond,A.M; O'Connor,M.J; and Wedd,A.G; Inorg.Chem; 1986; 25; 906.
- c. Bond,A.M; Haga,M; Creece,I.S; Robson,R; and Wilson,J.C; Inorg.Chem; 1989; 28; 559.
133. Nakamoto,K; 'Infrared and Raman Spectra of Inorganic and Coordination Compounds', (4th ed); Wiley Interscience; U.S.A; 1986.
134. Lever,A.P.B; 'Inorganic Electronic Spectroscopy', (2nd ed); 1984; Elsevier; Amsterdam.
135. Huheey,J.E; 'Inorganic Chemistry: Principles of Structure and Reactivity'; 1978; Harper and Row; New York.
136. Mockler,G.M; PhD Thesis; 1967; University of New South Wales.
137. Dooley,D.M; Rawlings,J; Dawson,J.H; Stephens,P.J; Andreasson,L.E; Malmstrom,B.G; and Gray,H.B; J.Am.Chem.Soc; 1979; 101; 5038.
138. Falk,K.E; and Reinhammar,B; Biochim.Biophys.Acta; 1972; 285; 84.

- 139a. Malkin,R; and Malmstrom,B.G; Adv.Enzymol; 1970; 33; 177.
- b. Solomon,E.I; Hare,J.W; and Gray,H.B; Biochim.Biophys.Acta; 1972; 285; 84.
140. Dawson,J.H; Dooley,D.M; Clark,R; Stephens,P.J; and Gray,H.B; J.Am.Chem.Soc; 1979; 101; 5046.
141. Herve,M; Garnier,A; Tosi,L; and Steinbuch,M; Biochem,Biophys.Res.Communi; 1978; 80; 797.
142. Avigliano,L; Davis,J.L; Graziani,M.T; Marchesini,A; Mims,W.B; Mardoui,B; and Peisach,J; F.E.B.S.Lett; 1981; 136; 80.
143. Dooley,D.M; Dawson,J.H; Stephens,P.J; and Gray,H.B; Biochemistry; 1981; 20; 2024.
144. Avigliano, L; Desideri,A; Urbanelli,S; Mondoli,B; and Marchesini,A; F.E.B.S.Lett; 1979; 100; 319.
145. Carlin,R; 'Magnetochemistry'; 1986; Springer-Verlag; Berlin.
146. Mabbs,F.E; and Machin,F.E; 'Magnetism and Transition Metal Complexes'; 1973; William Clowes and Sons Ltd; U.K.
147. Van Vleck,J.H; 'The Theory of Electric and Magnetic Susceptibilities'; 1932; Oxford University Press; Oxford.
148. Earnshaw,A; 'Introduction to Magnetochemistry'; 1968; Academic Press; London.
149. Bleaney,B; and Bowers,K.D; Proc.Roy.Soc; 1952; A214; 451.

150. Basch,D.H; and Cairns,C.J; Coord.Chem.Rev; 1986; 69; 1.
151. Crawford,V.H; Richardson,H.W; Wasson,J.R; Hodgson,D.J; and Hatfield , W.E; Inorg.Chem; 1976; 15; 2107.
- 152a. Charlot,M.F; Jeannin,S; Jeannin,Y; Kahn,O; Lucrece-Abaul,J; and Martin-Frere,J; Inorg.Chem; 1979; 18; 1675.
- b. Charlot,M.F; Kahn,O; Jeannin,Y; and Jeannin,S; Inorg.Chem; 1980; 19; 1410.
153. Bkouche-Waksman,I; Boillot,M.L; Kahn,O; and Sikorav,S; Inorg.Chem; 1984; 23; 4454.
154. Moss,T.H; and Vanngard,T; Biochim.Biophys.Acta; 1974; 371; 39.
155. Dooley,D.M; Scott,R.A; Ellinghaus,J; Soloman,E.I; and Gray,H.B; Proc.Natl.Acad.Sci.U.S.A; 1978; 75; 3019.
156. Peterson,L; Angstrom,J; and Ehrenberg,A; Biochim.Biophys.Acta; 1978; 526; 311.
- 157a. Hay,P.J; Thibeault,J.C; and Hoffman,R; J.Am.Chem.Soc; 1975; 97; 4884.
- b. Hay,P.J; Thibeault,J.C; and Hoffman,R; J.Am.Chem.Soc; 1981; 103; 7000.
158. Makino,N; McMahonill,P; Mason,H.S; and Moss,T.H; J.Biol.Chem; 1974; 249; 6062.
159. Fee,J.A; Malkim,R; Malstrom,B.G; and Vanngard,T; J.Biol.Chem; 1969; 244; 4200.

160. Malkin,R; Malmstrom,B.G; and Vanngard,T; Eur.J.Biochem; 1969; 10; 324.
161. Nakamura,T; Biochim.Biophys.Acta; 1958; 30; 44.
162. Reinhammar,B; 'Laccase' in 'Copper Proteins and Copper Enzymes,' Vol III;  
Lontie,R.(ed); C.R.C.Press; 1984; Boca Raton.
163. Reinhammar,B.R.M; Biochim.Biophys.Acta; 1972; 275; 245.
164. Reinhammar,B; and Malmstrom,B.G; 'Metal Ions in Biology', in 'Copper Proteins,'  
Vol 3; Spiro,T.G. (ed); John Wiley and Sons; 1981; New York.
165. Reinhammar,B; and Oda,Y; J.Inorg.Biochem; 1979; 11; 115.
166. Andreasson,L.-E; Branden,R; and Reinhammar,B; Biochim.Biophys.Acta; 1976; 438; 370.
167. Asa,R; Branden,R; Deinum,J; Malmstrom,B.G; Reinhammar,B; and Vanngard,T; F.E.B.S. Lett; 1976;  
61; 115.
168. Asa,R; Branden,R; Deinum,J; Malmstrom,B.G; Reinhammar,B; and Vanngard,T;  
Biochim.Biophys.Acta; 1976; 70; 1024.
169. Ryder,L; 'Ceruloplasmin', in 'Copper Proteins and Copper Enzymes,' Vol II;  
C.R.C.Press; 1984; Boca Raton.
170. Deinum,J; and Vanngard,T; Biochim.Biophys.Acta; 1973; 310; 321.

171. Mondovi,B; and Avigliano,L; 'Ascorbate Oxidase' in 'Copper Proteins and Copper Enzymes,' Vol II; C.R.C.Press; 1984; Boca Raton.
172. Armstrong,F; Merkle,H; Marchesini,A; and Kroneck,P; Cieni.Biol. (Portugal); 1980; 5; 91.
173. Greef,R; Peat,R; Peter,L.M; Pletcher,D; and Robinson,J; 'Instrumental Methods in Electrochemistry'; Kemp,T.J. (ed); John Wiley and Sons; 1985; Chichester.
174. Plambeck,J.A; 'Electroanalytical Chemistry: Basic Principles and Applications'; John Wiley and Sons; 1982; New York.
175. Galus,Z; 'Fundamentals of Electrochemical Analysis'; John Wiley and Sons; 1976; Poland.
176. Headridge,J.B; 'Electrochemical Techniques for Inorganic Chemists'; Academic Press; 1969; London.
177. Wilson,C.L; and Wilson.D.W. (eds); 'Comprehensive Analytical Chemistry,' Vol IID; Elsevier Scientific Publishing Company; 1975; Amsterdam.
- 178.a) Lingane,J.J; 'Electroanalytical Chemistry' (2nd Ed); Interscience; New York; 1958.  
  
b) Lingane,J.J; J.Am.Chem.Soc; 1945; 67; 1916.  
  
c) Lingane,J.J; Anal.Chim.Acta; 1948; 2; 584.  
  
d) McNevin,W.M; and Baker,B.B; Anal.Chem; 1952; 24; 986.  
  
e) Meites,G; Anal.Chem; 1959; 31; 1285.

179. Browning,D.R. (ed); 'Electrometric Methods'; McGraw-Hill; 1969; London.
180. Glasstone,S; 'An Introduction to Eletrochemistry'; Van Nostrand,D. Company, Inc; 1942; U.S.A.
181. Dick,J.G; 'Analytical Chemistry'; Robert,E.Kreiger Publishing Company; 1978; U.S.A.
182. Nishida,Y; Unoura,K; Watanabe,I; Yokomizo,T; and Kato,Y; Inorg.Chimica.Acta; 1991; 181; 141.
183. Owen,G.R; and reese,C.B; J.Chem.Soc.Section C; 1970; 2401.
184. Murase,I;Hatano,M; Tanaka,M; Veno,S; Okawa,H; and Kida,S; Bull.Chem.Soc.Japan; 1982; 55(8);  
2404.
185. Figgs,B.N; and Nyholm,R.S; J.Chem.Soc.Chem.Commun; 1959; 331.